



**HAL**  
open science

# Loi de comportement et modélisation numérique des sols artificiellement structurés

Victor Robin

► **To cite this version:**

Victor Robin. Loi de comportement et modélisation numérique des sols artificiellement structurés. Other. Université de Lorraine, 2014. English. NNT : 2014LORR0264 . tel-01751386

**HAL Id: tel-01751386**

**<https://hal.univ-lorraine.fr/tel-01751386>**

Submitted on 29 Mar 2018

**HAL** is a multi-disciplinary open access archive for the deposit and dissemination of scientific research documents, whether they are published or not. The documents may come from teaching and research institutions in France or abroad, or from public or private research centers.

L'archive ouverte pluridisciplinaire **HAL**, est destinée au dépôt et à la diffusion de documents scientifiques de niveau recherche, publiés ou non, émanant des établissements d'enseignement et de recherche français ou étrangers, des laboratoires publics ou privés.



## AVERTISSEMENT

Ce document est le fruit d'un long travail approuvé par le jury de soutenance et mis à disposition de l'ensemble de la communauté universitaire élargie.

Il est soumis à la propriété intellectuelle de l'auteur. Ceci implique une obligation de citation et de référencement lors de l'utilisation de ce document.

D'autre part, toute contrefaçon, plagiat, reproduction illicite encourt une poursuite pénale.

Contact : [ddoc-theses-contact@univ-lorraine.fr](mailto:ddoc-theses-contact@univ-lorraine.fr)

## LIENS

Code de la Propriété Intellectuelle. articles L 122. 4

Code de la Propriété Intellectuelle. articles L 335.2- L 335.10

[http://www.cfcopies.com/V2/leg/leg\\_droi.php](http://www.cfcopies.com/V2/leg/leg_droi.php)

<http://www.culture.gouv.fr/culture/infos-pratiques/droits/protection.htm>

---

# Analytical and numerical modelling of artificially structured soils

## Thèse de Doctorat

pour l'obtention du grade de

Docteur de l'Université de Lorraine

et

Docteur de l'Université d'Exeter

en

**Mécanique – Génie Civil**

par

**Victor Robin**

Présentée et soutenue publiquement le 11 Décembre 2014 devant le jury composé de

Prof. Cristina Jommi	University of Delft	Rapporteur
Prof. Fabrice Emeriault	Université de Grenoble	Rapporteur
Prof. Philippe Young	University of Exeter	Rapporteur
Prof. Pierre-Yves Hicher	Ecole Centrale de Nantes	Président
Prof. Farimah Masrouri	Université de Lorraine	Directeur de thèse
Prof. Akbar Javadi	University of Exeter	Directeur de thèse
Dr Olivier Cuisinier	Université de Lorraine	Co-Directeur



---

# Analytical and numerical modelling of artificially structured soils

## THESIS

Submitted by Victor Robin to the University of Exeter  
as a thesis for the degree of

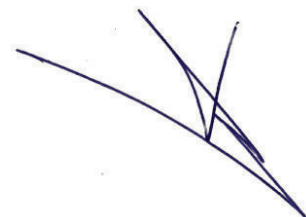
**Doctor of Philosophy in Engineering**

in December 2014

This thesis is available for Library use on the understanding that it is copyright material and that no quotation from the thesis may be published without proper acknowledgement.

I certify that all material in this thesis which is not my own work has been identified and that no material has previously been submitted and approved for the award of a degree by this or any other University.

Signature:





# Declaration

I, Victor Robin, hereby declare that this Ph.D. thesis report entitled

**”Analytical and numerical modelling of artificially structured soils”**

is written by me and that all material in this thesis which is not my own work has been identified and properly cited.

**Student’s Name:** Victor Robin



Signature:

Date: 30<sup>th</sup> September 2014





## Acknowledgements

My warmest gratitude should be expressed to my parents for having supported me through all these years. They gave me the chance to pursue my studies until the doctorate, and for that I shall be forever grateful.

I would like to thank my advisors Farimah Masrouri, Akbar Javadi and Olivier Cuisinier for their supervision and advice throughout these three years, and for having trusted me with this very interesting joint PhD program between the Université de Lorraine and the University of Exeter. It has been a fantastic experience during which I learnt a lot and that helped me to achieve my goals.

I have been honoured to have Cristina Jommi, Fabrice Emeriault, and Philippe Young as examiners of my thesis, and Pierre-Yves Hicher as chairman of my defense, and I was very pleased by their positive comments about my work.

I would like to thank the company Colas for having funded part of this PhD, and especially Jean Voirin for his support during this thesis and his valuable insight.

A special thank to Mélanie Coureau for her unconditioned help. I also thank all my colleagues for the fun we had, and a special thank to Hossein, Luc, and Wadood for their help before my viva.



## Abstract

The effects of lime treatment on the mechanical properties of soils are usually not accounted for in the design of geotechnical structures. As a result the potential of lime treatment has not been fully exploited. In this thesis, a comprehensive experimental program has been carried out to identify the key features of the mechanical behaviour of structured materials. The chemical modifications arising from lime treatment were quantified using thermal analysis methods. From these results a non-linear chemo-mechanical coupling was established between the concentration of cementitious compounds and the yield stress. Using these results, a new formulation to model the degradation of the structure at yield has been developed and implemented in a constitutive model for structured materials. This new model, developed in the framework of the Modified Cam Clay model, requires a limited number of additional parameters that all have a physical meaning and can all be determined from an isotropic compression test. The model has proven to be successful in reproducing the key features of structured materials and for the modelling of the mechanical behaviour of lime treated specimens under various stress paths. Due to similarities in behaviour, it is shown that the formulation is also suitable for naturally structured soils. To account for a structured material in the design of geotechnical structures, a fully functional finite element program for elasto-plastic problems was developed including the pre- and post-processing of the results. A thorough validation has confirmed the good implementation of the finite element method and its suitability for the modelling of complex geometries involving structured materials.

## Résumé

Le traitement des sols à la chaux est une méthode couramment utilisée pour améliorer les propriétés mécaniques de sols aux performances insuffisantes. Cependant, ces améliorations mécaniques ne sont pas prises en compte dans les calculs de dimensionnement. Cette thèse propose une méthodologie pour pallier à ce problème. Un programme expérimental approfondi est réalisé afin de décrire avec précision le comportement mécanique d'un sol traité et les processus associés à la structuration introduite par le traitement. La composition chimique, et notamment la quantité de composés cimentaires hydratés, est déterminée par analyses thermogravimétriques et thermo différentielles. Un couplage non-linéaire entre la quantité d'hydrates et la limite élastique se basant sur ces résultats expérimentaux est proposé. À partir de ces résultats, une nouvelle formulation a été développée afin de modéliser la dégradation de la structure en plasticité, et a servi au développement d'une nouvelle loi de comportement élasto-plastique basée sur le modèle de Cam Clay Modifié. Cette dernière a montré reproduire correctement les principaux traits de comportement spécifiques aux sols traités. Il est démontré que ce modèle est également adapté aux sols naturellement structurés. Afin de prendre en compte les effets du traitement et la présence de structure dans le dimensionnement, un programme basé sur la méthode des éléments finis, comprenant le pré- et le post-processing de la géométrie et des résultats du problème, a été développé. Une validation rigoureuse a confirmé l'implémentation correcte de la méthode et son potentiel pour l'optimisation du dimensionnement des ouvrages.



# Contents

<b>Abstract</b>	<b>vii</b>
<b>1 Introduction</b>	<b>1</b>
1.1 Context . . . . .	1
1.2 Motivations . . . . .	2
1.3 Structure of the thesis . . . . .	4
<b>2 Background of the study</b>	<b>7</b>
2.1 Introduction . . . . .	7
2.2 Chemical reactions in lime treated soils . . . . .	7
2.2.1 Short term reactions . . . . .	7
2.2.2 Long term reactions . . . . .	8
2.3 Mechanical behaviour of lime treated soils . . . . .	11
2.3.1 Behaviour of a lime treated soil under isotropic compression . . . . .	11
2.3.2 Analogy with naturally structured soils . . . . .	13
2.4 Theory of continuum mechanics and elasticity . . . . .	17
2.4.1 Concepts of continuum mechanics . . . . .	17
2.4.2 Mathematical theory of continuum mechanics . . . . .	18
2.4.3 Linear elasticity . . . . .	20
2.5 Theory of elasto-plasticity and application to soils . . . . .	23
2.5.1 Concept of plasticity . . . . .	23
2.5.2 Yield criteria . . . . .	25
2.5.3 The Modified Cam Clay model . . . . .	29
2.6 Conclusion . . . . .	35
<b>3 Chemo-mechanical modelling of lime treated soils</b>	<b>37</b>
3.1 Introduction . . . . .	37
3.2 Review of the methods for chemo-mechanical coupling . . . . .	37
3.2.1 Qualitative analysis . . . . .	38
3.2.2 Quantitative analysis . . . . .	38
3.2.3 Soil Water Transfer model . . . . .	39
3.2.4 Suitable approach for lime treated soils . . . . .	42
3.3 Materials and methods . . . . .	43
3.3.1 Characterization of the materials . . . . .	43
3.3.2 Specimens preparation . . . . .	44
3.3.3 Drained triaxial experiments . . . . .	46

3.3.4	Monitoring of the physico-chemical reactions . . . . .	49
3.4	Experimental results . . . . .	50
3.4.1	Mechanical behaviour . . . . .	51
3.4.2	Yield loci for lime treated soils . . . . .	55
3.4.3	Chemical analysis . . . . .	56
3.5	Discussion . . . . .	57
3.5.1	Influence of lime on mechanical parameters . . . . .	58
3.5.2	Chemo-mechanical coupling between physico-chemical process and yield stress . . . . .	59
3.6	Conclusion . . . . .	62
<b>4</b>	<b>A general formulation for degradation in structured soils</b>	<b>65</b>
4.1	Introduction . . . . .	65
4.2	Review of methods for the modelling of the structure . . . . .	66
4.2.1	Bounding surface theory . . . . .	66
4.2.2	Structured soils as cohesive-frictional materials . . . . .	67
4.2.3	Plastic strain damage . . . . .	67
4.2.4	Suitable approach for lime treated soils . . . . .	68
4.3	Structured Cam Clay model . . . . .	69
4.4	Features of structured soils . . . . .	72
4.4.1	Naturally structured soils . . . . .	73
4.4.2	Lime treated soils . . . . .	74
4.4.3	Summary . . . . .	77
4.5	Theoretical framework of the model . . . . .	78
4.5.1	Modelling the structure and its degradation under isotropic loading	78
4.5.2	Yield function $f$ . . . . .	84
4.5.3	Plastic potential $g$ . . . . .	85
4.5.4	Summary of the model parameters . . . . .	86
4.6	Stress-strain relationship . . . . .	86
4.6.1	Elastic behaviour . . . . .	86
4.6.2	Plastic behaviour . . . . .	86
4.7	Model evaluation . . . . .	89
4.7.1	Associated flow rule hypothesis . . . . .	89
4.7.2	Lime treated specimens . . . . .	90
4.7.3	Naturally structured soils . . . . .	96
4.7.4	Discussion: influence of the initial void ratio on the degradation mode . . . . .	101
4.8	Conclusion . . . . .	102
<b>5</b>	<b>Finite element modelling of structured materials</b>	<b>105</b>
5.1	Introduction . . . . .	105
5.2	Principles of the finite element method . . . . .	106
5.3	Mathematical theory of finite element method for elastic problems . . .	107
5.3.1	Strong formulation . . . . .	107
5.3.2	Weak formulation . . . . .	108

5.3.3	Weighted residual formulation . . . . .	109
5.4	Theory of plasticity in finite element method . . . . .	112
5.4.1	Yield criterion . . . . .	113
5.4.2	Flow rule . . . . .	114
5.4.3	Incremental stress-strain relationship . . . . .	114
5.5	Presentation of the finite element code FEMASS . . . . .	118
5.5.1	Pre-processing . . . . .	118
5.5.2	Processing . . . . .	119
5.5.3	Post-processing . . . . .	119
5.6	Validation of the finite element code FEMASS . . . . .	120
5.6.1	Objectives . . . . .	120
5.6.2	Simulation of a thick cylinder subjected to internal pressure . . . . .	122
5.6.3	Validation of the Modified Cam Clay . . . . .	127
5.6.4	Validation of the MASS . . . . .	128
5.6.5	Conclusion of the validation . . . . .	129
5.7	Potential of the code FEMASS for design optimisation . . . . .	129
5.7.1	Context . . . . .	129
5.7.2	Example of application . . . . .	130
5.8	Conclusion . . . . .	134
<b>6</b>	<b>Conclusion of the study</b>	<b>135</b>
<b>7</b>	<b>Recommendations for future work</b>	<b>139</b>
7.1	Introduction . . . . .	139
7.2	Further investigation for the chemo-mechanical modelling of lime treated soils . . . . .	139
7.2.1	Durability of lime treatment under water circulation . . . . .	139
7.2.2	Time-dependency of pozzolanic reactions and influence on the long term behaviour . . . . .	144
7.3	Improved yield criterion for structured materials . . . . .	145
	<b>Bibliography</b>	<b>158</b>
<b>A</b>	<b>Experimental program details</b>	<b>161</b>
<b>B</b>	<b>Finite element procedures</b>	<b>163</b>
B.1	Proof of Equation (5.7) . . . . .	163
B.2	Nodal interpolation . . . . .	163
B.3	Explicit formulation of the model MASS . . . . .	166
B.4	Pre-processing procedures . . . . .	167
B.5	Finite element algorithm for elasto-plastic problems . . . . .	175
B.6	Python script for vtk file generation . . . . .	176
<b>C</b>	<b>Paper published in <i>Applied Clay Science</i></b>	<b>179</b>
<b>D</b>	<b>Paper published in <i>Computers &amp; Geotechnics</i></b>	<b>189</b>





# Chapter 1

## Introduction

### 1.1 Context

With the world population constantly increasing the need for larger facilities and house buildings has become a key issue. However, simultaneously, the disastrous effects of the human activity on the environment has lead to new environmental regulations and the promotion of sustainable solutions (European Commission, 2013). The geotechnical industry is among the most important regarding employment and revenue, but is also responsible for a large share of the annual pollution (Kamon, 2001). Geotechnical industry therefore faces increasing pressure to meet the demand in new structures while reducing its impact on the environment. Three main challenges for the companies can be identified:

**Resources used.** Although not always noticed, earthworks like foundations, backfills, or embankments require large amount of natural resources. For instance foundations for Burj Khalifa, largest tallest man-made structure in the world (829.8 m), required 45 000 m<sup>3</sup> of concrete and involved 192 piles buried more than 50 m deep (Burj Khalifa, 2013). The companies are looking for alternative solutions to reduce these quantities by using, as much as possible, the resources available on-site (Constructing Excellence Limited, 2013).

**Wastes.** Earth structures, and especially foundations, have a key role in the stability of superstructures built on them. The mechanical properties of the materials involved must therefore fulfil strict requirements. In the event of an unsuitable material on-site, it is common to dispose of it in landfills. For large structures the amount of wastes can become significant, and for this reason companies are trying to recycle this waste as a resource or to produce energy (European Commission, 2013).

**Carbon footprint.** Construction industry is one of the main actors in the production of carbon dioxide, responsible for approximately 50% of the UK's total carbon dioxide (CO<sub>2</sub>) emissions (UK Green Building Council, 2012). A major part of CO<sub>2</sub> is produced by the geotechnical industry during earthworks such as earth-moving, levelling works or foundations. The fulfilment of a large project always requires the use of building site machinery, which usually have high energy consumption, with average fuel consumption of 250 L per hour.

## 1. INTRODUCTION

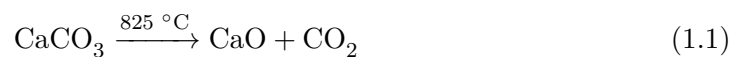
One of the main challenges for geotechnical companies is the use of materials available on site, which very often do not meet the mechanical characteristics required for the safety and stability of the construction. Before the environment regulations an unsuitable material would have been simply removed and disposed of in landfills. This resulted in an expensive cost in money, time, people, heavy machinery, fuel, and all the related environmental impact they come with (carbon footprint, wastes, use of landfills, etc...). The ability to deal with all the available resources could lead to significant savings and would help construction industry to meet their environmental objectives. Thus, it has become a key issue for companies to make use, as much as possible, of the available materials on-site. A possible solution to deal with such material is to proceed to an artificial treatment of the soil, which involves mixing the material with a chemical compound to improve the geotechnical properties. Soil treatment with quicklime (CaO) has significant effects on the mechanical properties at both short and long term and has been used successfully in a number of major construction projects: The New York Stock Exchange, Millau viaduct, or Burj khalifa in Dubai.

Nowadays, artificial treatment with lime is mostly used by construction industry for its short term effects such as the decrease of the water content and/or the increase of the bearing capacity. Those effects result in an easier handling of plastic materials and ease the traffic of heavy machineries. However, lime is also known to have long term effects leading to significant mechanical improvements of the material which are at the moment not accounted for in the design of the geotechnical structures. As a result the potential of lime treatment has not been fully exploited.

### 1.2 Motivations

#### Sustainability of lime treatment

The key element in lime treatment is the calcium oxide (CaO), known as *quicklime*, which is produced by thermal decomposition of calcium carbonates  $\text{CaCO}_3$ :



It can be seen from Equation (1.1) that 1 mol of carbon dioxide is produced per mol of calcium oxide, which corresponds to 0.8 t of  $\text{CO}_2$  per tonne of CaO produced. Lime can therefore hardly be referred to as a “green” product and should be used wisely.

From the methods used in the design of structures results the use of unnecessary large amount of material in order to satisfy the safety factors. In the event of a lime treatment, this also results in excessive use of a lime. Moreover, lime treatment is mostly used nowadays for its short term effects, and the mechanical improvements arising from the long term effects are ignored in the calculations. Accounting for the long term effects could result in an optimisation of the design which would lead to 1) a diminution of the resources required, 2) a smaller amount of lime needed for the treatment and 3) a reduced carbon footprint.

The strategy used at the moment by companies, which consists in over designing the structure and neglecting the long term effects of the lime treatment, appears to be the least sustainable (amount of material and carbon footprint wise) and economical

solution ( $\approx$ £15-20 per tonne of CaO). Important benefits, both environmental and economical, could arise by taking into account the long term improvements of the material in the calculations.

### Need for innovative methods

The development of sustainable solutions implies innovative methods and is problematic for construction companies. Most of the methods used for the design of geotechnical structures are based on theories developed between the 18<sup>th</sup> and early 20<sup>th</sup> centuries, and are constrained to strict assumptions on the material behaviour and simplifications of the problem. Some of the most popular and famous methods in geotechnics are given below:

*Coulomb's theory (1776)* is used in the design of retaining walls to determine the maximum lateral earth pressure on the wall before failure. Originally formulated for vertical wall only (Coulomb, 1776), it was generalised to account for the wall friction by Mayniel (1808).

*Rankine's theory (1857)* is also widely used in the design of retaining walls. It is a stress field solution in a soil mass when plastic equilibrium has been reached, and is useful to calculate the lateral earth pressure and locate where reinforcements might be necessary. However, it is only valid for a smooth (frictionless soil-wall interface) and vertical wall in a semi-infinite space (Rankine, 1857).

*Boussinesq equations (1885)* are used to calculate the stress increments anywhere in a massif due to a loading on the surface (point load or pressure). However, the solution is valid only for semi-infinite, homogeneous, isotropic solid, with a linear stress-strain relationship (Boussinesq, 1885).

These methods have the advantage to rely on resolutions of elastic problems and require a limited number of parameters that all have physical meanings. However, these models apply for ideal materials (homogeneous, isotropic, linear elastic behaviour) in ideal situations (frictionless walls, infinite massif), very different from real conditions (e.g. nonlinear behaviour, plastic deformation, boundary effects). For these reasons engineers have recourse to safety factors which consists in increasing the magnitude of the mechanical solicitations theoretically calculated and designing the structures accordingly. Consequently, this leads to an over design and an over consumption of resources. Nowadays priorities have changed and construction industry must face the challenge of evolving and developing new methods.

### Strategy for industrial use

The modelling of lime treatment is a complicated problem due to the number of processes involved to improve the mechanics properties. To account for the lime treatment in the design of the geotechnical structures, companies need 1) to be able to calculate the right lime content in order to match the mechanical characteristics required, 2) a framework to describe the mechanical behaviour of lime treated soils, and

## 1. INTRODUCTION

3) a numerical model to assess the effect of the treatment on the whole structure and optimize the design. Three distinct challenges can therefore be identified:

*A chemo-mechanical coupling* between the concentration in lime and the resulting mechanical improvements is not sufficient. The latter must be linked with the products of the chemical reactions following the treatment.

*A constitutive model* for lime treated soils. Since the mechanical properties are modified, the stress-strain relationship of the material might be changed as well. The understanding of the material under elastic and plastic deformations is therefore required to account for the treatment in the design.

*A numerical model* to evaluate the effects of the treatment and its degradation in the entire geotechnical structure for complex geometry.

### 1.3 Structure of the thesis

The purpose of this thesis is to meet the need of the industry to exploit the full potential of lime treatment by developing a methodology answering the three issues highlighted before. Considering the needs to optimise the design with lime treatment and the limitations of the current methods, this thesis is structured as follows:

1. The second chapter is a background of the current knowledge on artificial lime treatment for geotechnical applications. The chemical reactions involved in lime treatment and their short and long term effects on the mechanical behaviour are presented. The frameworks of continuum mechanics, elasticity, and plasticity are then introduced to identify the elements required for the development of a constitutive model.
2. The third chapter is dedicated to the establishment of a chemo-mechanical coupling between the concentration in lime and the resulting mechanical properties. First, the mechanical behaviour of a lime treated silt is extensively studied. Anticipating the need for experimental results for the evaluation of the constitutive law, triaxial experiments were carried out to allow complete determination of the stress tensor within the specimens. The chemical composition of a lime treated material is quantified using thermogravimetric analysis (TGA) and differential thermal analysis (DTA). The relevant compounds responsible for the mechanical improvement are identified, and a nonlinear coupling is developed between the yield stress and the concentration in hydrates.
3. The fourth chapter aims at developing a reliable elasto-plastic model for lime treated soils in the framework of the Modified Cam Clay. From the results of triaxial tests performed on lime treated specimens, a closed yield surface for this kind of material is developed. The plastic strain increments at yielding are used to assess the shape of the plastic potential. A new formulation to model the degradation in a structured soil is proposed and is implemented in the hardening and softening rules. The Model for Artificially Structured Soils (MASS) gives very satisfactory results for the modelling of lime treated soils

and appears to provide an accurate description of the mechanical behaviour of structured materials at yield. As part of the development of a methodology to account for artificial treatment in the design, the model relies on meaningful parameters only, all determined from a single isotropic compression test.

4. The fifth chapter is about the assessment of the effects of lime treatment for complex geometries and the optimisation of the design using the finite element method (FEM). A fully functional FEM program for elasto-plastic problems was developed in this thesis, including the pre- and post-processing of the results. The constitutive model developed for lime treated soils was included as well as the Modified Cam Clay and other classic yield criteria (Von Mises, Tresca, Mohr-Coulomb, Drucker-Prager).
5. The sixth chapter gives a conclusion of the thesis. As recommendations for future work, the seventh chapter discusses the potential and success of the methodology developed in this thesis for an industrial use as well as its limitations and the possible remedies. The stability of lime treatment under aggressive water conditions is a major aspect to be clarified for the assessment of the durability of the treatment. A first approach to assess the consequences of a leaching of the soil due to water circulation was developed using the finite difference method. In addition, the time-dependency of the chemical reactions involved in lime treatment and the possible effects on the stability of structures is highlighted. Finally, we discuss about improvement of the yield criterion of the model MASS to increase the accuracy of the predictions for low confining pressures.

## 1. INTRODUCTION

# Chapter 2

## Background of the study

### 2.1 Introduction

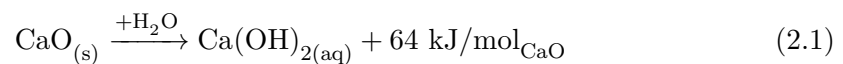
Three requirements have been identified to take into consideration a lime treatment in the design of geotechnical structures: a chemo-mechanical coupling, a constitutive law, and a numerical model suitable for lime treated soils. We give in this chapter the background related to lime treatment and the three issues.

First, we give a description of the chemical reactions happening in the soil after the addition of lime. The purpose is to identify 1) the type of components newly formed in the soil for a future experimental quantification and 2) the effects on the mechanical parameters (e.g. cohesion and Young's modulus). Then, we give a description of the specific features of artificially structured soils subjected to mechanical loading, the purpose being to identify the mechanisms involved in the degradation of the treatment. Finally, we give an introduction to the main concepts of continuum mechanics, elasticity, and plasticity, in order to identify the limits of the current methods for the modelling of artificially treated soils.

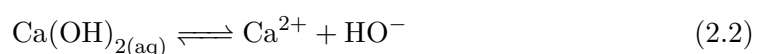
### 2.2 Chemical reactions in lime treated soils

#### 2.2.1 Short term reactions

When added to the soil, quicklime ( $\text{CaO}$ ) reacts with the free water to produce hydrated lime, known as portlandite  $\text{Ca}(\text{OH})_2$ :



This first reaction is responsible for the decrease of the water content  $w$ . The portlandite dissolved in aqueous medium dissociates in ions  $\text{Ca}^{2+}$  and  $\text{HO}^-$  according to the equilibrium reaction



Cation exchange process induced by the presence of large amounts of calcium ions adsorbed on the clay particles surface lead to a reduction of the size of the Gouy-Chapman diffuse double-layer of the clay particles. This results in the lowering of the repelling forces between clay particles and thereby gives rise to the flocculation of the

## 2. BACKGROUND OF THE STUDY

clay particles (Schofield and Samson, 1953; Mathew and Rao, 1997). It is generally accepted that cation exchange and flocculation processes occur immediately after the addition of lime, and result in a decrease of the soil plasticity and the modification of the engineering properties like the bearing capacity or the Atterberg's limits (e.g. Sherwood, 1993; Little, 1995). Lime treatment increases the plastic limit ( $w_p$ ) without changing the liquid limit ( $w_l$ ) (Figure 2.1).

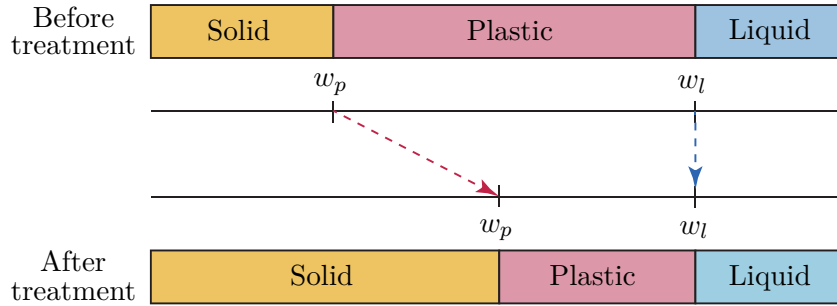


Figure 2.1: Consequences of aggregation on Atterberg Limits – after SETRA (2007) modified.

During the short term reactions the ions  $\text{Ca}^{2+}$  and  $\text{HO}^-$  are adsorbed by minerals in order to satisfy the electrochemical equilibrium of the soil, and are therefore not available yet for other reactions (Schofield and Samson, 1953). During this process, known as lime fixation, all the ions resulting from the dissociation of the portlandite are adsorbed by minerals. This process goes on until no more ions can be adsorbed and is reached to a concentration called *lime fixation point*. A lime content greater than the lime fixation point does not lead to any additional modification of the Atterberg's limits (Clare and Cruchley, 1957; Hilt and Davidson, 1960) but results in the accumulation in the solution of ions  $\text{Ca}^{2+}$  and  $\text{HO}^-$  that can be involved in other chemical processes.

### 2.2.2 Long term reactions

The increase of concentration in hydroxide ions in the solution results in an increase of the pH. An alkaline environment enables the dissolution of both silica and alumina present in the soil minerals and their reaction with calcium ions (Diamond and Kinter, 1965, 1966). The reactivity of these reactions, known as *pozzolanic reactions*, is maximum when the pH is around 12.4, which gives the maximum solubility for the silicon and aluminium ions and the portlandite (Eades and Grim, 1966; Müller, 2005). Pozzolanic reactions result in the production of cementitious gel such as calcium silicate hydrates (CSH), calcium aluminate hydrates (CAH), and calcium aluminosilicate hydrates (CASH) (e.g. Eades and Grim, 1960; Croft, 1967; Bell, 1996; Narasimha Rao and Rajasekaran, 1996).

Pozzolanic reactions are time dependent (Mitchell and Hooper, 1961) and it is now well accepted that cementitious compounds are responsible for most of the mechanical improvements of the material (e.g. Ingles, 1964; Broms and Boman, 1975) such as the unconfined compressive strength (Bell, 1996), the cohesion and friction angle (Brandl, 1981), the optimum water content (Davidson et al., 1962; Locat et al., 1990), the yield stress (Tremblay et al., 2001), or Young's modulus (Broms and Boman, 1979; Bell,



1996) (Figure 2.2). However, it was observed that there also exists a lime content above which there is no more mechanical improvements (e.g. Bell, 1996). Al-Rawi (1981) even reported that a large amount in lime can sometimes lower the mechanical properties compared to the original untreated material.

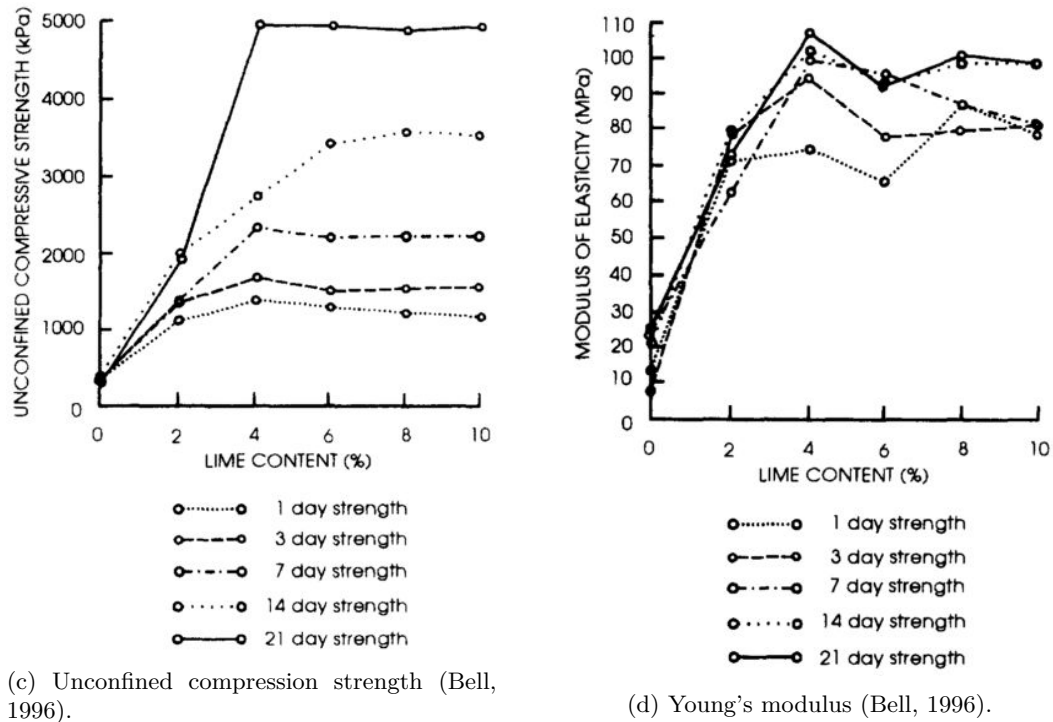
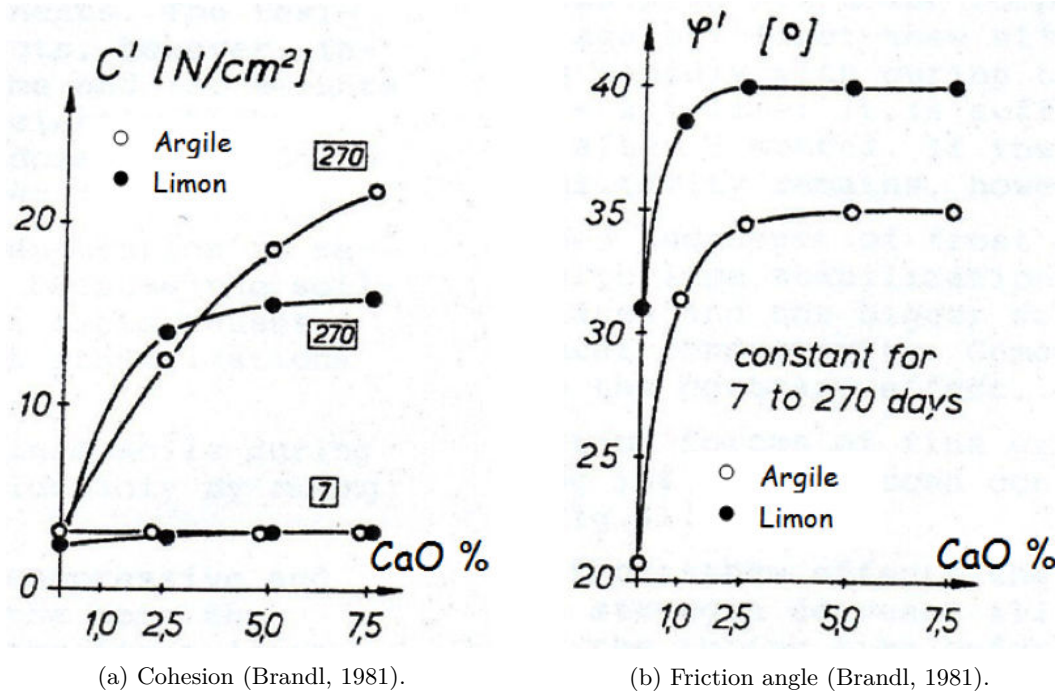
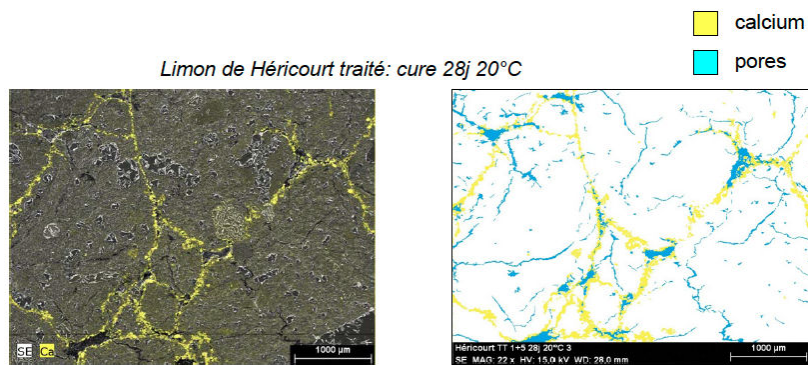


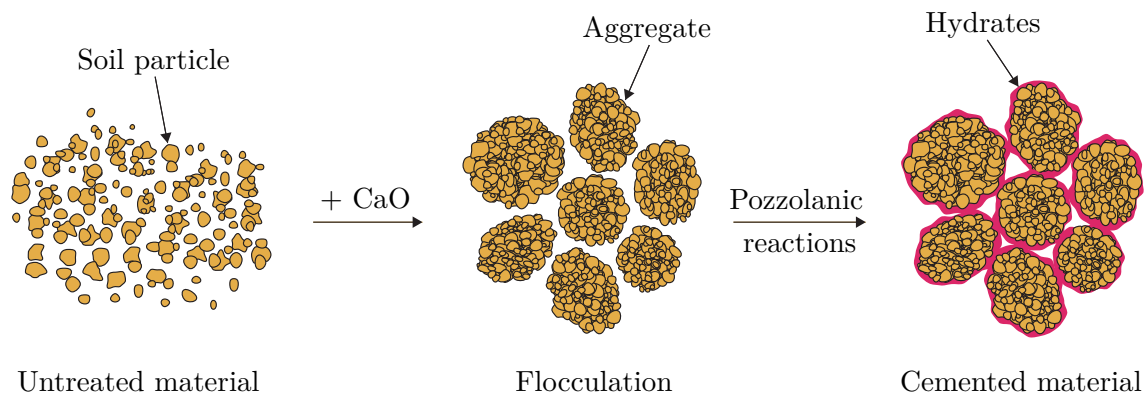
Figure 2.2: Influence of a lime treatment on some mechanical parameters and time dependency.

## 2. BACKGROUND OF THE STUDY

Several studies have reported the engineering applications of lime treatment to solve geotechnical problems (e.g. Little, 1995; Broms and Boman, 1975). The understanding of the chemical reactions involved in lime treatment appears to be the key for the establishment of a chemo-mechanical coupling. Figure 2.3a shows the repartition of the calcium after 28 days in a lime treated silt. Since calcium is involved in the pozzolanic reactions, it can be used to trace the cementitious compounds within the treated material. One can see that most of the calcium, and therefore the hydrates, appears to be located around the aggregates resulting from the short term effects, and forming a coat binding soil particles together. Figure 2.3b sums up the different processes experienced by soil particles during lime treatment (Choquette et al., 1987).



(a) Localisation of the calcium and voids in a lime treated silt after 28 days (Deneele and Lemaire, 2012).



(b) Schematic representation of flocculation and cementation

Figure 2.3: Process of cementation following a lime treatment.

The study of the chemical reactions involved in a lime treatment has shown that the modifications of the mechanical parameters are directly related to the lime content. The latter also determines the amount of hydrated compounds produced by pozzolanic reactions and therefore the “amount” of bonding of the soil particles. To account for the treatment in the design, the effects of the cementation on the mechanical behaviour and its durability under mechanical loading must be understood.

## 2.3 Mechanical behaviour of lime treated soils

Having described the effects of lime treatment on the chemical and mechanical properties of the soil, we now look at the mechanical behaviour of such engineered material under mechanical loading and the analogy with naturally structured soils.

### 2.3.1 Behaviour of a lime treated soil under isotropic compression

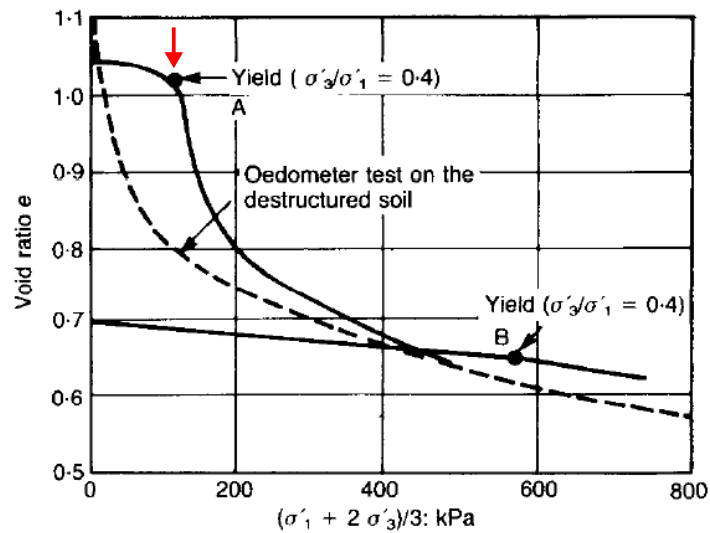
The mechanical behaviour of artificially treated materials have been extensively studied (e.g. Balasubramaniam et al., 2005; Lo and Wardani, 2002; Locat et al., 1996, 1990; Oliveira et al., 2013). The isotropic behaviour is a convenient way to assess the effects of lime treatment. It consists in carrying out triaxial tests which, unlike the oedometer test, allows a full determination of the stress tensor  $\underline{\underline{\sigma}}$  in the sample. An isotropic compression consists in increasing the cell pressure applied on a saturated sample and measuring the variation of volume  $\Delta V$  associated with the increment of cell pressure  $\Delta P$ . This allows the calculation of the variation of the specific volume  $v$  which is plotted as a function of the effective mean stress  $p' = \frac{1}{3}(\sigma_1 + \sigma_2 + \sigma_3)$  (spherical part of the stress tensor). There is no shear deformation in the sample with this stress path ( $\underline{\underline{s}} = \underline{\underline{0}}$ ).

To assess the mechanical improvements induced by chemical treatment, the treated soil is compared with the untreated material which is used as reference. Figure 2.4 shows the general behaviour of an isotropic compression performed on an untreated material. Two domains can be identified:

- For  $p' \leq p'_y$ , the material has an elastic behaviour, almost reversible along this stress path, and linear in a natural log scale until it reaches the yield stress  $p'_y$ .
- For  $p' > p'_y$  plasticity begins associated with a sudden variation of the specific volume. The behaviour is also linear in log scale but material experiences plastic deformations that are no longer reversible. If unloaded, the material goes back into the elastic domain, deformations become reversible again, and the yield stress is equal to the largest effective mean stress experienced by the material.

The effects of the artificial treatment can therefore be assessed with the increase of the yield stress  $\Delta p'_y$ , which leads to an increase of the additional void ratio  $\Delta e$  compared to the untreated material, maximum at  $p' = p'_{y,t}$  and noted  $\Delta e_i$  (Figure 2.4b). When the treated soil reaches the yield stress, plastic deformations occur within the material and are associated with a diminution of the additional void ratio  $\Delta e$ . This process, called *degradation*, corresponds to the alteration of the mechanical improvements arising from the treatment (Leroueil and Vaughan, 1990).

## 2. BACKGROUND OF THE STUDY



(a) Artificially treated soil (Maccarini, 1987; Leroueil and Vaughan, 1990).

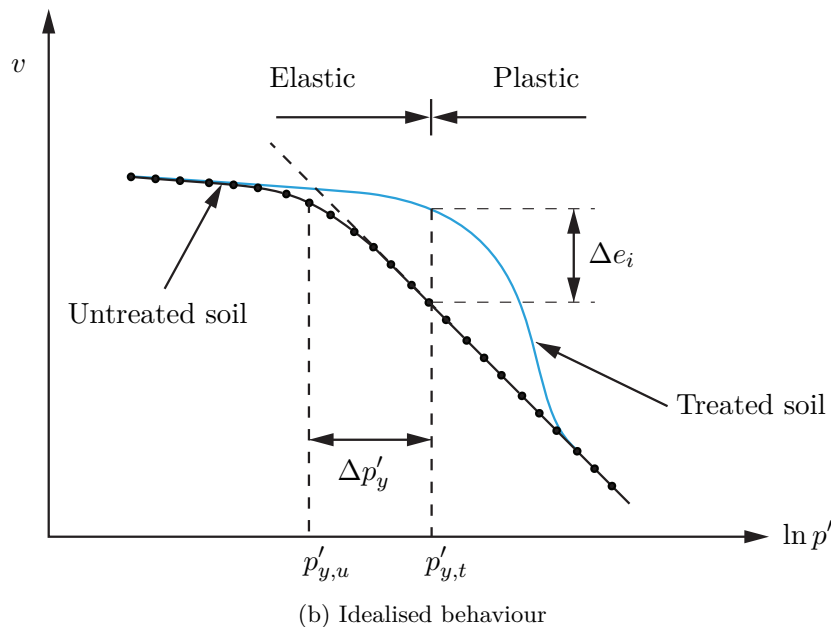


Figure 2.4: Elastic and plastic behaviour of an artificially structured soil under isotropic compression –  $p'_{y,u}$ : yield stress of the untreated soil,  $p'_{y,t}$ : yield stress of the lime treated soil,  $\Delta p'_y$ : increase of the yield stress due to treatment,  $\Delta e_i$ : additional void ratio at yield.

The mechanical improvements, such as the increase of the yield stress, are the results of the combination of the short term and long term effects. First, aggregates arise from the flocculation of the soil particles, which already improves the bearing capacity. Then, in a second phase, long term (or pozzolanic) reactions result in the production of cementitious compounds. These products, also called *hydrates*, coat the aggregates and act as a skeleton binding the particles together and constitute the *structure* (Figure 2.3b). This structure, more like a gel-like, has been observed experimentally using scanning electron microscope (SEM) by Eades and Grim (1960) and Croft (1964). This structure is responsible for the global enhancements of the material. In this thesis, structure refers to Burland's definition (Burland et al., 1996) and describes the combination of the fabric and the bonding of the soil skeleton. Fabric

accounts for the arrangement of the particles, which depends on the state of compaction and their geometry.<sup>1</sup>

### 2.3.2 Analogy with naturally structured soils

Naturally structured soils have been extensively studied (e.g. Liu and Carter, 2003; Callisto and Rampello, 2004). For such materials structure is the result of natural processes occurring under specific conditions such as:

- Solution and deposition of silica at particle contacts in sands,
- Modification of adsorbed water layer and inter-particle attractive forces in clays,
- Deposition of organic matter,
- Deposition of carbonates and hydrates.

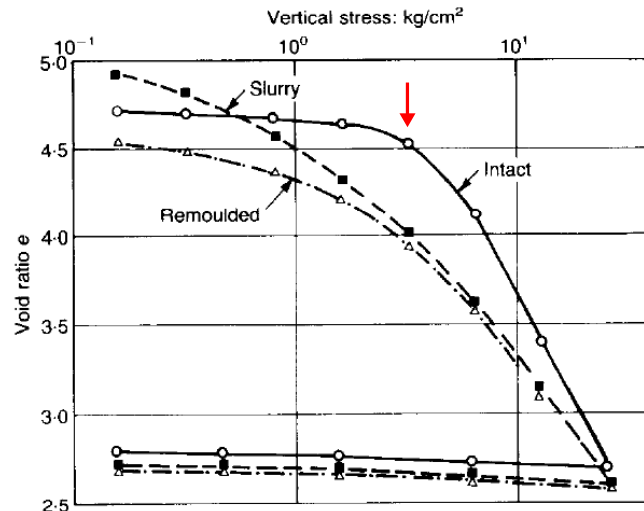
This last process is to be linked with the chemical reactions involved in lime treatment. Although time scale is completely different, natural carbonation and artificial treatment result in the production of a similar cement coating binding soil particles together. Similarities in the mechanical behaviour have been identified between naturally and artificially structured soils (Leroueil and Vaughan, 1990).

***Isotropic compression behaviour*** The typical behaviours of a naturally structured material and an artificially treated soil are compared in Figure 2.5, which presents one-dimensional compression curves performed on both materials.

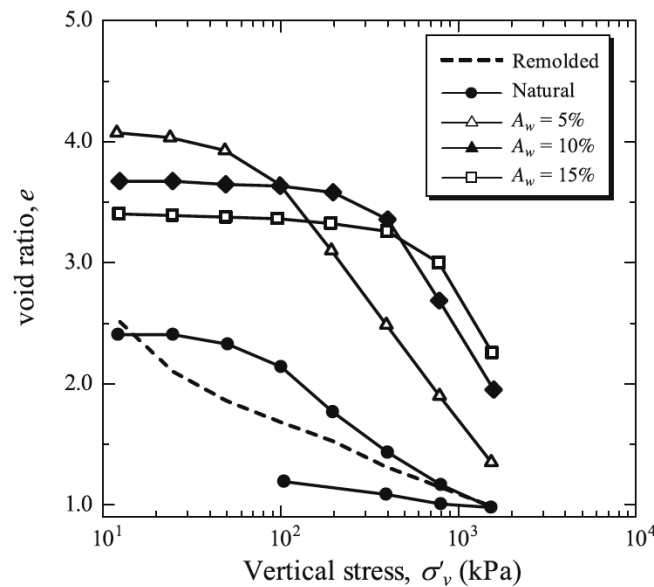
---

<sup>1</sup>Various terminologies can be found in the literature to describe the structure and the state of the material (e.g. structured, cemented, destructured, reconstituted or remoulded). For clarity, structure and cementation will be used equally in this thesis.

## 2. BACKGROUND OF THE STUDY



(a) Naturally structured (Wesley, 1973)



(b) Artificially cemented (Lorenzo and Bergado, 2004; Horpibulsuk et al., 2010a)

Figure 2.5: One-dimensional compression curves for (a) naturally structured, (b) and artificially treated –  $A_w$ : Cement content.

It can be seen from Figure 2.5 that both structured materials have a greater yield stress compared to their respective destructured state and experience a loss of structure at yield associated with the decrease of the additional void ratio. This indicates that, regardless of the origin of the cementation, structure leads to a similar mechanical behaviour and suggests a similar process of degradation of the structure at yield.

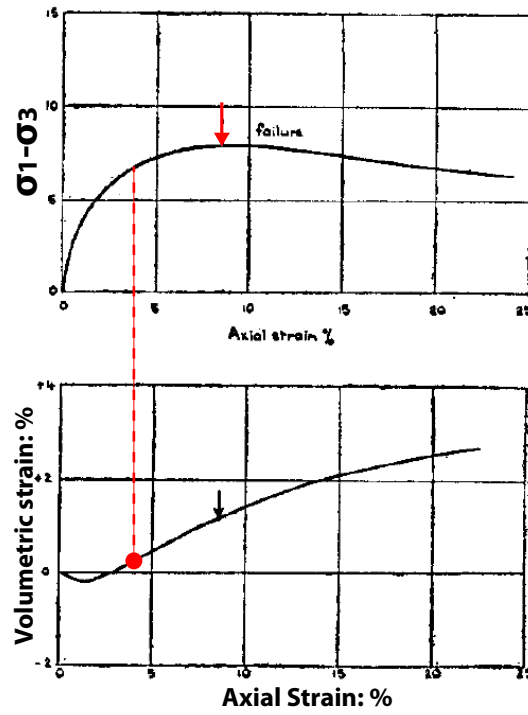
**Stress-strain curves** By comparing the shear behaviour of naturally and artificially structured materials at yield, Leroueil and Vaughan (1990) shed light on the process of degradation and proved the existence of a specific mechanism due to the structure. Figure 2.6 shows drained triaxial test results performed on three different materials. Figure 2.6a gives the typical behaviour of an unstructured material, Figure 2.6b of a naturally structured soil, and Figure 2.6c of an artificially structured material. The

qualitative values of the variables put aside, all three materials can experience a softening behaviour. This corresponds to the deviatoric stress  $q$  reaching a maximum value (failure) before progressively decreasing and converging toward a stable state called *critical state*. Regarding the volumetric deformations, the material experiences contraction followed by dilation.

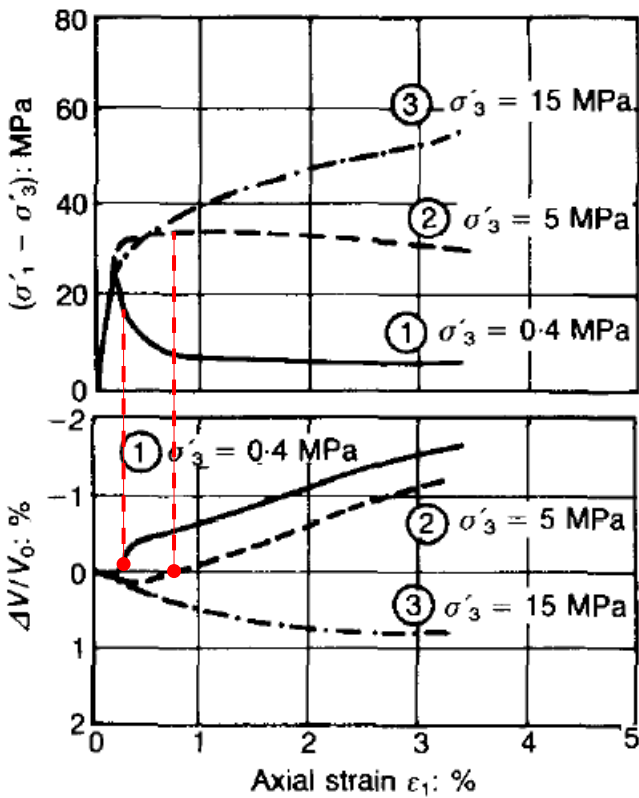
The origin of the change in the volumetric deformations (contraction-dilation) has been extensively studied and explained by Rowe (1962). As the deviatoric stress increases, particles within the sample proceed to a rearrangement towards a more compact state (contraction) until there is no other choice but to overcome interlocking (dilation) (Burland et al., 2008). At this moment the rate of dilation  $d\varepsilon_p/d\varepsilon_a$  is maximum, but because of the frictional resistance between the particles the deviatoric stress keeps increasing until interlocking and friction are both completely overcome. For this reason, the maximum rate of dilation in unstructured soils is always before the deviatoric stress peak (Craig, 2004).

Figures 2.6b and 2.6c show that both naturally and artificially structured materials experiencing dilation do not follow this rule and present a maximum rate of dilation after the peak. This is due to the structure and for such materials another mechanism is involved in addition to interlocking and friction. Structure results in the binding of the particles and should therefore be degraded first. Cementation prevails on interlocking and friction and deviatoric stress keeps increasing until bonding between particles is completely degraded. This marks the release of the particles that can move freely (dilation). For this reason, the rate of dilation in structured materials is observed after the deviatoric stress peak, and is not related to the origin of the cementation. More details can be found in Leroueil and Vaughan (1990).

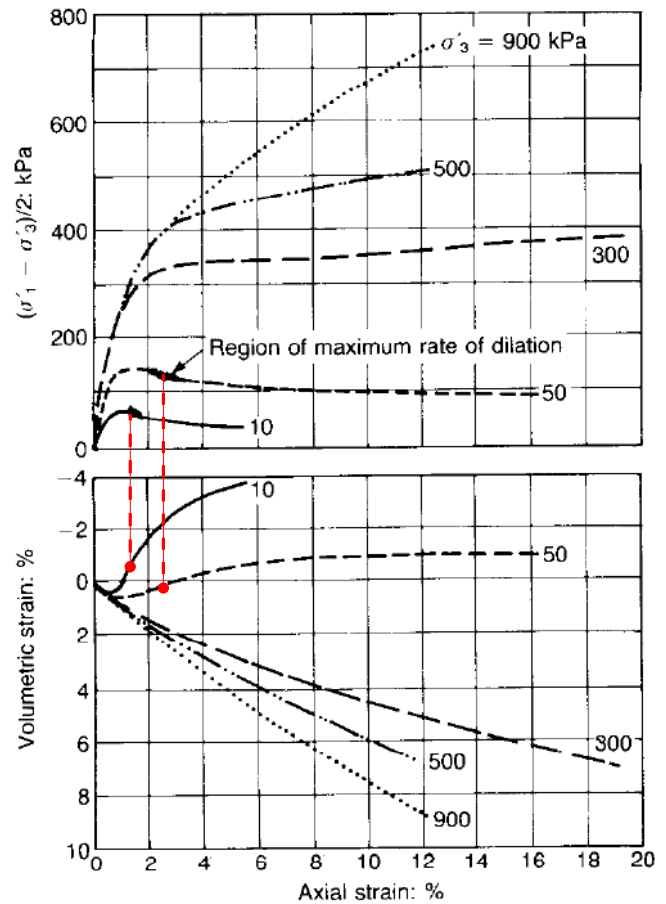
## 2. BACKGROUND OF THE STUDY



(a) Overconsolidated (Henkel, 1956)



(b) Naturally structured (Leroueil and Vaughan, 1990)



(c) Artificially cemented (Leroueil and Vaughan, 1990)

Figure 2.6: Drained triaxial compression tests on (a) overconsolidated, (b) naturally structured and (c) artificially treated soils.



The analysis of the mechanical behaviour of lime treated soils has revealed specific mechanisms in structured soils that do not exist in unstructured materials. For this reason, methods described in Section 1.2 are not suitable for the modelling of lime treated soils. Moreover, most of the studies of degradation of structured soils have focused on the one-dimensional behaviour (oedometer test). However, this experiment presents limitations and allows a complete determination of the stress tensor only if the lateral stresses are measured during the test (Salençon, 2007; Giraud, 2011). In order to identify the precise needs for the modelling of lime treated soils we present the concepts of continuum mechanics and the concepts involved in elasto-plasticity.

## 2.4 Theory of continuum mechanics and elasticity

The study of the mechanical behaviour of lime treated soils has revealed the existence of specific mechanisms due to structure. The latter appears to expand the elastic domain, but experiences degradation at yield due to plastic strains. This implies that a pure elastic constitutive law is not enough to describe the whole process of degradation of the structure.

We first introduce the main concepts in continuum mechanics that constitute the basis for constitutive modelling and the finite element method. The theory for the stress-strain relation of an elastic, isotropic and homogeneous material is then addressed. Finally, we present the theory of plasticity, the most common yield criteria, and discuss their limitations for the modelling of lime treated soils. We end this section by describing the Modified Cam Clay, an elasto-plastic model for soils.

### 2.4.1 Concepts of continuum mechanics

An ideal model for granular material would account for every particle of the solid and its interaction with the others. A numerical method, called Discrete Element Method (Cundall, 1979), intends to model a granular material this way. However the method is extremely computer expensive and is limited by the number of particles, the size distribution, and their shapes. Great progresses have been made over the last few years (Rougier et al., 2004; Nitka et al., 2011; Scholtès and Donzé, 2013) but its use on large-scale structures is not possible yet.

Continuum mechanics has a different approach and considers any solid as continuous at a macroscopic scale. It ignores the discontinuity of the matter and averages the local behaviour. This approach gives accurate results for length scales much greater than the particles size of the solid, but is obviously not suitable for the modelling of the solid at the particle scale. However, it verifies all the fundamental laws of physics such as the conservation of mass, Cauchy momentum equations and the laws of thermodynamics for instance (Salençon, 2007; Le Tallec, 2011).

A constitutive model gives an explicit relationship between the stresses and strains. These physical properties are represented in solid mechanics by tensors, which are used to describe linear relations between sets of geometrics vectors, and present therefore the advantage to be independent of the coordinate system (Sokolnikoff, 1951). The next section presents the conceptual framework of continuum mechanics and its importance in the development of constitutive law and in the finite element method.

## 2. BACKGROUND OF THE STUDY

### 2.4.2 Mathematical theory of continuum mechanics

Assume a body in its initial state, called reference configuration  $\kappa_0$ , of volume  $\Omega_0$ , and the point  $M_0 \in \Omega_0$  (Figure 2.7). The deformed state of  $\kappa_0$  subjected to the transformation  $\tau$  is called current configuration  $\kappa_t$ , of volume  $\Omega_t$ . We call  $M \in \Omega_t$  the image of  $M_0 \in \Omega_0$  by the linear mapping  $\phi : \Omega_0 \rightarrow \Omega_t$ .

#### Lagrangian description

It describes particles as they move through space and time. The transformation of the initial configuration  $\underline{X} = \underline{OM}_0$  by  $\tau$  called  $\underline{x} = \underline{OM}$  is defined as

$$\forall t, \forall M_0 \in \Omega_0 \quad \underline{x} = \underline{\phi}(\underline{X}, t) \quad (2.3)$$

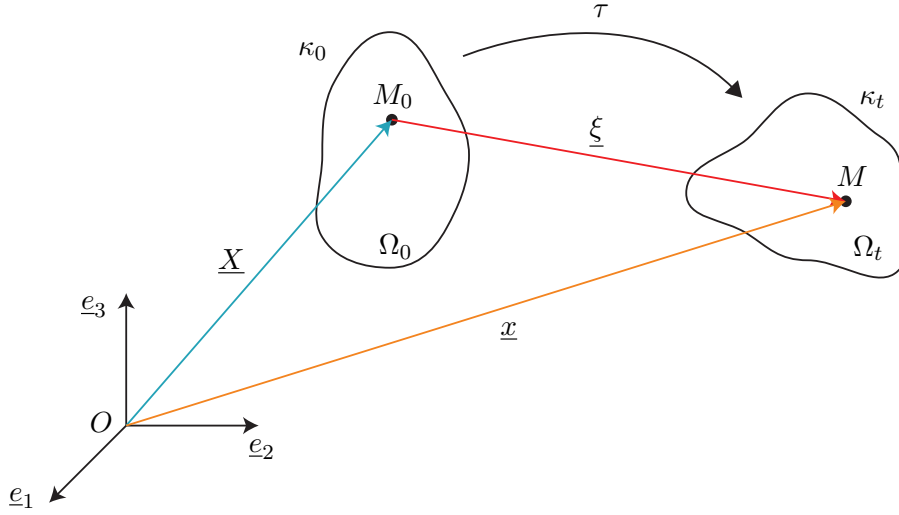


Figure 2.7: Configuration of the system. After Salençon (2007).

Since every particle in  $\Omega_0$  is assumed to be affected by the transformation (onto) and every  $\underline{x}$  is the image of a unique antecedent  $\underline{X}$  (one-to-one), the mapping function  $\phi$  is an automorphism  $\phi: \mathbb{R}^3 \rightarrow \mathbb{R}^3$  and continuous with respect to space and time variables. Consequently, by the implicit function theorem (Lublimer, 2008), its Jacobian determinant, given by

$$\forall (\underline{x}, \underline{X}) \in (\mathbb{R}^3)^2 \quad J(\underline{X}, t) = \begin{vmatrix} \frac{\partial x_1}{\partial X_1} & \frac{\partial x_1}{\partial X_2} & \frac{\partial x_1}{\partial X_3} \\ \frac{\partial x_2}{\partial X_1} & \frac{\partial x_2}{\partial X_2} & \frac{\partial x_2}{\partial X_3} \\ \frac{\partial x_3}{\partial X_1} & \frac{\partial x_3}{\partial X_2} & \frac{\partial x_3}{\partial X_3} \end{vmatrix} \quad (2.4)$$

must be invertible (non-singular) and therefore neither null or infinite

$$0 < J(\underline{X}, t) < \infty \quad (2.5)$$

The dilation (volume change) between  $\kappa_0$  and  $\kappa_t$  following particle  $M_0$  is linked to the

Jacobian determinant  $J(\underline{X}, t)$  by

$$d\Omega_t = J(\underline{X}, t) d\Omega_0 \quad (2.6)$$

which illustrates the conditions on the sign of the  $J(\underline{X}, t)$ ; a sub-element keeps the same sign during the transformation and its volume cannot become infinite or null. This first condition insures that the model follows the laws of thermodynamics, i.e. no creation or disappearance of matter. This condition of the determinant of the Jacobian matrix play a key role in the finite element method that will be developed in Chapter 5.

### Concept of transport

The deformation gradient tensor, noted  $\underline{F}$ , gives the gradient of the mapping function  $\underline{\phi}$  between  $\kappa_0$  and  $\kappa_t$  and links any vector  $\underline{v} \in \Omega_0$  with its transformation  $\underline{V} \in \Omega_t$

$$\forall \underline{v} \in \Omega_t \quad \forall \underline{V} \in \Omega_0 \quad \underline{v} = \underline{F}(t) \cdot \underline{V} \quad (2.7)$$

with  $\underline{F} = \underline{\nabla} \underline{\phi} = \phi_{i,j} \underline{e}_i \otimes \underline{e}_j$ . It can be noted that we have  $J(\underline{X}, t) = \det \underline{F}(t)$  which makes  $\underline{F}$  responsible for the mapping function  $\phi$  being bijective and therefore  $\Omega_t = \Omega_0 \det \underline{F}$ .

### Dilation and deformation

Tensor  $\underline{F}$  only describes the local transformation of a vector by linear mapping. Therefore, it does not contain any information on the variation of the dilation of the solid. To access this information about deformation of the solid between  $\kappa_0$  and  $\kappa_t$  we look at the variation of the dot product of two vectors  $(\underline{V}, \underline{W}) \in \Omega_0^2$ . From Equation (2.7), we have

$$\forall (\underline{V}, \underline{W}) \in \Omega_0^2 \quad (\underline{v}, \underline{w}) \in \Omega_t^2 \quad \underline{v} = \underline{F} \cdot \underline{V} \quad \text{and} \quad \underline{w} = \underline{F} \cdot \underline{W} \quad (2.8)$$

$$\therefore \underline{v} \cdot \underline{w} = (\underline{F} \cdot \underline{V}) \cdot (\underline{F} \cdot \underline{W}) = \underline{V} \cdot (\underline{F}^T \cdot \underline{F}) \cdot \underline{W} = \underline{V} \cdot \underline{C} \cdot \underline{W} \quad (2.9)$$

with  $\underline{C} = \underline{F}^T \cdot \underline{F}$  the right Cauchy-Green deformation tensor whose eigenvalues/eigenvectors give the dilations/principal dilation directions respectively (Salençon, 2007).

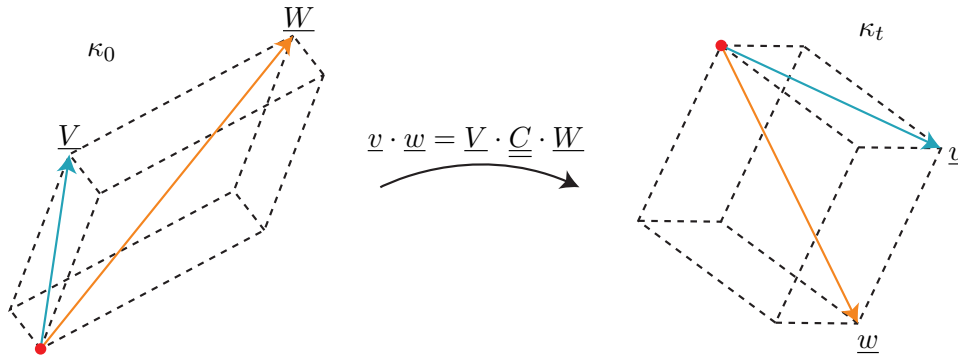


Figure 2.8: Variation of dot product and relation with Cauchy tensor.

## 2. BACKGROUND OF THE STUDY

However, it is not possible to measure experimentally the dot product  $\underline{v} \cdot \underline{w}$  since it is in a static configuration. Nevertheless, what can be measured is the variation of a dot product between  $\kappa_0$  and  $\kappa_t$  during the transformation  $\tau$ :

$$\underline{v} \cdot \underline{w} - \underline{V} \cdot \underline{W} = \underline{V} \cdot \underline{\underline{C}} \cdot \underline{W} - \underline{V} \cdot \underline{\underline{1}} \cdot \underline{W} \quad (2.10)$$

$$\begin{aligned} &= \underline{V} \cdot (\underline{\underline{C}} - \underline{\underline{1}}) \cdot \underline{W} \\ &= 2 \underline{V} \cdot \underline{\underline{e}} \cdot \underline{W} \end{aligned} \quad (2.11)$$

with

$$\underline{\underline{e}} \doteq \frac{1}{2} (\underline{\underline{C}} - \underline{\underline{1}}) = \frac{1}{2} (\underline{\underline{\nabla\xi}} + \underline{\underline{\nabla\xi^T}} + \underline{\underline{\nabla\xi^T}} \cdot \underline{\underline{\nabla\xi}}) \quad (2.12)$$

the Green-Lagrange strain tensor<sup>2</sup>. Since  $\underline{\underline{C}}$  is symmetric, then so is  $\underline{\underline{e}}$ .

### Infinitesimal finite strain

The formulation of  $\underline{\underline{e}}$  is valid for any kind of strain, large (macroscopic) or small (microscopic). However, Equation (2.12) shows the non-linearity between the displacement field and the deformation/strain field of Green-Lagrange due to a quadratic term. In solid mechanics, bodies are frequently subjected to very small displacements. In these conditions, the quadratic term can be neglected compared to the linear terms (Salençon, 2007) which leads to the

**Definition 2.1** *For infinitesimal deformations of a continuum solid, in which the displacements and the displacement gradients are such as  $\|\xi\| \ll 1$  and  $\|\underline{\underline{\nabla\xi}}\| \ll 1$ , the second-order terms of the Green-Lagrangian strain tensor  $\underline{\underline{e}}$  can be neglected which gives the infinitesimal strain tensor  $\underline{\underline{\varepsilon}}$  defined as*

$$\underline{\underline{e}} \approx \underline{\underline{\varepsilon}} = \frac{1}{2} (\underline{\underline{\nabla\xi}} + \underline{\underline{\nabla\xi^T}}) \quad (2.13)$$

and corresponds to the symmetric part of the displacement gradient tensor  $\underline{\underline{F}}$ .  $\underline{\underline{\varepsilon}}$  is called the infinitesimal strain tensor or Cauchy's strain tensor. This assumption on the magnitude of the displacements leads to significant simplification of the calculations for analytical and numerical applications such as finite elements.

### 2.4.3 Linear elasticity

#### Elasticity tensor

The mechanical characteristics of a material are often expressed as a maximum admissible stress [Pa]. The strain tensor  $\underline{\underline{\varepsilon}}$  previously formulated must therefore be related to the stress tensor  $\underline{\underline{\sigma}}$ . Such relationship is called constitutive or stress-strain relationship.

The constitutive law in linear elasticity for an anisotropic homogeneous body, known as the Hooke's law, postulates that the two second-rank tensor fields  $\underline{\underline{\sigma}}$  and  $\underline{\underline{\varepsilon}}$  can be linearly mapped using a fourth-order tensor

$$\underline{\underline{\sigma}} = \mathbb{C} : \underline{\underline{\varepsilon}} \quad \Leftrightarrow \quad \sigma_{ij} = C_{ijkl} \varepsilon_{lk} \quad (2.14)$$

---

<sup>2</sup> $\underline{\underline{x}} = \underline{\underline{X}} + \underline{\underline{\xi}} \Rightarrow \underline{\underline{\nabla\xi}} = \underline{\underline{\nabla\phi}} - \underline{\underline{1}}$

with  $\mathbb{C}$  the tensor of elasticity which has the physical dimension of a stress and is symmetric. It can be shown (Salençon, 2002) that the energy density of a deformed material is given by

$$W = \frac{1}{2} \underline{\underline{\varepsilon}} : \mathbb{C} : \underline{\underline{\varepsilon}} = \frac{1}{2} e_{ij} C_{ijkl} e_{kl} \quad (2.15)$$

The double inner product in this quadratic term introduces 81 components and in this form  $\mathbb{C}$  can be represented by  $9 \times 9$  matrix. However, to protect the symmetry of  $\underline{\underline{\varepsilon}}$  and  $\underline{\underline{\sigma}}$  certain symmetry relations can be applied on the elasticity tensor, called *minor symmetry*:

$$C_{ijkl} = C_{jikl} = C_{ijlk} = C_{jilk} \quad (2.16)$$

which corresponds to 45 independent symmetric classes. Accordingly, the tensor  $\mathbb{C}$  can be represented by a  $6 \times 6$  matrix with 36 components.

Another class of symmetry between the groups of indices  $(i, j)$  and  $(k, l)$  can be noticed, called *major symmetry*. For  $(i, j) \neq (k, l)$  we distinguish the terms  $e_{ji} C_{ijkl} e_{lk}$  and  $e_{lk} C_{klij} e_{ji}$  and therefore

$$\forall (i, j) \neq (k, l) \quad C_{ijkl} = C_{klij} \quad (2.17)$$

which gives 15 additional independent symmetric classes. In total, the minor and major symmetries imply 60 independent relations of symmetry on  $\mathbb{C}$  and therefore 21 independent parameters are necessary to describe an anisotropic material with no particular symmetry in a general stress space (Itin and Hehl, 2013).

Using Voigt notation, a second-order symmetric tensor can be written as vectors of 6 components. Therefore, Hooke's law for a linear elastic material can be represented in matrix form by

$$\begin{pmatrix} \sigma_{11} \\ \sigma_{22} \\ \sigma_{33} \\ \sqrt{2}\sigma_{23} \\ \sqrt{2}\sigma_{13} \\ \sqrt{2}\sigma_{12} \end{pmatrix} = \begin{pmatrix} C_{1111} & C_{1122} & C_{1133} & \sqrt{2}C_{1123} & \sqrt{2}C_{1131} & \sqrt{2}C_{1112} \\ * & C_{2222} & C_{2233} & \sqrt{2}C_{2223} & \sqrt{2}C_{2231} & \sqrt{2}C_{2212} \\ * & * & C_{3333} & \sqrt{2}C_{3323} & \sqrt{2}C_{3331} & \sqrt{2}C_{3312} \\ * & * & * & 2C_{2323} & 2C_{2331} & 2C_{2312} \\ * & * & * & * & 2C_{3131} & 2C_{3112} \\ * & * & * & * & * & 2C_{1212} \end{pmatrix} \cdot \begin{pmatrix} \varepsilon_{11} \\ \varepsilon_{22} \\ \varepsilon_{33} \\ \sqrt{2}\varepsilon_{23} \\ \sqrt{2}\varepsilon_{13} \\ \sqrt{2}\varepsilon_{12} \end{pmatrix} \quad (2.18)$$

### Constitutive law for an isotropic linear elastic material

Assume the one-dimensional case of a material subjected to  $\sigma_{11}$  only:  $\underline{\underline{\sigma}} = \sigma_{11} \underline{\underline{e}}_1 \otimes \underline{\underline{e}}_1$ . From Hooke's law we have

$$\varepsilon_{11} = \frac{1}{E} \sigma_{11} \quad \text{and} \quad \varepsilon_{22} = \varepsilon_{33} = -\nu \varepsilon_{11} \quad (2.19)$$

## 2. BACKGROUND OF THE STUDY

with  $E$  the Young's modulus and  $\nu$  the Poisson's ratio. Proceeding this way for the other directions (Sokolnikoff, 1956):

$$\varepsilon_{11} = \frac{1}{E} [(1 + \nu) \sigma_{11} - \nu \text{tr}(\underline{\underline{\varepsilon}})] \quad (2.20)$$

$$\varepsilon_{22} = \frac{1}{E} [(1 + \nu) \sigma_{22} - \nu \text{tr}(\underline{\underline{\varepsilon}})] \quad (2.21)$$

$$\varepsilon_{33} = \frac{1}{E} [(1 + \nu) \sigma_{33} - \nu \text{tr}(\underline{\underline{\varepsilon}})] \quad (2.22)$$

$$\varepsilon_{12} = \frac{1 + \nu}{E} \sigma_{12} \quad (2.23)$$

$$\varepsilon_{23} = \frac{1 + \nu}{E} \sigma_{23} \quad (2.24)$$

$$\varepsilon_{13} = \frac{1 + \nu}{E} \sigma_{13} \quad (2.25)$$

and applying the superposition principle to Equation (2.20) to (2.25) gives the stress-strain relationship

$$\underline{\underline{\varepsilon}} = \frac{1 + \nu}{E} \underline{\underline{\sigma}} - \frac{\nu}{E} \text{tr}(\underline{\underline{\sigma}}) \underline{\underline{1}} \quad (2.26)$$

or its equivalent form

$$\underline{\underline{\sigma}} = 2\mu \underline{\underline{\varepsilon}} + \lambda \text{tr}(\underline{\underline{\varepsilon}}) \underline{\underline{1}} \quad (2.27)$$

with  $\lambda$  and  $\mu$  the Lamé parameters given by

$$\lambda = \frac{\nu E}{(1 - 2\nu)(1 + \nu)} \quad \mu = \frac{E}{2(1 + \nu)} \quad (2.28)$$

Therefore, only two parameters are sufficient to describe the behaviour of an isotropic elastic material, which gives the following formulation for the elastic tensor

$$\begin{pmatrix} \sigma_{11} \\ \sigma_{22} \\ \sigma_{33} \\ \sigma_{23} \\ \sigma_{13} \\ \sigma_{12} \end{pmatrix} = \begin{pmatrix} \lambda + 2\mu & \lambda & \lambda & 0 & 0 & 0 \\ * & \lambda + 2\mu & \lambda & 0 & 0 & 0 \\ * & * & \lambda + 2\mu & 0 & 0 & 0 \\ * & * & * & \mu & 0 & 0 \\ * & * & * & * & \mu & 0 \\ * & * & * & * & * & \mu \end{pmatrix} \cdot \begin{pmatrix} \varepsilon_{11} \\ \varepsilon_{22} \\ \varepsilon_{33} \\ 2\varepsilon_{23} \\ 2\varepsilon_{13} \\ 2\varepsilon_{12} \end{pmatrix} \quad (2.29)$$

Assuming the material isotropic and elastic leads to significant simplifications of the problem since knowing one of the set of parameters  $(E, \nu)$  or  $(\lambda, \mu)$  is enough to completely describe the material and the stress-strain relationship. Most of the methods used by industry and presented in Section 1.2 are based on the assumption of an isotropic elastic material, especially because only two parameters, easy to determine, are required.

Unfortunately, geomaterials rarely behave only elastically when subjected to increasing mechanical loading, and especially lime treated soils whose mechanical behaviour relies on processes absent from classic elastic materials. There exists a level of stress at which irrecoverable deformation, called *plastic deformation*, occurs and lead to a nonlinear behaviour of the material that can be radically different from the elastic

solution. For a more accurate modelling of a soil, an elasto-plastic model describing the material in the elastic domain and when plasticity occurs is preferred.

## 2.5 Theory of elasto-plasticity and application to soils

### 2.5.1 Concept of plasticity

The object of a plasticity model is to provide an explicit relationship between  $\underline{\sigma}$  and  $\underline{\varepsilon}$  for a material experiencing elasto-plastic deformations. A solid behaves elastically until a certain stress state, called yield stress  $\sigma_y$ , is reached (Figure 2.9). As long as the stress state remains lower than the yield stress, the deformations are reversible. If the mechanical loading bring the stress state beyond  $\sigma_y$ , plastic deformations appear within the solid. Plasticity is characterised by irreversible deformations that are not time dependent, which means that, if unloaded, the material does not go back to its original state (Hill, 1950). From a thermodynamic point of view, it can be seen as a fraction of the energy given to the system during the loading that is dissipated and won't be returned in the event of an unloading. However, if unloaded, solid behaves elastically again.

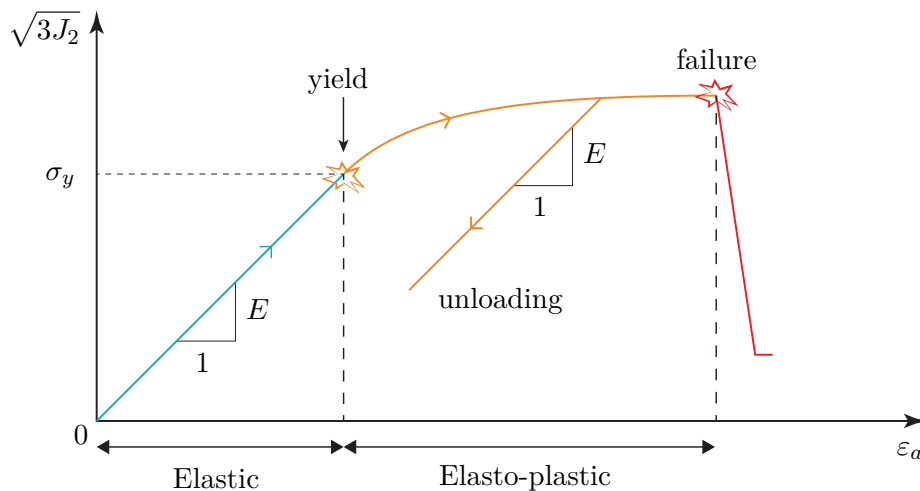


Figure 2.9: General elasto-plastic behaviour

This introduces the concept of yield function describing all the stress states for which plasticity occurs. In the general stress space, the yield function can be represented by a surface inside which the behaviour is assumed elastic. Once the stress state reaches the yield surface, the behaviour becomes elasto-plastic. One should note that stress state lying outside the yield surface are not permitted. If the material is perfectly plastic, the yield function is independent of the degree of plasticity and remains fixed, which implies that the stress state remains on the yield surface and is therefore constant (Figure 2.10a). However for most materials the yield surface will evolve with the degree of plastic straining, and in this case the yield stress does not remain constant. Such phenomenon is called *hardening* if the yield surface expands (Figure 2.10b) or *softening* if the yield surface shrinks (Figure 2.10c).

## 2. BACKGROUND OF THE STUDY

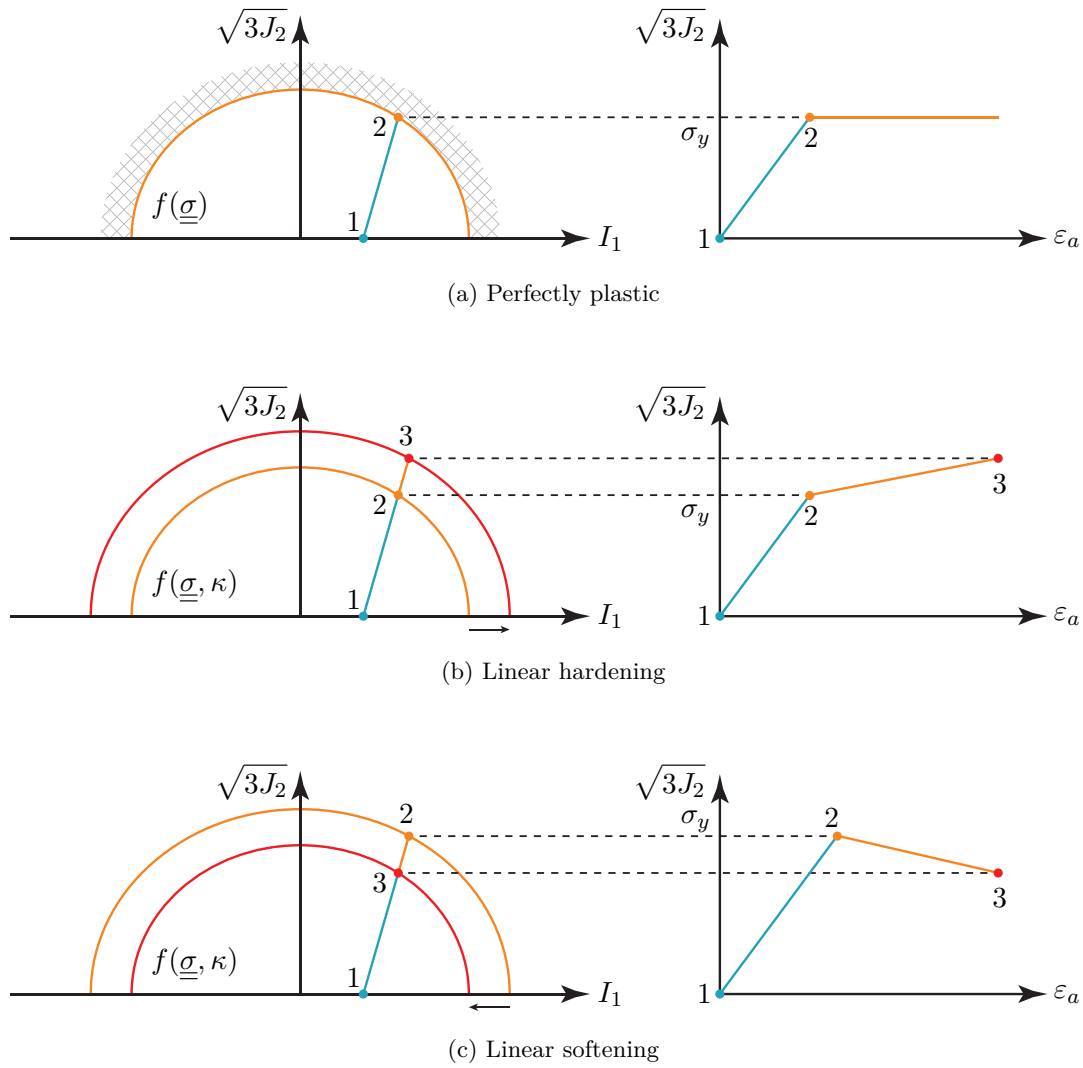


Figure 2.10: Theoretical representation of strain hardening and softening at yield

In order to model the elasto-plastic behaviour of a solid, the following elements are required (Hinton and Owen, 1980; Muir Wood, 1990):

1. **Elastic properties** A relationship between stresses and strains for which the material has an elastic behaviour,
2. **Yield criterion** A yield criterion, noted  $f(\underline{\sigma})$ , that describes the elastic/plastic limit in the general stress space,
3. **Plastic potential** A function, noted  $g(\underline{\sigma})$ , that links the stress increment with the magnitude of plastic strains,
4. **Hardening rule** A relationship between the magnitude of plastic strains and the size of the elastic domain,
5. **Elasto-plastic relationship** A relationship between the stress and strains at yield when strain is made of an elastic and plastic component.

Elastic properties have been introduced in Section 2.4.3. We now present some yield criteria that are commonly used in the industry and discuss about their suitability for soils.



### 2.5.2 Yield criteria

The yield criterion, noted  $f$ , describes the stress level at which plastic deformations begin, and is expressed as a function of  $\underline{\underline{\sigma}}$  defined in the general stress space

$$f(\underline{\underline{\sigma}}) = k(\kappa) \quad (2.30)$$

with  $k$  a material parameter, such as the yield stress, to be determined experimentally, and  $\kappa$  the hardening parameter describing the variation of the yield stress with the degree of plastic straining (Hinton and Owen, 1980).

A convenient way is to write the yield criterion as a function of the three invariants of the stress tensor  $\underline{\underline{\sigma}}$

$$I_1 \doteq \text{tr} \underline{\underline{\sigma}} \quad I_2 \doteq \frac{1}{2} \text{tr} (\underline{\underline{\sigma}} \cdot \underline{\underline{\sigma}}) \quad I_3 \doteq \frac{1}{2} \text{tr} (\underline{\underline{\sigma}} \cdot \underline{\underline{\sigma}} \cdot \underline{\underline{\sigma}}) \quad (2.31)$$

and of the two invariants<sup>3</sup> of the stress deviator tensor  $\underline{\underline{s}} \doteq \underline{\underline{\sigma}} - \frac{I_1}{3} \underline{\underline{I}}$

$$J_2 \doteq \frac{1}{2} \text{tr} (\underline{\underline{s}} \cdot \underline{\underline{s}}) \quad J_3 \doteq \frac{1}{2} \text{tr} (\underline{\underline{s}} \cdot \underline{\underline{s}} \cdot \underline{\underline{s}}) \quad (2.32)$$

Because the invariants are independent of the coordinate system, this gives a general formulation of the yield criterion expressed in the principal stress space  $(\sigma_1, \sigma_2, \sigma_3)$  (Neto et al., 2009). The formulation of classic yield criteria is presented to illustrate their relationship with the invariants.

#### The Von Mises yield criterion (1913)

This criterion was originally developed for ductile materials based on experimental observations. For metals yield does not appear to depend on the hydrostatic pressure, but mostly on shear. The yield criterion was therefore written as a function of the second invariant of the deviatoric stress tensor  $J_2$  and independent of the spherical part of  $\underline{\underline{\sigma}}$ :

$$f(\underline{\underline{\sigma}}) = \sqrt{J_2} - k' \quad (2.33)$$

where  $k'$  is the yield stress of the material in pure shear. It is frequently written as a function of the yield stress  $\sigma_y$  in tension which is proportional to  $k$ :

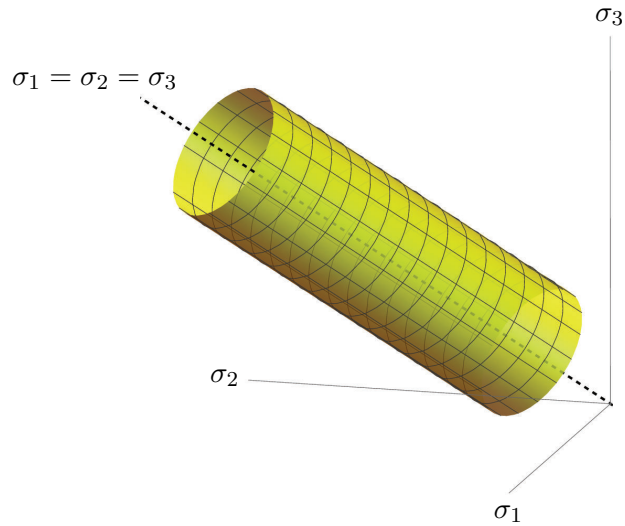
$$f(\underline{\underline{\sigma}}) = \sqrt{3J_2} - \sigma_y \quad (2.34)$$

The Von Mises criterion can be represented in the principal stress space as an infinite cylinder centred around the hydrostatic axis  $\sigma_1 = \sigma_2 = \sigma_3$  (Figure 2.11a). The stress state of an isotropic compression lies on the hydrostatic axis, and since  $f$  is independent of  $I_1$ , plasticity is only reached in shear when the second invariant  $J_2$  reaches a critical value equal to the radius of the cylinder ( $\sqrt{3J_2}$ ) in the deviatoric plane  $\pi : \sigma_1 + \sigma_2 + \sigma_3 = 0$  (Figure 2.11b).

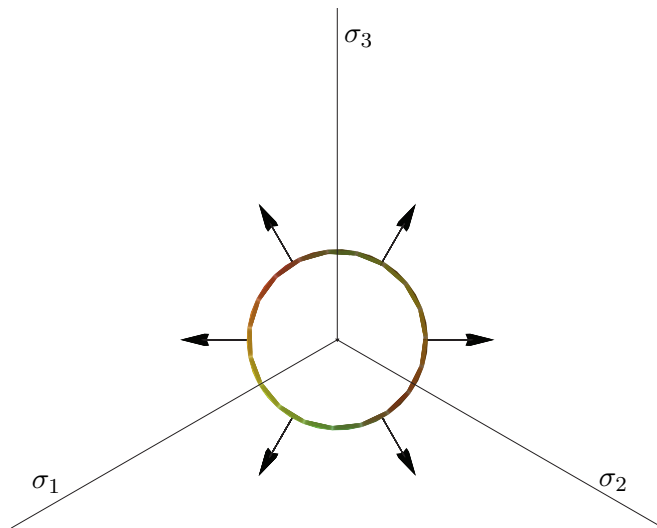
---

<sup>3</sup>By definition,  $J_1 = \text{tr} \underline{\underline{s}} = 0$ .

## 2. BACKGROUND OF THE STUDY



(a) Von-Mises yield criterion in the general stress space



(b) Von-Mises yield criterion in the deviatoric  $\pi$  plane

Figure 2.11: General representation of the Von Mises yield criterion in the principal stress space and the deviatoric plane  $\pi$ .

This criterion gives good agreement with experimental results for most metals and has a simple formulation. However soils can experience plastic straining under isotropic compression. Also, it often overestimates the yield loci in shear for granular materials, and the determination of the yield stress in tension for rocks and soils is not straightforward. This criterion is therefore not the most suitable choice for soils.

### The Mohr-Coulomb and Drucker-Prager yield criteria

The Mohr-Coulomb criterion in the general stress space is obtained by generalisation of Coulomb friction failure law developed in 1773 and is defined by

$$\tau = c - \sigma_n \tan \phi \quad (2.35)$$

with  $\tau$  the magnitude of the shear stress and  $\sigma_n$  the normal stress. It depends on two parameters, the cohesion  $c$  and the friction angle  $\phi$  of the material, which

are meaningful for granular material and easily determined experimentally. It gives relatively good results on concrete, rock, and soils. For this reason, the Mohr-Coulomb criterion is frequently used by industry.

The generalisation in the principal stress space was presented in 1882 by Mohr and is given, for  $\sigma_1 \geq \sigma_2 \geq \sigma_3$ , by

$$\underbrace{-\frac{1}{2}(\sigma_1 - \sigma_3) \cos \phi}_{\tau} = c - \underbrace{\left( \frac{\sigma_1 + \sigma_3}{2} - \frac{\sigma_1 - \sigma_3}{2} \sin \phi \right)}_{\sigma_n} \tan \phi \quad (2.36)$$

The Mohr-Coulomb criterion can be presented in the principal stress space by a conical prism (Figure 2.12a), and in the  $\pi$  plane by an irregular hexagon (Figure 2.12b). The conical shape is due to the fact that the hydrostatic stress included in the last term in Equation (2.36) can lead to yielding. As the hydrostatic stress gets closer to the apex (A in Figure 2.12b) of coordinates  $\sigma_1 = \sigma_2 = \sigma_3 = -c \cot \phi$ , the section of the hexagon in the  $\pi$  plane progressively decreases. However this criterion presents 6 singularities, which can be problematic for a numerical implementation.

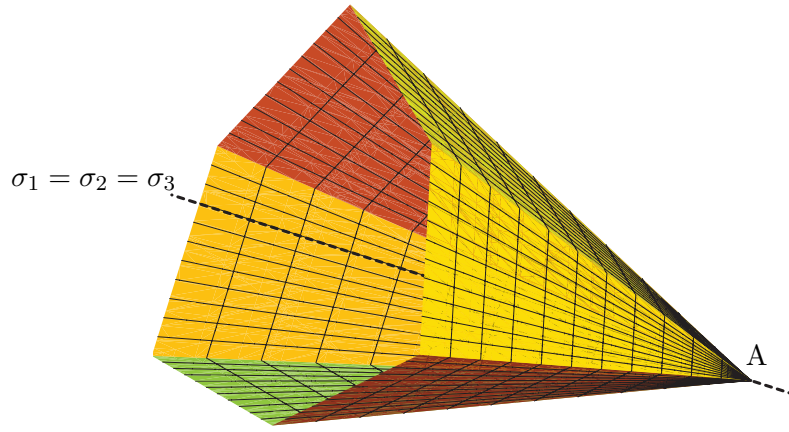
An approximate solution of the Mohr-Coulomb criterion was proposed in 1952 by Drucker and Prager, based on the Von Mises criterion. The goal was, similarly to Mohr-Coulomb, to account for the influence of the first invariant  $I_1$  on the yielding. This was done by adding a term to Equation (2.33) to give

$$\alpha I_1 + \sqrt{J_2} = \beta \quad (2.37)$$

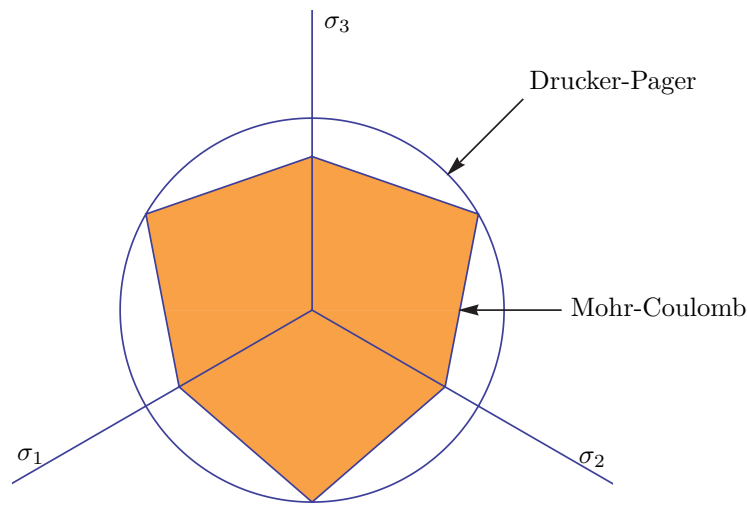
with  $\alpha$  and  $\beta$  two constants functions of  $c$  and  $\phi$  (Hinton and Owen, 1980). The Drucker-Prager criterion, although based on Von Mises formulation, is therefore closely related to Mohr-Coulomb and can be represented in the principal stress space by a circular cone whose apex coincides with Mohr-Coulomb's (Figure 2.12a), and by a circle in the  $\pi$  plane which coincides with some of Mohr-Coulomb's apices.  $\alpha$  and  $\beta$  can be determined in order to make Drucker-Prager criterion passing through either the inner or outer apices.

The formulation of this criterion leads to a continuous yield surface that makes it convenient for a numerical use, and accounts for the mean stress  $I_1$  on the yielding. It is frequently used for  $I_1$ -dependent materials such as concrete, rocks and soils, but also polymers and foams. However, the cylindric shape due to the square root of the second invariant of the deviatoric stress tensor increases the section of the elastic domain compared to Mohr-Coulomb and, like Von Mises, overestimates the yield loci for soils.

## 2. BACKGROUND OF THE STUDY



(a) Mohr-Coulomb yield criterion in the principal stress space



(b) Mohr-Coulomb and Drucker-Prager yield criteria in the  $\pi$  plane.

Figure 2.12: General representation of the Mohr-Coulomb yield criterion in the principal stress space and the deviatoric plane  $\pi$ .

These last two criteria are frequently used by industry to model concrete, rocks, and soils mostly for their simplicity and the limited number of parameters. However, they both present a major drawback: despite accounting for the mean stress  $I_1$ ) yielding under isotropic compression can only be reached in tension. In the compression domain both criteria remains opened, which means even an infinite isotropic compression ( $\sigma_1 = \sigma_2 = \sigma_3 = \sigma_m \rightarrow +\infty$ , will never lead to the failure of the material and, in other words, will only have an elastic behaviour. This assumption might be valid for some concretes and rocks whose elastic limit is very large compared to the mechanical loading. In this case only a semi-infinite surface is acceptable. However, this assumption is known to be wrong for weaker materials like soils. To model correctly the elastic limit of such materials, a closed yield surface in the principal stress space is required to account for yielding under isotropic compression.

### 2.5.3 The Modified Cam Clay model

To account for the influence of the yield stress on yielding in soils subjected to isotropic compression, several closed yield surfaces have been proposed (e.g. Matsuoka and Nakai, 1982; Lubliner et al., 1989; Bigoni and Piccolroaz, 2004). The Modified Cam Clay model (MCC) was developed in 1968 by Roscoe and Burland (1968) based on the original Cam Clay proposed in 1963 by Roscoe et al. (1963). The simplicity of the model and its suitability for numerical computation has made it very popular for the constitutive modelling of soils. The model was developed in the framework of the critical state theory (Schofield and Wroth, 1968; Muir Wood, 1990) to describe the elasto-plastic behaviour of clays in conventional triaxial tests. However it can be easily generalised for any stress path in the principal stress space. We describe in this section the 5 elements required for an elasto-plastic model.

#### Elastic behaviour

The behaviour of the soil is assumed isotropic and can therefore be defined by two elastic parameters (Equation (2.27)). The formulation for the elastic behaviour is based on the results of isotropic compression tests plotted in the  $(\ln p', v)$  plane. The framework chosen in the MCC model for a typical isotropic compression is given in Figure 2.13. One can note that this representation leads to a linear behaviour between the natural log of the effective mean stress and the specific volume for both the elastic domain ( $p' \in ]0, p'_y]$ ) and plastic domain ( $p' > p'_y$ ) and justifies the choice of this representation as framework of reference for the model. The specific volume is therefore given by

$$v(p') \doteq \begin{cases} N_\kappa - \kappa \ln p' & \text{if } p' \leq p'_y \\ N_\lambda - \lambda \ln p' & \text{if } p' > p'_y \end{cases} \quad (2.38a)$$

$$(2.38b)$$

with  $\kappa$  and  $\lambda$  (to be distinguished from the Lamé coefficient), two soil constants describing the slope of the url/ncl<sup>4</sup> respectively, and  $N_\kappa/N_\lambda$  the specific volume at  $p' = 1$  kPa of the url/ncl respectively.

---

<sup>4</sup>url: unloading-reloading line, ncl: normal compression line.

## 2. BACKGROUND OF THE STUDY

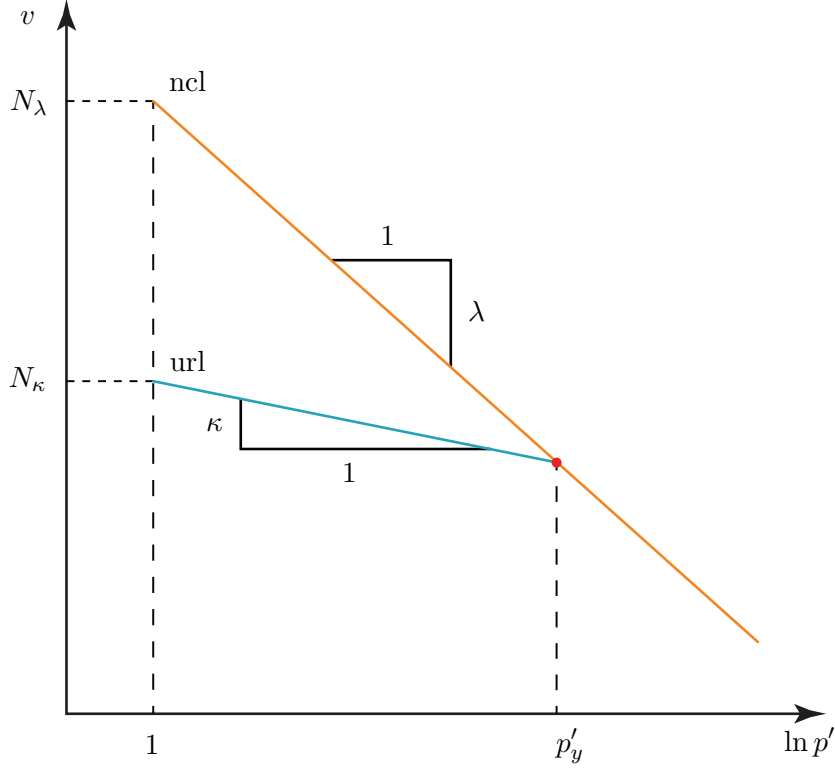


Figure 2.13: General elasto-plastic behaviour

From Equation (2.38a) the elastic volumetric strain increment<sup>5</sup>  $\delta\varepsilon_p^e = -\frac{\delta v}{v}$  can be written

$$\forall p' \leq p'_y \quad \delta\varepsilon_p^e = -\frac{\delta v}{v} = \frac{\kappa}{v} \frac{\delta p'}{p'} \quad (2.39)$$

By definition, the elastic parameter bulk modulus  $K$  is defined as

$$K \doteq -v \frac{\delta p'}{\delta v} \quad (2.40)$$

which, combined with Equation (2.39) links the stress state to one of the elastic parameters:

$$K = \frac{\delta p'}{\delta\varepsilon_p^e} = \frac{vp'}{\kappa} \quad (2.41)$$

By analogy,  $K$  replaces the first Lamé parameter ( $\lambda$ ) in Equation (2.27) and accounts for the volumetric (or spherical) part of the strain tensor  $\underline{\underline{\varepsilon}}$  ( $\varepsilon_p^e = \text{tr} \underline{\underline{\varepsilon}}^e$ ). One can note that this framework leads to a formulation of stress-dependent bulk modulus, which leads to a nonlinear elastic law. Alternatively, this is equivalent to a non-constant Young's modulus.

The second elastic Lamé parameter is used for the deviatoric strains. In soil mechanics,  $\mu$  is replaced by  $G$  and called *shear modulus*. By definition

$$G \doteq \frac{\delta q}{3\delta\varepsilon_q^e} \quad (2.42)$$

In the framework of the MCC, the two most suitable elastic constants for the

<sup>5</sup>By convention, symbol ' $\delta$ ' will refer to an increment, and ' $\partial$ ' to the derivative.

modelling of soils appear to be  $K$  and  $G$ . The first arises from the linear behaviour of the specific volume  $v$  with  $\ln p'$ , and the second is directly related to  $\delta\varepsilon_q^e$  (Muir Wood, 2004). However, it is frequent to have  $E$  and  $\nu$  as input of a model because they are easy to determine experimentally. The value for the bulk modulus is immediately given for any stress state by Equation (2.40), and  $G$  can be written as a function of  $(K, E)$  or  $(K, \nu)$ :

$$G = K \frac{3(1 - 2\nu)}{2(1 + \nu)} = K \frac{3KE}{9K - E} \quad (2.43)$$

which introduce some contradictions due to the stress-dependency of  $K$ . If  $G$  is assumed constant, which is a relevant assumption for soils, then from Equation (2.43) either  $E$  or  $\nu$  cannot be constant, and a choice has to be made to decide which one to be considered constant (Muir Wood, 2004). The Young's modulus has units of pressure and can be easily deduced from the  $\varepsilon_a : q$  curve. Poisson's ratio  $\nu$  is dimensionless and, appart from being not as straightforward as  $E$  to determine, arises from energetic considerations and is bound by the first law of thermodynamic to take its values in  $[-1, \frac{1}{2}]$  in order to ensure the reversibility of the deformation (Le Tallec, 2011). At Poisson's ratio greater than  $\frac{1}{2}$  the solid dissipates more energy than what it actually receives from the source of the deformation.

To set  $\nu$  as a constant appears a safer choice since  $E$  has fewer restrictions on its value, but then implies that  $K$  and  $G$  have to change together which is known to lead to thermodynamic inconsistencies, the system generating or dissipating energy on elastic cycles of stress change (Zytynski et al., 1978). However, since this kind of cyclic loading is not considered in this study, one can assume that  $\nu$  being constant does not lead in this context to significant violation of any thermodynamic laws.

### Yield criterion

The yield function  $f$  for the Modified Cam Clay model (Roscoe and Burland, 1968) is expressed as the function of  $p'$  ( $I_1$ ) and  $q$  ( $J_2$ ) (Potts and Zdravkovic, 2000):

$$f(\underline{\sigma}, p_0, \kappa') = q^2 - M^2 p' (p'_0 - p') = 0 \quad (2.44)$$

with  $M$  the slope of the critical state line and  $p'_0$  the initial isotropic yield stress. This yield function can be represented in the  $(p'q)$  plane by an ellipse (Figure 2.14) and in the general stress space by an ellipsoid (Figure 2.15–2.16).

## 2. BACKGROUND OF THE STUDY

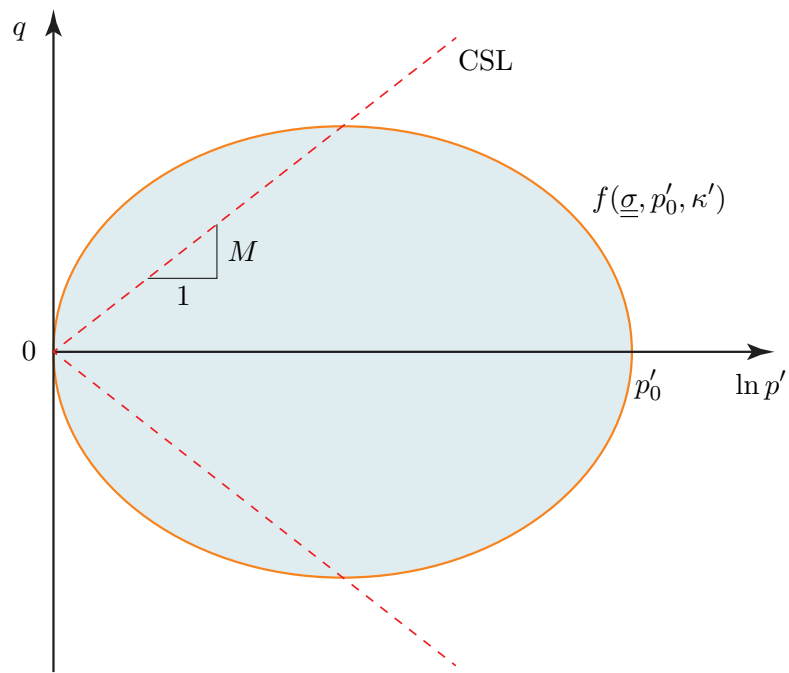


Figure 2.14: Cam Clay model yield function in the  $(p', q)$  plane –  $p'_0$ : initial yield stress, CSL: Critical State Line,  $M$ : Slope of the CSL.

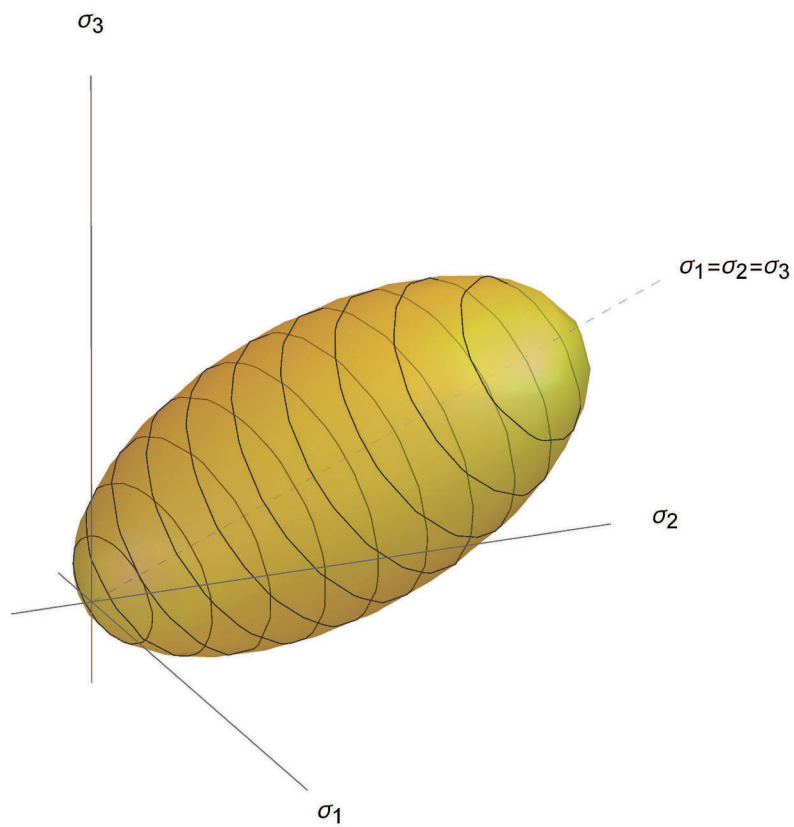
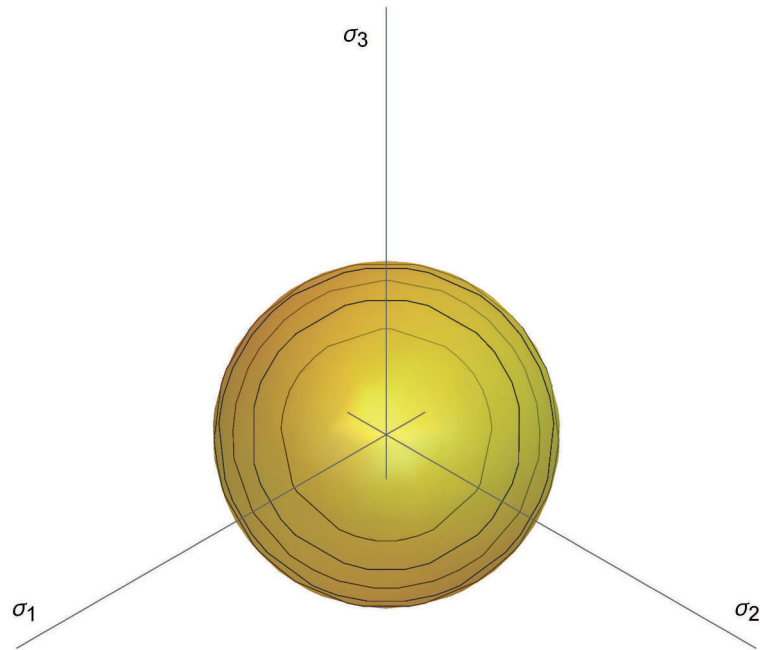


Figure 2.15: Cam Clay model yield function in the principal stress space




 Figure 2.16: Cam Clay model yield function in the  $\pi$  plane

### Plastic potential

It is assumed that yield function  $f$  and plastic potential  $g$  are associated. Therefore,

$$g(\underline{\sigma}) \equiv f(\underline{\sigma}, p_0, \kappa') = q^2 - M^2 p' (p'_0 - p') = 0 \quad (2.45)$$

which means the plastic strain increments are normal to the yield surface, and is known as the *normality rule* (Figure 2.17).

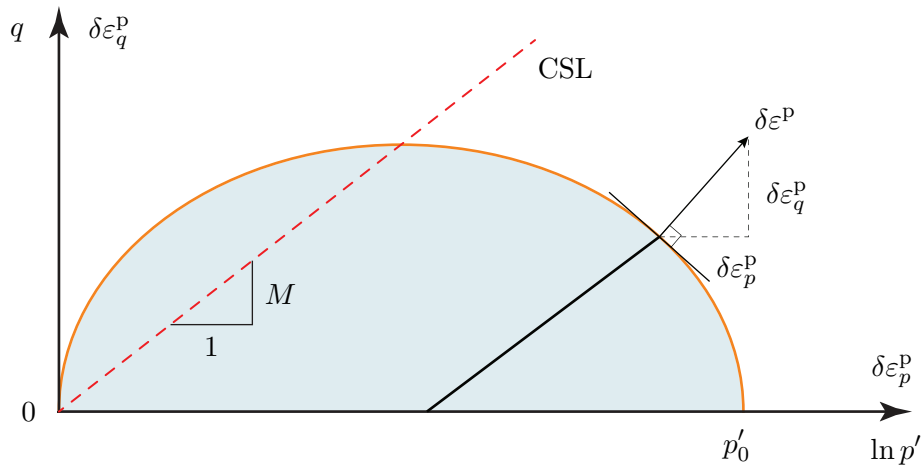


Figure 2.17: Normality rule

The flow rule of the material is therefore given by

$$\frac{\delta \varepsilon_p^P}{\delta \varepsilon_q^P} = \frac{\partial g / \partial p'}{\partial g / \partial q} = \frac{M^2 - \eta^2}{2\eta} \quad (2.46)$$

with  $\eta = q/p'$ .

## 2. BACKGROUND OF THE STUDY

### Hardening rule

The hardening rule links the change in size of the yield surface with the magnitude of plastic strain

$$\delta p'_0 \approx dp'_0 = \frac{\partial p'_0}{\partial \varepsilon_p^P} \delta \varepsilon_p^P + \frac{\partial p'_0}{\partial \varepsilon_q^P} \delta \varepsilon_q^P \quad (2.47)$$

In the MCC model hardening is assumed to be controlled by the plastic volumetric deformation  $\varepsilon_p^P$  only. From Equation (2.38a) we can link  $\delta \varepsilon_p^P$  with  $\delta p'_0$

$$\delta \varepsilon_p^P = \left( \frac{\lambda - \kappa}{v} \right) \frac{\delta p'_0}{p'_0} \quad (2.48)$$

and assuming infinitesimal increments the elements for the hardening relationship (Equation (2.47)) are given by

$$\frac{\partial p_0}{\partial \varepsilon_p^P} = \frac{vp'_0}{\lambda - \kappa} \quad (2.49)$$

$$\frac{\partial p_0}{\partial \varepsilon_q^P} = 0 \quad (2.50)$$

One can note that a yield loci situated in the left part of the ellipse ( $p' < \frac{p'_0}{2}$ ) leads to the dilation of the specimen ( $\delta \varepsilon_p^P < 0$ ) and the shrinkage of the yield surface ( $\delta p'_0 < 0$ ). This case is called *softening* and describes materials that are highly overconsolidated.

### Elasto-plastic relationship

Combining the four previous sections gives all the elements to write the stress-strain relationship. The total strain increment ( $\delta \varepsilon$ ) can be divided into an elastic and a plastic components:

$$\delta \varepsilon = \delta \varepsilon^e + \delta \varepsilon^P \quad (2.51)$$

$$= \delta \varepsilon_p + \delta \varepsilon_q \quad (2.52)$$

From Equation (2.41) and (2.42) the elastic stress:strain response can be written in matrix form as

$$\begin{bmatrix} \delta \varepsilon_p^e \\ \delta \varepsilon_q^e \end{bmatrix} = \begin{bmatrix} \kappa/vp' & 0 \\ 0 & 1/3G \end{bmatrix} \cdot \begin{bmatrix} \delta p' \\ \delta q \end{bmatrix} \quad (2.53)$$

The general plastic stress:strain relationship accounting for the hardening rule is given by (Muir Wood, 1990)

$$\begin{bmatrix} \delta \varepsilon_p^P \\ \delta \varepsilon_q^P \end{bmatrix} = \frac{-1}{\left[ \frac{\partial f}{\partial p'_0} \left[ \frac{\partial p'_0}{\partial \varepsilon_p^P} \frac{\partial g}{\partial p'} + \frac{\partial p'_0}{\partial \varepsilon_q^P} \frac{\partial g}{\partial q} \right] \right]} \begin{bmatrix} \frac{\partial f}{\partial p'} \frac{\partial g}{\partial p'} & \frac{\partial f}{\partial q} \frac{\partial g}{\partial p'} \\ \frac{\partial f}{\partial p'} \frac{\partial g}{\partial q} & \frac{\partial f}{\partial q} \frac{\partial g}{\partial q} \end{bmatrix} \cdot \begin{bmatrix} \delta p' \\ \delta q \end{bmatrix} \quad (2.54)$$

which, by combining Equation (2.44) to (2.49), is equivalent for the MCC model to

$$\begin{bmatrix} \delta \varepsilon_p^P \\ \delta \varepsilon_q^P \end{bmatrix} = \frac{\lambda - \kappa}{vp'(M^2 + \eta^2)} \begin{bmatrix} M^2 - \eta^2 & 2\eta \\ 2\eta & 4\eta^2/(M^2 - \eta^2) \end{bmatrix} \cdot \begin{bmatrix} \delta p' \\ \delta q \end{bmatrix} \quad (2.55)$$

## 2.6 Conclusion

This chapter has presented a review of the main chemical reactions and mechanical processes involved in lime treatment. The study of the chemical reactions between the soil and the lime has revealed the production of several compounds: the hydrated lime (portlandite) and the cementitious compounds (CSH, CAH, CASH). A chemo-mechanical coupling cannot therefore rely on the lime content alone and requires these compounds to be quantified. Regarding the mechanical behaviour it has been proven that the development of structure introduces new mechanisms that classic yield criteria and constitutive models do not account for.

In order to answer the three main issues identified to take into account lime treatment in the design of the geotechnical structure, the following three criteria must be met:

1. A protocol to quantify the concentrations in the different products of the short and long term reactions. A chemo-mechanical coupling will be developed by finding a correlation between one of these compounds and a pertinent mechanical parameter for lime treated soils.
2. An elasto-plastic model for the modelling the structure, especially the softening behaviour and the influence of the structure and its degradation of the volumetric strains.
3. A numerical model, including the two previous items, in order to consider the influence of the treatment on the global behaviour of geotechnical structures.

The next three chapters intend to answer each one of these three items, which will lead to a complete modelling of lime treated soils and the possibility of exploiting the full potential of lime treatment for an industrial use.

## 2. BACKGROUND OF THE STUDY

## Chapter 3

# Chemo-mechanical modelling of lime treated soils

### 3.1 Introduction

The background of the study (Chapter 2) has broached the chemical and mechanical aspects of lime treatment separately in order to describe the key features, and three issues have been identified to account for lime treatment in the design. The objective of this chapter is to address the first issue and to establish a coupling between the chemical modifications of the soils and the mechanical improvements arising from the treatment. This requires an advanced understanding of the mechanical behaviour of lime treated soils. To this end, this chapter will develop the two following aspects:

- a) How can the effects of a lime treatment on a material and its effects on the mechanical properties be described?
- b) How can a chemo-mechanical coupling be established between the mechanical improvements and the chemical modifications?

First we give a review of the methods proposed for the determination of the chemical composition of a lime treated soil in the scope of chemo-mechanical modelling. Then, an extensive experimental program is carried out to study the effects of lime treatment. The mechanical behaviour is assessed using drained triaxial experiments and the chemical composition with thermogravimetric analysis (TGA) and differential thermal analysis (DTA). Finally, a non-linear chemo-mechanical coupling between the yield stress and the concentration in cementitious compounds is proposed.

### 3.2 Review of the methods for chemo-mechanical coupling

A key aspect of lime stabilization is the fact that the structure, and therefore the mechanical behaviour, relies on physico-chemical processes that need to be quantified. In Chapter 2, it was shown that hydration of quicklime can produce portlandite and cementitious compounds. In addition, lime can also react with atmospheric carbon dioxide to produce carbonates ( $\text{CaCO}_3$ ). In the end, three types of compounds can be used to monitor the transformation of quicklime during a lime treatment: portlandite, hydrates, and carbonates (Figure 3.1).

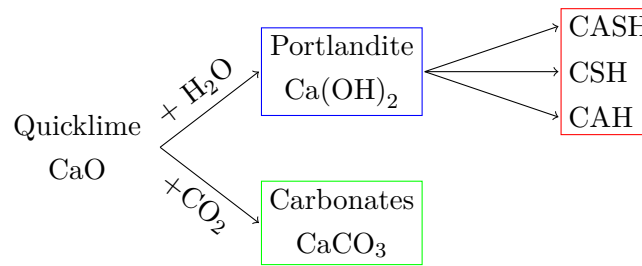


Figure 3.1: Three possible transformations of quicklime during soil treatment.

Different approaches have been proposed to establish a coupling between the mechanical behaviour and the products of soil treatment. We present the qualitative and quantitative methods used for the determination of the chemical composition of lime treated soils and how mechanical behaviour and chemistry have been coupled.

### 3.2.1 Qualitative analysis

The micro-structure of the cementitious compounds (CSH, CAH, CASH) has been qualitatively studied by methods such as X-ray crystallography (Chew et al., 2004) and scanning electron microscopy (Narasimha Rao and Rajasekaran, 1996). Some relationships have been proposed between micro-structure, porosity and strength of the soil (Kendall et al., 1983).

### 3.2.2 Quantitative analysis

Methods originally developed for medical imaging have been used for the study of construction materials and soils. Tomography consists of taking 2D slice images of the material, the global 3D representation being rendered by the assembling of the slices. This family of methods allow great accuracy and are non-destructive. However, the size of the sample is limited and the computational resources get very important as the size and the number of slices increase. Methods such as nuclear magnetic resonance (NMR) or X-ray tomography that rely on hydrogen atom have been successfully applied for the analysis of water composition. Anderson et al. (1988) used tomography for the determination of the water content, including the water located in the vicinity of the particles. It has then been used for different purposes like the analysis of porous media (Ketcham and Carlson, 2001; Ketcham, 2005). The proton RMN ( $H_2O$ ) was used to determine the chemical composition of artificially treated materials (Pomakhina et al., 2012; De Windt et al., 2014) (Figure 3.2). The main potential of this method is that each peak is associated to a chemical compound and the area under the curve can be related to the concentration in the element.

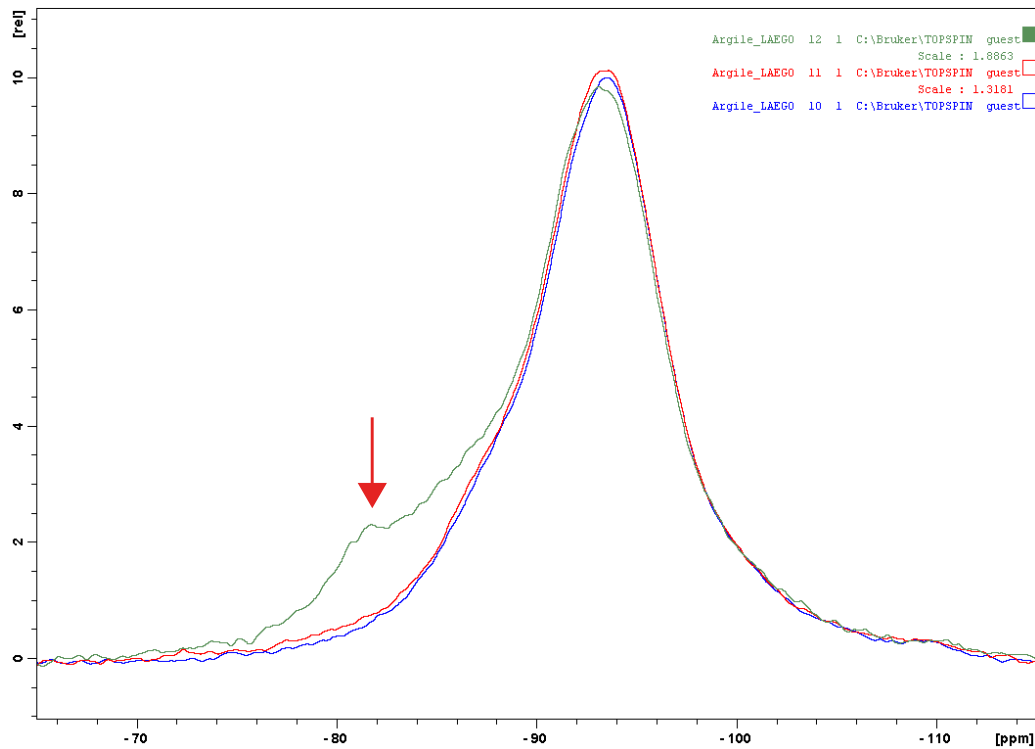


Figure 3.2: Proton RMN spectrum of lime treated bentonite. The red arrow indicates the apparition of a compound following a lime treatment.

### 3.2.3 Soil Water Transfer model

Zhu et al. (2007) proposed a framework based on the soil-water mechanism to quantify the amount of hydrates formed in a cement treated dredge material. Water in soils can exist in three different phases based on the binding forces acting on water molecules (Mitchell and Soga, 2005): the hydrated water (hw) as part of the mineral structure, the bound water (bw) adsorbed on soil particles which constitutes the double diffuse layer, and the free water (fw) loosely retained in the soil by surface tensional forces and gravity. The model postulates that only the pore water (pw) is available for the hydration of the cement and results in the combination of the free water and the bound water, the hydrated water trapped in the minerals being assumed unreachable. The hydration process consumes preferentially the free water to form new hydrated compounds and increases the amount of bounded water. Since the latter precipitates, a double diffuse layer is created using the remaining free water, which also increases the fraction of bounded water. Calling  $m_{pwo}$  the initial mass of pore water and  $m_{bwo}$  the initial mass of bounded water in the sample, the framework of the soil water transfer model describing the effects of an artificial treatment on the three different phases is given in Figure 3.3.

### 3. CHEMO-MECHANICAL MODELLING OF LIME TREATED SOILS

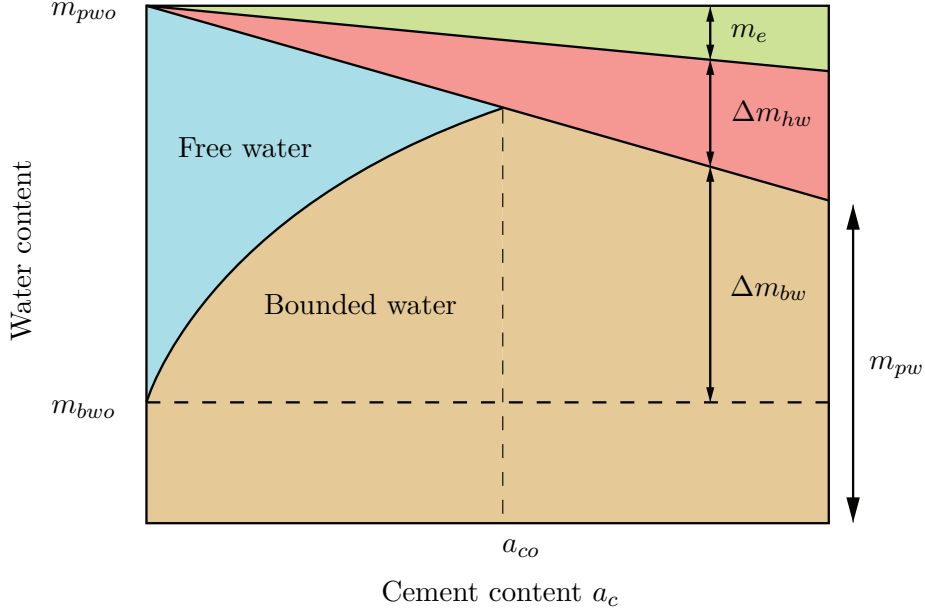


Figure 3.3: Soil water transfer model for cement-treated dredge materials.  $a_c$ : cement content,  $m_{pwo}$ : mass of pore water,  $m_{hw}$ : mass of hydrated water,  $m_{bw}$ : mass of bounded water,  $m_{fw}$ : mass of free water,  $m_e$ : mass of evaporated water. After Chiu et al. (2009).

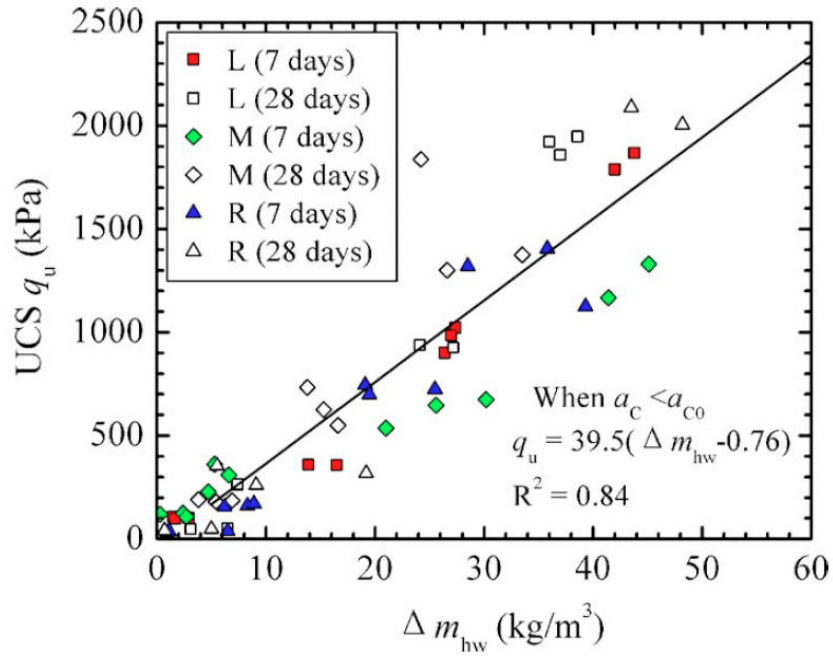
From the mass conservation law it can be written:

$$m_{pwo} = \begin{cases} m_{fw} + m_{bwo} + \Delta m_{bw} + \Delta m_{hw} + m_e & \text{if } a_c < a_{co} \\ m_{bwo} + \Delta m_{bw} + \Delta m_{hw} + m_e & \text{if } a_c \geq a_{co} \end{cases} \quad (3.1)$$

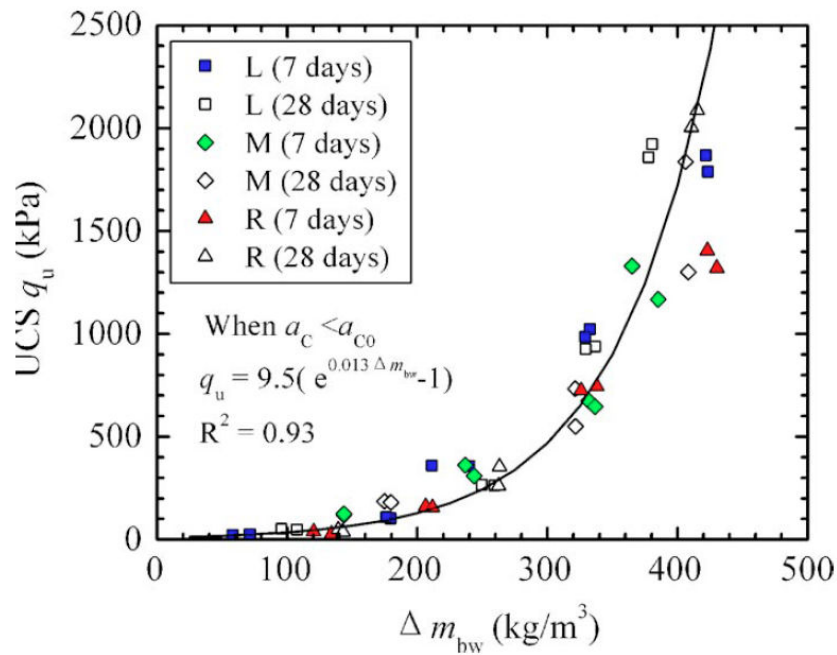
with  $a_{co}$  the cement content leading to the total consumption of the free water, and  $m_e$  the mass of evaporated water resulting from the heat generated by the hydration of lime. The products of pozzolanic reactions responsible can be indirectly quantified using  $\Delta m_{hw}$  and  $\Delta m_{bw}$ , which can be experimentally measured by oven drying and centrifuge method.

The method was successfully applied by Zhu et al. (2007) and Chiu et al. (2009) to establish a nonlinear coupling between the mass increments  $\Delta m_{hw}$  and  $\Delta m_{bw}$  and the unconfined compressive strength (Figure 3.4a–3.4b), the cohesion (Figure 3.4c), and the yield stress (Figure 3.4d). This proves that the determination of all the products of pozzolanic reactions is not required and that a single parameter describing the total amount in hydrates can be sufficient to establish a coupling with a mechanical parameter. However, the method relies on the measurement of bounded water and pore water which makes it suitable only for materials with high water content ( $w > 70\%$ ).

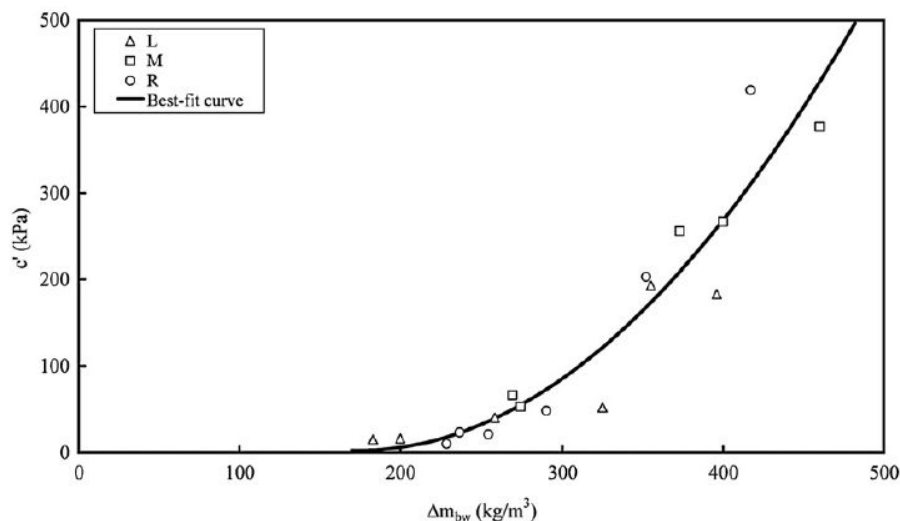




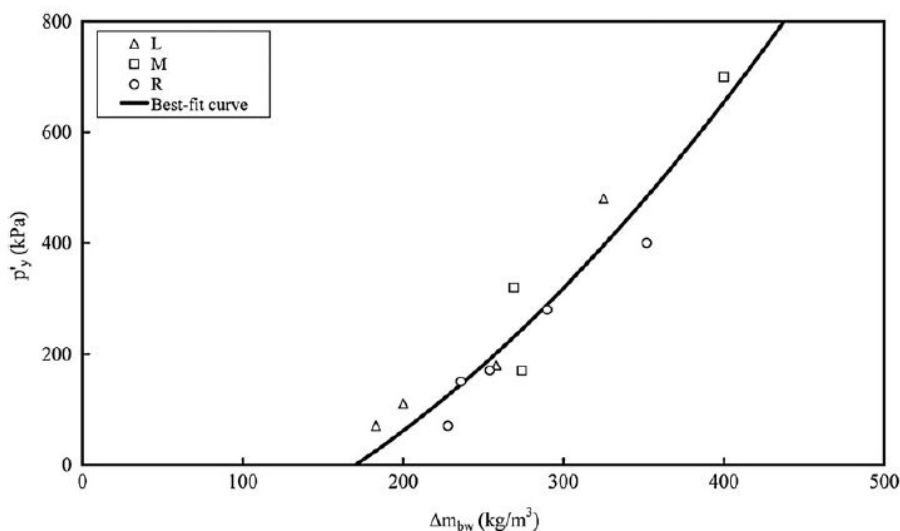
(a) Chemo-mechanical coupling between the UCS and the changes in hydrated water (Zhu et al., 2007)



(b) Chemo-mechanical coupling between the UCS and the changes in bonded water (Zhu et al., 2007) – L: lake sediment, M: marine sediment, R: river sediment



(c) Chemo-mechanical coupling between the cohesion and the changes in bonded water (Chiu et al., 2009)



(d) Chemo-mechanical coupling between the yield stress and the changes in bonded water (Chiu et al., 2009)

Figure 3.4: Chemo-mechanical coupling between some mechanical parameters and the changes in hydrated or bonded water using the soil water transfer model – UCS: unconfined compressive strength.

### 3.2.4 Suitable approach for lime treated soils

None of these methods appear actually suitable for the establishment of a chemo-mechanical coupling for lime treated soils; X-ray analysis only allows qualitative descriptions, the large number of hydrated cementitious compounds makes difficult the use of NMR, and the soil water transfer model requires materials with high water contents. For materials with lower water content ( $w = 20 - 30\%$ ), like the compacted soils used in geotechnical structures, the method cannot be applied.

In this thesis we investigated the suitability of thermal analysis (Kissinger, 1957; Wendlandt, 1974; Ramachandran et al., 2002; Pansu and Gautheyrou, 2006; Plante et al., 2009) to assess the chemical composition of lime treated soils. Maubec (2010) has proposed a method using thermogravimetric analysis (TGA) and differential thermo

analysis (DTA) to measure quantitatively the amount of portlandite and cementitious compounds. The method was cross-validated using the results of NMR and a chemo-mechanical coupling was developed between the mass loss over a specific range of temperature and the unconfined compressive strength. More details can be found in Maubec (2010).

### 3.3 Materials and methods

#### 3.3.1 Characterization of the materials

The material selected in this study is a silt from the east part of France. These granular materials result from abrasive processes of a bedrock and are very abundant in Europe. For this reason, geotechnical companies have to deal frequently with this kind of silt. However, the mechanical properties are usually too low for an immediate use in geotechnical structures and an artificial treatment with quicklime is therefore most of the time performed. The particle size distribution curve and the main geotechnical characteristics are given in Figure 3.5 and Table 3.1 respectively.

Table 3.1: Characteristics of the silt

	Mineral composition
Quartz (%)	55.0
Kaolinite (%)	12.0
Feldspar (%)	11.0
Illite (%)	10.0
Montmorillonite (%)	4.0
Chlorite (%)	1.0
Goethite (%)	6.4
Carbonates (%)	0.6
	Geotechnical properties
Liquid limit $w_l$ (%)	31.2
Plastic limit $w_p$ (%)	7.8
Plasticity index PI (%)	23.4
Particle density $\rho_s$ (Mg.m <sup>-3</sup> )	2.66
Methylene blue value (g/100 g of dry soil)	2.1
USCS <sup>a</sup>	ML

<sup>a</sup>USCS: Unified Soil Classification System.

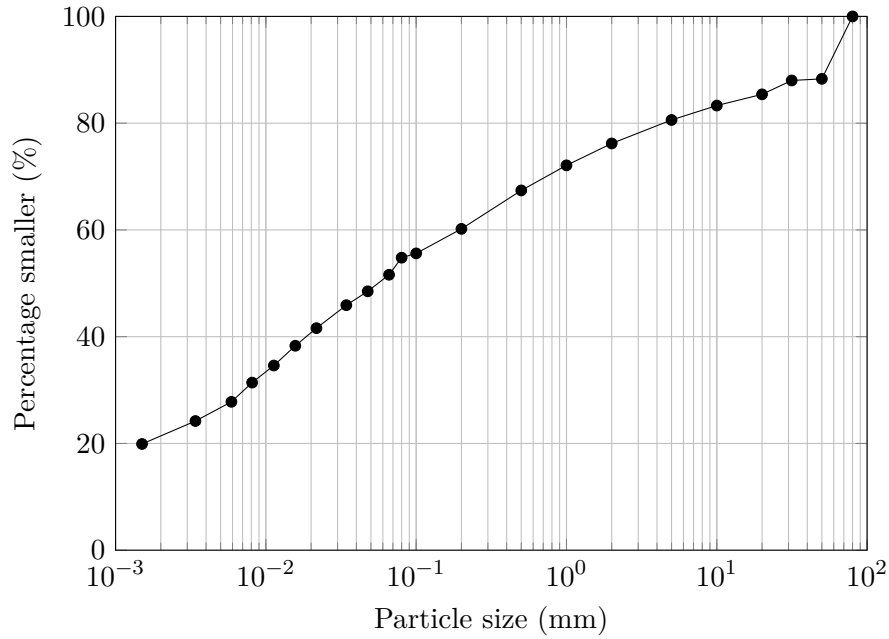


Figure 3.5: Particle size distribution curve

### 3.3.2 Specimens preparation

#### Initial conditions of the specimens

All the specimens used for the mechanical characterisation of the soil, with or without treatment, were prepared at the same moisture content and dry density. Indeed, the optimal moisture content and maximum dry density of the silt used in this study were not significantly modified by the lime-treatment (Figure 3.6 and Figure 3.7). Therefore, all the specimens have been prepared at the same mean initial water content of 20% and a dry density of  $1.68 \text{ Mg}\cdot\text{m}^{-3}$ . Thus, any modification of the mechanical behaviour of the soil after treatment can be attributed mostly to structure modification, i.e. fabric and bonding, but not to density. The lime fixation point is near 1% and was determined according to the ASTM Standard D6276 (2006).

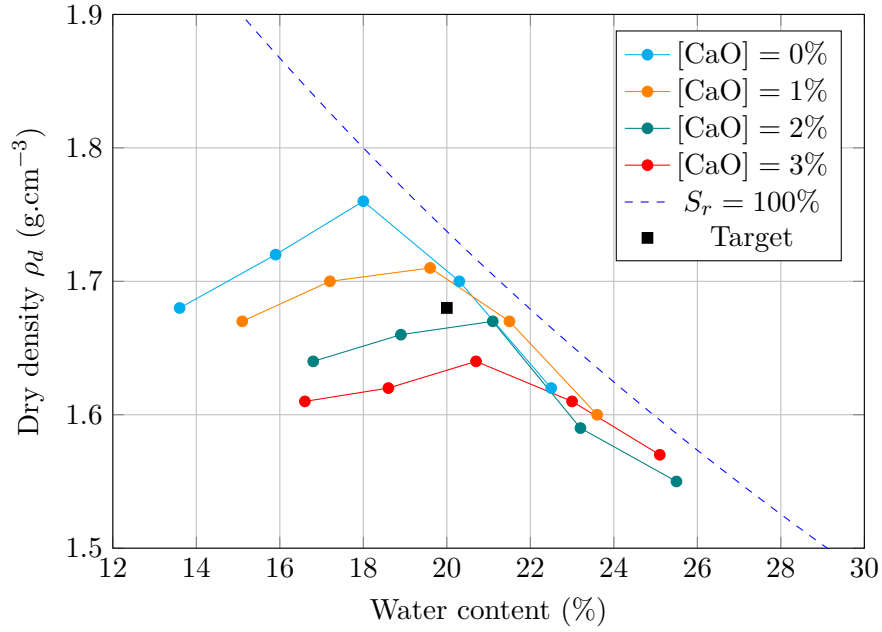


Figure 3.6: Influence of the lime content on the dry density-water content curves. –  $S_r$ : degree of saturation.

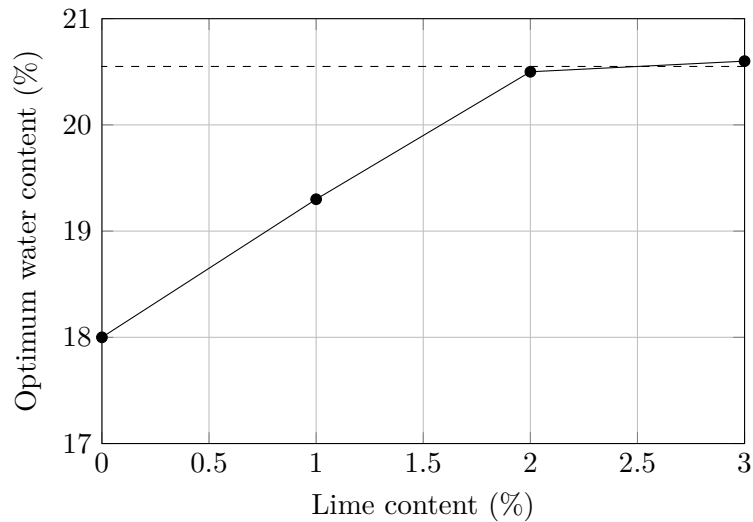


Figure 3.7: Evolution of the optimum water content with the lime content.

### Moulding of the specimens

The soil was first prepared at the target water content. After an equilibration period of 3 days, quicklime was added to the soil, both being mixed thoroughly until a homogeneous mixture was obtained. Before the specimens were compacted, the quicklime-soil mixture was sealed in hermetic plastic bags for one hour before compaction. Then, 35 mm x 70 mm triaxial specimens were statically compacted up to target the dry density. After these steps, the actual water content of the specimens was determined. It varied between 19.6% and 20.2%. The specimens were then wrapped in plastic bags to prevent any exchange with the atmosphere (Bell, 1996), and a conventional curing time of 28 days was respected (SETRA, 2007). A detailed protocol for the preparation of lime treated specimens is given in Appendix A.

### 3.3.3 Drained triaxial experiments

#### Apparatus

Triaxial experiment is widely used to assess the stress:strain relationship of a material. It consists in immersing the sample in the triaxial cell (Figure 3.8) and a confined pressure can be applied. This feature is particularly suitable for loose samples. A rubber membrane isolates the sample from the cell which allows to apply a different pressure in the sample than the cell pressure. Unlike the oedometer test, the surface of the sample is not restrained which allows a full determination of the stress tensor in the specimen. More details about the experiment can be found in Bishop and Henkel (1957); Muir Wood (1990). The stress paths performed in this thesis are given in Figure 3.9.

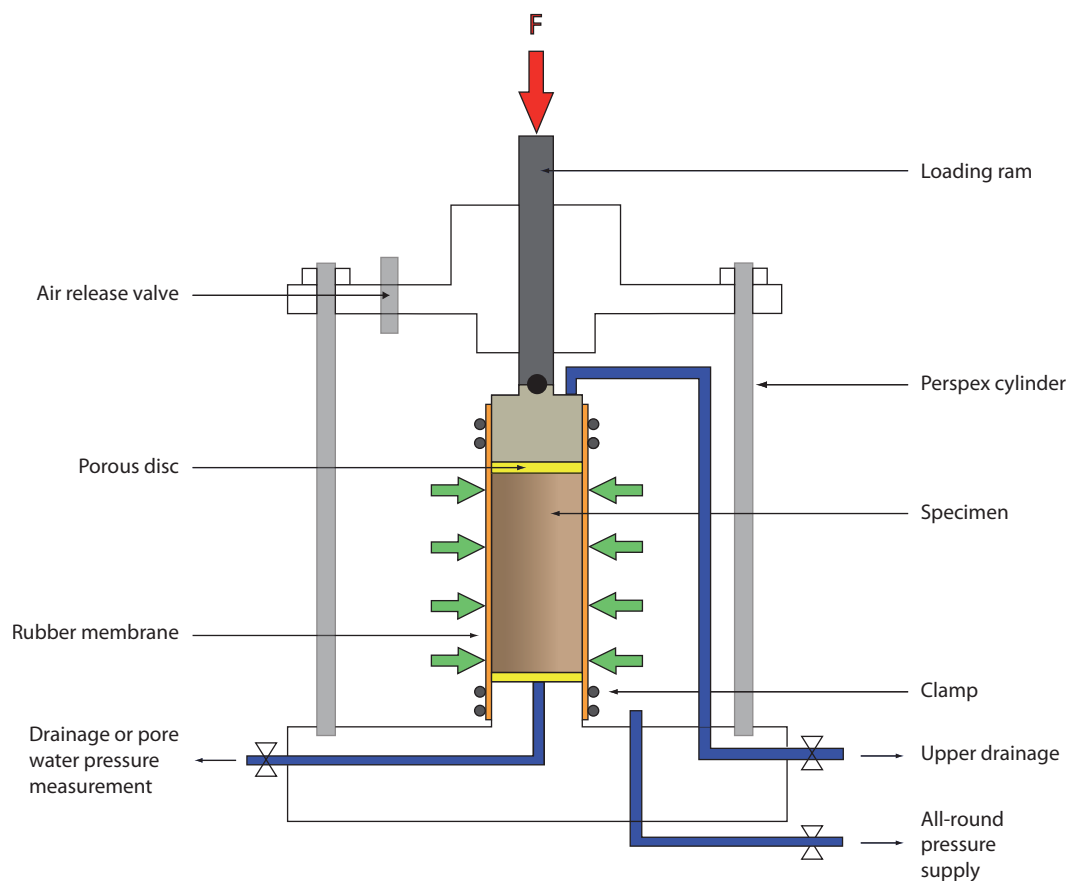


Figure 3.8: Triaxial apparatus. After Craig (2004).

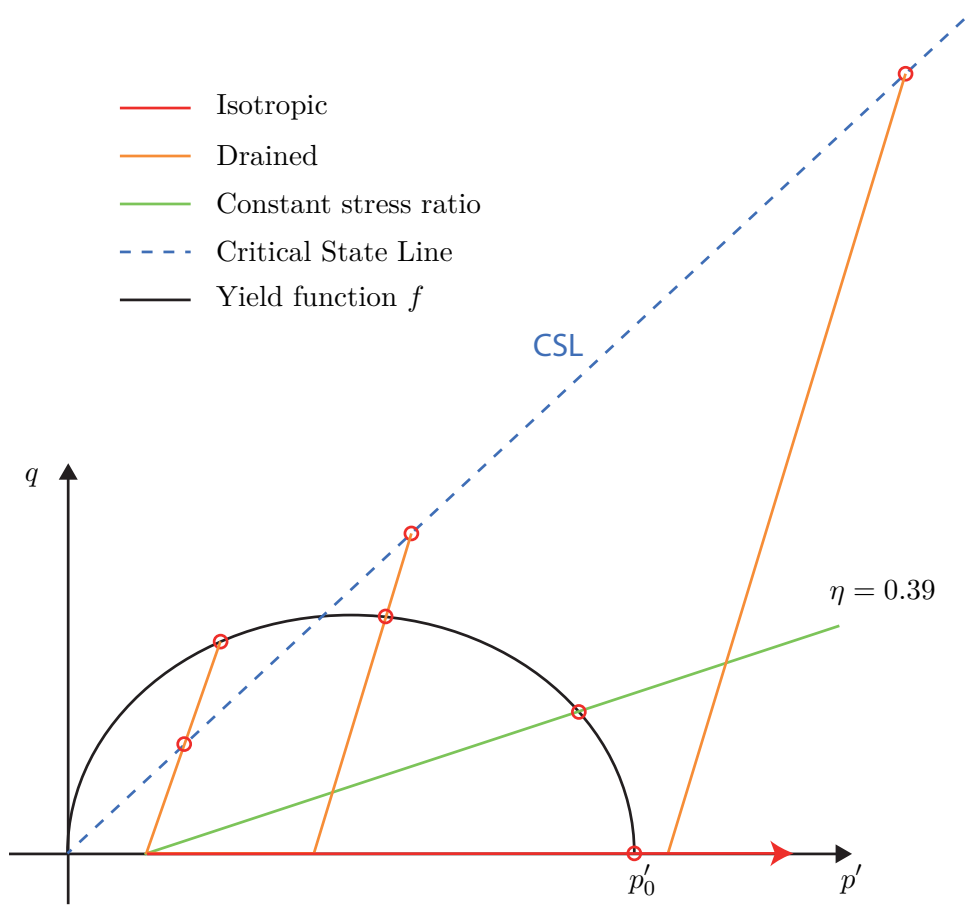


Figure 3.9: Stress paths carried out with triaxial experiments on lime treated soils: isotropic compression, drained shear, and constant stress ratio tests.

### Preparation & Saturation

Saturation was achieved by first creating an upward water flow through the specimen. This was achieved by applying a pressure gradient between the bottom and the top of the specimen. Demineralised and deaerated water was used to maximize the dissolution of air. Pore pressure was then increased in three stages (Table 3.2) while maintaining a constant effective mean stress.

After every triaxial experiment, saturation of the specimen was checked by determining the degree of saturation with paraffin according to the ASTM Standard D7263-09 (2009).

Table 3.2: Saturation stages performed

Duration	(Days)	Stage 1	Stage 2	Stage 3
		$\approx 7$	$\approx 7$	$\approx 7$
$\sigma_3$	(kPa)	50	100	200
$P_{bottom}$	(kPa)	30	80	180
$P_{top}$	(kPa)	20	70	170
$\bar{\sigma}'_3$	(kPa)	25	25	25

$P_{bottom}/P_{top}$ : pressure at the bottom/top of the specimen

### 3. CHEMO-MECHANICAL MODELLING OF LIME TREATED SOILS

To ensure full drainage of the specimens during the experiments, filter paper strips were applied to the surface of the specimens (Figure 3.10). Low rates of consolidation and axial deformation were chosen in order to generate small excess of pore pressure. An external probe was used to measure accurately the pore pressure at the bottom of the specimen during shearing.

For isotropic consolidation, a rate of  $3.47 \text{ Pa}\cdot\text{s}^{-1}$  was chosen and specimens were consolidated up to a total effective stress of 3,320 kPa. Validation tests were performed to verify that there was no excess pore pressure in the specimen under this rate.

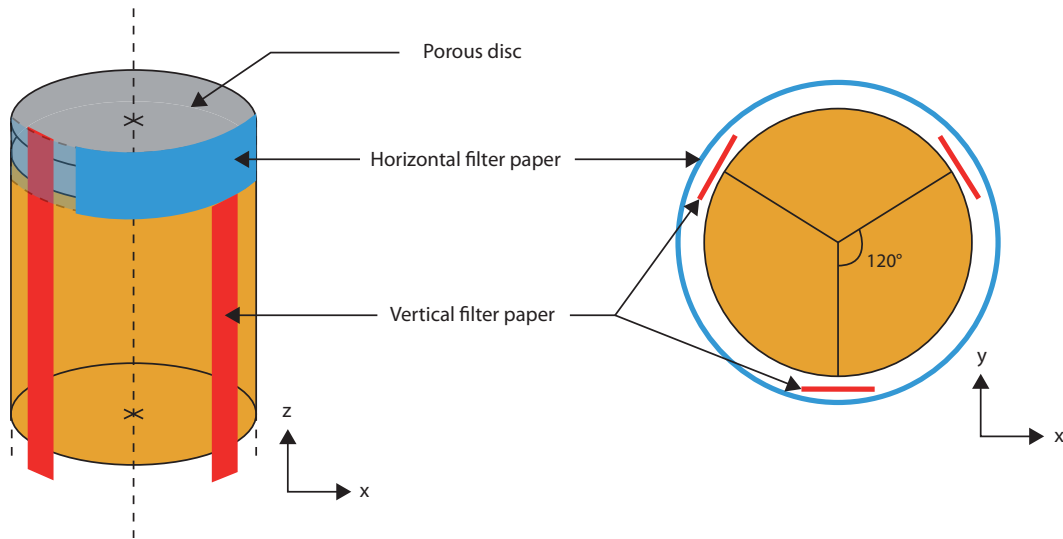


Figure 3.10: Disposition of the filter paper strips on the sample.

Triaxial compression tests were carried out with an axial displacement rate of  $2.46 \mu\text{m}\cdot\text{min}^{-1}$ , leading to an axial deformation of about 5% per day. Validation tests confirmed the suitability of this rate. All the experiments were performed following the procedure described in the ASTM Standard D7181-11 (2011). The initial conditions of the specimens are given Table 3.3. The saturation of the specimen was checked after each experiment (Figure 3.11) and always showed a value greater than 98%. Values can be found in Appendix A.

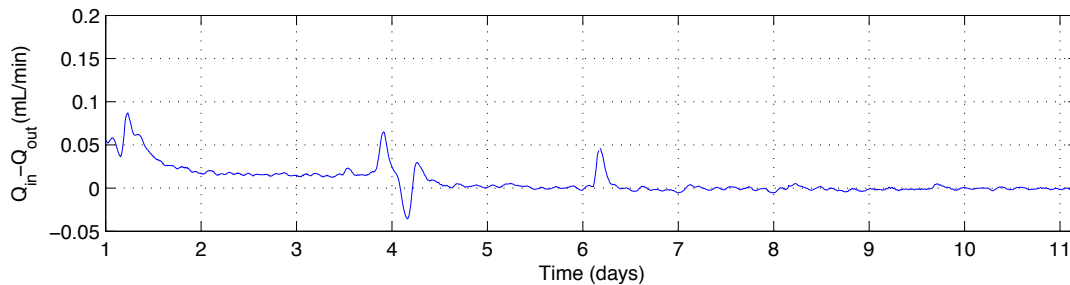


Figure 3.11: Control of the saturation of the samples



Table 3.3: Initial characteristics of the specimens

Lime content (%)	Water content (%)	$\rho_d$ (Mg · cm <sup>-3</sup> )	$v_0$ (-)	Hydraulic conductivity $k$ (m · s <sup>-1</sup> )
0	20.0	1.67 ± 0.01	1.60 ± 0.02	10 <sup>-9</sup> – 10 <sup>-8</sup>
0.5	19.6	1.67 ± 0.01	1.60 ± 0.01	10 <sup>-9</sup> – 10 <sup>-8</sup>
1	20.2	1.67 ± 0.01	1.60 ± 0.01	10 <sup>-9</sup> – 10 <sup>-8</sup>
2	19.6	1.67 ± 0.01	1.60 ± 0.01	10 <sup>-8</sup> – 10 <sup>-7</sup>
5	20.2	1.66 ± 0.01	1.60 ± 0.02	10 <sup>-8</sup> – 10 <sup>-7</sup>

### 3.3.4 Monitoring of the physico-chemical reactions

To monitor the progress of the physico-chemical processes in the specimens, it is necessary to determine the amount of portlandite, hydrates, and carbonates. Thermogravimetric analysis (TGA) consists of measuring the mass loss of a specimen as a function of the increasing temperature. This test is completed with a differential thermal analysis (DTA), which compares any temperature difference between the specimen and an inert reference (MacKenzie, 1970). Each peak on the curves is correlated to a chemical compound. Using the associated mass loss, the mass concentration of the species can be estimated (MacKenzie, 1972).

TGA/DTA analysis was first used successfully to determine the chemical composition of cements and concretes in hydrated products, portlandite, and carbonates. Some studies have shown that the decarboxylation processes of these three compounds are associated with three temperature domains (Das et al., 1996; Saikia et al., 2002; Alarcon-Ruiz et al., 2005). Recent studies have applied TGA/DTA analysis on artificially treated soils to assess the mass concentration in portlandite (unreacted lime), cementitious compounds, and calcium carbonates in artificially treated specimens (Horpibulsuk et al., 2010b; Maubec, 2010). The procedure for the determination of the chemical composition is illustrated on Figure 3.12. TGA/DTA analysis provides three different curves: the variation of the energy (DTA), the mass loss (TG), and the first derivative of the weight loss (DTG). First, TDA and DTG results were used to determine accurately the three temperature domains (Table 3.4).

Each peak on the DTG curve (Figure 3.12) is associated to a variation of the weight loss and corresponds to the decarboxylation of a chemical compound. The two temperatures delimitating the peak correspond to the temperature domains, and the chemical compound is assumed to have completely disappeared when the upper temperature limit was reached. Therefore, the variation of weight (TG curve) between these two temperatures gives the mass of the chemical compound. Analyses were performed using a NETZSCH STA 409 PC/PG device. The accuracy of the TGA weighing scale was 0.01 mg.

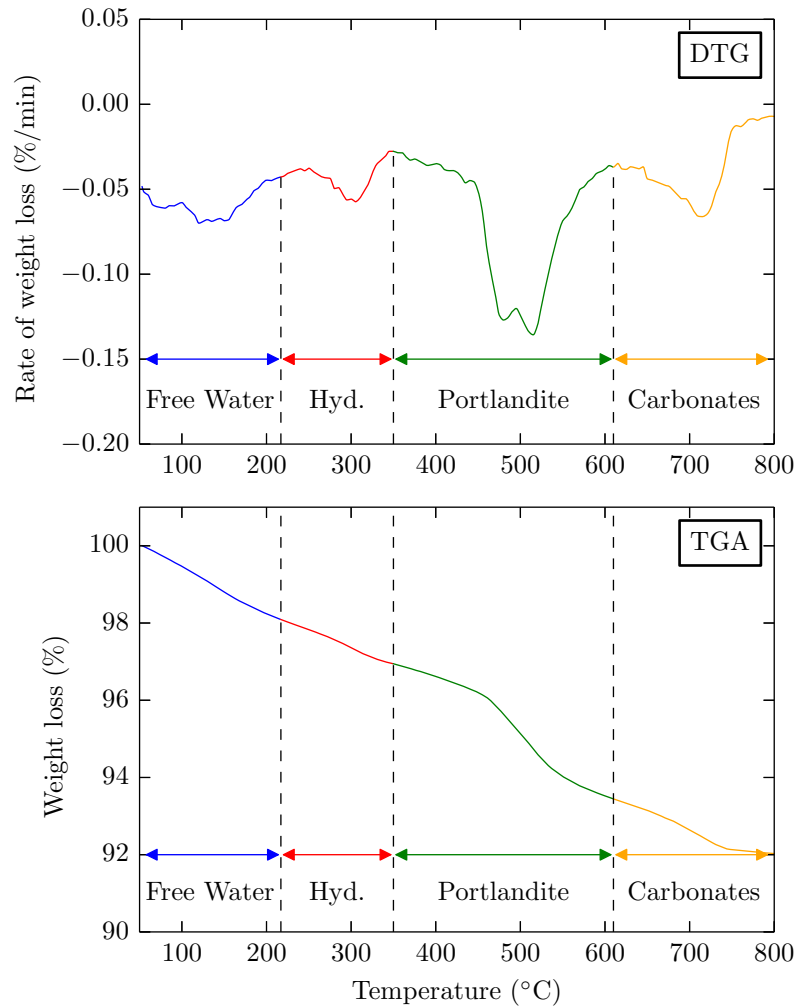


Figure 3.12: TGA/DTA results for a lime treated specimen with the three temperatures domains — Hyd.: Hydrates, DTG: Differential Thermo Gravimetric, TGA: Thermo Gravimetric Analysis

Table 3.4: Ranges of temperatures used for the determination of the TGA/DTA

Range of temperature	Chemical compound
20 °C – 217 °C	Free and adsorbed water
217 °C – 350 °C	Cementitious compounds
350 °C – 610 °C	Portlandite ( $\text{Ca}(\text{OH})_2$ )
610 °C – 800 °C	Carbonates ( $\text{CaCO}_3$ )

### 3.4 Experimental results

The experiments performed in this chapter aimed: 1) to determine the effects of the quicklime on the intrinsic parameters of soils, 2) to assess the shape of the yield function in order to choose the most suitable model for lime-treated soils, and 3) to measure the concentrations in portlandite, hydrates, and carbonates of lime treated specimens.

### 3.4.1 Mechanical behaviour

#### Isotropic consolidation

To assess the effects of the treatment on the yield stress, isotropic consolidation tests were performed on 0, 0.5, 1, 2, and 5% lime-treated specimens. For concentrations greater than 1%, three isotropic tests were carried out to ensure the highest representativeness. Only one result is reported in Figure 3.13. The yield stress was determined using Casagrande's method, the variation of the incremental work, and the variation of the volumetric and deviatoric deformations.

Yield occurred for an effective mean stress of about  $177 \pm 5$  kPa for the untreated specimen (Figure 3.13). When lime was added to the soil, the yield stress was increased even for low lime content of 0.5%. The evolution of the yield stress as a function of the lime content is given in Figure 3.14. For concentrations between 0.5% and 2%, the gradient of the curve was significantly increased. Above 2% the slope decreased, and as concentration increased, yield stress value seemed to approach 2,000 kPa. One can note that there exists a one-to-one correspondence between the lime content and the resulting yield stress after 28 days of curing.

At yield the treated soil displayed higher specific volume compared to the reference state (Figure 3.13). This could be due to the structure. When the effective mean stress reached the yield stress, the additional specific volume began to decrease as the effective mean stress was increased until a new normal compression line was reached, parallel to the one of the non-treated state. This decrease of the additional specific volume corresponds to the loss of the structure. Only 0.5% lime treated specimen has shown to completely lose the additional specific volume at high mean stresses. In this case, the normal compression line matched the one of the non-treated state. For lime contents greater than 1%, specimens did not appear to converge to the non-treated state for mean effective stresses lower than 3,320 kPa. At some point, a secondary normal compression line, different from the non-treated state but still parallel, seems to be reached. This feature is particularly noteworthy for the 1% treated specimen. The 2% and 5% lime-treated specimens have shown such significant improvements in mechanical properties that this feature could not be seen because of the limits of the applied pressure in triaxial cell (3,500 kPa).

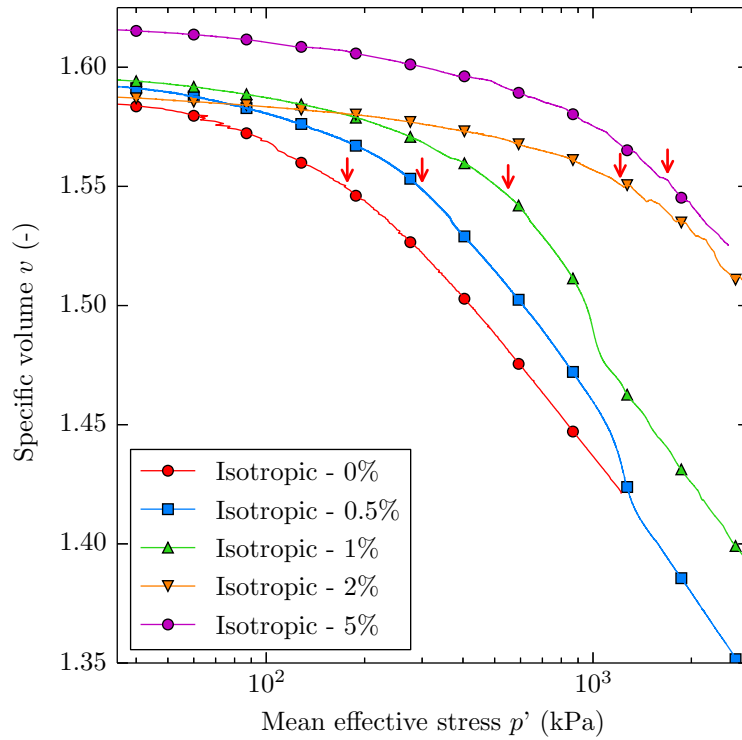


Figure 3.13: Isotropic consolidation curves for five concentrations in lime.

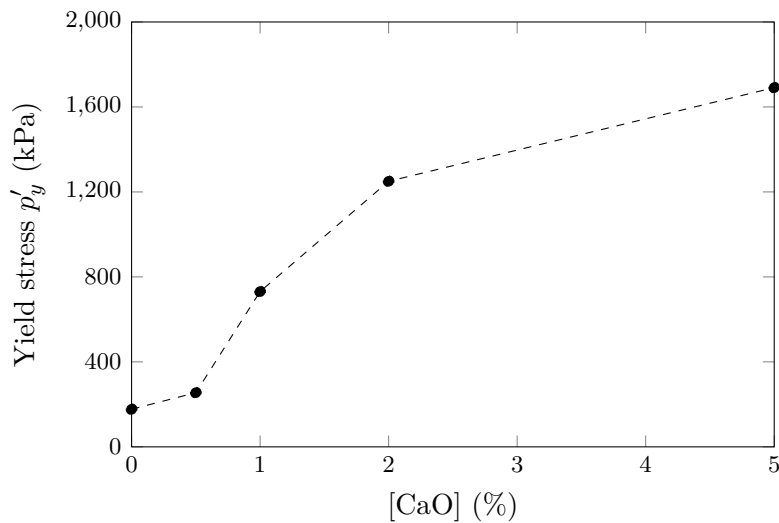


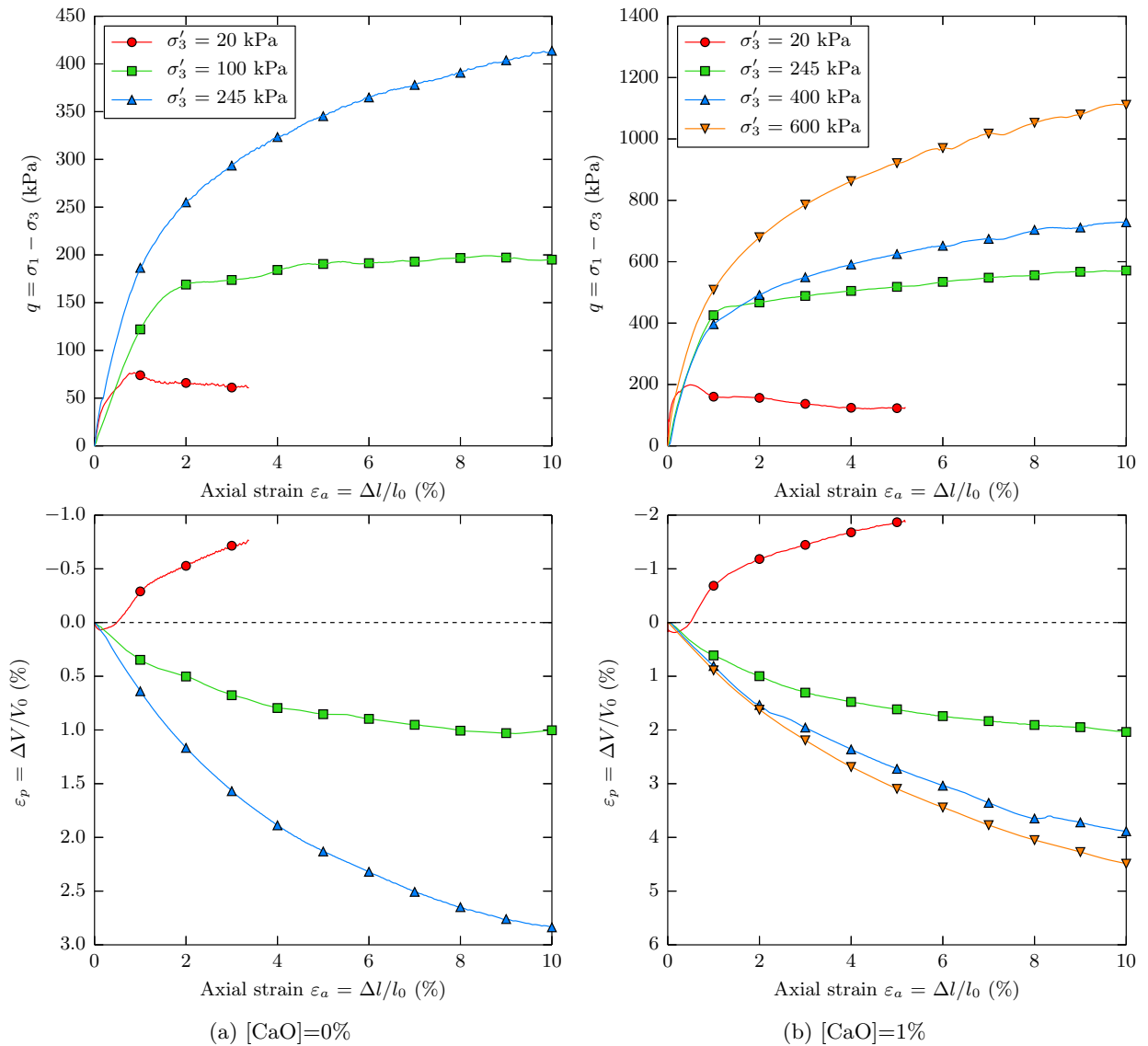
Figure 3.14: Evolution of the yield stress with the lime content after 28 days of curing.

### Shear behaviour

Drained triaxial experiments were performed to assess the shape of the yield function and the gradient of the critical state line. Different stress paths and pre-consolidation pressures were performed (Figure 3.9) on 0, 1, 2, and 5% lime-treated specimens (Figure 3.15).

The shear behaviour of the non-treated specimens (Figure 3.15a) was significantly improved with 5% lime treatment (Figure 3.15d). For an isotropic pre-consolidation pressure of 245 kPa, the yield locus of the reference state was reached for a deviatoric stress of 400 kPa. With 5% of lime, this value was increased up to 1,250 kPa.

As the confining pressure was increased, one can see that contraction behaviour was gradually observed. This feature was particularly marked for the 5% lime-treated specimens (Figure 3.15d). For a confining pressure of 20 kPa, the specimens had significant dilation behaviour. As the confining pressure increased, the specimens started to exhibit a contraction behaviour.



### 3. CHEMO-MECHANICAL MODELLING OF LIME TREATED SOILS

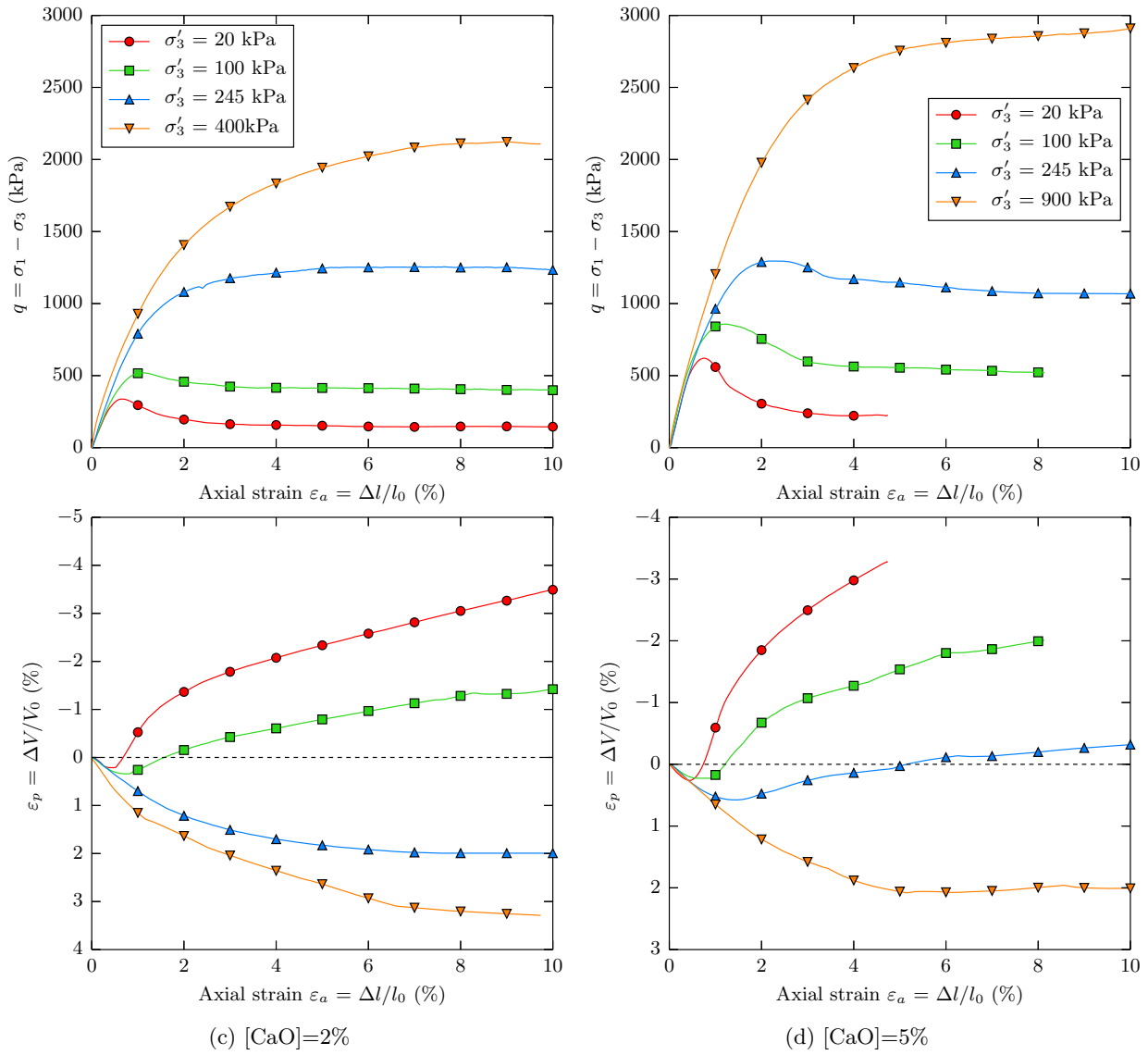


Figure 3.15: Drained triaxial results on (a) untreated, (b) 1%, (c) 2% and (d) 5%.

### 3.4.2 Yield loci for lime treated soils

Yield loci and critical states were determined from the previous results by combining the different techniques available, such as the variation of the incremental work or of the volumetric and deviatoric deformations, and plotted in the  $(p', q)$  plane (Figure 3.16). The results from the same stress ratio paths ( $\eta = 0.39$ ) were also included. To use these results in a constitutive model, yield loci and critical states were determined based on the critical state theory (Muir Wood, 1990). Yield was assumed to occur when plastic deformation appeared ( $\varepsilon_q^p > 0$ ), and critical state was reached when:

$$\frac{\partial p'}{\partial \varepsilon_q} = \frac{\partial q}{\partial \varepsilon_q} = \frac{\partial v}{\partial \varepsilon_q} = 0 \quad (3.2)$$

The elastic domain showed to be significantly increased with increasing the lime content, without any significant anisotropic behaviour (no noticeable trends), and the critical state lines appeared to be modified with the treatment. The gradient and the y-intercept of the critical state lines both increased with increasing the amount in lime. The results appear to be well described by the Modified Cam Clay model.

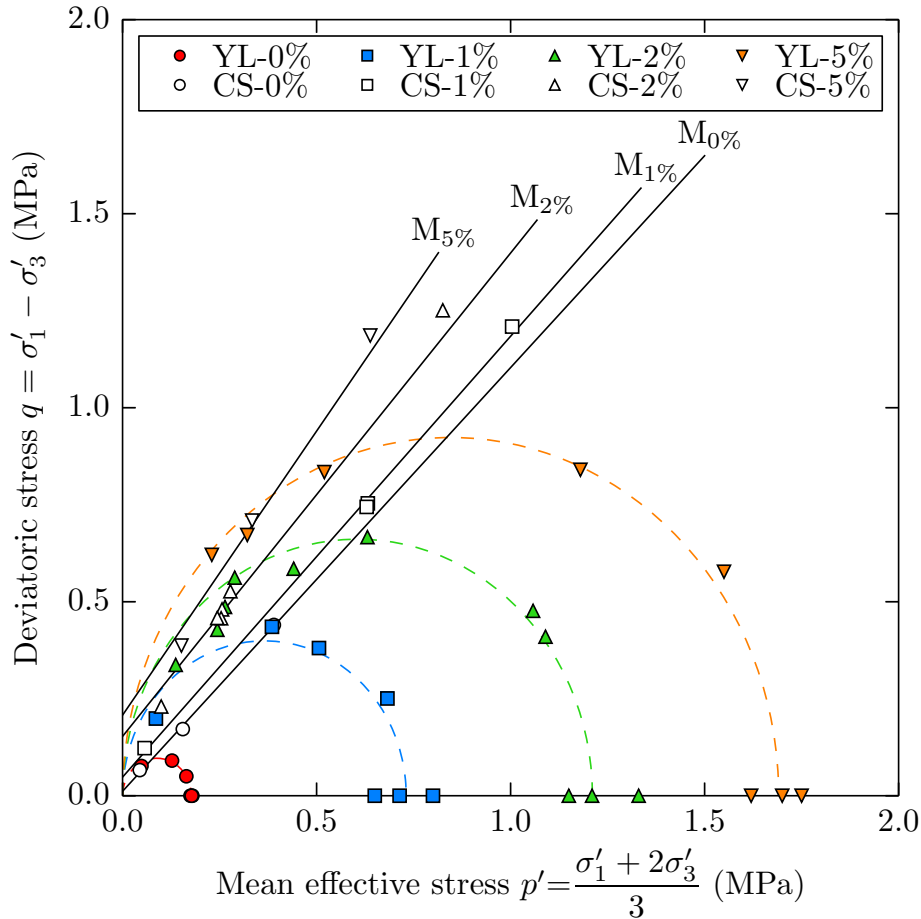


Figure 3.16: Yield loci and critical state of 0%, 1%, 2% and 5% lime treated specimens – YL: Yield loci, CS: Critical state, M: Gradient of the critical state line.

#### 3.4.3 Chemical analysis

In parallel with the analysis of the mechanical behaviour, we investigated the chemical properties of the tested samples after 28 of curing. The results of TGA/DTA tests to measure the chemical composition in portlandite, hydrates, and carbonates on 0, 0.5, 1, 2, and 5% lime treated specimens are plotted in Figure 3.17. The y-axis values correspond to the variation of mass compared to the untreated specimen.

The chemical composition of the soil appears to be modified after addition of lime and a curing time of 28 days. Concentration in portlandite is increased only for lime contents greater than 0.5%. The latter is used by pozzolanic reactions to produce cementitious compounds. For a concentration of 0.5%, all the portlandite produced by the hydration of the quicklime was used by pozzolanic reactions.

Concentration in hydrates was increased for all the lime contents. It is worth to note that there is a one-to-one correspondence between the lime content and the mass concentration in hydrates. The fact that neo-portlandite is measured for high lime contents means that pozzolanic reactions are unfinished and concentration in hydrates is likely to evolve if the curing time is extended.

Concentration in carbonates revealed to be increased only for high lime contents. Probability of carbonation is higher at high lime contents and this could explain the formation of carbonates. It is more likely that these new carbonates are the result of the reaction of the unhydrated lime (calcium oxide) with the atmospheric carbon dioxide.



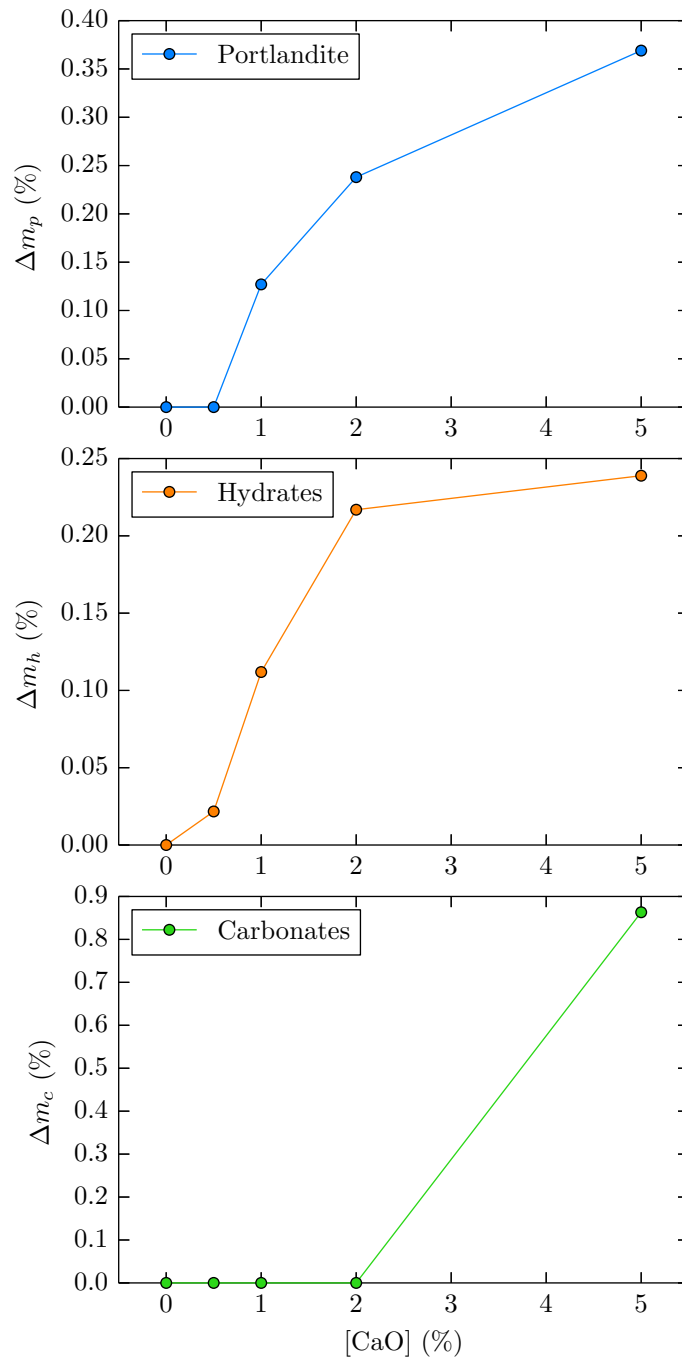


Figure 3.17: Influence of a lime treatment on the variation of the mass concentration in portlandite, hydrates (cementitious compounds), and carbonates for a curing time of 28 days –  $\Delta m_p$ : mass concentration in portlandite,  $\Delta m_h$ : mass concentration in hydrates,  $\Delta m_c$ : mass concentration in carbonates.

### 3.5 Discussion

In the first part of the discussion section, the influence of lime on the mechanical properties of soil is discussed. Moreover, a quantification of the physico-chemical processes induced by lime-treatment after 28 days of curing is provided. The main objective of the second part of the discussion section is to highlight the coupling between the mechanical behaviour and the amount of the different compounds formed during the curing period, and to propose a formulation for the coupling. In the last part, a framework to account for the effects of the treatment on the intrinsic parameters is

proposed.

### 3.5.1 Influence of lime on mechanical parameters

Lime has appeared to modify the mechanical behaviour of the soil, and parameters like the position of the virgin consolidation line and the slope of the critical state line,  $M$ . Following the definition proposed by Burland (1990), “structure” consists of the combination of the cementation and the fabric. In the case of structured soils, Leroueil and Vaughan (1990) showed that isotropic consolidation induced a progressive loss of structure at yield (cf. Section 2.3). After total loss of structure, the normal compression line of the structured soil converges to that of the same soil prepared in a remoulded state before compression.

In the case of a treated soil with quicklime, this assumption was only valid for a soil treated with 0.5% of quicklime. Isotropic consolidation results revealed a full loss of the structure for 0.5% lime treated specimens, which displayed the same virgin consolidation line as the non-treated specimens at a mean stress value of 1,340 kPa. However, for concentrations greater or equal than 1% it could be assumed that the position of the virgin consolidation line following the destructuration is shifted. This feature is usually controlled by the fabric, and especially by the geometry of the particles. Therefore, one may assume that the geometry of the particles is modified by the treatment and is lime content-dependant. This observation is corroborated by the drained triaxial test results, which revealed a modification of the critical state line. The increase of the  $y$ -intercept is a result of the cementation (Figure 3.16). The slope of the critical state line,  $M$ , is a direct function of the angle of friction (Schofield and Wroth, 1968) and describes the relationship between the particles and their geometry. A modification of  $M$  (Table 6) implies a modification of the angle of friction, and therefore of the geometry of the particles (Stocker, 1974; Wissa, 1965). Therefore, in the framework of the lime-treated soils, our results show that these mechanical parameters are modified.

Parameters like  $M$  and the normal compression line are considered as intrinsic and invariable in the framework of naturally structured soils (Liu and Carter, 2002). For these materials, reconstituted state is used as reference to assess the mechanical improvements due to the structure. In this case, the soil particles have already experienced cementation processes. The soils particles of the untreated state have not been in contact with lime and hence no modification of their geometry has occurred. From this point of view, the use of the mechanical parameters of the non-treated state as reference appears to be inappropriate to assess the effects of the treatment. This is important to describe the improvements, but not enough to fully describe the mechanical behaviour of treated soils. To do this, an intermediate state appears to be required, the destructured state of the lime treated soil. This state would account for the effects of the treatment on the mechanical parameters.

These results have shown that mechanical parameters of a soil are modified with the addition of quicklime. Therefore, it appears of the greatest interest to compare those with the chemical modifications arising from the treatment.

### 3.5.2 Chemo-mechanical coupling between physico-chemical process and yield stress

It has appeared that lime treatment modified the nature of the soil by altering parameters classically considered as intrinsic. In the light of these results and using the approach proposed by Chiu et al. (2009), the yield stress was chosen as the mechanical coupling parameter. Apart from controlling the size of the initial yield function in most of the constitutive models, there is a one-to-one correspondence between the lime content and the resulting yield stress. The mechanical results and the chemical compositions are plotted in a scatterplot matrix (Figure 3.18) to assess the trends between the yield stress and the mass concentration in cementitious compounds, portlandite, and carbonates.

The trends between the yield stress and the portlandite, and carbonates and hydrates are given in Figure 3.18. The results show a linear correlation between the yield stress and the portlandite. Hydrates also appear to be linearly correlated to the yield stress. The production of hydrates was noted for every lime content and a one-to-one correspondence with the lime content. A second trend can be noticed between the yield stress and the portlandite. Chemical analysis revealed that all the portlandite has been consumed by pozzolanic reactions for low lime-contents ( $< 0.5\%$ ). However, mechanical results showed that this lime-content is enough to increase the yield stress. Therefore, portlandite cannot be considered as a relevant parameter for a chemo-mechanical coupling.

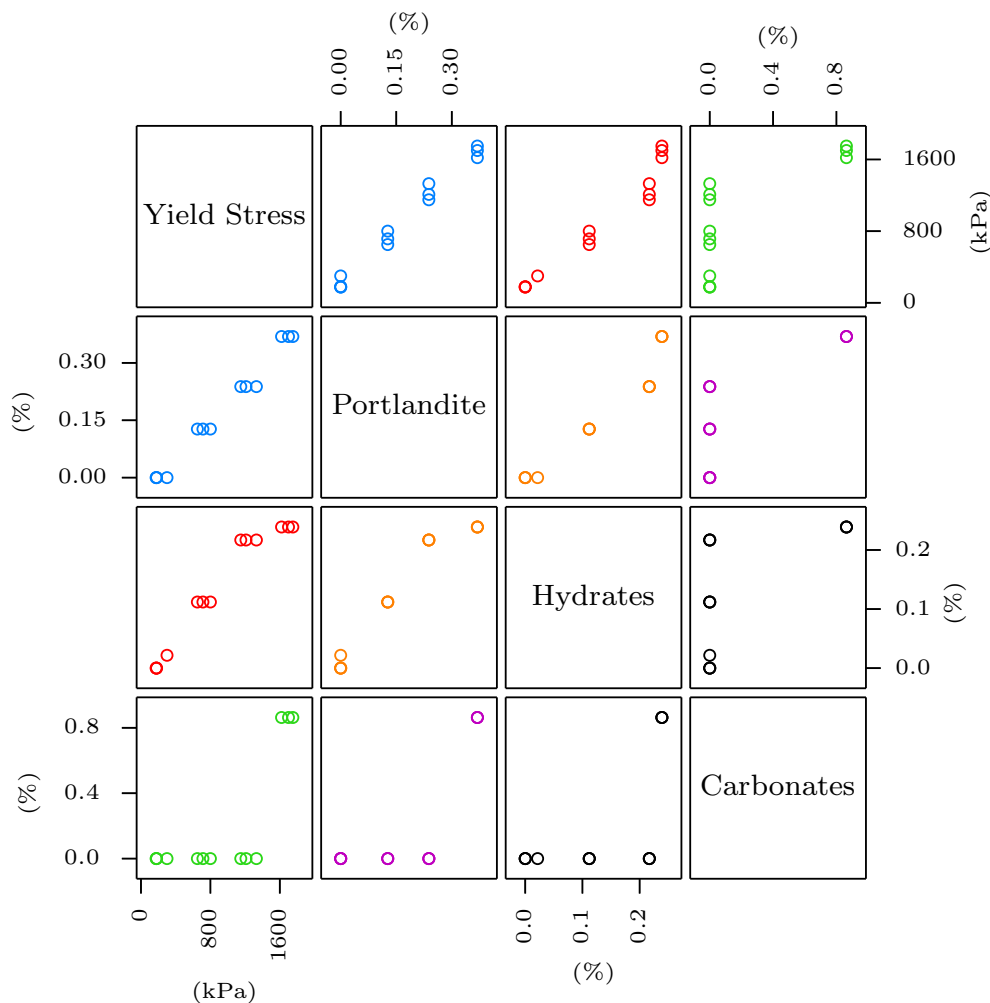


Figure 3.18: Scatterplot matrix between the yield stress and the mass concentration in cementitious compounds (hydrates), portlandite and carbonates.

Production of carbonates was only observed for concentrations greater than 2%, but mechanical improvements can be measured for small lime contents. Maubec (2010) has shown that the contribution of the carbonates in the mechanical behaviour can be neglected. For the same reasons as the portlandite, carbonates are not suitable for a chemo-mechanical coupling. Lime can be easily carbonated in contact with  $\text{CO}_2$  (Figure 3.1).

In the light of these observations, mass concentration in hydrates is the only parameter systematically modified by the addition of lime and presenting a one-to-one correspondence with the lime content. Since yield stress has also a one-to-one correspondence with the lime content, a coupling between these two parameters appears to be the most relevant choice. In order to establish a coupling, a relationship was established between yield stress and the mass concentration in hydrates. To model accurately a lime-treated soil, the regression function must fulfil the following criteria:

- (a) The point of lime fixation describes the minimum lime-content required to measure mechanical improvements. Thus, for low concentrations in hydrates ( $< 0.05\%$ ), regression function must show a low gradient,

- (b) Above a critical lime content, yield stress does not increase anymore (Rotta et al., 2003). To account for this feature in the coupling, the interpolation function must converge toward a finite value for high concentrations in hydrates.

To account for these two conditions, we chose a generalised logistic function of the form

$$\forall \Delta m_h \in \mathbb{R}^+ \quad f(\Delta m_h) = p_{y,\min} + \frac{p_{y,\max} - p_{y,\min}}{1 + e^{-\vartheta(\Delta m_h - \Delta x)}} \quad (3.3)$$

with:

- $p_{y,\min}$  : The lower asymptote
- $p_{y,\max}$  : The upper asymptote
- $\vartheta$  : The growth rate
- $\Delta x$  :  $\Delta m_h$  value for which the first derivative is maximum and  $\frac{df^2}{d^2\Delta m_h} = 0$

Using a non-linear least square method, the 4 variables  $p_{y,\min}$ ,  $p_{y,\max}$ ,  $\vartheta$ , and  $\Delta x$  were calculated to determine the optimal set of parameters (Table 3.5) based on the results of the isotropic tests. For lime concentrations greater than 1%, three isotropic tests were performed to improve the robustness of the interpolation. The formulation for the coupling appears to satisfactorily describe the results (Figure 3.19) and fulfil the conditions (a) and (b). The same procedure can be applied to link the mass concentration in hydrates with the lime content and will result in a direct coupling between the amount in lime introduced in the soil and the resulting yield stress. This correlation is allowed since there is a systematic one-to-one correspondence between all the variables, which proves that a robust coupling between the mechanical behaviour and chemical composition exists.

Table 3.5: Optimal set of parameters for logistic interpolation for chemo-mechanical coupling in lime treated soils

Parameter	$p_{y,\min}$	$p_{y,\max}$	$\vartheta$	$\Delta x$
Value	100	2000	17.4	0.16

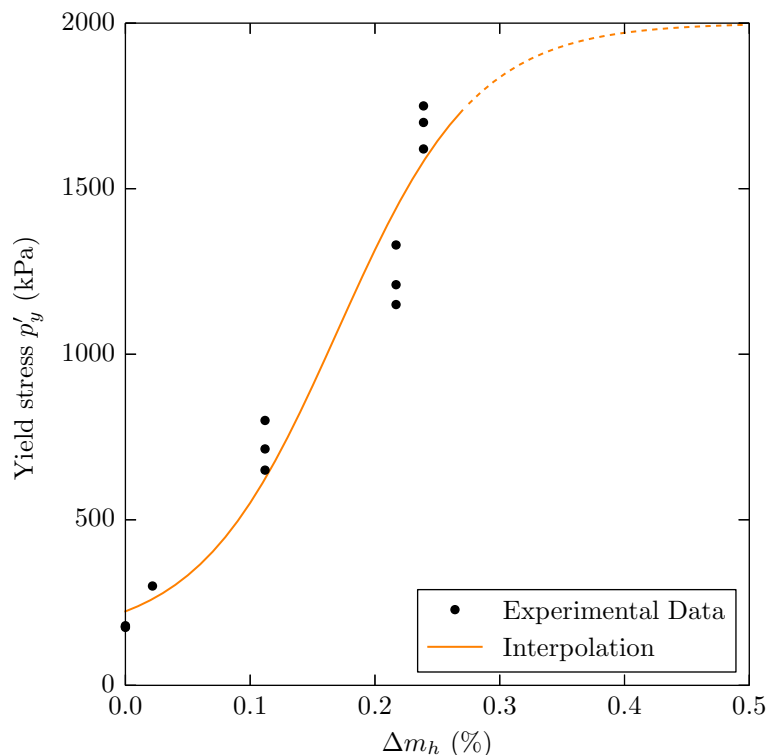


Figure 3.19: Logistic interpolation for a chemo-mechanical coupling in lime treated soils –  $\Delta m_h$ : mass concentration in hydrates.

### 3.6 Conclusion

This experimental study has shown the potential of lime treatment to improve the mechanical properties of materials initially unsuitable for geotechnical structures. Thus, a chemo-mechanical coupling to account for the treatment in the design is of greatest interest.

This chapter aimed first at describing in details the effects of lime on the mechanical behaviour of a soil and also on parameters usually considered as constant in the presence of structure. The results have shown that there was an improvement of the mechanical parameters due to the chemical reactions occurring after addition of the lime. For lime contents greater than 1%, the specimens converged toward a normal compression line different from the untreated state, but parallel to it. Therefore, in the framework of the lime treated soils, the mechanical parameters of treated soils could be different from those of the untreated state.

The chemical composition of lime treated specimens has been successfully assessed using thermogravimetric and thermodifferential analyses. The results have shown that concentrations in cementitious compounds and portlandite increased with the lime content. They permitted to explain the mechanical results and especially the modification of some parameters such as the angle of friction. The production of the cementitious compounds involves several preliminary reactions where soil particles experience dissolution due to the high pH. From this point of view, the nature of soil is seriously altered, leading to an evolution of the mechanical parameters. Chemical results revealed that cementitious compounds were produced for every concentration tested. A chemo-mechanical coupling was established using a logistic function between

the amount of cementitious compounds and the yield stress. The proposed equation appears to describe accurately the observations, and ensures a one-to-one correspondence between the mass concentration in cementitious compounds and the yield stress.

Now that all the key features regarding the effects of lime treatment on the mechanical parameters and behaviour of a soil have been identified, it is possible to address the second main issue of this thesis and develop a constitutive model specifically designed for artificially treated materials.

### 3. CHEMO-MECHANICAL MODELLING OF LIME TREATED SOILS



## Chapter 4

# A general formulation for degradation in structured soils

### 4.1 Introduction

In the previous chapter the mechanical behaviour of lime treated soils has been extensively studied and some specific mechanical features due to cementation have been identified. A constitutive model for lime treated soils should therefore properly reproduce these key features. The concept of similarity between naturally structured soils and artificially treated soils was approached in section 2.3. It starts from the observation that, despite arising from different processes, the structure formed by natural cementation and the one developed after an artificial treatment both lead to a similar mechanical behaviour and involve the same process of destructuration at yield. From this statement, models originally developed for naturally structured soils might be suitable for lime treated soils.

The main objective of this chapter is to propose a general formulation capable of fulfilling some fundamental criteria regarding the degradation of the structure. This model should be capable of modelling the most relevant kind of degradations, and require a limited number of parameters to account for the maximum number of features of structured materials. These parameters should be readily obtained from classic experimental tests, and they must all have a physical meaning. To this end, this chapter will focus on two aspects:

- How can the key features of structured or lime treated materials be described?
- How can these features be efficiently accounted for in a constitutive model?

First we give a summary of the methods and models proposed to account for the effect of structure on the mechanical behaviour. As a conclusion of this literature review we discuss the suitability of each method for practical modelling of the structure. Secondly, we present an original formulation to model the degradation of the structure at yield which is used in a new model for artificially structured soils (MASS) developed in the framework of Modified Cam Clay model. The model MASS is validated with the experimental results of this study given in Chapter 3. Finally, the suitability of the model for structured materials is assessed on naturally structured calcarenite.

## 4.2 Review of methods for the modelling of the structure

Several yield criteria have been used or proposed to model the elastic limit of structured soils (e.g. Roscoe et al., 1958; Roscoe and Burland, 1968; Matsuoka and Nakai, 1982; Lubliner et al., 1989; Lagioia et al., 1996), and most of them give satisfactory results for the yield loci. However, the difficulty for structured materials lies in the modelling of the destructuration at yield for hardening and softening. Different frameworks have been proposed to account for the structure in the mechanical behaviour at yield. We now present the approaches proposed for the modelling of the structure and its degradation in regard to their suitability for practical use.

### 4.2.1 Bounding surface theory

Several models have been proposed within the framework of bounding surface plasticity (Dafalias and Popov, 1975; Dafalias, 1986). This framework, based on the observation that there is no purely elastic stress path, allows plastic straining within the elastic domain using two surfaces (Figure 4.1). Pekau and Gocevski (1989) were amongst the first to propose a model for cemented sandy sediments based on the theory of bounding surface plasticity and using a non-associated flow rule with a closed yield surface. Cotecchia and Chandler (2000) introduced the Sensitivity framework to simulate the structure which is assumed to be made of a *stable* and a *metastable* components. Since then many models have been developed upon this framework to improve the modelling of destructuration and the relationship between change in sensitivity and plastic strain (e.g. Kavvas and Amorosi, 2000; Baudet and Stallebrass, 2004).

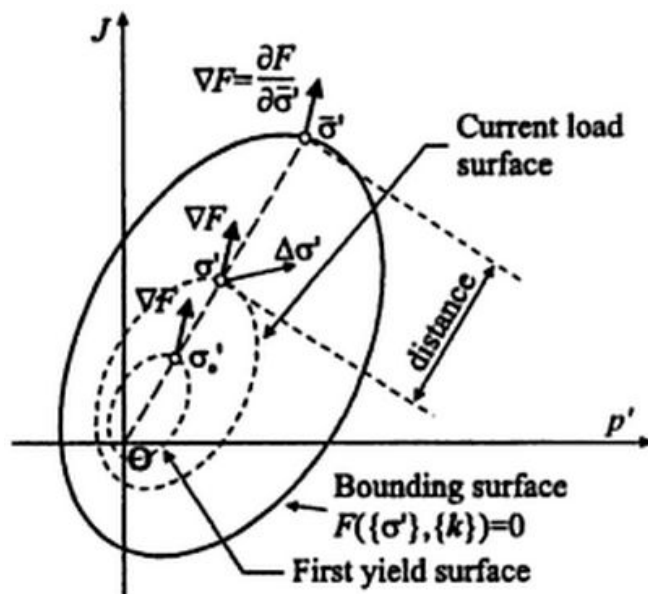


Figure 4.1: Schematic illustration of the bounding surface (Potts and Zdravkovic, 1999).

### 4.2.2 Structured soils as cohesive-frictional materials

Soil skeleton and structure can be seen as two different solids that can be considered separately. Such approach can be described by a two-element rheological model similar to the Kelvin-Voigt model. The overall response of the material at yield is obtained by superposition of the two behaviours (Liu et al., 2006).

As any model the coupling must respect the laws of thermodynamic (Salençon, 2002), which can lead to some difficulties in the formulation. Haeri and Hamidi (2009) and Tengattini et al. (2014) proposed two models for cemented granular materials based on thermomechanical considerations, but a large number of meaningless parameters were introduced. Vatsala et al. (2001) proposed a model based on the Modified Cam Clay (Roscoe and Burland, 1968) for the soil skeleton and another elasto-plastic model for the structure degradation (two springs in parallel, Figure 4.2a). However, this approach lacks of practicality since the mechanical behaviour of the structure cannot be assessed easily and requires advanced methods such as micro-indentation techniques. Chazallon and Hicher (1995, 1998) proposed a model coupling elasto-plasticity with a damage-type mechanism for destructuration (one spring and a sliding frictional element in parallel with a single spring, Figure 4.2b). The mechanical behaviour of the soil skeleton, modelled using Hujeux's model (Aubry et al., 1982; Hujeux, 1985), is coupled with an elastic damage model depending on the damage energy rate release. This elastic damage formulation verifies the Clausius-Duhem inequality (Chazallon and Hicher, 1998). The model gives a good agreement with the experimental results but the determination of some parameters requires calibration.

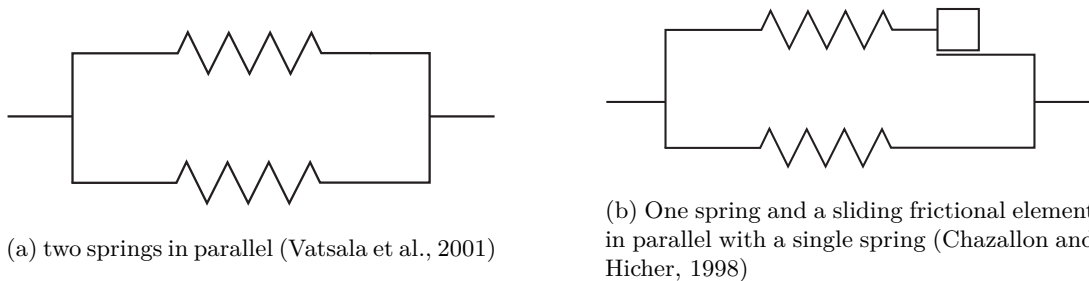


Figure 4.2: Rheological models used for the modelling of structured soils.

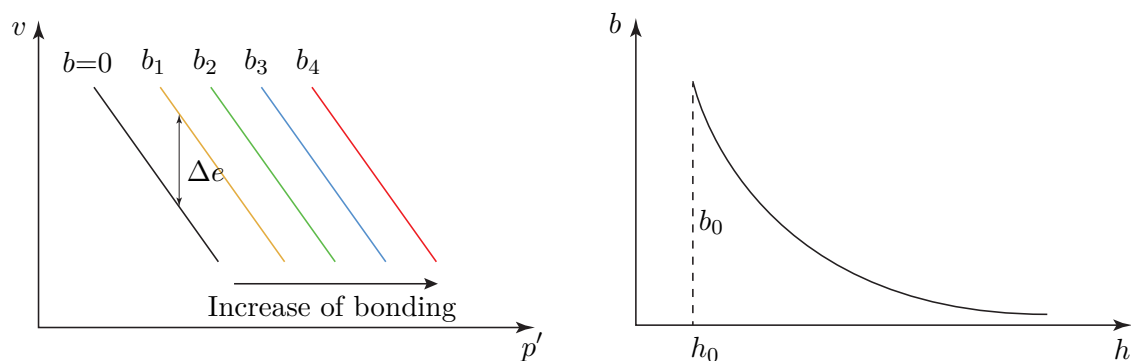
### 4.2.3 Plastic strain damage

Gens and Nova (1993) have proposed a general framework to account for the structure in natural or artificial materials based on the observations made by Leroueil and Vaughan (1990). The amount of structure in the soil is described using a quantitative variable  $b$  (Figure 4.3a) that is embedded in the elasto-plastic model chosen for the soil skeleton. Degradation is assumed to be due to plastic strains only, and the amount of structure decreases with the amount of plastic strain. The determination of this quantitative variable is therefore the key issue in this approach. This framework leads to simpler formulations with a smaller number of parameters compared to the other methods previously described.

As an example in their paper (Gens and Nova, 1993), the behaviour of the skeleton is described by the model given in Nova (1988), which is an enhancement of the Cam Clay

#### 4. A GENERAL FORMULATION FOR DEGRADATION IN STRUCTURED SOILS

model. However, these enhancements come at the cost of additional parameters whose physical meaning and determination are not straightforward such as the parameter  $h$  describing the damage (Figure 4.3b). The degradation of the structure starts with the development of plastic strains, referred to as damage. The model is successful in describing qualitatively the main features of structured soils, but the agreement with the experimental results was not conclusive. Several other models have proven the suitability of this approach to reproduce some of the key features observed in structured soils. The most common approach is to include the amount of the structure in the hardening rule; a large number of models (e.g. Lagioia and Nova, 1995; Liu and Carter, 2002; Nova et al., 2003; Arroyo et al., 2012) have been developed under this assumption using different elasto-plastic models (e.g. Roscoe et al., 1958; Roscoe and Burland, 1968; Matsuoka and Nakai, 1982; Lagioia et al., 1996).



(a) Virgin isotropic consolidation lines for materials with various degrees of bonding

(b) Reduction of bonding,  $b$ , with increasing damage,  $h$

Figure 4.3: Conceptual framework for bonded soils and weak rocks (Gens and Nova, 1993).

#### 4.2.4 Suitable approach for lime treated soils

The methods described above have very interesting features but not all of them are suitable for a practical use. The bounding surface theory gives satisfactory results but the resolution relies on mapping algorithm (Borja and Lee, 1990; Potts and Zdravkovic, 1999; Borja et al., 2001) which is an iterative and computationally expensive process. Moreover, the framework introduces several meaningless additional parameters whose determination requires calibration. Despite several interesting features, models developed in the framework of the boundary surface theory are rather descriptive than predictive. The second approach, which consists in considering the structure as a separate phase and using the superposition principle, is also interesting but the physical meaning of the parameters may not always be straightforward and require calibration.

Using a quantitative variable to describe the amount of structure appears to be a good trade-off between accuracy of the predictions and complexity of the model. Although this approach is known to introduce significant simplifications of the processes involved in the degradation, a lot of models have tried to use this framework to model the structure as a separate element as it was done by Chazallon and Hicher (1998). This has resulted in a large complexity of the formulations (e.g. Tamagnini et al., 2002; Nova et al., 2003; Arroyo et al., 2012) and has driven the formulation away from

a practical suitability.

Liu and Carter (2002) developed a simple approach in the framework of the Modified Cam Clay (Roscoe and Burland, 1968). It has been used as a framework for several other models because of its simplicity (e.g. Horpibulsuk et al., 2010a; Suebsuk et al., 2010). The original form introduces only 3 additional parameters, two of which have a physical meaning and can be determined from a single isotropic compression test. This kind of formulation is therefore easy-to-use in practice and very interesting for an industrial purpose as a predictive tool. The original formulation gives acceptable agreement with the experimental results but fails to model some of the typical features of structured soils such as the residual additional void ratio  $\Delta e_r$ , which shows that the influence of the structure at yield on the mechanical behaviour is not properly modelled. Some enhancements have been developed to account for microstructural considerations (Horpibulsuk et al., 2010b) or the bounding surface theory (Suebsuk et al., 2011). Unfortunately they come at the cost of additional parameters that are difficult to assess.

We now present the original framework of the Structured Cam Clay model and discuss its suitability for modelling of lime treated soils.

### 4.3 Structured Cam Clay model

The approach proposed by Liu and Carter (2002) is interesting from a conceptual point of view. The formulation of the degradation relies only on two parameters that makes it very suitable for a practical use. The model accounts for the amount of structure using the additional void ratio at yield  $\Delta e$  compared to the destructured state, the soil skeleton behaviour being described by the Modified Cam Clay model (Figure 4.4). While the stress state lies within the yield surface the material behaves elastically and the structure is assumed to remain intact. Once plastic strains appear the structure is assumed to experience degradation. We now present the pros and cons of this framework for practical modelling of lime treated soils.

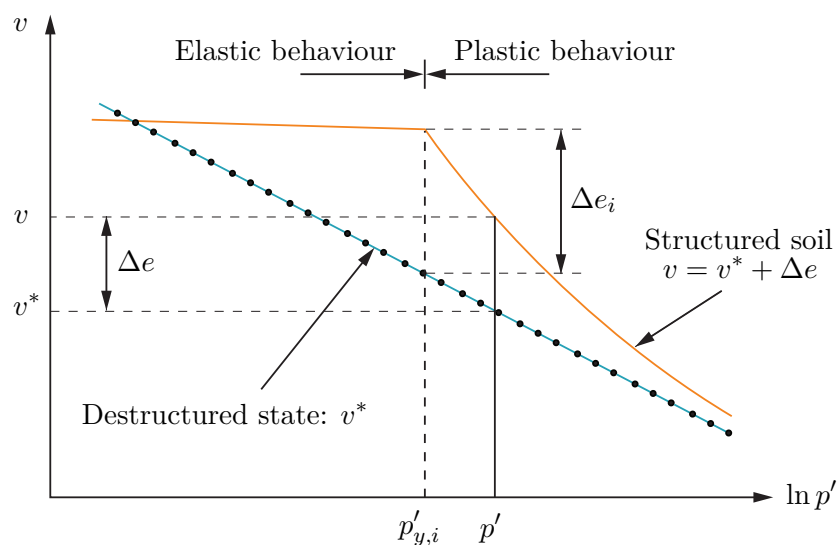


Figure 4.4: Idealization of the isotropic compression behaviour of reconstituted and structured soils. After (Liu and Carter, 2002).

#### 4. A GENERAL FORMULATION FOR DEGRADATION IN STRUCTURED SOILS

**Influence of structure on virgin isotropic compression** In the Structured Cam Clay model, the additional void ratio  $\Delta e$  compared to the destructured state is used as a quantitative variable to assess the amount of structure in the soil:

$$v = v^* + \Delta e \quad (4.1)$$

where  $v^*$  is the void ratio of the destructured state given by the equation of the normal compression line (ncl) (Equation (2.38b)), and  $\Delta e$  is the additional void ratio induced by the soil structure.

Liu and Carter (2002) proposed the following formulation to model the degradation of structure at yield:

$$\forall p' \geq p'_y \quad \Delta e = \Delta e_i \left( \frac{p'_{y,i}}{p'} \right)^b \quad (4.2)$$

where  $\Delta e_i$  is the additional voids ratio at  $p' = p'_{y,i}$ , and  $b$  is the *destructuring index*, a parameter quantifying the rate of destructuring. The value of  $b$  depends on the soil type and structure. Usually, we have  $b \geq 1$  for soft structured clays and  $b < 1$  for stiff clays.

**Yield surface** The presence of structure is assumed to lead to an increase of the yield stress  $\Delta p'_y$  only. The equation of the yield criterion is therefore identical to the Modified Cam Clay and is given by

$$f(\underline{\sigma}, p_0, \kappa') = q^2 - M^2 p' (p'_0 - p') = 0 \quad (4.3)$$

Originally developed for naturally structured soils, the critical state of the structured and destructured state is assumed to be the same. In this case, the reference state is obtained by destructuration of the natural material in which soil particles have already experienced the process of cementation. In the case of an artificially structured soil this assumption must be verified since the reference (untreated soil) has not experienced the chemical reactions involved in lime treatment which is likely to alter the soil particles and the fabric.

**Volumetric deformations** From Equations (4.1) and 4.2 the volumetric deformations accounting for the structure are given by

$$\delta \varepsilon_p = \underbrace{\frac{\kappa}{v} \frac{\delta p'}{p'}}_{\delta \varepsilon_p^e} + \underbrace{\frac{(\lambda - \kappa)}{v} \frac{\delta p'_0}{p'_0}}_{\delta \varepsilon_p^p} + b \Delta e \frac{\delta p'_0}{v p'_0} \quad (4.4)$$

In this formulation the degradation is only due to  $p' = I_1/3$ , the spherical part of the stress tensor. However, it is fair to assume that shear is also involved in the process of degradation. For these reasons, the authors have introduced an additional term in

Equation (4.4) to account the effects of shear stress on the degradation:

$$\delta\varepsilon_p = \frac{\kappa}{v} \frac{\delta p'}{p'} + \frac{(\lambda - \kappa)}{v} \frac{\delta p'_0}{p'_0} + b\Delta e \underbrace{\left( \frac{M}{M - \eta} \right)}_{\text{Shear}} \frac{\delta p'_0}{vp'_0} \quad (4.5)$$

with  $\eta = q/p'$  the shear stress ratio.

**Flow rule** The Structured Cam Clay model (SCCM) assumes that structured material follows an associated flow rule and therefore  $f \equiv g$ . Therefore, the SCCM and MCC should follow the same flow rule given by:

$$\frac{\delta\varepsilon_p^p}{\delta\varepsilon_q^p} = \frac{\partial g / \partial p'}{\partial g / \partial q} = \frac{M^2 - \eta^2}{2\eta} \quad (4.6)$$

which is in contradiction with Equation (4.5), the influence of shear strains not being reflected in the flow rule. To account for the degradation of the structure in the flow rule, the authors proposed a modified formulation:

$$\frac{\delta\varepsilon_p^p}{\delta\varepsilon_q^p} = \frac{\partial g / \partial p'}{\partial g / \partial q} = \frac{M^2 - \eta^2}{2 \underbrace{(1 - \omega\Delta e)}_{0 < \cdot \leq 1} \eta} \geq \frac{M^2 - \eta^2}{2\eta} \quad (4.7)$$

with  $\omega$  a parameter to account for the structure in the flow rule to be determined. This parameter is a constant, independent from the stress state, and is determined by calibration with experimental results. This leads to a non-associated flow rule (Figure 4.5), although the stress-strain relationship is calculated assuming an associated flow rule. Moreover, the compliance matrix (Equation (2.54)) is not symmetric any more, despite using the same equations for the yield surface and plastic potential.

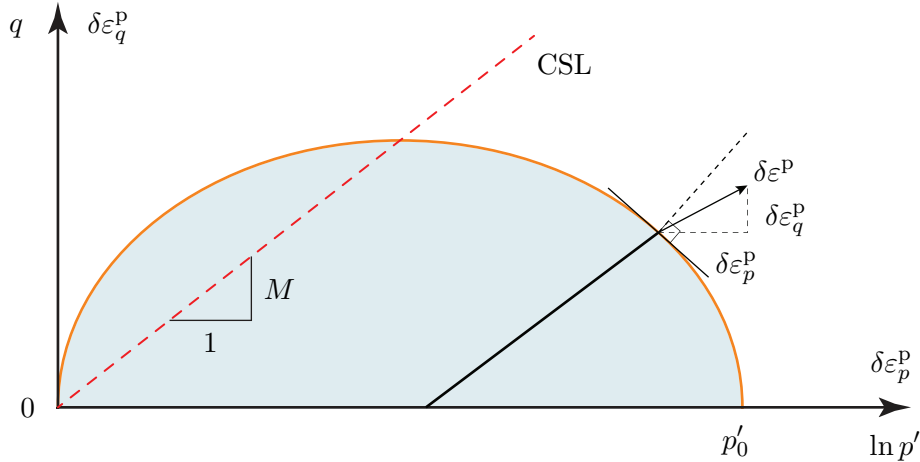


Figure 4.5: Non-associated flow rule for the Structured Cam Clay model

The model gives a reasonable agreement with the experimental data but fails to model some key features than can be observed in lime treated materials (e.g. residual void ratio at large effective mean stress). Also, the formulation of the flow rule may lead, in some cases, to the contraction of samples experiencing softening ( $\sigma'_3 = 294$  kPa in Figure 4.6). However, the physical meaning of the parameters  $\Delta e_i$  and  $b$  is an

interesting feature and gives a practical formulation.

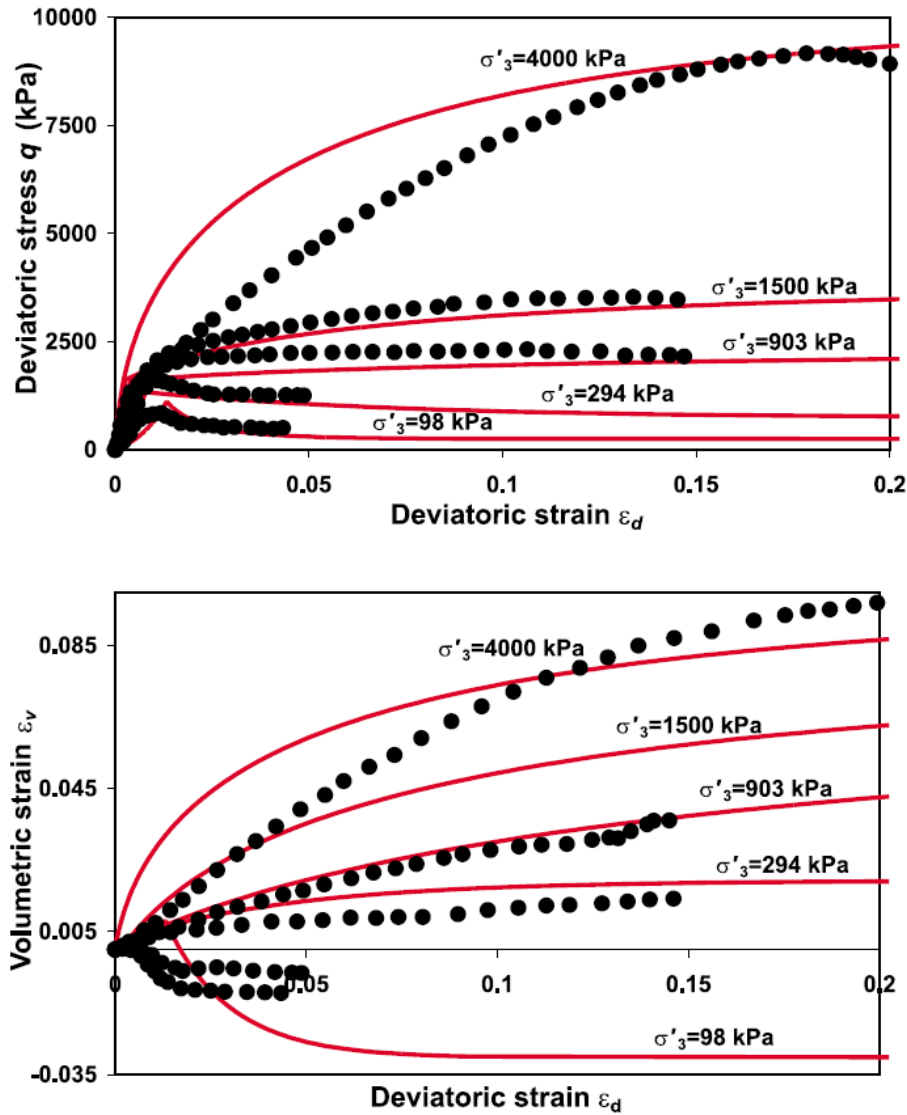


Figure 4.6: Capabilities of the Structured Cam Clay for modelling of structured materials. Sample might experience contraction behaviour at softening. From Liu and Carter (2002).

Before presenting the constitutive model developed in the framework of the Structured Cam Clay, we proceed to a rigorous and exhaustive study of the features in common between naturally and artificially structured soils to motivate the choice of the assumptions made in the model. This analysis will later be used as a check-list to verify the success of the model to describe the main features of structured soils and of the degradation of the structure at yield.

#### 4.4 Features of structured soils

The mechanical behaviour of naturally and artificially structured material has been extensively studied (Leroueil and Vaughan, 1990; Burland et al., 1996; Malandraki and Toll, 2001; Cuisinier et al., 2008, 2011; Consoli et al., 2011; Oliveira, 2013) and some specific features have been identified. Several studies have pointed out that naturally and artificially structured soils have a similar mechanical behaviour. In this section,



we identify the key features common to naturally and artificially structured soils that should be properly reproduced by a model.

#### 4.4.1 Naturally structured soils

It has been shown that naturally structured soils have a higher yield stress compared to the destructured state (Burland et al., 1996), the latter being usually considered as the reference state. For the same stress state, a higher yield stress leads to a higher void ratio at yield compared to the destructured state, called the additional void ratio  $\Delta e$ . Once plastic deformations take place, one can observe that the additional void ratio decreases. Depending on the material, the additional void ratio can quickly or slowly decrease until the material reaches a normal compression line (ncl), which can correspond to the ncl of the reference state ( $ncl_d$ ), or a different one, parallel to the reference ncl but vertically translated along the  $v$  axis ( $ncl_r$ ) (Baudet and Stallebrass, 2004; Callisto and Rampello, 2004; Suebsuk et al., 2011). More generally, 4 modes of degradation can be identified (Figure 4.7):

**Mode 1:** Destructuration takes place immediately at yield. The additional void ratio progressively decreases until it converges toward the destructured state (Lagioia and Nova, 1995; Yong and Nagaraj, 1977).

**Mode 2:** Destructuration takes place immediately at yield, but it does not converge toward its destructured state. A different ncl appears parallel to the destructured state, but a residual additional void ratio still remains (Rampello and Callisto, 1998; Burland et al., 1996).

**Mode 3:** No significant destructuration is observed immediately after yield. The process of degradation is initiated later on for a higher effective mean stress and the additional void ratio completely disappears (Callisto and Rampello, 2004).

**Mode 4:** No destructuration is observed immediately after yield. The process of degradation is initiated later on for a higher effective mean stress. However, a residual additional void ratio remains (Rotta et al., 2003).

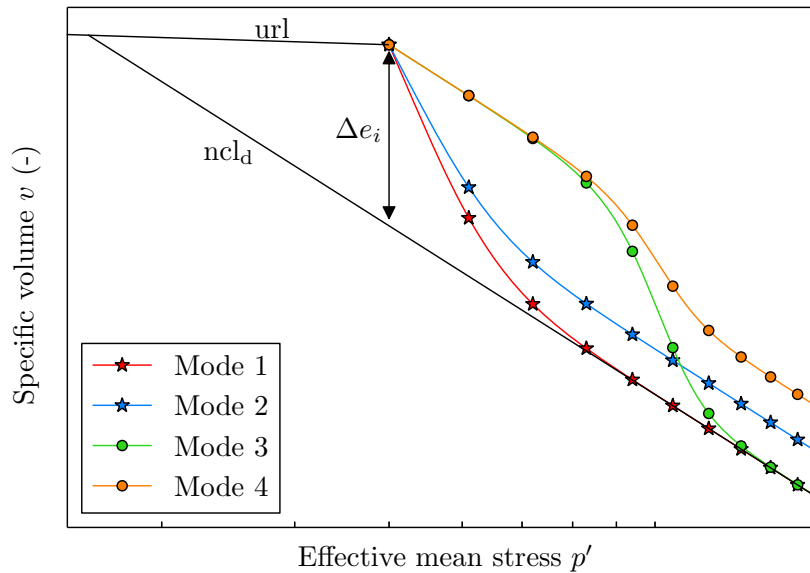


Figure 4.7: The four different modes of destructuration in structured soils –  $ncl_d$ : Normal compression line of the destructured state,  $url$ : Unloading-reloading line.

Additionally, the volumetric behaviour of naturally structured soils was compared with the destructured state by Leroueil and Vaughan (1990) on heavily overconsolidated specimens from drained triaxial test results. They identified two different mechanisms taking place. While the maximum rate of dilation was measured before the peak of the deviatoric stress for the destructured soil, it was observed after the peak of the deviatoric stress for structured soils. This is due to the structure, which binds soil particles together. To allow the particles to move freely, the structure has to be degraded first to release particles (Leroueil and Vaughan, 1990).

#### 4.4.2 Lime treated soils

Several studies have shown that addition of lime leads to an increase of the yield stress compared to the untreated state (Tremblay et al., 2001; Ahnberg, 2007). As for naturally structured soils, the additional void ratio appears to decrease at yield, i.e. the degradation of the artificial structure takes place. During the experimental program (Chapter 3) we have assessed the mechanical behaviour of a lime treated silt under isotropic loading (Figure 4.8). It can be seen that the mode of degradation depends on the amount of lime. For 0.5% in lime, the additional void ratio completely disappears at high stress states (Mode 3), when it is not the case for 1% lime treated specimens (Mode 4). This latter reaches a different  $ncl$  compared to the untreated specimen.

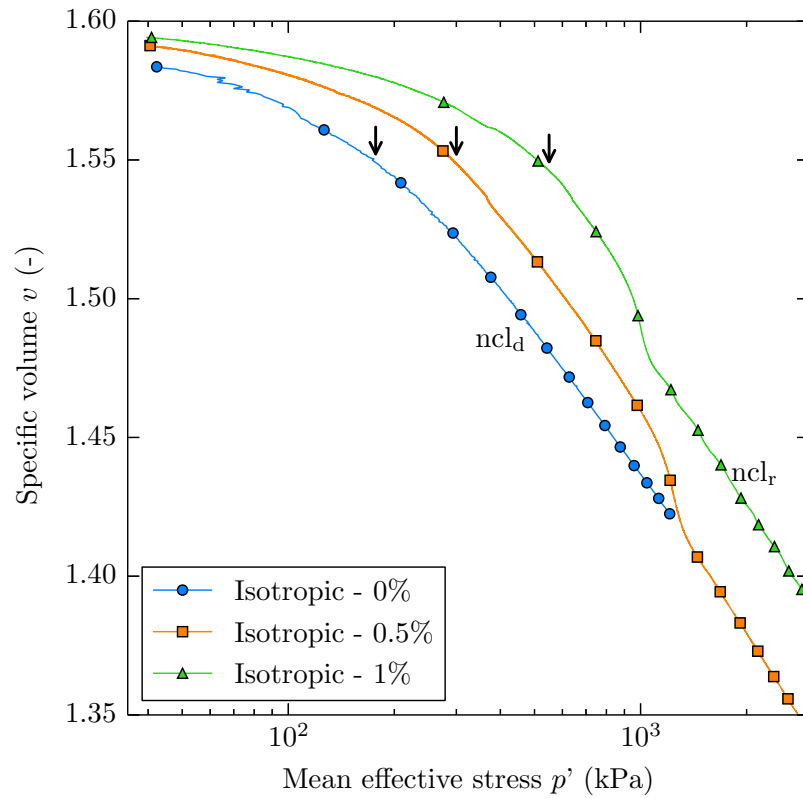
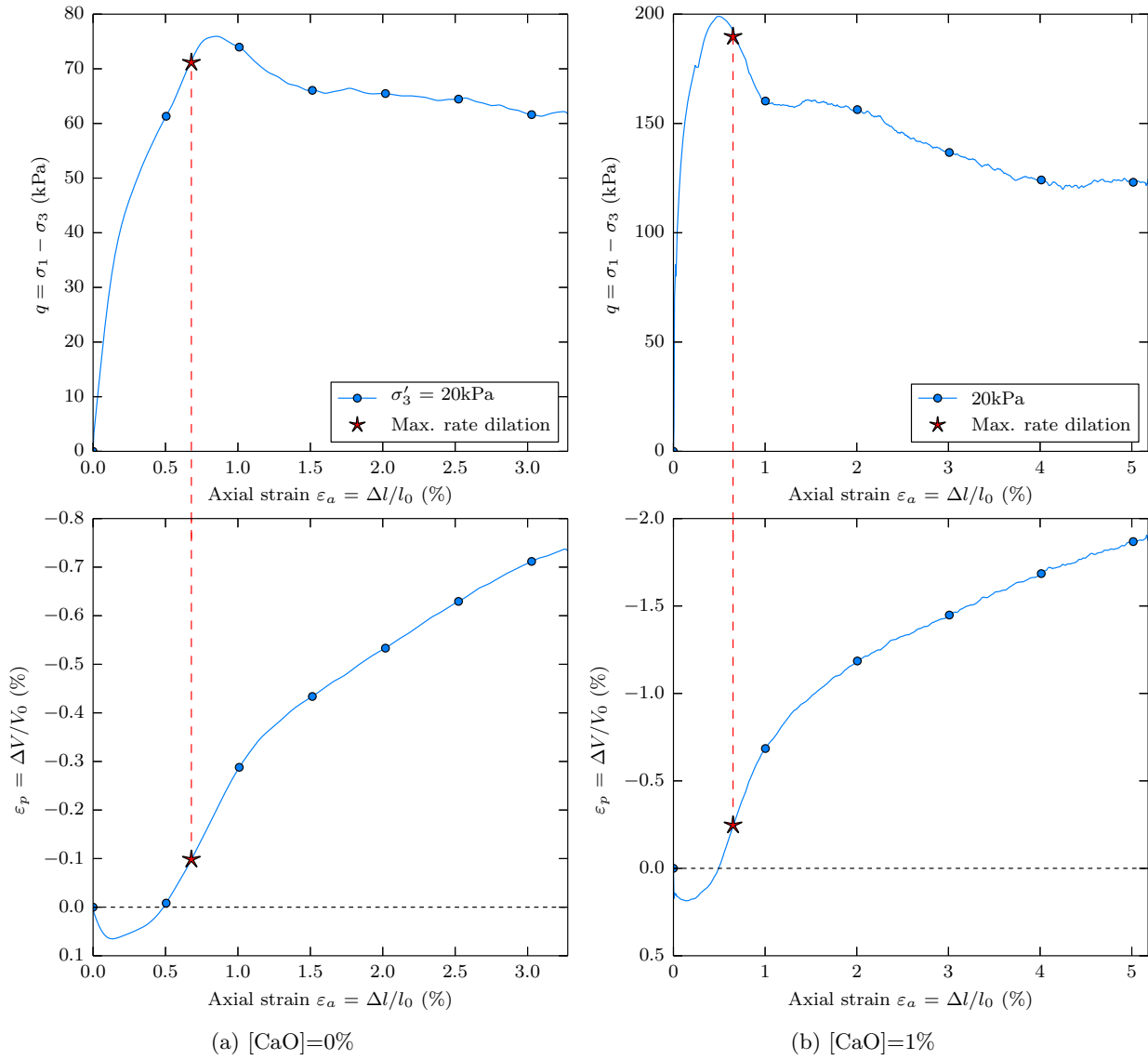


Figure 4.8: Isotropic consolidation curves obtained from specimens of silt treated at 0.5% and 1% in lime – Arrows mark the yield stress  $p'_y$ ,  $ncl_d$ : Normal compression line of the destructured state,  $ncl_r$ : Normal compression line of the residual state.

The maximum rate of dilation at shear for specimens experiencing softening also appears after the peak for artificially structured soils, which indicates that the same kind of mechanism is taking place. This common feature was pointed out by Leroueil and Vaughan (1990), and was also observed for the lime treated specimens from the current study (Figure 4.9).

#### 4. A GENERAL FORMULATION FOR DEGRADATION IN STRUCTURED SOILS



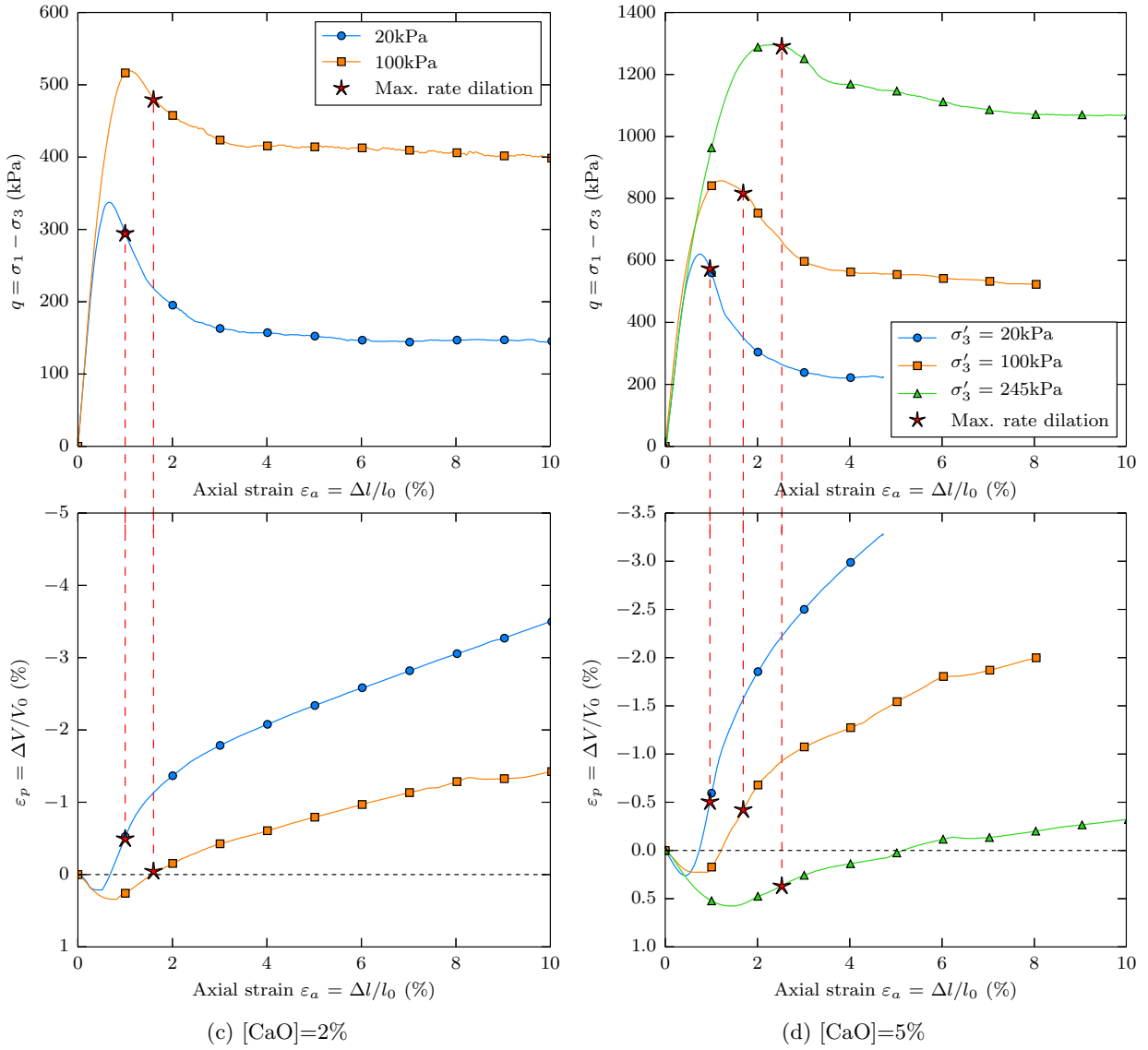


Figure 4.9: Drained triaxial results on (a) untreated and (b) lime treated soils – Stars mark the location where the rate of dilation is maximum.

The influence of a lime treatment on the cohesion and the friction angle has been studied by several authors (Wissa, 1965; Balasubramaniam et al., 2005). Both cohesion and friction angle appear to increase with the amount of lime. The slope of the critical state line is directly related to the friction angle, and the increase of cohesion, which increases the tensile strength, has an influence on the shape of the yield function. Therefore, in the framework the critical state theory, these features should be accounted for in the model.

#### 4.4.3 Summary

Based on the previous observations, a model for lime treated soils might be suitable for naturally structured soils, and therefore should be able to reproduce the four modes of destructuration and account for the following features:

- The cohesion increases following pozzolanic reactions,
- The yield stress increases for lime treated soils compared to the reference state,

## 4. A GENERAL FORMULATION FOR DEGRADATION IN STRUCTURED SOILS

- At yield, there exists an additional void ratio compared to the reference state,
- At yield, degradation of the structure takes place, which follows one of the four modes identified previously,
- Overconsolidated specimens at shear show a maximum rate of dilation after the peak, describing the degradation of the structure,
- The friction angle is modified due to the effects of the chemical reactions on the texture of the soil, and therefore the critical state as well.

### 4.5 Theoretical framework of the model

The model proposed in this chapter was developed in the framework of the Modified Cam Clay model (MCC) to model the key features of lime treated soils previously identified. We introduced only parameters with a physical meaning that can be determined from isotropic compression tests. We present in this section a new formulation to model the four modes of degradation in structured soils under isotropic loading. This will then be used as a hardening rule for the determination of the compliance matrix.

#### 4.5.1 Modelling the structure and its degradation under isotropic loading

To model the degradation of the structure under isotropic loading, we propose the framework given in Figure 4.10. We introduce the *primary yield stress*  $p_y^I$ , which corresponds to the apparition of plastic deformations. To situate the stress states for which the degradation of the structure takes place (hatched area in Figure 4.10), we also introduce the *degradation stress*  $p_y^{II}$ . In the case of an immediate degradation of the structure at yield (modes 1 & 2 in Figure 4.7), which can happen for some structured soils, we have  $p_y^{II} = p_y^I$ . The additional void ratio  $\Delta e_i$  at  $p_y^I$  quantifies the initial additional void ratio at yield.  $\Delta e_c$  is measured at an effective mean stress above which the additional void ratio remains constant ( $p' \gg p_y^{II}$ ). By setting the parameters as given in Table 4.1, this framework is capable of describing the four modes of degradation.

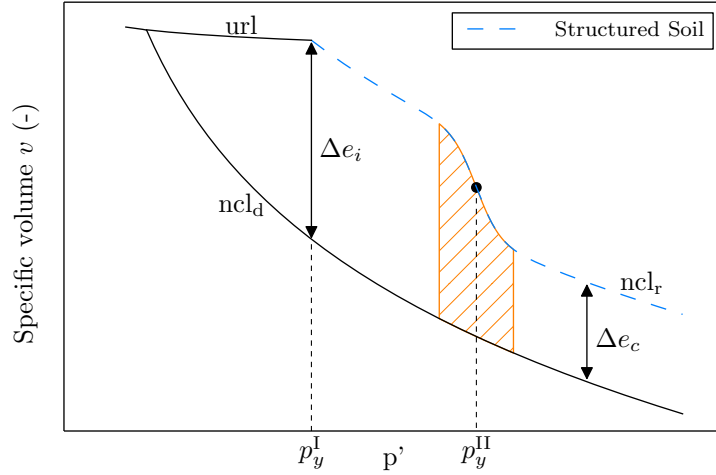


Figure 4.10: General framework of the degradation of structured soils –  $\Delta e_i$ : Initial additional void ratio,  $\Delta e_c$ : Residual additional void ratio,  $p_y^I$ : Primary yield stress,  $p_y^{II}$ : degradation stress, hatched area: degradation of the structure,  $ncl_d$ : Normal compression line of the destructured state,  $ncl_r$ : Normal compression line of the residual state, url: Unloading-reloading line.

Table 4.1: Conditions on the parameters  $p_y^{II}$  and  $\Delta e_c$  for the 4 modes of degradation

Parameters	Values			
	Mode 1	Mode 2	Mode 3	Mode 4
$p_y^{II}$	$p_y^I$	$p_y^I$	$> p_y^I$	$> p_y^I$
$\Delta e_c$	0	$> 0$	0	$> 0$

In this study, the structure is quantified through the additional void ratio in comparison to the  $ncl_d$  and is assumed to be made of two components. The first one, referred to as the *available structure*, corresponds to the part of structure that will be available during the process of destructuration ( $\Delta e_i - \Delta e_c$ ). The second one, referred to as the *residual structure*, corresponds to the persisting additional void ratio at high effective mean stress ( $\Delta e_c$  at  $p' \gg p_y^I$ ). The latter can be the consequences of chemical reactions, e.g. a lime treatment, which leads to a permanent modification of the fabric of the soil (cf. Chapter 3).

### Mathematical Formulation

To model these four mechanisms, a flexible formulation using all the parameters previously introduced is required. Richards's equation (Richards, 1959) for the sigmoid provides many degrees of freedom to control the shape of the function. This function is frequently used for the modelling natural phenomena where there exists a threshold above which a process is activated, in this case the degradation. This equation can be written as follows:

$$\forall p' \in [p_y^I, +\infty[ \quad \pi(p') = 1 - \frac{1}{1 + e^{-\beta(p' - p_y^{II})}} \quad (4.8)$$

#### 4. A GENERAL FORMULATION FOR DEGRADATION IN STRUCTURED SOILS

where  $p_y^{\text{II}}$  [Pa] corresponds to the position of the inflection point ( $\pi''(p_y^{\text{II}}) = 0$ ) and describes the stress state for which the degradation occurs (hatched area in Figure 4.10), and  $\beta$  [ $\text{Pa}^{-1}$ ] describes the rate of degradation.

Therefore, we have

$$\forall p' \in \mathbb{R} \quad 0 \leq \pi(p') \leq 1 \quad (4.9)$$

##### Scaling of $\pi$

The function  $\pi$  is scaled to ensure that  $\forall \beta, \forall p_y^{\text{II}} \quad \pi(p_y^{\text{I}}) = 1$ , which leads to the following final formulation:

$$\forall p' \in \left[ p_y^{\text{I}}, +\infty \right[ \quad \pi(p') = \frac{e^{\beta p_y^{\text{I}}} + e^{\beta p_y^{\text{II}}}}{e^{\beta p'} + e^{\beta p_y^{\text{II}}}} \quad (4.10)$$

which verifies  $\pi(p_y^{\text{I}}) = 1$  and  $\lim_{p' \rightarrow +\infty} \pi(p') = 0$ .

The ability to control the rate of degradation at yield of this formulation is demonstrated in Figure 4.11. It can be seen that the function  $\pi$  can either slowly decrease with a low  $\beta$  or quickly with a high  $\beta$  as  $p'$  gets close to  $p_y^{\text{II}}$ .

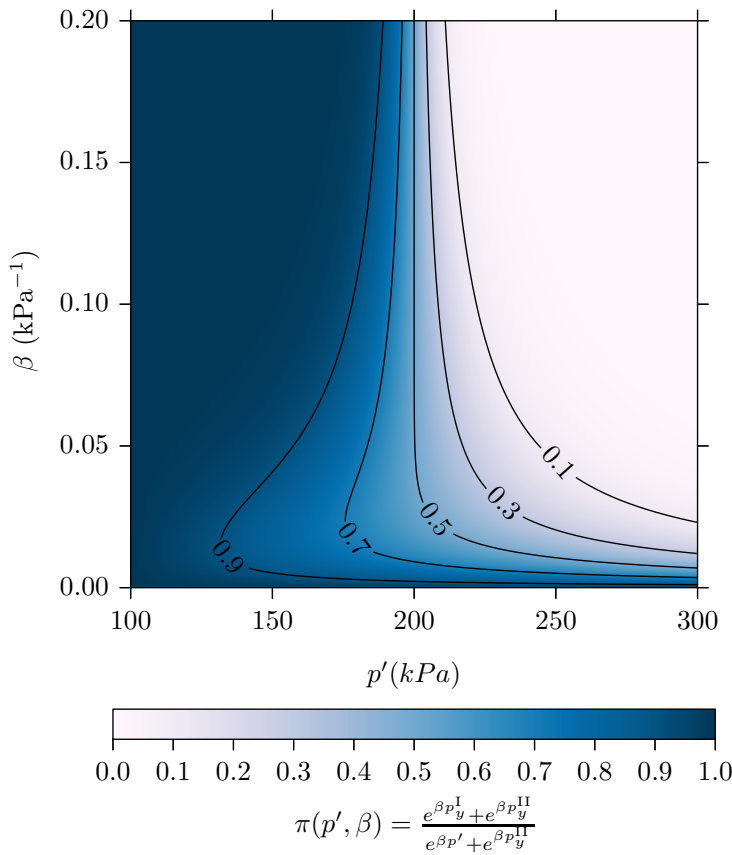


Figure 4.11:  $\pi$  values as a function of  $p_y^{\text{II}}$  and  $\beta$  –  $p_y^{\text{I}}=100$  kPa,  $p_y^{\text{II}}=200$  kPa.

##### Relationship between the specific volume and the effective mean stress for structured soils

The presence of structure can be accounted for in the relationship between the specific volume and the effective mean stress ( $v : p'$  relationship) using the following



general formulation:

$$\forall p' \in \mathbb{R}_+^* \quad v(p') = N_\lambda - \lambda \ln(p') + \Delta e(p') \quad (4.11)$$

with  $N_\lambda$  the intercept on the reference normal compression line  $\text{ncl}_d$  and  $\lambda$  the slope of the reference ncl in  $v : \ln(p')$  plane.

Using the function  $\pi$  (Equation (4.10)), the equation for the additional void ratio is given by:

$$\forall p' \in [p_y^I, +\infty[ \quad \Delta e(p') = (\Delta e_i - \Delta e_c) \cdot \left[ \frac{e^{\beta p_y^I} + e^{\beta p_y^{II}}}{e^{\beta p'} + e^{\beta p_y^{II}}} \right] + \Delta e_c \quad (4.12)$$

which fulfils the boundary value problems:

$$\Delta e(p') = \begin{cases} \Delta e_i & \text{if } p' = p_y^I \\ \Delta e_c & \text{if } p' \rightarrow +\infty \end{cases} \quad (4.13)$$

Introducing Equation (4.12) in Equation (4.11) gives the final equation of the specific volume for structured soils at yield:

$$\forall p' \in [p_y^I, +\infty[ \quad v_s(p') = N_\lambda - \lambda \ln(p') + (\Delta e_i - \Delta e_c) \cdot \left[ \frac{e^{\beta p_y^I} + e^{\beta p_y^{II}}}{e^{\beta p'} + e^{\beta p_y^{II}}} \right] + \Delta e_c \quad (4.14)$$

### Determination of $\beta$

$\beta$  can be directly determined from the results of an isotropic compression test. Practically,  $\beta$  is related to the gradient  $\xi$  on the  $v : p'$  curve at  $p' = p_y^{II}$  (Figure 4.12). For consistency and stability, the function  $v_s$  for the specific volume in the  $v : p'$  plane must be strictly monotonic decreasing on  $[p_y^I, +\infty[$ , which imposes  $\beta \geq 0$ .

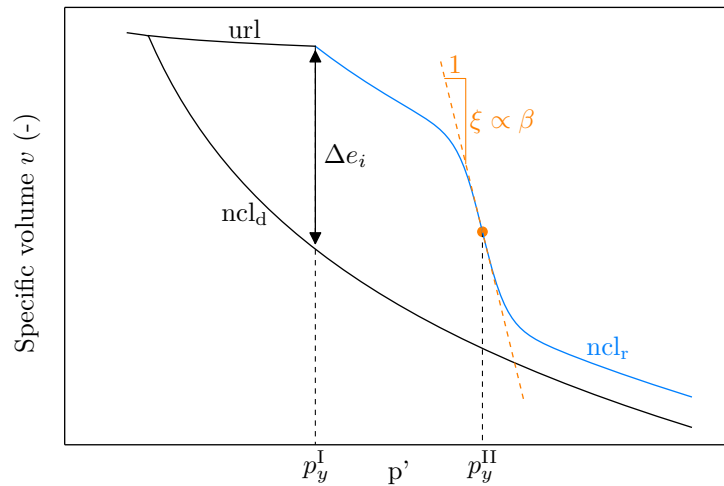


Figure 4.12: Physical meaning of  $\beta$  –  $\text{ncl}_d$ : Normal compression line of the destructured state,  $\text{ncl}_r$ : Normal compression line of the residual state,  $\text{url}$ : Unloading-reloading line.

Calling  $\xi$  the gradient of the specific volume curve at  $p' = p_y^{II}$ , the appropriate value

#### 4. A GENERAL FORMULATION FOR DEGRADATION IN STRUCTURED SOILS

for  $\beta$  is obtained by solving the following equation:

$$\left(\frac{dv}{dp'}\right)_{p'=p_y^{\text{II}}} = \xi \quad \Leftrightarrow \quad -\frac{1}{4} \left(1 + e^{\beta(p_y^{\text{I}} - p_y^{\text{II}})}\right) \times \beta(\Delta e_i - \Delta e_c) - \frac{\lambda}{p_y^{\text{II}}} = \xi \quad (4.15)$$

There is no analytical solution to this equation, known as the Lambert W function, due to the non-linearity in  $\beta$ . However, this equation can be solved graphically or numerically using methods such as the Newton-Raphson algorithm (Corless et al., 1996).

##### Suitability of the formulation

The  $v : p'$  relationship (Equation 4.14) is used to demonstrate the ability of the formulation to describe the four modes (Figure 4.13). Parameters used for the simulations are given in Table 4.2. The influence of the parameters  $\beta$  (Figure 4.14) and the degradation stress  $p_y^{\text{II}}$  (Figure 4.15) is assessed and the case  $p_y^{\text{I}} = p_y^{\text{II}}$  is considered in Figure 4.16.

Figure 4.14 shows that it is possible to describe the mode 3. Changing the value of  $\beta$  permits to achieve different rates of degradation. In this figure, a nonzero  $\Delta e_c$  was chosen ( $\Delta e_c > 0$ ), but mode 4 can be achieved by setting  $\Delta e_c = 0$ . The influence of  $p_y^{\text{II}}$  is shown in Figure 4.15. One can see that this parameter controls the initiation of the process of degradation, and is successful in describing modes 2 and 4. As previously, modes 1 and 3 can be achieved by setting  $\Delta e_c = 0$ . Finally, the case  $p_y^{\text{I}} = p_y^{\text{II}}$  is considered in Figure 4.16. This case corresponds to an immediate loss of structure at yield. This case does not lead to any instabilities of the formulation.

Table 4.2: Model parameters used for simulations of the four modes in Figure 4.13

Mode	$p_y^{\text{I}}$ (kPa)	$p_y^{\text{II}}$ (kPa)	$\Delta e_i$	$\Delta e_c$	$\beta$ (kPa <sup>-1</sup> )
Mode 1	600	600	0.104	0.0	0.025
Mode 2	600	600	0.104	0.026	0.02
Mode 3	600	900	0.104	0.0	0.025
Mode 4	600	900	0.104	0.052	0.02

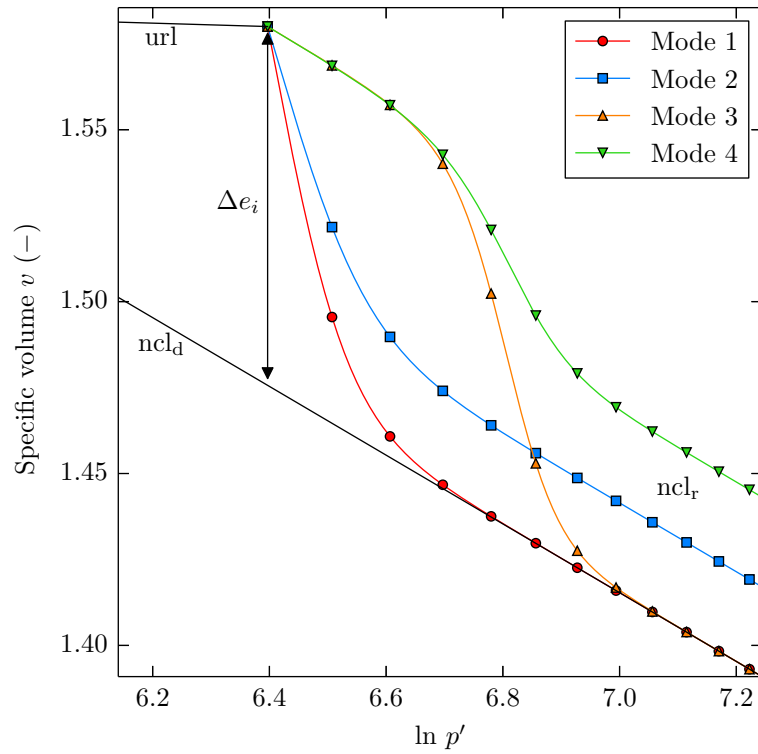


Figure 4.13: Possibility of the formulation to model the four modes –  $ncl_d$ : Normal compression line of the untreated state,  $url$ : Unloading-reloading line.

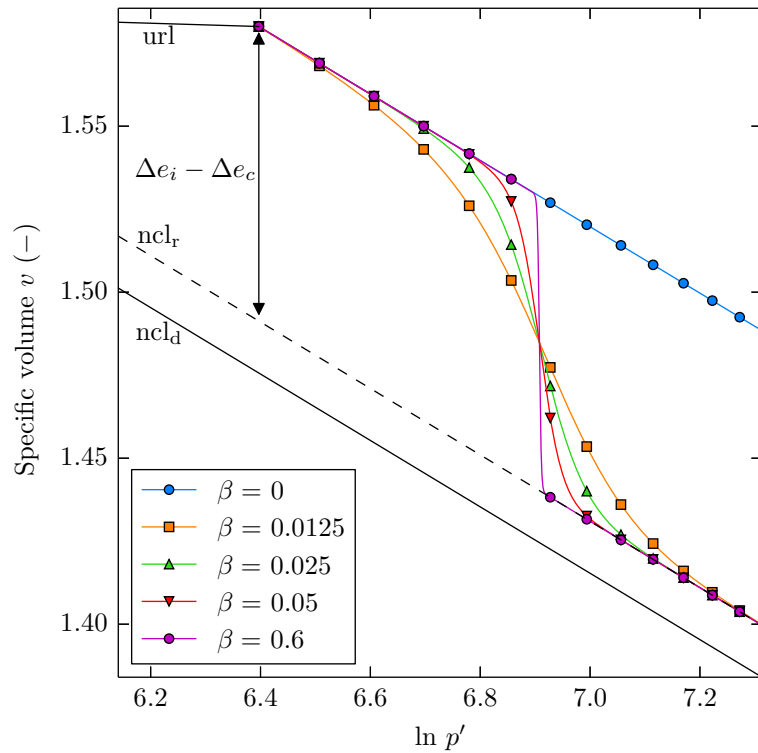


Figure 4.14: Influence of  $\beta$ :  $p_y^I = 600$  kPa,  $p_y^{II} = 1000$  kPa,  $\Delta e_c > 0$  – Mode 4.

#### 4. A GENERAL FORMULATION FOR DEGRADATION IN STRUCTURED SOILS

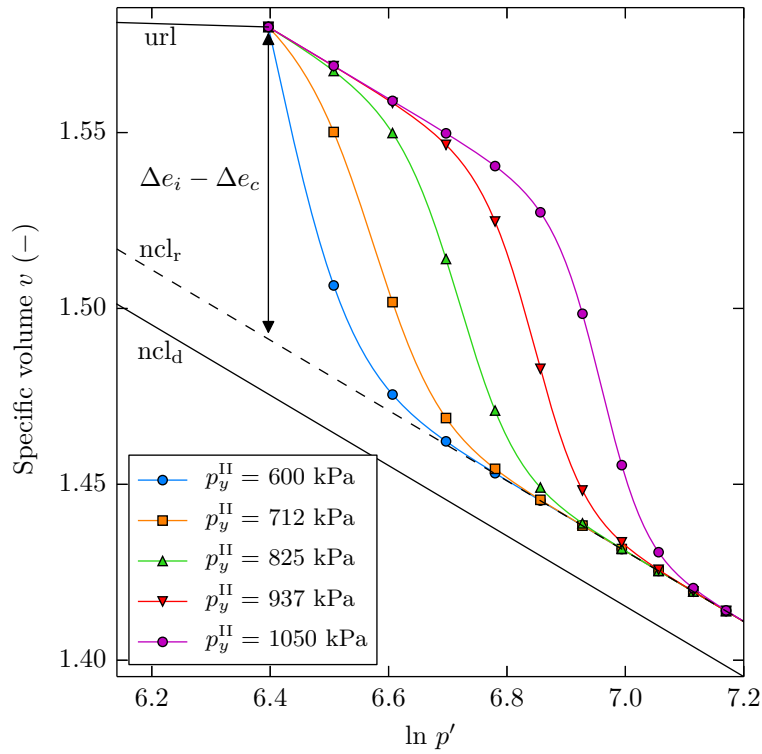


Figure 4.15: Influence of  $p_y^{\text{II}}$ :  $p_y^{\text{I}} = 600$  kPa,  $\beta = 0.025$ ,  $\Delta e_c > 0$  – Modes 2 and 4.

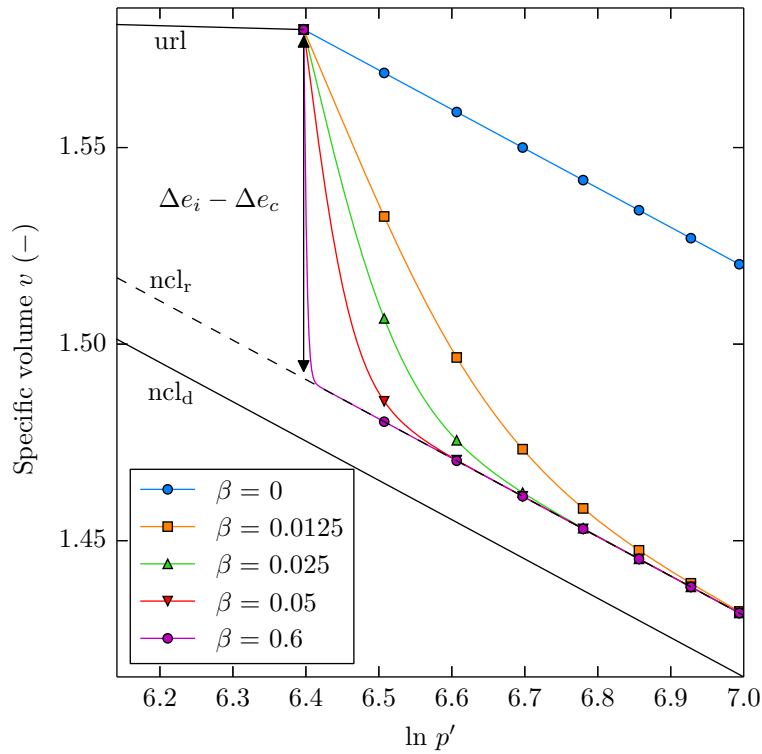


Figure 4.16: Influence of  $\beta$ :  $p_y^{\text{II}} = p_y^{\text{I}} = 600$  kPa,  $\Delta e_c > 0$  – Mode 2.

#### 4.5.2 Yield function $f$

The addition of lime leads to an increase of the cohesion and the friction angle compared to the untreated soil. Therefore, the equation of the MCC for the yield function  $f$  is not sufficient in its original form. One way to account for the increase of

cohesion is to consider it as an increase of the tensile strength. This can be modelled by expanding the yield function in the negative stress domain (Figure 4.17). The parameter  $p_b$  is introduced to control the expansion of the yield function due to the increase of the cohesion and is directly obtained from the equation of the CSL. The critical state line does not necessarily pass through the origin anymore.

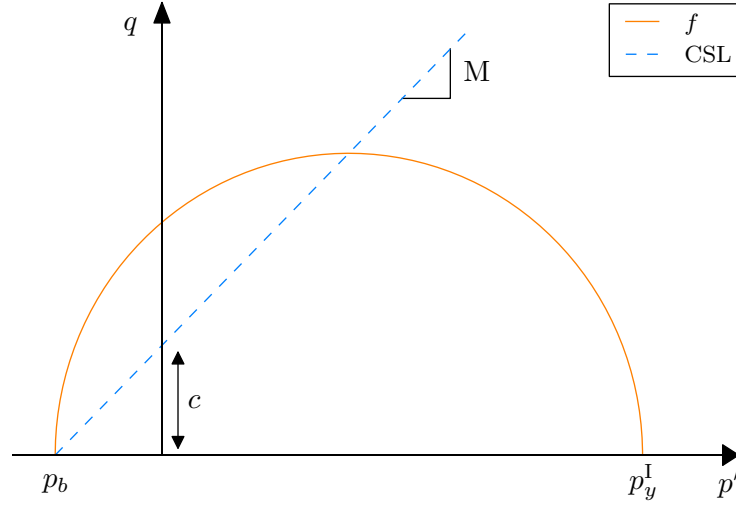


Figure 4.17: Theoretical yield function for lime treated soils.

The equation chosen for the yield function can therefore be expressed as:

$$f \equiv q^2 + M^2(p' - p_y^I)(p' - p_b) \equiv 0 \quad (4.16)$$

### 4.5.3 Plastic potential $g$

The choice of the formulation for the plastic potential  $g$  is a major issue in the constitutive modelling of soils. The use of non-associated potentials comes at the cost of several additional parameters with, in most of the cases, no straightforward physical meaning and whose values can rarely be determined from experimental results. This study aims to develop a model based on meaningful parameters determined from classic experimental tests. To this end, this model assumes that lime treated materials follow an associated flow rule and therefore

$$g \equiv f \quad \Rightarrow \quad g \equiv q^2 + M^2(p' - p_y^I)(p' - p_b) \quad (4.17)$$

which leads to the following flow rule for lime treated materials:

$$\frac{\delta \varepsilon_p^P}{\delta \varepsilon_q^P} = \frac{\partial g / \partial p'}{\partial g / \partial q} = \frac{M^2(p' - p_b)}{2p'\eta} - \frac{p'\eta}{2(p' - p_b)} \quad (4.18)$$

with  $\eta = q/p'$ . The suitability of this hypothesis will be verified during the model evaluation in Section 4.7.1.

#### 4.5.4 Summary of the model parameters

Using the sigmoid equation, a new formulation has been developed to model the degradation of structure at yield for lime treated soils (Equation 4.14). This formulation has the significant advantage to add only 4 additional parameters to the original MCC, which all have a physical meaning and can all be determined from an isotropic consolidation test performed on the lime treated material. To model the influence of the cohesion on the deviatoric behaviour the parameter  $p_b$ , directly related to the equation of the CSL, was introduced. Finally, 6 parameters appear sufficient to account for the effects of a lime treatment on the mechanical behaviour of a material:

- $p_y^I$  : Primary yield stress
- $p_y^{II}$  : Degradation stress
- $\Delta e_i$  : Additional void ratio at  $p_y^I$
- $\Delta e_c$  : Residual additional void ratio for  $p' \rightarrow +\infty$
- $\beta$  : Rate of degradation
- $p_b$  : Tensile strength due to the increase of the cohesion

### 4.6 Stress-strain relationship

#### 4.6.1 Elastic behaviour

It is assumed that only elastic deformation occurs for stress states lying within the yield surface. According to the Modified Cam Clay model, the elastic volumetric increments are given by

$$\delta \varepsilon_p^e = \kappa \frac{\delta p'}{vp'} \quad (4.19)$$

$$\delta \varepsilon_q^e = \frac{\delta q}{3G'} \quad (4.20)$$

#### 4.6.2 Plastic behaviour

##### Compliance matrix for hardening case

The general plastic stress-strain relationship for axisymmetric problem is given by

$$\begin{bmatrix} \delta \varepsilon_p^p \\ \delta \varepsilon_q^p \end{bmatrix} = \frac{-1}{\left[ \frac{\partial f}{\partial p'_0} \left[ \frac{\partial p'_0}{\partial \varepsilon_p^p} \frac{\partial g}{\partial p'} + \frac{\partial p'_0}{\partial \varepsilon_q^p} \frac{\partial g}{\partial q} \right] \right]} \begin{bmatrix} \frac{\partial f}{\partial p'} \frac{\partial g}{\partial p'} & \frac{\partial f}{\partial q} \frac{\partial g}{\partial p'} \\ \frac{\partial f}{\partial p'} \frac{\partial g}{\partial q} & \frac{\partial f}{\partial q} \frac{\partial g}{\partial q} \end{bmatrix} \cdot \begin{bmatrix} \delta p' \\ \delta q \end{bmatrix} \quad (4.21)$$

The new formulation of the  $v : p'$  relationship given by Equation (4.14) is now used as the new hardening rule. For the sake of simplicity, it was assumed that hardening is only controlled by the plastic volumetric strains ( $f(\boldsymbol{\sigma}, \varepsilon_p^p)$ ). The volumetric plastic

strains for lime treated soils is therefore expressed as

$$\delta\varepsilon_p^p = \left[ \left( \frac{M^2(2p' - p'_0 - p_b) + 6q}{M^2(p' - p_b)} \right) \left( \frac{\partial p'_0}{\partial \varepsilon_p^p} \right)^{-1} \right] \cdot \delta p' \quad (4.22)$$

with

$$\frac{\partial p'_0}{\partial \varepsilon_p^p} = \frac{v}{\frac{e^{p'_0\beta} \left( e^{p_y^I\beta} + e^{p_y^{II}\beta} \right) \beta (\Delta e_i - \Delta e_c)}{\left( e^{p'_0\beta} + e^{p_y^{II}\beta} \right)^2} + \frac{\lambda - \kappa}{p'_0}} \quad (4.23)$$

$$\frac{\partial p'_0}{\partial \varepsilon_q^p} = 0 \quad (4.24)$$

Combining Equations (4.21) to (4.24) gives the final formulation of the plastic volumetric strains

$$\delta\varepsilon_p^p = \frac{\left( M^2(p' - p_b) + p'\eta \left( 6 - \frac{p'\eta}{p - p_b} \right) \right)}{M^2(p' - p_b)v} \left( \frac{e^{p'\beta \left( 1 + \frac{p'\eta^2}{M^2(p' - p_b)} \right)} \left( e^{p_y^I\beta} + e^{p_y^{II}\beta} \right) \beta (\Delta e_i - \Delta e_c) + \frac{\lambda - \kappa}{p' + \frac{p'^2\eta^2}{M^2(p' - p_b)}}}{\left( e^{p_y^{II}\beta} + e^{p'\beta \left( 1 + \frac{p'\eta^2}{M^2(p' - p_b)} \right)} \right)^2} + \frac{\lambda - \kappa}{p' + \frac{p'^2\eta^2}{M^2(p' - p_b)}} \right) \delta p' \quad (4.25)$$

The deviatoric plastic strains can be calculated using the flow rule from Equation (4.18):

$$\delta\varepsilon_q^p = \left[ \frac{M^2(p' - p_b)}{2p'\eta} - \frac{p'\eta}{2(p' - p_b)} \right]^{-1} \cdot \delta\varepsilon_p^p \quad (4.26)$$

### Compliance matrix for softening case

Lime treated specimens experiencing softening at shear show a maximum rate of dilation after the peak due to the degradation of the structure. If Equation (4.12) is used to model the softening behaviour on  $]0, p_y^I]$ , the formulation leads to  $\Delta e \geq \Delta e_i$  and no degradation of the structure is modelled. To model the softening behaviour, we propose a new softening rule in the same framework as the one chosen for the hardening case, where the degradation of the structure is described by the sigmoid equation. To avoid the addition of meaningless parameters, an automatic procedure is proposed based on experimental considerations.

Since  $\Delta e_c$  arises from the lime treatment and modifies the texture of the soil, it is assumed that the material converges toward the same  $ncl_r$  as under isotropic loading. Based on experimental observations made from the results obtained on artificially structured soils (Chapter 3) the inflexion point, called  $p_{y,s}^{II}$ , was chosen as the intersection of the  $url$  and the  $ncl_r$  (Figure 4.18) and is given by

$$p_{y,s}^{II} = \exp \left( \frac{N_\lambda - N_\kappa + \Delta e_c}{\lambda - \kappa} \right) \quad (4.27)$$

which does not require any additional parameter. This leads to the following ex-

#### 4. A GENERAL FORMULATION FOR DEGRADATION IN STRUCTURED SOILS

pression of the softening rule:

$$\forall p' \in ]0, p_y^I] \quad v_s(p') = N_\lambda - \lambda \ln(p') + (\Delta e_i - \Delta e_c) \cdot \left[ \frac{e^{-\beta_s p_y^I} + e^{-\beta_s p_{y,s}^{II}}}{e^{-\beta_s p'} + e^{-\beta_s p_{y,s}^{II}}} \right] + \Delta e_c \quad (4.28)$$

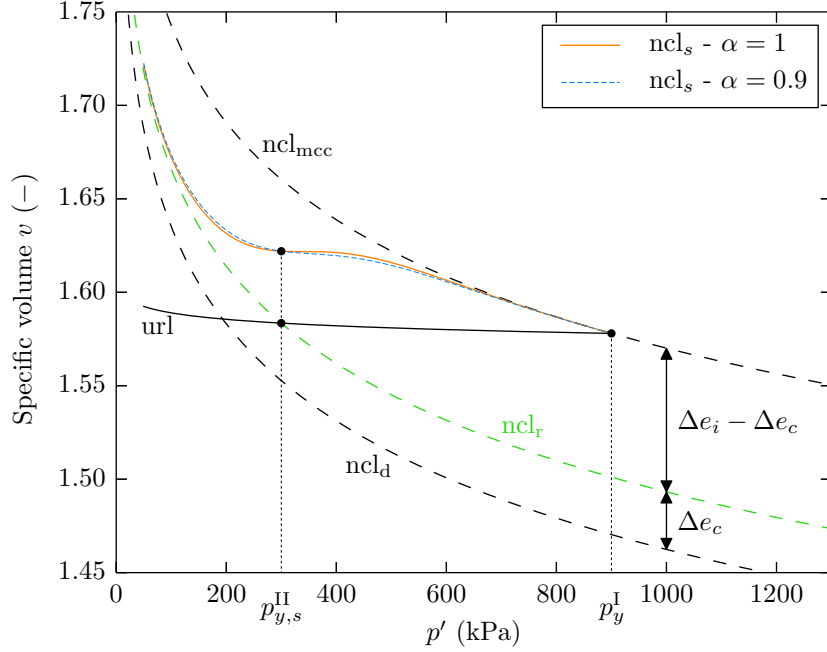


Figure 4.18: Modelling of the behaviour at yield for softening case.

The parameter  $\beta_s$  describes the rate of destructuration which is calculated automatically. During the post-yield behaviour, the maximum rate of dilation is observed right after the deviatoric stress reaches its maximum. This is due to the structure experiencing an extensive degradation. Such feature can be modelled by using as  $\beta_s$ , the maximum rate of degradation  $\beta_0$ , leading to  $v_s$  monotonically decreasing (not strictly). In this case, the first derivative being zero only for a single effective mean stress (which is not necessarily  $p_{y,s}^{II}$ ). This method presents the advantage that  $\beta_0$  can easily be determined graphically or numerically. However, for consistency and numerical stability,  $v_s$  is preferred to be strictly monotonically decreasing on  $]0, p_y^I]$ . For this purpose, we introduced a constant  $\alpha$  such that

$$\beta_s = \alpha \times \beta_0 \quad (4.29)$$

the bijection (one-to-one correspondence) being ensured by  $\alpha \in ]0, 1[$ . Practically,  $\alpha$  can control the smoothness of the process of destructuration. In this model,  $\alpha$  is arbitrarily set to 0.9, which ensures a bijective function and an appropriate rate of degradation at yield (Figure 4.18).

This two-step method is the simplest and most reliable way to calculate  $\beta_s$ , simply because the determination of  $\beta_0$  is independent of the stress state and does not require information about the gradient at  $p_{y,s}^{II}$ , which can not be determined from experimental results, and may lead to numerical instabilities. The suitability of this method will be demonstrated during the model evaluation in Section 4.7.



The stress-strain relationship for the softening case is obtained by introducing Equation (4.28) into Equation (2.54). Such softening rule respects the associated potentials hypothesis.

## 4.7 Model evaluation

The robustness of the model for artificially structured soils (MASS) is assessed in predicting the behaviour of artificially and naturally structured materials under isotropic loading and drained paths for different confining pressures. As a first step, we assess the suitability of an associated flow rule for the modelling of lime treated soils using the experimental results from Chapter 3. Then, the model is used to predict the behaviour of silt specimens treated with different lime contents (0.5%, 1%, 2%, and 5% CaO) of the present study. The model is finally tried out on naturally structured specimens of calcarenite (Lagioia and Nova, 1995). For both cases, the additional parameters to the Modified Cam Clay were determined from a single isotropic compression test performed on the structured specimens (Table 4.3).

Table 4.3: Values of the model parameters

Parameters		[CaO]				Lagioia and Nova (1995)
		Present study				
		0.5%	1%	2%	5%	
MCC	$p_y^I$ (kPa)	255	600	1260	1900	2300
	$N_\lambda$ (-)	1.95	1.99	1.97	2.00	3.76
	$\lambda$ (-)	0.08	0.08	0.08	0.08	0.23
	$\kappa$ (-)	0.019	0.032	0.014	0.015	0.020
	M (-)	-	1.15	1.22	1.42	1.42
	E (kPa)	-	45000	55000	70000	77000
MASS	$p_y^{II}$ (kPa)	1200	1000	2200	3500	2300
	$\Delta e_i$ (-)	0.027	0.065	0.129	0.159	0.134
	$\Delta e_c$ (-)	0.0	0.046	0.109	0.136	0.0
	$p_b$ (kPa)	-	-41.8	-120.3	-144.7	-25.6
	$\beta$ (kPa <sup>-1</sup> )	0.020	0.035	0.020	0.020	0.047

MCC: Modified Cam Clay model, MASS: Model for Artificially Structured Soils.

### 4.7.1 Associated flow rule hypothesis

In this section, we assess the validity of an associated flow rule for lime treated soils. Plastic strain increment vectors from drained triaxial tests performed on specimens treated with 1%, 2%, and 5% in lime were determined. The yield loci values were normalized with respect to the primary yield stress  $p_y^I$ . Figure 4.19 shows that it seems reasonable to assume that plastic strain increment vectors are normal to the yield surface. The hypothesis of an associated flow rule for the modelling of lime

## 4. A GENERAL FORMULATION FOR DEGRADATION IN STRUCTURED SOILS

treated soils appears therefore suitable.

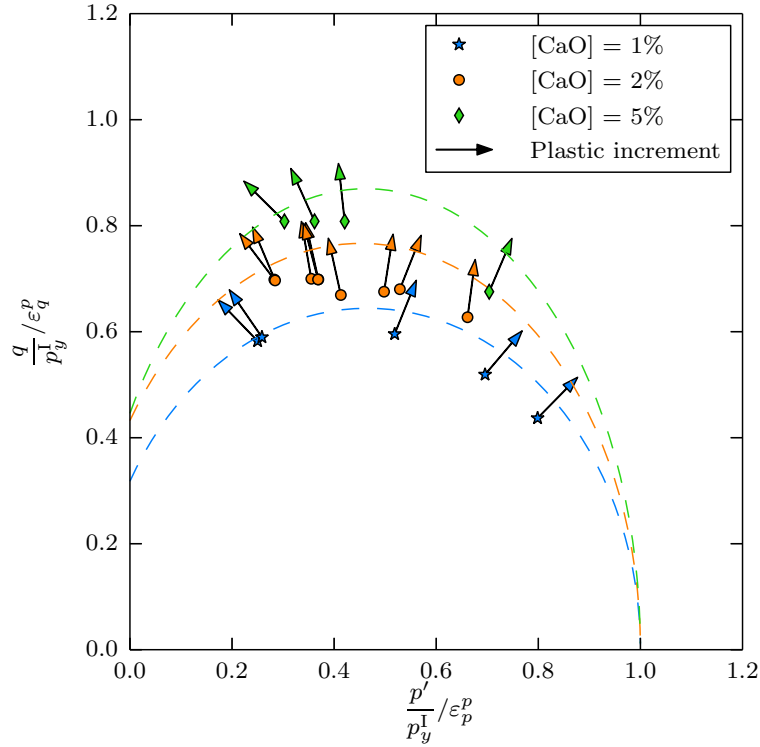


Figure 4.19: Vectors of plastic strain increment plotted at yield points obtained from drained triaxial tests on lime treated specimens.

### 4.7.2 Lime treated specimens

#### Isotropic consolidation

The new formulation to model the degradation of the structure at yield (Equation 4.14) was applied on lime treated specimens. Two sets of experimental results of isotropic compression tests were used to verify the general nature of the formulation. The first set was treated with 0.5% CaO and follows the mode 3 ( $\Delta e_c = 0$ ), and the second with 1% CaO and follows the mode 4 ( $\Delta e_c > 0$ ) (Figure 4.20). For the two sets the parameter  $\beta$  was determined from the gradient of the curve at  $p' = p_y^{\text{II}}$  using the Newton-Raphson algorithm.

The use of the sigmoid equation appears very appropriate to model the degradation experienced at yield by lime treated materials. For both concentrations in lime, there is a very good agreement between the experimental results and the model. The degradation is initiated at the right effective mean stress and with the correct rate, and both sets converge toward the correct normal compression line.

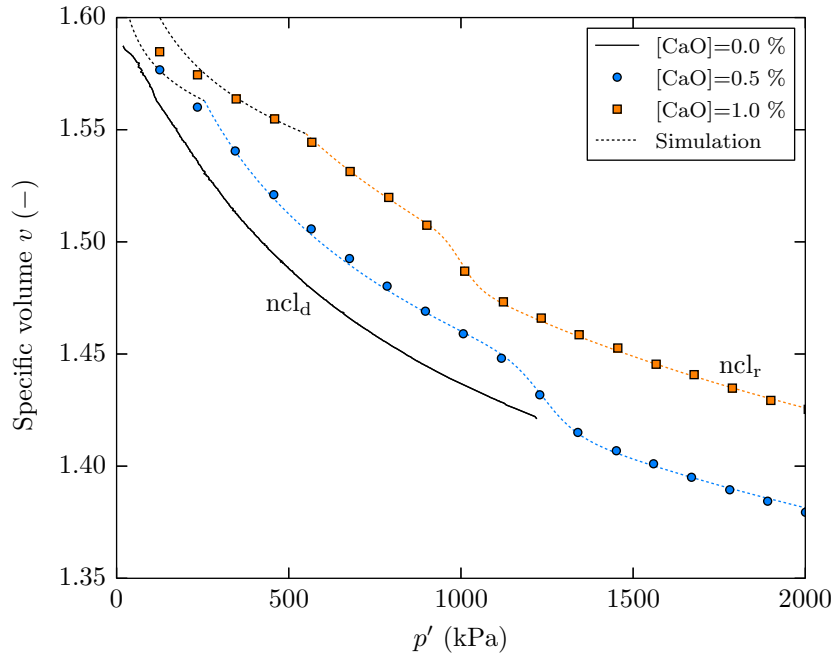


Figure 4.20: Evaluation of the formulation on 0.5% and 1% lime treated specimens –  $ncl_d$ : normal compression line of the untreated state,  $ncl_r$ : normal compression line of the residual state.

### Shear behaviour

No additional parameters to the MCC are required by this model to describe the degradation of the structure at shear apart from  $p_b$  that is derived from the equation of the CSL. The model was applied on lime treated specimens along different drained stress paths and confining pressures (Figures 4.21-4.23). Three concentrations in lime were tested to consider various degrees of structure: 1%, 2% and 5% CaO.

The yield loci and critical states appear satisfactory modelled for all the lime contents tested. They confirm the appropriateness of the equation of the yield function  $f$  and the suitability of the parameter  $p_b$  to account for the influence of the lime treatment on the cohesion and the critical state.

For both hardening and softening cases, the volumetric deformations are very accurately predicted by the model. This supports the assumption of the volumetric deformations being mostly controlled by the structure. The evolution of the specific volume for the softening case is particularly accurate (Figure 4.24). The model is successful to reproduce the dilation post-yield of the specimens and the maximum rate of dilation after the deviatoric stress peak, which is one of the key features of structured soils.

The framework chosen for the softening case appears suitable and very powerful. The assumptions made to calculate automatically in the background the parameters  $p_{y,s}^{\text{II}}$  and  $\beta_s$  (Figure 4.18) are therefore relevant and successful to reproduce the majority of the main features of behaviour of lime treated soils, and that using only information from isotropic test results. It also ensures that the material experiences dilation at yield for samples in the dry side.

#### 4. A GENERAL FORMULATION FOR DEGRADATION IN STRUCTURED SOILS

The MASS appears very satisfactory to model the key features of lime treated soils considering the limited number of parameters and the straightforwardness of their determination. Nevertheless, the model tends to deviate from the experimental results during the post-yield stage before converging back toward the critical state at high axial strains for some samples subjected to a high preconsolidation pressure (600 kPa in Figure 4.21, 900 kPa in Figure 4.22). In this model, potentials  $f$  and  $g$  are associated and hardening is controlled by the plastic volumetric deformations  $\varepsilon_p^p$  only ( $f(\boldsymbol{\sigma}, \varepsilon_p^p)$ ). This has for consequences to reflect the degradation of the structure on the deviatoric stress. However, lime treated specimens experiencing hardening do not show any sign of this phenomenon for any of the concentrations tested. This might come from the fact that the contribution of  $\varepsilon_q^p$  was neglected in this model, and/or that the ‘amount’ of structure is too low to significantly affect the stresses.

For samples in the dry side, the model predicts larger values for the yield loci than what is experimentally observed. One of the known limitations of the MCC is that it overestimates the values in such situation; the fact that we extended the yield function in the tensile domain with  $p_b$  amplifies this feature.

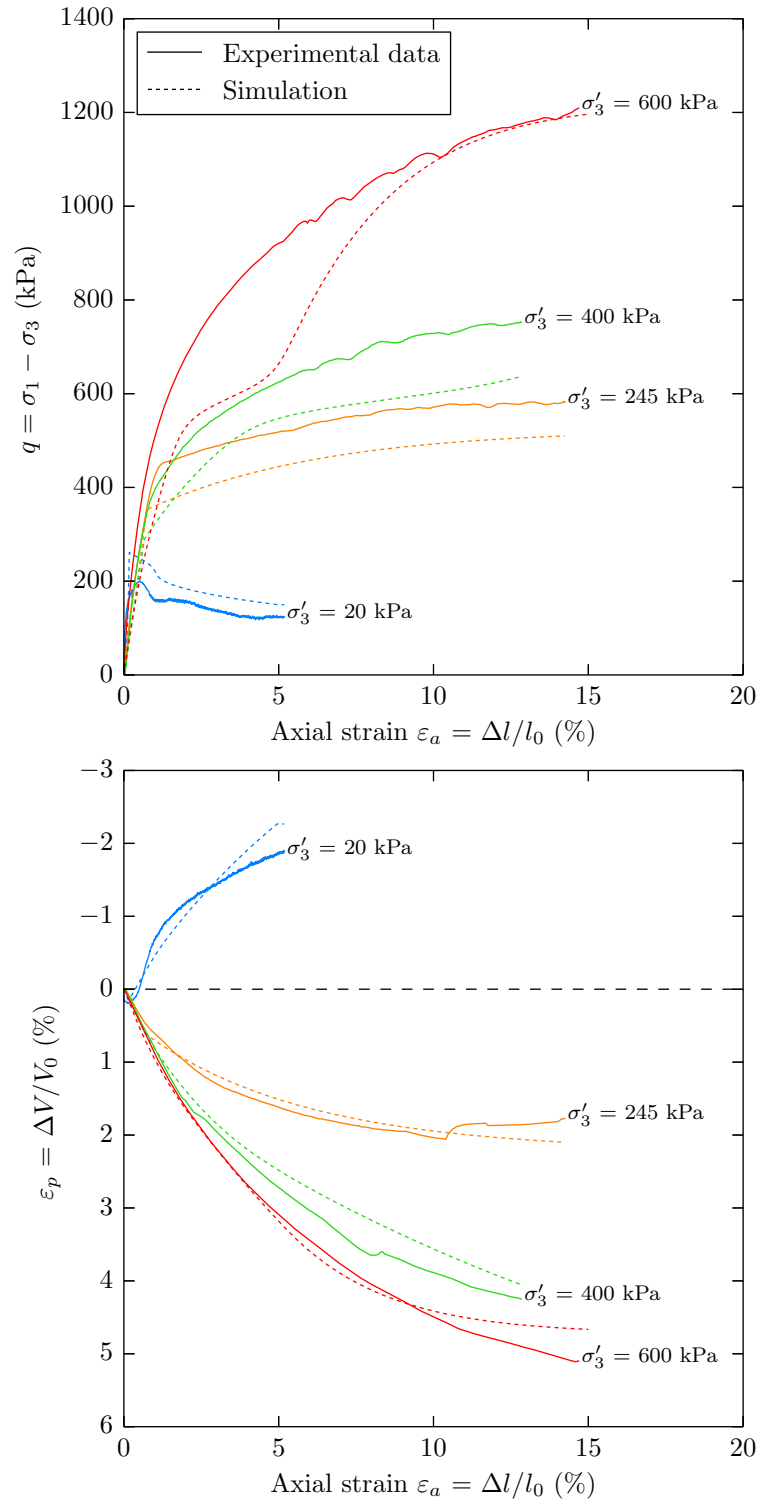


Figure 4.21: Comparison between experimental results and the model of drained tri-axial tests performed on lime treated specimens with 1% CaO.

4. A GENERAL FORMULATION FOR DEGRADATION IN STRUCTURED SOILS

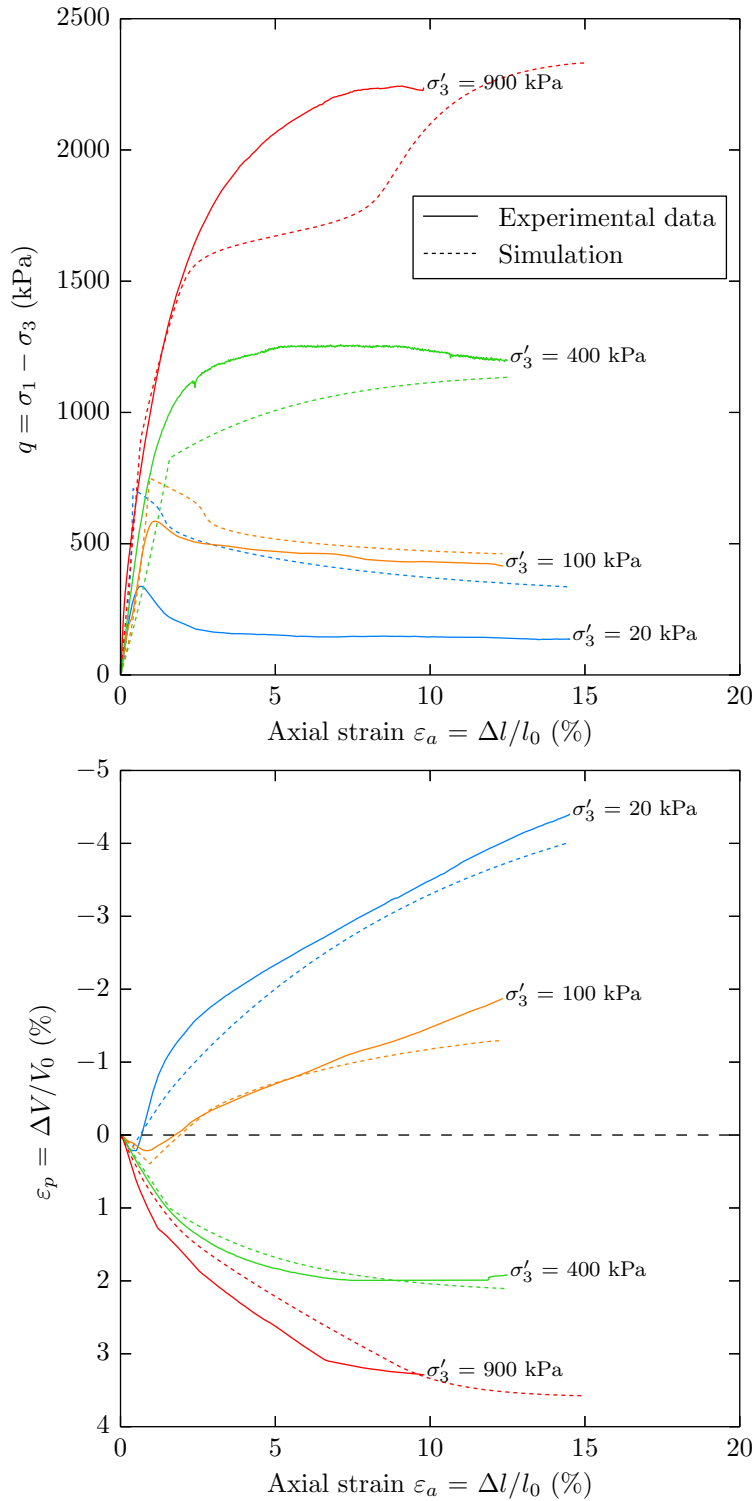


Figure 4.22: Comparison between experimental results and the model of drained tri-axial tests performed on lime treated specimens with 2% CaO.

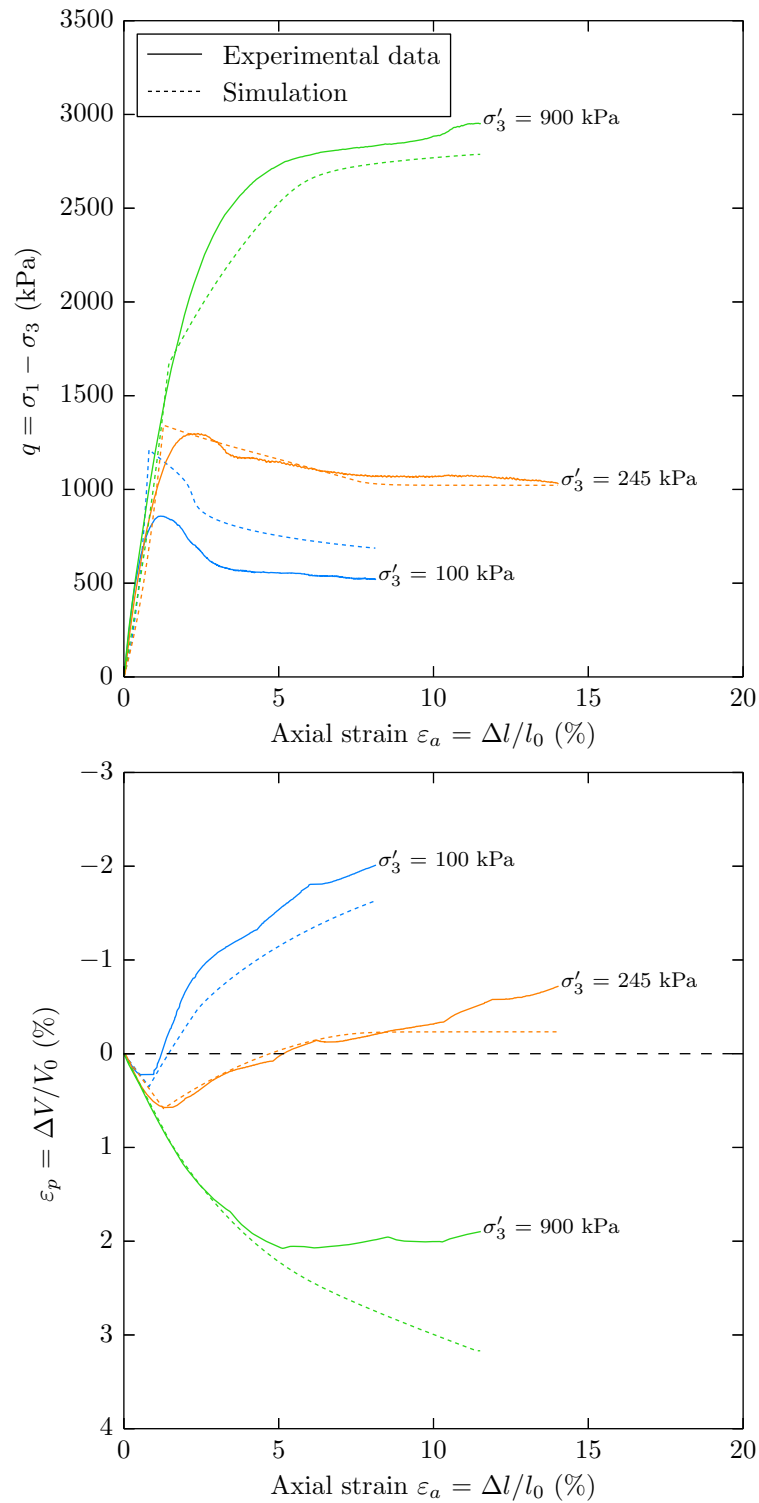


Figure 4.23: Comparison between experimental results and the model of drained tri-axial tests performed on lime treated specimens with 5% CaO.

#### 4. A GENERAL FORMULATION FOR DEGRADATION IN STRUCTURED SOILS

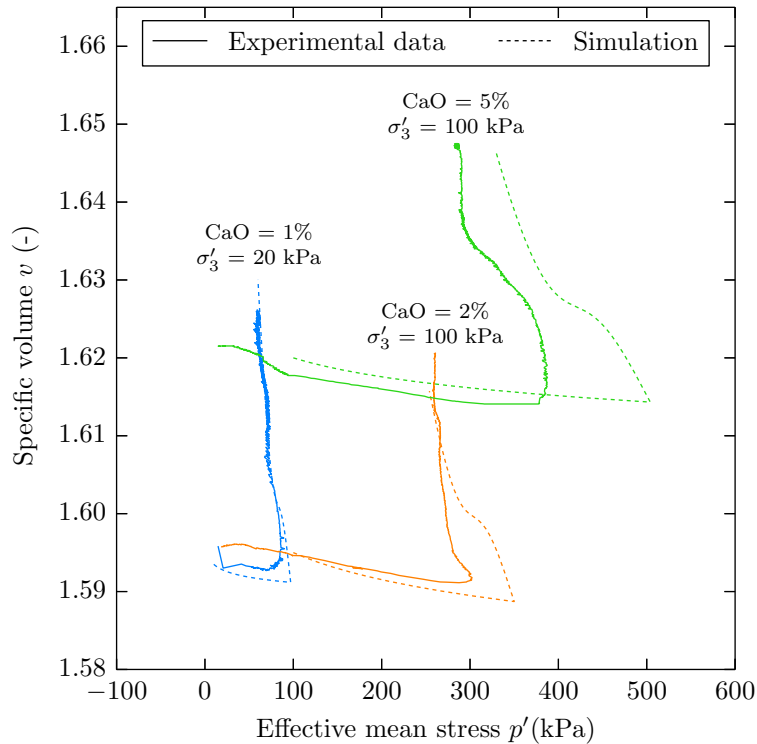


Figure 4.24: Comparison between drained triaxial results and the model of the specific volume for different lime contents.

#### 4.7.3 Naturally structured soils

Although the formulation was originally designed for lime treated soils, there are several common features of behaviour between artificially and naturally materials that could also make it suitable for the latter.

##### Isotropic consolidation

The suitability of the formulation to model the degradation of naturally structured soils under isotropic loading is verified using the results from Lagioia and Nova (1995) on natural calcarenite (Figure 4.25). Likewise the lime treated specimens, calcarenite experiences a degradation of the structure at yield but that occurs immediately at yield ( $p_y^I = p_y^{II}$ ) and at a very high rate. Again,  $\beta$  was solved numerically using the Newton-Raphson procedure. There is no information about the behaviour of the destructured calcarenite under isotropic loading, and therefore no information is given about the value of the residual void ratio  $\Delta e_c$ . However, Lagioia and Nova (1995) considered that calcarenite converges toward the ncl of the destructured state. Thus, it is assumed that calcarenite has no residual void ratio ( $\Delta e_c = 0$ ) and follows the mode 1. The parameters used for the simulations are given in Table 4.3. Though the origin of the cementation is different, the MASS appears suitable to model naturally structured materials under isotropic loading. As for the lime treated specimens, the degradation is initiated at the right effective mean stress and at the correct rate till it reaches the normal compression line of the destructured state.



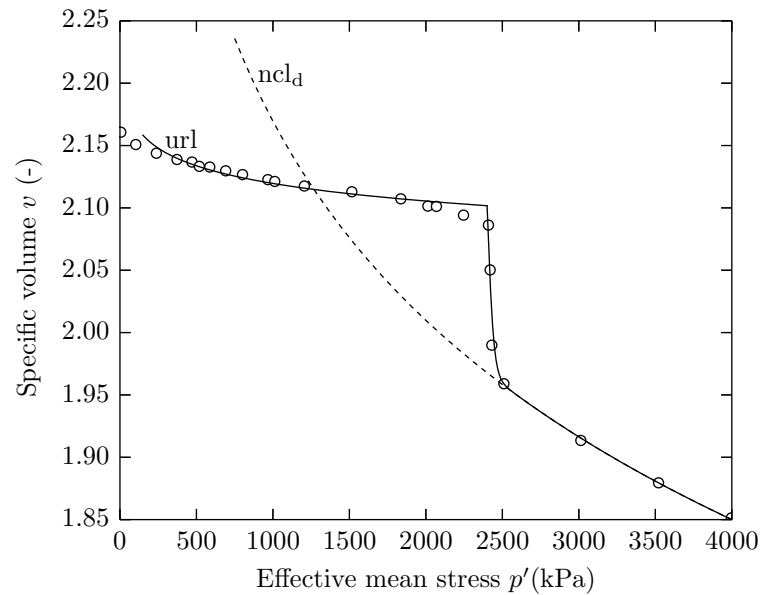


Figure 4.25: Validation of the formulation on natural calcarenite (Lagioia and Nova, 1995) –  $ncl_d$ : normal compression line of the destructured state.

### Shear behaviour

The model is now tried to reproduce the behaviour of samples naturally structured calcarenite at shear submitted to drained triaxial tests. The parameter  $p_b$  was determined from the equation of CSL given in Lagioia and Nova (1995).

For samples of calcarenite experiencing hardening (Figure 4.26) the MASS gives a very good agreement with the experimental results of the yield loci and the critical state. At yield, the degradation of the structure seems to affect the deviatoric stress, which is successfully described by model. The specific volume at yield (Figure 4.27) is accurately modelled and the trends of the volumetric deformations (Figure 4.26) are satisfactory, although the values appear underestimated at large deformations.

For samples experiencing softening (Figure 4.28) the MASS gives an accurate prediction of the yield loci and the critical state. However, samples revealed an unusual behaviour in the framework of the MCC and the critical state theory regarding the volumetric deformations. It is generally accepted that for the softening case samples experience dilation at yield. However, the calcarenite seems to behave differently and keeps contracting at yield, although the deviatoric stress decreases.

#### 4. A GENERAL FORMULATION FOR DEGRADATION IN STRUCTURED SOILS

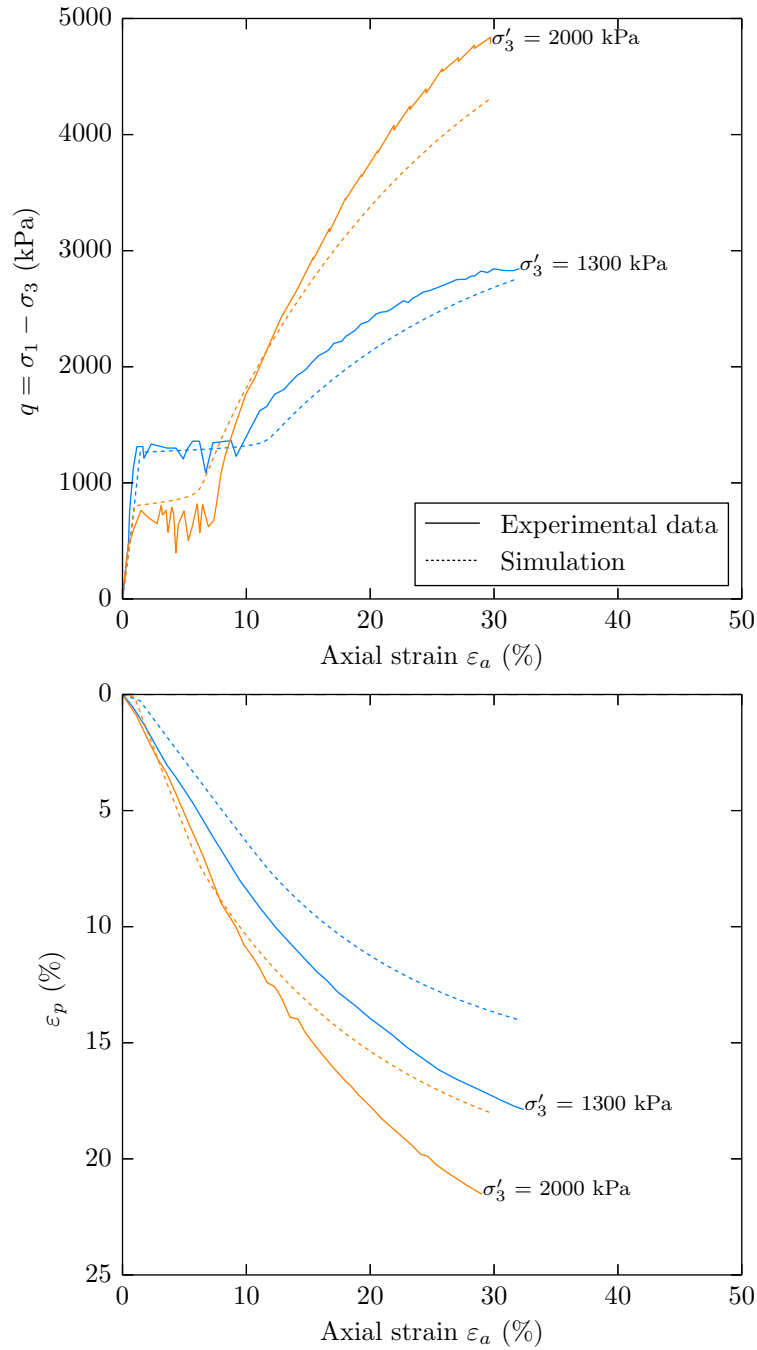


Figure 4.26: Comparison between experimental results and the model of drained tri-axial tests performed on calcarenite and experiencing hardening (Lagioia and Nova, 1995).

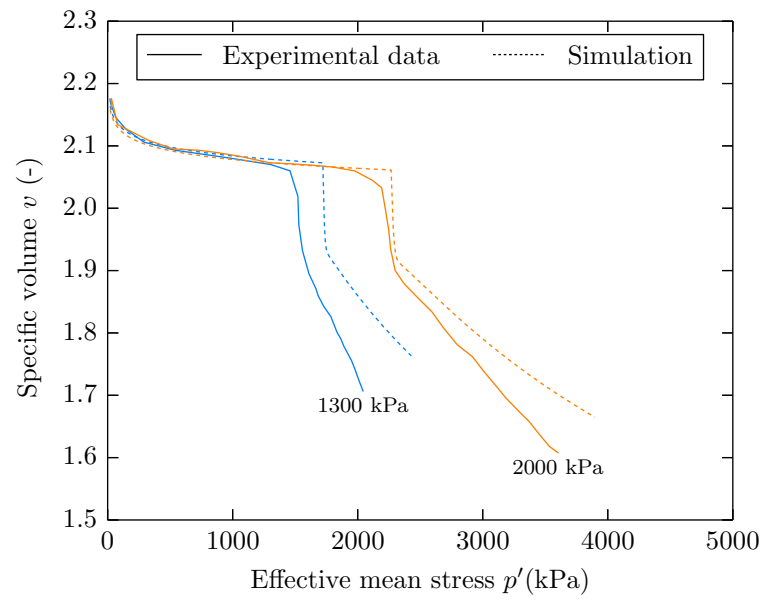


Figure 4.27: Comparison between the experimental results and the model for the specific volume (Lagioia and Nova, 1995)

#### 4. A GENERAL FORMULATION FOR DEGRADATION IN STRUCTURED SOILS

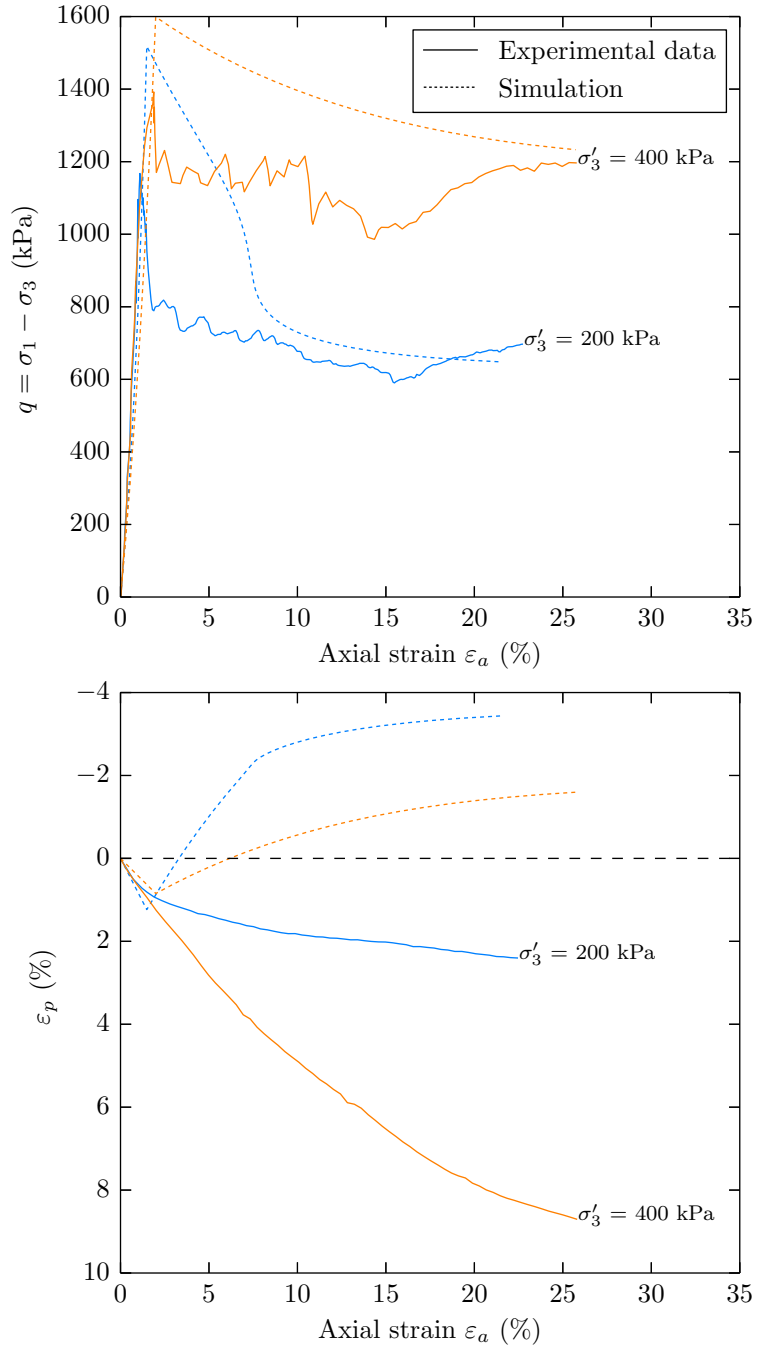


Figure 4.28: Comparison between experimental results and the model of drained triaxial tests performed on calcarenite and experiencing softening (Lagioia and Nova, 1995).

#### 4.7.4 Discussion: influence of the initial void ratio on the degradation mode

The MASS can successfully reproduce a large number of features of both lime treated soils and naturally structured soils. However, the model deviates from the experimental results for 1) lime treated specimens subjected to high preconsolidation pressures experiencing hardening, and 2) samples of calcarenite experiencing softening. In this section, we propose a hypothesis to explain these limitations using the initial void ratio of the material.

During the early post-yield stage, the degradation of the structure seems to affect the stress:strain response for samples of calcarenite experiencing hardening, but not for the lime treated specimens. Furthermore, for the softening case, lime treated specimens experience dilation, as predicted by the critical state theory, but this is not the case for the samples of calcarenite, which experience contraction despite the decrease of deviatoric stress at yield.

For the calcarenite, the initial additional void ratio at yield  $\Delta e_i$  and the range of stresses are similar to those measured on lime treated soils with 5% CaO. The only difference between the two materials lies in the initial specific volume (around 1.6 for the lime treated specimens and 2.2 for the calcarenite). When the calcarenite starts yielding, the structure is rapidly degraded due to the brittleness of the material. Lagioia and Nova (1995) stated that some softening could take place under isotropic loading, and explained that the plateau of the deviatoric stress is associated with debonding. However, what was interpreted as *softening* under isotropic loading is more likely to be collapse since the specific volume decreases during the deconstruction. Once the particles are released from the cementation, they immediately collapse and start filling the voids as the axial deformation increases. During this stage, there is no effective friction inside the material and therefore no additional deviatoric stress is necessary to increase the axial deformation. The effective friction is restored once the particles are close enough and the porosity is significantly reduced, which leads to an increase of the deviatoric stress followed by convergence toward the critical state. This mechanism also explains why samples experiencing softening do not have a dilatant behaviour at yield as predicted by the critical state theory. The dilation process is the direct result of the interlocking of the particles; in the case of the calcarenite, the fast degradation of the structure leads to the collapsing of the particles and therefore to the contraction of the sample. Although the deviatoric stress decreases at yield, since there is no interlocking of the particles, there is no dilation of the sample.

For the lime treated specimens of this study, the initial conditions were chosen to match those used on-site and obtained from the Proctor compaction test. In these conditions, the void ratio is too low to generate a noticeable collapse in the material, and the deconstruction is a slower process. The degradation of the structure takes place but particles are already in contact, which maintains a friction between them and leads to increase in the deviatoric stress with the axial deformation. Therefore, the degradation of the structure is not observed directly on the stress:strain response. If the conditions imply strain softening, interlocking happens and therefore dilation, which is observed on the experimental results and properly reproduced by the MASS.

#### 4. A GENERAL FORMULATION FOR DEGRADATION IN STRUCTURED SOILS

In light of these observations, it appears that the initial void ratio has a key impact on the behaviour of the material than the degree and the origin of cementation. As a matter of fact, the mode of degradation of a large number of structured materials seems to be closely related to the initial void ratio (Table 4.4). Further work must be carried out to identify the parameters responsible for the different behaviours. Nevertheless, the MASS appears to reproduce the main features of behaviour of lime treated soils, and is also successful in modelling the main trends that are observed in naturally structured soils.

Table 4.4: Correlation between the initial void ratio and the mode of degradation

	Origin of structure	Material	$v_i$ (-)	Study
Mode 1	Natural	Pisa clay	2.8	Callisto and Calabresi (1998)
	Artificial	St-Alban clay	6.0	Tremblay et al. (2001)
Mode 2	Natural	Louiseville clay	3.0	Lapierre et al. (1990)
	Artificial	Louiseville clay	$\gg 3$	Tremblay et al. (2001)
Mode 3	Natural	Corinth marl	1.6	Anagnostopoulos et al. (1991)
	Artificial	Silt	1.6	Present study
Mode 4	Natural	Vallericca clay	1.8	Callisto and Rampello (2004)
	Artificial	Sandstone	$<1.6$	Rotta et al. (2003)

$v_i$ : initial specific volume.

### 4.8 Conclusion

A new model in the framework of the Modified Cam Clay model was developed for lime treated soils. In order to introduce only relevant parameters, the most important features of lime treated materials and naturally structured soils that should be reproduced by a model were identified. Experimental results reveal that both naturally and artificially soils have a very similar mechanical behaviour at yield.

To account for the effects of structure on the behaviour of soils, a new formulation was developed based on Richards's equation. In the framework of the simplicity and easiness, only 4 new additional parameters to the MCC were introduced to model the degradation: the degradation stress  $p_y^{\text{II}}$ , the rate of degradation  $\beta$ , the additional void ratio at  $p_y^{\text{I}}$ , and the additional void ratio  $\Delta e_c$  at  $p' \rightarrow +\infty$ . A fifth parameter  $p_b$  was introduced to account for the increase of cohesion due to the structure. The power of this model is that all the additional parameters have a physical meaning and can be determined from a single isotropic consolidation test performed on the structured material. A transparent and powerful procedure was developed for the softening rule. The two parameters required by the sigmoid function to model the degradation are automatically determined from the 4 parameters obtained from the isotropic tests.

The model was applied for lime treated soils and naturally structured samples of calcarenite. The formulation is in good agreement with the experimental results and

the main trends are properly reproduced. The formulation proposed as softening rule is successful to model the dilation observed on lime treated samples at yield and the maximum rate of dilation after the peak, one of the most representative features of structured soils. However, the results on the calcarenite have risen interesting considerations for the modelling of the structured materials in general, naturally or artificially.

The initial porosity appeared to be the key parameter controlling the influence of the degradation of the structure on the mechanical behaviour of lime treated specimens and the calcarenite. Once the material starts yielding the degradation of the bonding structure takes place, and therefore the release of the particles. Depending on the initial void ratio, the material can either experience dilation (particles are in contact and expand due to the interlocking) or collapse until particles start interacting again. This can lead to contraction even for heavily over consolidated samples. Further work must be carried out to develop a model capable of accounting for the influence of the initial void ratio on the post-yield behaviour.

#### 4. A GENERAL FORMULATION FOR DEGRADATION IN STRUCTURED SOILS



## Chapter 5

# Finite element modelling of structured materials

### 5.1 Introduction

The work carried out in Chapter 4 has led to the development of a new constitutive model for structured materials – naturally or artificially – and has proven to give a good agreement with the experimental results. However, the partial differential equations (PDE) governing the behaviour are only valid locally and cannot therefore be applied in their current form for the modelling of complex geometries.

The finite element method is one of the most popular approaches for the resolution of non-linear partial differential equations on complex geometry and, since its transfer during the 1950s and 1960s from the aerospace industry to engineering, it has been extensively applied by industry and a large number of numerical codes are now available.

Although this thesis focused on the modelling of the mechanical behaviour of structured soils, it also fits in the larger project of developing a complete chemo-mechanical model accounting for all the features involved in soil treatment (e.g. pozzolanic reactions, time dependency, mechanical behaviour, durability). For this reason, one of the ambitions of this thesis was to develop a fully functional finite element program incorporating the elasto-plastic model MASS developed for structured soils, as a first step toward the complete modelling of soil treatment. To this end, this chapter aims at addressing the three following issues:

- How can we implement the finite element method for geotechnical applications?
- How can we introduce the model MASS in the finite element model?
- How can we use such finite element model for design optimisation of lime treated structures?

In the first section we briefly outline the principles and the applications of the finite element method for geotechnical problems. Then, we give a review of the mathematical framework of the FEM for elastic and plastic problems, and we formulate the model MASS in a form suitable to be implemented in a finite element code. Then, we present the main features of the Finite Element Model for Artificially Structured

Soils (FEMASS) developed in this study, followed by its validation on a benchmark problem. Finally, we demonstrate the potential of the numerical method for design optimisation.

## 5.2 Principles of the finite element method

The Finite Element Method (FEM) was developed to solve non-linear partial differential equations on complex geometries in the framework of efficiency and accuracy (Aziz, 1972). It is one of the most popular methods based on *discretisation*, especially for solid mechanics.

By definition, the resolution of partial differential equations on a continuous solid involves an infinite number of degrees freedom (Figure 5.1a). The main concept of FEM is to subdivide the system into smaller and non-overlapping elements (or subdomains) of simpler geometry than the original (Figure 5.1b).

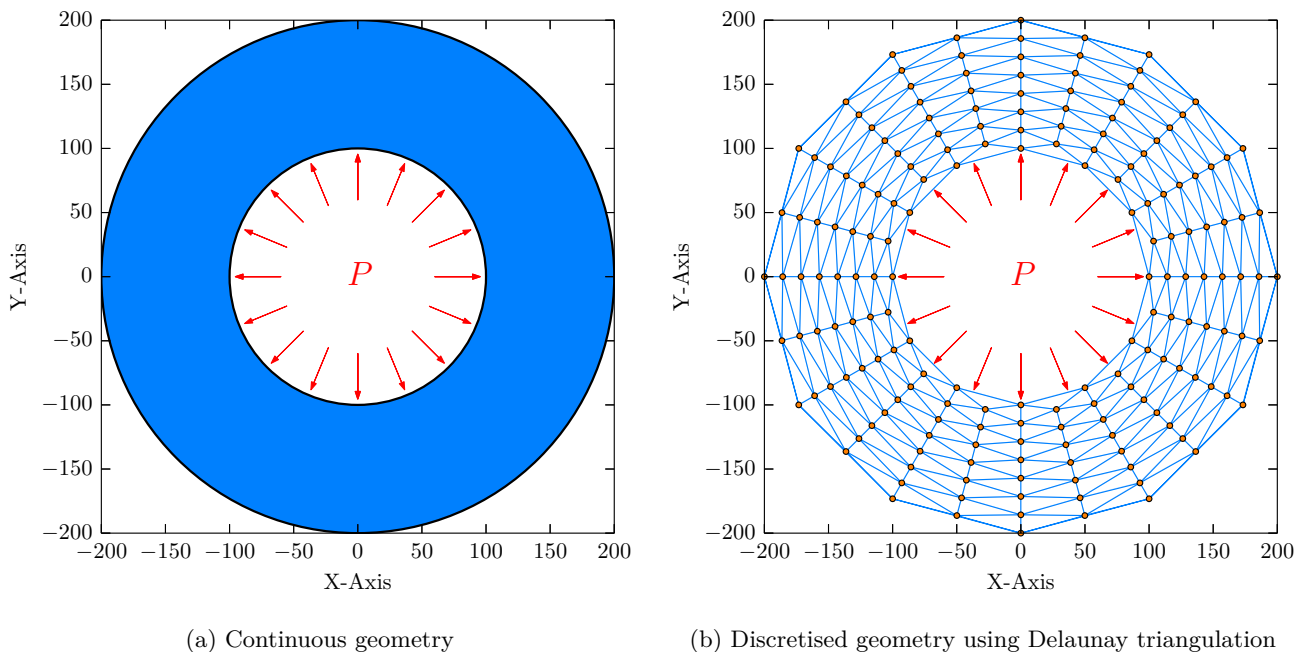


Figure 5.1: Principle of discretisation in finite element method for the modelling of a thick cylinder subjected to an internal pressure  $P$ .

This considerably reduces the number of degrees of freedom (i.e. unknowns) of the problem, each element being made of a finite number of nodes at which the unknowns of the problem (e.g. displacements, stresses, temperature) are calculated. The main idea is that the response of the original system can be approximated by assembling the response of every subdomain using the connectivity between the elements (Zienkiewicz and Taylor, 1989).

Physical processes are usually governed by partial differential equations in space and time describing a variable locally. This form, called *strong* form, is only valid on a continuum solid. The finite element method consists in writing this strong form valid on an infinite-dimensional space in a variational form, called *weak* form, valid on a finite-dimensional space. We present in the next section the method to formulate the strong form of an equation in a suitable form for finite element use.

## 5.3 Mathematical theory of finite element method for elastic problems

### 5.3.1 Strong formulation

Consider a continuum body of volume  $\Omega$  (Figure 5.2) assumed to behave elastically and being subjected to infinitesimal strains.

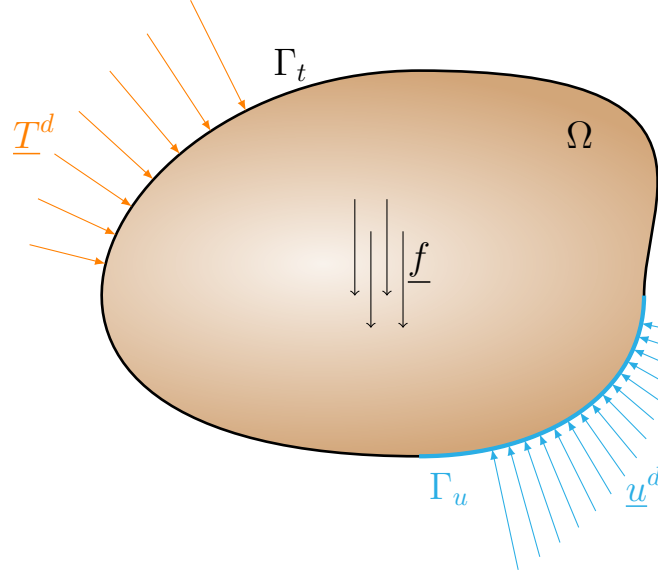


Figure 5.2: Configuration of the system.

From section 2.4 we can introduce the following definitions (Bonnet and Frangi, 2006; Legay, 2012):

**Definition 5.1 (Compatibility conditions)** *Given a solid  $\Omega$  subjected to body forces  $\underline{f}$ , prescribed displacements  $\underline{u}^d$  on  $\Gamma_u$ , and boundary tractions  $\underline{T}^d$  on  $\Gamma_t$ , and calling  $\underline{u}$  the displacements field,  $\underline{\varepsilon}$  the strain tensor, and  $\underline{\sigma}$  the stress tensor, the equilibrium of the solid is governed by*

$$\underline{\varepsilon} = \frac{1}{2} [\underline{\nabla u} + (\underline{\nabla u})^T] \quad \text{in } \Omega \quad (5.1a)$$

$$\underline{f} + \underline{\nabla} \cdot \underline{\sigma} = \underline{0} \quad \text{in } \Omega \quad (5.1b)$$

$$\underline{\sigma} = \mathbb{D} : \underline{\varepsilon} \quad \text{in } \Omega \quad (5.1c)$$

with the boundary conditions

$$\underline{u} = \underline{u}^d \quad \text{on } \Gamma_u \quad (5.2a)$$

$$\underline{\sigma} \cdot \underline{n} = \underline{T}^d \quad \text{on } \Gamma_t \quad (5.2b)$$

with  $\mathbb{D}$  the fourth-order elasticity tensor introduced in section 2.4.3. Equation (5.1a) corresponds to the infinitesimal deformations hypothesis ( $\|\underline{u}\| \ll 1$  and  $\|\underline{\nabla u}\| \ll 1$ ), Equation (5.1b) to the compatibility conditions of the stress tensor, Equation (5.1c) to the stress-strain relationship of the solid (cf. section 2.4.3, Equation (2.14)), Equation (5.2a) to Dirichlet boundary conditions and Equation (5.2b) to Neumann boundary condition.

From Definition (5.1), the laws of thermodynamic are respected for the displacements and stress tensor following the two definitions (Bonnet and Frangi, 2006; Legay, 2012):

**Definition 5.2 (Admissible stress states)**  $\underline{\underline{\sigma}}$  is kinematically admissible if and only if

$$\underline{\underline{\sigma}} \in \mathcal{S} \doteq \left\{ \begin{array}{l} \underline{\underline{\sigma}} \quad \left| \quad \begin{array}{ll} \sigma_{ij,j} + f_i = 0 & \text{in } \Omega \\ \sigma_{ij}n_j = T_i^d & \text{on } \Gamma_t \end{array} \right. \end{array} \right\} \quad (5.3)$$

**Definition 5.3 (Admissible displacements)**  $\underline{u}$  is kinematically admissible if and only if

$$\underline{u} \in \mathcal{U} \doteq \left\{ \begin{array}{l} \underline{u} \quad \left| \quad u_i = u_i^d \text{ on } \Gamma_u \end{array} \right. \right\} \quad (5.4)$$

The equations given in Definition (5.1) are sufficient to completely describe the response of a solid subjected to boundary conditions and loadings while respecting of the laws of thermodynamic. However, in their present forms, called *strong formulation*, the equations are valid for a continuum solid only. For a finite element they must be reformulated in order to be valid on a discretised domain.

### 5.3.2 Weak formulation

The weak form is a variational statement of the problem in which we integrate against a test function to be defined later. This has the effect of relaxing the problem: instead of finding an exact solution, we are finding a solution that satisfies the strong form on average over the domain. A solution of the strong form will always satisfy the weak form, but not reciprocally.

The test function is chosen as an arbitrary virtual displacement  $\underline{\delta u} \in \mathcal{U}$ . Therefore, the weak form of Equation (5.1b) is given by

$$\forall \underline{\delta u} \in \mathcal{U} \quad \int_{\Omega} (\nabla \cdot \underline{\underline{\sigma}}) \cdot \underline{\delta u} \, d\Omega + \int_{\Omega} \underline{f} \cdot \underline{\delta u} \, d\Omega = 0 \quad (5.5)$$

Integrating by parts and using Ostrogradsky's theorem the boundary conditions (5.2a-5.2b) are introduced into Equation (5.5), which gives the

**Definition 5.4 (Virtual work principle)**

$$\forall \underline{\delta u} \in \mathcal{U} \quad \int_{\Omega} (\underline{\underline{\sigma}} : \underline{\nabla \delta u}) \, d\Omega - \int_{\Gamma_u} (\underline{\underline{\sigma}} \cdot \underline{n}) \cdot \underline{\delta u} \, d\Gamma - \int_{\Gamma_t} (\underline{T}^d \cdot \underline{\delta u}) \, d\Gamma - \int_{\Omega} \underline{f} \cdot \underline{\delta u} \, d\Omega = 0 \quad (5.6)$$

The reaction  $\underline{T} = \underline{\underline{\sigma}} \cdot \underline{n}$  on  $\Gamma_u$  can be eliminated by restraining Equation (5.6) to the virtual displacements equal to zero. This kinematic aspect is then accounted for in the space  $\mathcal{U}$  in which there is the unknown  $\underline{u}$ . Moreover, we have

$$\underline{\underline{\sigma}} : \underline{\nabla \delta u} = \underline{\underline{\sigma}} : \underline{\delta \varepsilon} \quad (5.7)$$

The proof is given in Appendix B.1. This leads to a convenient reformulation of the virtual work principle given by

**Definition 5.5 (Variant of the virtual work principle)**  $\underline{u}$  is solution of the problem  $\Leftrightarrow$  find  $\underline{u} \in \mathcal{U}$  such that  $\forall \delta \underline{u} \in \mathcal{U}(\underline{0}) = \{\underline{u} \mid \underline{u} = \underline{0} \text{ on } \Gamma_u\}$

$$\int_{\Omega} (\underline{\sigma} : \delta \underline{\varepsilon}) d\Omega - \int_{\Gamma_u} (\underline{T}^d \cdot \delta \underline{u}) d\Gamma - \int_{\Omega} \underline{f} \cdot \delta \underline{u} d\Omega = 0 \quad (5.8)$$

This equation is an all-in-one formulation of the Equations (5.1) and (5.2). However it is still valid on  $\Omega$  only, and therefore further refinement must be performed to get a formulation suitable on a subvolume  $\Omega_i \in \Omega$ . More details regarding the calculations can be found in (Legay, 2012).

### 5.3.3 Weighted residual formulation

The notion of elements and their nodal values are still to be introduced into Equation (5.8). The Galerkin method aims at discretising the problem by transforming the integral of volume into a sum of integrals on elementary elements.

#### Galerkin's method

Galerkin methods are used to convert a continuous problem, valid on an infinite dimensional space  $\Omega$ , to a discrete problem valid on a finite dimensional space  $\Omega_i \in \Omega$  ( $\cup \Omega_i = \Omega$ ,  $\cap \Omega_i = \emptyset$ ). Several variants of this method exist; we present here the weighted residual method that leads to the formulation of the stiffness matrix. The methodology is similar to the variational method, except the test function  $v$  and the unknown displacements  $\underline{u}$  are expressed as a linear combination of kinematically admissible displacements  $\underline{\psi}_i \in \mathcal{U}$  (Bonnet and Frangi, 2006):

$$\underline{u}(x) \approx \hat{\underline{u}}(x) = \sum_{i=1}^n \alpha_i \underline{\psi}_i(x) \quad \delta \underline{u}(x) \approx \delta \hat{\underline{u}}(x) = \sum_{i=1}^n \beta_i \underline{\psi}_i(x) \quad (5.9)$$

with  $n$  the total number of nodes in the mesh,  $\boldsymbol{\alpha} = \{\alpha_1, \alpha_2, \dots, \alpha_n\}^T \in \mathbb{R}^n$  the generalised variables of the element,  $\delta u_i$  the virtual nodal displacement at the node  $i$ ,  $\boldsymbol{\psi} = \{\psi_1, \psi_2, \dots, \psi_n\}^T$  a finite basis, and  $\boldsymbol{\beta} = \{\beta_1, \beta_2, \dots, \beta_n\}^T$  a set of arbitrary scalars.

The approximation of the admissible displacements field is therefore the keystone of the finite element method. One convenient way is to write  $\hat{\underline{u}}$  as a linear combination of the nodal values (Zienkiewicz and Taylor, 2000):

$$\hat{\underline{u}}(x) = \sum_{i=0}^n \mathbf{N}_i \underline{u}_i \quad (5.10)$$

with  $\mathbf{N}_i = N_i \mathbf{I}_{p \in \{1,2,3\}}$  and  $N_i$  the *global shape function*<sup>1</sup> associated to node  $i$ . More details about the notion of nodal interpolation and the relationship between the generalised variables and the nodal displacements are given in Appendix B.2. A systematic procedure for the construction of the shape functions based on polynomial interpolation can be found in Dhatt and Touzot (1984). The finite element approximation is

<sup>1</sup> $\mathbf{I}_p$  the  $p \times p$  identity matrix. The value  $p$  depends on the problem. For more details see Hinton and Owen (1980); Zienkiewicz and Taylor (2000).

therefore a Galerkin formulation of the weighted residual method applied on the strong form of the equilibrium equations.

### Discretisation of the virtual work principle equation

**Notation for numerical use** For a numerical use, it is often more convenient to make use of the symmetry of the  $2^{nd}$  order stress and strain tensors and write them as vectors using Voigt Notation. The following notations replace the previous one<sup>2</sup>:

$$\begin{aligned} \underline{\underline{\sigma}} &\equiv \boldsymbol{\sigma} = \{\sigma_{xx}, \sigma_{yy}, \sigma_{zz}, \tau_{yz}, \tau_{xz}, \tau_{xy}\}^T \\ \underline{\underline{\varepsilon}} &\equiv \boldsymbol{\varepsilon} = \{\varepsilon_{xx}, \varepsilon_{yy}, \varepsilon_{zz}, 2\varepsilon_{yz}, 2\varepsilon_{xz}, 2\varepsilon_{xy}\}^T \\ \underline{\underline{T}}^d &\equiv \mathbf{t} \\ \underline{\underline{f}} &\equiv \mathbf{f} \\ \underline{\underline{u}} &\equiv \mathbf{u} \\ \mathbb{D} &\equiv \mathbf{D} \end{aligned}$$

**Discretisation** For any solid the virtual work principle (Equation (5.8)) can be written as a function of the displacements only

$$\int_{\Omega} [\delta \boldsymbol{\varepsilon}]^T \boldsymbol{\sigma} d\Omega - \int_{\Omega} [\delta \mathbf{u}]^T \mathbf{f} d\Omega - \int_{\Gamma_t} [\delta \mathbf{u}]^T \mathbf{t} d\Gamma = 0 \quad (5.11)$$

From Galerkin's method (Equation (5.10)), the displacements  $\mathbf{u}$  and the virtual displacements  $\delta \mathbf{u}$  are expressed by

$$\mathbf{u} = \sum_{i=1}^n N_i \mathbf{d}_i \quad \delta \mathbf{u} = \sum_{i=1}^n N_i \delta \mathbf{d}_i \quad (5.12)$$

and the strains  $\boldsymbol{\varepsilon}$  and the virtual strains  $\delta \boldsymbol{\varepsilon}$  by

$$\boldsymbol{\varepsilon} = \sum_{i=1}^n \mathbf{B}_i \mathbf{d}_i \quad \delta \boldsymbol{\varepsilon} = \sum_{i=1}^n \mathbf{B}_i \delta \mathbf{d}_i \quad (5.13)$$

with  $n$  the total number of nodes in the whole mesh,  $\mathbf{d}_i$  the vector of nodal variables and  $\mathbf{B}_i$  the global strain-displacement matrix given by

$$\mathbf{B}_i = \begin{bmatrix} \frac{\partial N_i}{\partial x} & 0 \\ 0 & \frac{\partial N_i}{\partial y} \\ \frac{\partial N_i}{\partial y} & \frac{\partial N_i}{\partial x} \end{bmatrix} \quad (5.14)$$

for two-dimensionnal plane stress and plane strain problems<sup>3</sup> (Hinton and Owen, 1980; Zienkiewicz and Taylor, 1989). Substituting Equations (5.12) and (5.13) into Equation (5.11) leads to the discretisation of the virtual work principle on all the nodes of

<sup>2</sup>Lowcase letters denote a vector and capital letters a matrix.

<sup>3</sup>A different formulation is required for axisymmetric problems.

the mesh

$$\int_{\Omega} \left( \sum_{i=1}^n [\delta \mathbf{d}_i]^T [\mathbf{B}_i]^T \right) \boldsymbol{\sigma} d\Omega - \int_{\Omega} \left( \sum_{i=1}^n [\delta \mathbf{d}_i]^T [\mathbf{N}_i]^T \right) \mathbf{f} d\Omega - \int_{\Gamma_t} \left( \sum_{i=1}^n [\delta \mathbf{d}_i]^T [\mathbf{N}_i]^T \right) \mathbf{t} d\Gamma = 0 \quad (5.15)$$

which can be written as a sum over each node of the mesh

$$\sum_{i=1}^n [\delta \mathbf{d}_i]^T \left\{ \int_{\Omega} [\mathbf{B}_i]^T \boldsymbol{\sigma} d\Omega - \int_{\Omega} [\mathbf{N}_i]^T \mathbf{f} d\Omega - \int_{\Gamma_t} [\mathbf{N}_i]^T \mathbf{t} d\Gamma \right\} = 0 \quad (5.16)$$

Since Equation (5.16) must be true for any virtual displacements  $\delta \mathbf{d}_i$ , the vector of nodal displacements  $\mathbf{d}_i$ , solution of the problem, is obtained by solving

$$\int_{\Omega} [\mathbf{B}_i]^T \boldsymbol{\sigma} d\Omega - \int_{\Omega} [\mathbf{N}_i]^T \mathbf{f} d\Omega - \int_{\Gamma_t} [\mathbf{N}_i]^T \mathbf{t} d\Gamma = 0 \quad (5.17)$$

The unknowns  $\mathbf{d}_i$  are introduced by using the stress-strain relationship (Equation (5.1c)). For each element, we have

$$\boldsymbol{\sigma}^{(e)} = \mathbf{D}^{(e)} \boldsymbol{\varepsilon}^{(e)} = \mathbf{D}^{(e)} \left( \sum_{j=1}^r \mathbf{B}_j^{(e)} \mathbf{d}_j^{(e)} \right) \quad (5.18)$$

with  $r$  the number of nodes per element. Therefore, the contribution of element  $e$  to Equation (5.17) is given as

$$\sum_{j=1}^r \left( \underbrace{\int_{\Omega^{(e)}} [\mathbf{B}_i^{(e)}]^T \mathbf{D}^{(e)} \mathbf{B}_j^{(e)} d\Omega}_{\mathbf{K}_{ij}^{(e)}} \right) \mathbf{d}_j^{(e)} = \underbrace{\int_{\Omega^{(e)}} [\mathbf{N}_i^{(e)}]^T \mathbf{f}^{(e)} d\Omega}_{\mathbf{f}_{B_i}^{(e)}} + \underbrace{\int_{\Gamma_t^{(e)}} [\mathbf{N}_i^{(e)}]^T \mathbf{t}^{(e)} d\Gamma}_{\mathbf{f}_{T_i}^{(e)}} \quad (5.19)$$

where  $\mathbf{K}_{ij}^{(e)}$  is the positive-definite submatrix of the element stiffness matrix  $\mathbf{K}^{(e)}$  linking nodes  $i$  and  $j$ . For a  $r$ -noded element with  $n_d$  degrees of freedom per node, Equation (5.19) gives a set of  $(r \cdot n_d)$  equations which, in matrix notation, gives the  $(r \cdot n_d) \times (r \cdot n_d)$  element stiffness matrix

$$\mathbf{K}^{(e)} = \int_{\Omega^{(e)}} [\mathbf{B}^{(e)}]^T \mathbf{D}^{(e)} \mathbf{B}^{(e)} d\Omega \quad \left( \mathbf{K}^{(e)} \in \mathcal{M}_{r \cdot n_d}(\mathbb{R}) \right) \quad (5.20)$$

with  $\mathbf{B}^{(e)} = [\mathbf{B}_1^{(e)} \mathbf{B}_2^{(e)} \dots \mathbf{B}_r^{(e)}]$ . The integration is performed in the local coordinate system  $\boldsymbol{\xi} = (\xi, \eta)$  of the element. The discretised elemental volume is given as:

$$d\Omega^{(e)} = h^{(e)} \det \mathbf{J}^{(e)} d\xi d\eta \quad (5.21)$$

with  $h^{(e)}$  the thickness of the element and  $\mathbf{J}^{(e)}$  the Jacobian matrix. Therefore,

$$\mathbf{K}_{ij}^{(e)} = \int_{-1}^{+1} \int_{-1}^{+1} [\mathbf{B}^{(e)}]^T \mathbf{D}^{(e)} \mathbf{B}^{(e)} h^{(e)} \det \mathbf{J}^{(e)} d\xi d\eta \quad (5.22)$$

In an isoparametric representation the same shape functions are used to approximate

the unknowns and the geometry:

$$\begin{bmatrix} x^{(e)} \\ y^{(e)} \end{bmatrix} = \sum_{i=1}^r \begin{bmatrix} N_i^{(e)} & 0 \\ 0 & N_i^{(e)} \end{bmatrix} \begin{bmatrix} x_i^{(e)} \\ y_i^{(e)} \end{bmatrix} \quad (5.23)$$

Assuming an isoparametric representation we evaluate the Jacobian matrix as

$$\mathbf{J}^{(e)} = \begin{bmatrix} \frac{\partial x}{\partial \xi} & \frac{\partial y}{\partial \xi} \\ \frac{\partial x}{\partial \eta} & \frac{\partial y}{\partial \eta} \end{bmatrix} = \begin{bmatrix} \sum_{i=1}^r \frac{\partial N_i^{(e)}}{\partial \xi} x_i^{(e)} & \sum_{i=1}^r \frac{\partial N_i^{(e)}}{\partial \xi} y_i^{(e)} \\ \sum_{i=1}^r \frac{\partial N_i^{(e)}}{\partial \eta} x_i^{(e)} & \sum_{i=1}^r \frac{\partial N_i^{(e)}}{\partial \eta} y_i^{(e)} \end{bmatrix} \quad (5.24)$$

The determinant of  $\mathbf{J}^{(e)}$  is evaluated using the expression

$$[\mathbf{J}^{(e)}]^{-1} = \frac{1}{\det \mathbf{J}^{(e)}} \begin{bmatrix} \frac{\partial y}{\partial \eta} & -\frac{\partial y}{\partial \xi} \\ -\frac{\partial x}{\partial \eta} & \frac{\partial x}{\partial \xi} \end{bmatrix} \quad (5.25)$$

Equations (5.24) and (5.25) are linked with the concept of bijectivity introduced in section 2.4.2; one can see that the finite element method follows and respects the main assumptions of continuum mechanics.

**Assembled stiffness matrix** These element stiffness matrices assembled together gives the global stiffness matrix  $\mathbf{K} \in \mathcal{M}_{n \cdot n_d}(\mathbb{R})$ . The nodal displacements  $\mathbf{d}$  of the  $n$  nodes of the mesh are obtained by solving

$$[\mathbf{K}] \{\mathbf{d}\} = \{\mathbf{f}_{B_i} + \mathbf{f}_{T_i}\} \quad (5.26)$$

which corresponds to a set of  $n \cdot n_d$  linear equations to be solved simultaneously. The concept introduced in Section 5.2 about the overall response being approximated by assembling the response of all the elements appears clearly in Equations (5.22) and (5.26).

This section has been the opportunity to show in detail the transformation of the constitutive equations into a suitable form for finite element use. Especially, Equations (5.18) and (5.19) have shown how the stress-strain relationship is introduced in the virtual work principle. For elasto-plastic applications, the concept of plasticity will be introduced at this step.

## 5.4 Theory of plasticity in finite element method

The purpose of the previous section was to give an insight of the main steps involved in the discretisation of the strong formulation for the FEM, and to point out when the stress-strain relationship is involved (Equations (5.18)-(5.19)). We now consider a material experiencing plasticity and describe the methodology for the implementation of elasto-plastic models in FEA.



The object of plasticity is to describe the behaviour of a material which experiences irrecoverable deformations taking place once certain stress state is reached. Three requirements have to be met in order to model numerically plastic deformations:

- A yield criterion describing the stress state at which irrecoverable deformation occurs
- A stress-strain relationship when the deformation is made up of elastic and plastic components
- A formulation for evaluation of the elasto-plastic matrix  $\mathbf{D}_{ep}$

First the methodology to write a yield criterion in a suitable form for numerical modelling is presented. We will then focus on the implementation of hardening and softening using the framework of the Modified Cam Clay model. Finally, we generalize the stress-strain relationship for elasto-plastic behaviour and introduce the elasto-plastic matrix  $\mathbf{D}_{ep}$ . At the same time, we will formulate the model MASS into a suitable form for finite element modelling.

### 5.4.1 Yield criterion

The yield criterion  $F$ <sup>4</sup> is a function of the stress state  $\underline{\underline{\sigma}}$  that describes the limit between the elastic and plastic behaviour. However, the formulation of  $F$  can become highly complex if it is expressed as a function of  $\sigma_{ij}$ . A convenient way is to make use of the properties of the stress tensor and write the yield criterion such that it does not depend upon the coordinate system, and therefore should be a function of the three stress invariants:

$$I_1 \doteq \text{tr} \underline{\underline{\sigma}} \quad I_2 \doteq \frac{1}{2} \text{tr} (\underline{\underline{\sigma}} \cdot \underline{\underline{\sigma}}) \quad I_3 \doteq \frac{1}{2} \text{tr} (\underline{\underline{\sigma}} \cdot \underline{\underline{\sigma}} \cdot \underline{\underline{\sigma}}) \quad (5.27)$$

and of the two deviatoric stress invariants of the stress deviator tensor  $\underline{\underline{s}} \doteq \underline{\underline{\sigma}} - \frac{I_1}{3} \underline{\underline{I}}$

$$J_2 \doteq \frac{1}{2} \text{tr} (\underline{\underline{s}} \cdot \underline{\underline{s}}) \quad J_3 \doteq \frac{1}{2} \text{tr} (\underline{\underline{s}} \cdot \underline{\underline{s}} \cdot \underline{\underline{s}}) \quad (5.28)$$

The formulation proposed for structured and lime treated soils was developed in the framework of the Modified Cam Clay model. The yield function of this model, originally suitable for triaxial case, is expressed as a function of the effective mean stress  $p'$  and the deviatoric stress  $q$ . By noticing that

$$q = \sqrt{3J_2} \quad \text{and} \quad p' = \frac{I_1}{3} \quad (5.29)$$

the yield function (Equation (2.44)) can be written in terms of  $I_1$  and  $J_2$  (Potts and Zdravkovic, 1999)

$$F(\underline{\underline{\sigma}}, p_0, \varepsilon_p^p) = 3J_2 - I_1(I_1 - p_0)M^2 = 0 \quad (5.30)$$

which makes it suitable for the general stress space  $(\sigma_I, \sigma_{II}, \sigma_{III})$ . For the model MASS,

<sup>4</sup>Capital letter is used to avoid confusion with the body forces vector.

the yield function written in terms of the invariants is very similar and is given by

$$F(\underline{\sigma}, p_0, \varepsilon_p^p) = 3J_2 - (p_0 - I_1)(I_1 - p_b)M^2 = 0 \quad (5.31)$$

We now have a convenient formulation to determine if the stress state lies inside or outside the yield surface. This was the first of the three challenges identified supra. We now describe the relationship between the plastic straining and the stress state at yield.

#### 5.4.2 Flow rule

The flow rule gives the relationship between the plastic deformation and the stress state. By definition (Zienkiewicz and Taylor, 1991), we have

$$d\varepsilon^p \doteq d\lambda \frac{\partial G}{\partial \sigma} \quad (5.32)$$

or for any component  $i$

$$d\varepsilon_i^p \doteq d\lambda \frac{\partial G}{\partial \sigma_i} \quad (5.33)$$

with  $d\varepsilon^p$  the plastic strain increment,  $G$  the plastic potential, and  $d\lambda$  the plastic multiplier a scalar to be determined.

As it was pointed out previously, the determination of the plastic potential from experimental results is not an easy task. A frequent hypothesis chosen by many models, e.g. the Modified Cam Clay, consists in assuming  $F \equiv G$ . Under this assumption, called *normality rule*, the vector of plastic strain increment is normal to the yield surface in the stress space. It was shown in Section 4.7.1 that normality rule can be assumed for lime treated materials. Thus we have for the model MASS

$$d\varepsilon^p = d\lambda \frac{\partial F}{\partial \sigma} \quad (5.34)$$

This formula, called *flow rule*, links the plastic strain increment to the stress increment and will be of great importance for the formulation of the elasto-plastic stress-strain relationship.

#### 5.4.3 Incremental stress-strain relationship

By definition, strain changes are assumed to be made of an elastic and a plastic component:

$$d\varepsilon = d\varepsilon^e + d\varepsilon^p \quad (5.35)$$

The elastic strain increment is related to the stress increment by the elastic matrix  $\mathbf{D}$ . Combining Equations (5.1c), (5.34) and (5.35) gives

$$d\varepsilon = [\mathbf{D}]^{-1}d\sigma + d\lambda \frac{\partial F}{\partial \sigma} \quad (5.36)$$

The yield surface is updated using the hardening parameter  $\kappa$  which links the plastic deformations with the variation of the yield surface. The "amount" of plastic straining due to the stress increment  $d\sigma$  is calculated using Equation (5.34), and requires the

determination the plastic multiplier  $d\lambda$ . When plastic loading is occurring, the stress state remains on yield surface<sup>5</sup> ( $F(\underline{\sigma}, \kappa) = 0$ ). By differentiating  $F(\underline{\sigma}, \kappa)$  we have:

$$dF = \frac{\partial F}{\partial \underline{\sigma}} d\underline{\sigma} + \frac{\partial F}{\partial \kappa} d\kappa = 0 \quad (5.37)$$

or

$$dF = \frac{\partial F}{\partial \sigma_x} d\sigma_x + \frac{\partial F}{\partial \sigma_y} d\sigma_y + \dots + \frac{\partial F}{\partial \kappa} d\kappa = 0 \quad (5.38)$$

Using matrix notation for numerical use, Equation (5.38) is equivalent to

$$dF = \left\{ \frac{\partial F}{\partial \boldsymbol{\sigma}} \right\}^T d\boldsymbol{\sigma} + \frac{\partial F}{\partial \kappa} d\kappa = 0 \quad (5.39)$$

in which we make the following substitutions

$$A = -\frac{1}{d\lambda} \frac{\partial F}{\partial \kappa} d\kappa \quad \text{and} \quad \mathbf{a}^T = \left\{ \frac{\partial F}{\partial \boldsymbol{\sigma}} \right\}^T = \left[ \frac{\partial F}{\partial \sigma_x}, \frac{\partial F}{\partial \sigma_y}, \frac{\partial F}{\partial \sigma_z}, \frac{\partial F}{\partial \tau_{yz}}, \frac{\partial F}{\partial \tau_{zx}}, \frac{\partial F}{\partial \tau_{xy}} \right] \quad (5.40)$$

with  $\mathbf{a}$  the flow vector. Equation (5.39) becomes

$$dF = \mathbf{a}^T d\boldsymbol{\sigma} - Ad\lambda = 0 \quad (5.41)$$

Equation (5.36) can be rewritten as follows

$$\mathbf{a}^T \mathbf{D} d\boldsymbol{\varepsilon} = \mathbf{a}^T d\boldsymbol{\sigma} + d\lambda \mathbf{a}^T \mathbf{D} \mathbf{a} \quad (5.42)$$

which, combined with Equation (5.41), gives

$$\mathbf{a}^T \mathbf{D} d\boldsymbol{\varepsilon} = Ad\lambda + d\lambda \mathbf{a}^T \mathbf{D} \mathbf{a} \quad (5.43)$$

from which we obtain the plastic multiplier  $d\lambda$

$$d\lambda = \frac{\mathbf{a}^T \mathbf{D}}{A + \mathbf{a}^T \mathbf{D} \mathbf{a}} d\boldsymbol{\varepsilon} \quad (5.44)$$

Thus, the incremental stress-strain relationship (Equation (5.36)) can be written as

$$d\boldsymbol{\sigma} = \mathbf{D} d\boldsymbol{\varepsilon} - d\lambda \mathbf{D} \mathbf{a} \quad (5.45)$$

which is equivalent to

$$d\boldsymbol{\sigma} = \underbrace{\left( \mathbf{D} - \frac{\mathbf{D} \mathbf{a} \mathbf{a}^T \mathbf{D}}{A + \mathbf{a}^T \mathbf{D} \mathbf{a}} \right)}_{\mathbf{D}_{ep}} d\boldsymbol{\varepsilon} \quad (5.46)$$

and gives the equation of the elasto-plastic matrix  $\mathbf{D}_{ep}$ :

$$\mathbf{D}_{ep} = \mathbf{D} - \frac{\mathbf{D} \mathbf{a} \mathbf{a}^T \mathbf{D}}{A + \mathbf{a}^T \mathbf{D} \mathbf{a}} \quad (5.47)$$

<sup>5</sup>The case  $F(\underline{\sigma}, \kappa) > 0$  being not permitted.

$\mathbf{D}_{ep}$  is symmetric as long as the yield function and the plastic potential are associated ( $F \equiv G$ ). One can notice that there is still no sign of the hardening parameter in  $\mathbf{D}_{ep}$ . Indeed, one unknown remains: the parameter  $A$  which is still expressed as a function of  $d\lambda$ . If hardening is considered, its formulation – in which the parameter  $\kappa$  should appear – must be fully determined. In the Modified Cam-Clay model, hardening/softening is only due to the plastic volumetric strains; therefore,  $\kappa = \varepsilon_p^p$ . By definition, we have

$$d\kappa = d\varepsilon_p^p = \text{tr } d\underline{\underline{\varepsilon}}^p = d\varepsilon_x^p + d\varepsilon_y^p + d\varepsilon_z^p = d\lambda \left( \frac{\partial F}{\partial \sigma_x} + \frac{\partial F}{\partial \sigma_y} + \frac{\partial F}{\partial \sigma_z} \right) \quad (5.48)$$

which combined with Equation (5.40) and using the chain rule gives

$$A = -\frac{\partial F}{\partial d\varepsilon_p^p} \left( \frac{\partial F}{\partial \sigma_x} + \frac{\partial F}{\partial \sigma_y} + \frac{\partial F}{\partial \sigma_z} \right) \quad (5.49)$$

$$= -\frac{\partial F}{\partial p'_0} \frac{\partial p'_0}{\partial \varepsilon_p^p} \left( \frac{\partial F}{\partial \sigma_x} + \frac{\partial F}{\partial \sigma_y} + \frac{\partial F}{\partial \sigma_z} \right) \quad (5.50)$$

Some of the terms in  $A$  were explicitly calculated in Section 4.6.2, and the explicit formulations of the flow vector  $\mathbf{a}$  and the parameter  $A$  are given in Appendix B.3. But as one can see, calculations can quickly become complicated, especially the determination of the elasto-plastic matrix. Fortunately, the explicit evaluation of the flow vector  $\mathbf{a}$  for numerical computations is not required. The flow vector can be rewritten as a function of alternative stress invariants, called Nayak's coefficient (Nayak and Zienkiewicz, 1972). This method gives a general formulation of the flow vector and requires only 3 constants for any criterion:

$$\mathbf{a} = C_1 \mathbf{a}_1 + C_2 \mathbf{a}_2 + C_3 \mathbf{a}_3 \quad (5.51)$$

with  $\mathbf{a}_1$ ,  $\mathbf{a}_2$ ,  $\mathbf{a}_3$  three vectors independent of the yield criterion and therefore constant:

$$\mathbf{a}_1^T = \frac{\partial I_1}{\partial \boldsymbol{\sigma}} = \{1, 1, 0, 1\} \quad (5.52)$$

$$\mathbf{a}_2^T = \frac{\partial (J_2)^{1/2}}{\partial \boldsymbol{\sigma}} = \frac{1}{2\sqrt{J_2}} \{s_x, s_y, 2\tau_{xy}, s_z\} \quad (5.53)$$

$$\mathbf{a}_3^T = \frac{\partial J_3}{\partial \boldsymbol{\sigma}} = \left\{ \left( s_y s_z + \frac{J_2}{3} \right), \left( s_x s_z + \frac{J_2}{3} \right), -2s_z \tau_{xy}, \left( s_y s_y - \tau_{xy}^2 + \frac{J_2}{3} \right) \right\} \quad (5.54)$$

and  $C_1$ ,  $C_2$ ,  $C_3$  the Nayak's coefficients specific for each criterion to be determined:

$$C_1 = \frac{\partial f}{\partial I_1} \quad C_2 = \left( \frac{\partial f}{\partial (J_2)^{1/2}} - \frac{\tan(3\theta)}{(J_2)^{1/2}} \frac{\partial f}{\partial \theta} \right) \quad C_3 = \frac{-\sqrt{3}}{2 \cos(3\theta)} \quad (5.55)$$

with  $\theta$  a term related to the Lode angle  $\Gamma$  and given by  $\Gamma = -\sqrt{3} \tan \theta$  to locate the stress state in the deviatoric  $\pi$  plane.

This method leads to significant simplifications of the equations and is particularly suitable in a finite element program in which different yield criteria are implemented.

Moreover the explicit formulation of the elasto-plastic matrix, which can require heavy calculations, is not required anymore. The Nayak's coefficient of the criteria implemented in the finite element program FEMASS developed in this study are given in Table 5.1. One can note that criteria with circular sections in the  $\pi$  plane (i.e. Von Mises, Drucker-Prager, MCC, MASS) are independent of  $\theta$ , and criteria independent of the hydrostatic pressure (i.e. Tresca and Von Mises) have their coefficients  $C_1$  equal to zero.

Table 5.1: Nayak's coefficients for the 6 yield criteria implemented in the FEM program

Yield criterion	C1	C2	C3
Mohr-Coulomb	$\frac{1}{3} \sin \phi$	$\cos \theta \left[ (1 + \tan \theta \tan 3\theta) + (\tan 3\theta - \tan \theta) \frac{\sin \phi}{\sqrt{3}} \right]$	$\frac{\sqrt{3} \sin \theta + \cos \theta \sin \phi}{2J_2 \cos 3\theta}$
Tresca	0	$2 \cos \theta (1 + \tan \theta \tan 3\theta)$	$\frac{\sqrt{3}}{J_2} \frac{\sin \theta}{\cos 3\theta}$
Von Mises	0	$\sqrt{3}$	0
Drucker-Prager	$\alpha$	1.0	0
Modified Cam Clay	$\frac{1}{9} (2I_1 + 3p'_0)$	$\frac{6(J_2)^{1/2}}{M^2}$	0
MASS	$\frac{1}{9} (2I_1 + 3(p'_0 + p'_b))$	$\frac{6(J_2)^{1/2}}{M^2}$	0

We finally gathered all the elements necessary for the development of a finite element program for elasto-plastic problem. The strong formulation of continuum mechanics has been written in a form suitable to be used on a discretised geometry. Moreover, we formulated the parameters required for the implementation of the model MASS. We now present the structure of the finite element program developed during this thesis.

## 5.5 Presentation of the finite element code FEMASS

This thesis is incorporated within the larger framework of developing a model for the chemo-mechanical modelling of soil treatment. As a first step, a completely functional Finite Element Model for Artificially Structured Soils (FEMASS) has been developed in this thesis for elasto-plastic problems. It includes the pre- and post-processing of the problem and is suitable for several geotechnical applications. The structure of the code FEMASS is given in Figure 5.3.

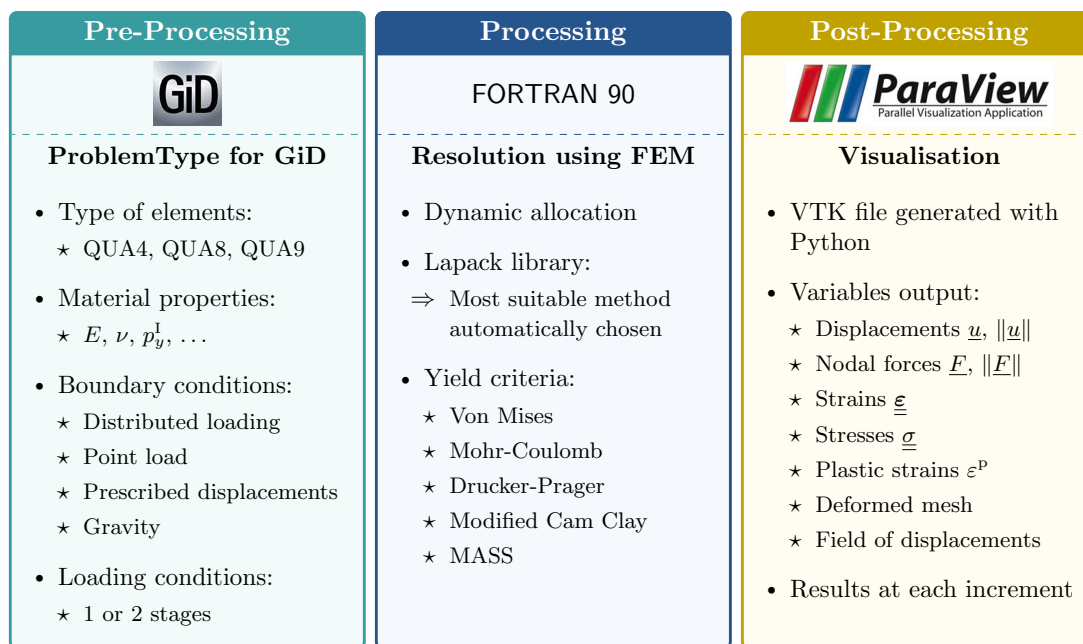


Figure 5.3: Structure of the finite element program FEMASS

We now explain the motivations behind the choice of the methods used in the program FEMASS.

### 5.5.1 Pre-processing

GiD is an open-source cross-platform pre-processor for numerical simulation in science and engineering (GiD User Manual, 2014). It gives the possibility to generate a mesh from any kind of geometry (2D or 3D) as well as to inform the characteristics of the materials and the boundary conditions of the problem.

The interesting feature that motivated the use of GiD is the framework of the ProblemType. Chosen by the user, a ProblemType gives the possibility to export all the information of a problem in a predefined format (GiD Customization Manual, 2014). GiD is therefore a versatile software particularly adapted to finite element. In this thesis a ProblemType was specifically developed for the modelling of 2D-geotechnical problems. Once loaded, a graphic interface allows the user to add all the information related to the problem and export them with the mesh in text file containing all the details of the simulation.

This file is used as input file for the processing of the finite element calculations. The listing of the ProblemType developed for the FEMASS and an example of input file are given in Appendix B.4.

### 5.5.2 Processing

The FEMASS was developed in the framework of the method proposed by Hinton and Owen (1980). It gives the general procedures inherent of finite element modelling and provides a background for the implementation of a finite element program.

We chose Fortran 90 for the implementation of the numerical procedures. Although it might be considered nowadays as an outdated language, Fortran remains one of the most efficient for the manipulation of large arrays and benefits from years of experience. The FEMASS uses as much as possible the new functions introduced in Fortran 90, which includes dynamic memory allocation of vectors and matrices, derived structured data type, and the use of modules instead of common blocks for global variables.

The resolution uses the initial stiffness method, and the linear systems are solved using Lapack and Blas libraries (Anderson, 1992). These libraries support multithreading, which reduces significantly the computational time (Anderson et al., 1990), and automatically chooses the most suitable method depending on the stiffness matrix (e.g. symmetric, non-symmetric, banded, sparse, etc . . .). In the event of plastic strains resulting from a stress state lying outside the yield surface, the stress state is brought back on the yield surface using a refinement algorithm. The pseudocode of the elastoplastic procedure implemented in the FEMASS is given in Appendix B.5, and more details about this algorithm can be found in Hinton and Owen (1980).

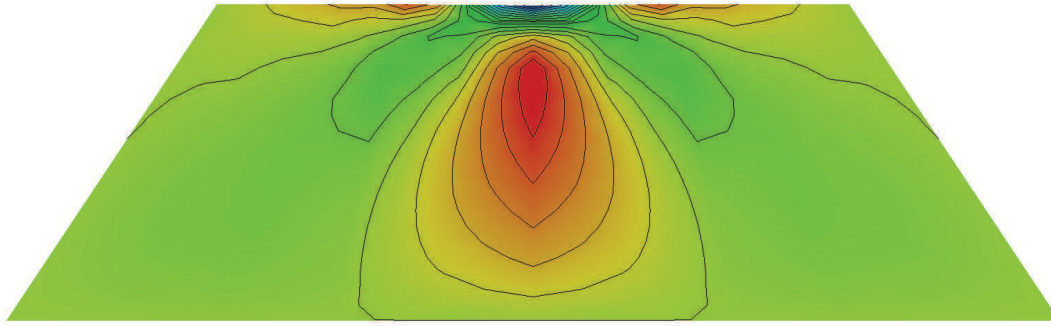
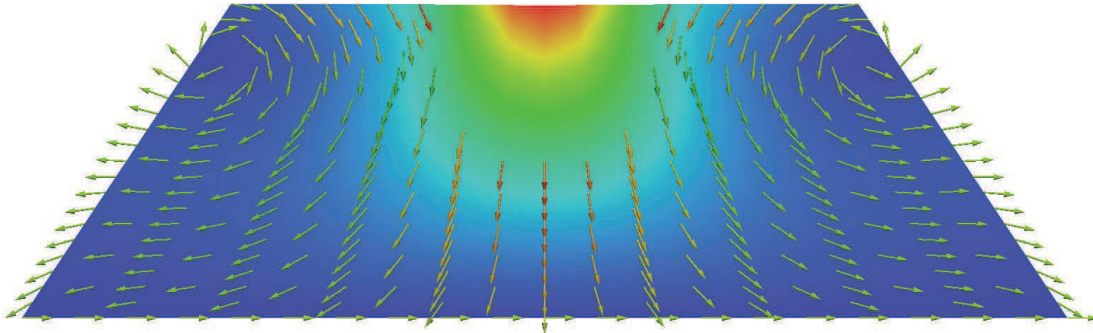
At the end of each increment, all the results of the simulation ( $\mathbf{d}$ ,  $\boldsymbol{\varepsilon}$ ,  $\boldsymbol{\sigma}$ ,  $\varepsilon^P$ , etc. . .) are output in a text file that will be used for the post-processing of the simulation.

### 5.5.3 Post-processing

One of the most interesting features of numerical modelling is the possibility to visualise the distribution of the unknown variables inside the structure. However, at the end of the calculations, the unknowns of the problem are given at the nodes or Gauss points and are saved in vectors or matrices. Before it can be read by a post-processing software, results must be exported in a suitable format.

In this thesis, results were saved using the *Visualization Toolkit* (VTK) which is a popular data file format to visualize the results of computer simulations such as analysis (VTK User's Guide, 2010). It provides a convenient framework to save the data and can be read by a large number of post-processing software, including ParaView which is an open-source, multi-platform data analysis and visualisation application (ParaView User's Guide, 2012). It allows the post-processing of simulations on complex geometries and offers many interesting features, such as contours lines and vector field visualisation (Figure 5.4).

The VTK format is quite straightforward and consists in a file containing the node coordinates, the connectivity table, and the unknowns at the nodal points. More details regarding the programming of the VTK format can be found in VTK User's Guide (2010). A Python script was developed for the program FEMASS to convert the output files created during the processing in the VTK format. The listing can be found in Appendix B.6.

(a) Contour lines for  $\varepsilon_{xy}$ 

(b) Magnitude of displacements and field displacements

Figure 5.4: Post-processing of the results produced by the FEMASS with ParaView of an embankment subjected to a distributed loading on the surface.

## 5.6 Validation of the finite element code FEMASS

### 5.6.1 Objectives

In Sections 5.3 and 5.4 we introduced the main steps of finite element modelling, such as the evaluation of the element stiffness matrix  $\mathbf{K}$  or the flow vector  $\mathbf{a}$ . However many other procedures, such as the evaluation of the shape functions, numerical integration, or computation of the invariants, are also involved. A finite element program is therefore made of a large number of subroutines that interact together. For this reason, the results produced by the code FEMASS must be validated on a benchmark test to ensure the validity of the complete procedure implemented. The main steps involved in a finite element model are given in Figure 5.5.



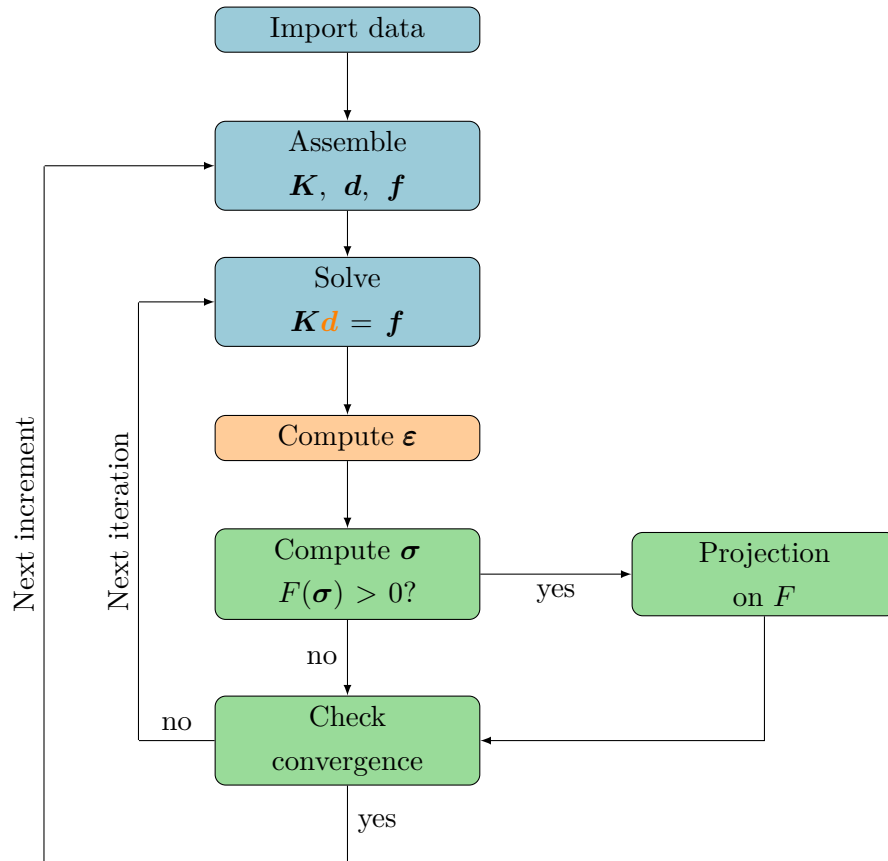


Figure 5.5: Flowchart of the main finite element procedures

Three main stages can be distinguished in Figure 5.5 and must be validated:

**Computation of the nodal displacements (blue):** This stage includes the importation of the mesh, connectivity table, and all the information regarding the problem to be modelled. Boundary conditions are converted into nodal forces and are used to assemble and reduce the global stiffness matrix, load vector, and nodal displacements vectors. These 3 arrays are then used as input by the Lapack library for the determination of the nodal displacements  $\mathbf{d}$ .

**Computation of the strain tensor (orange):** The strain tensor  $\boldsymbol{\varepsilon}$  is computed at each Gauss point using the nodal displacements of the element previously calculated. This stage involves the evaluation of the shape functions and their derivatives at any Gauss point in the local and Cartesian coordinate system, of the Jacobian matrix and its determinant, and numerical integration using Gauss-Legendre method.

**Computation of the stress tensor (green):** The stress tensor  $\boldsymbol{\sigma}$  is calculated from the strain tensor using the elastic stress-strain relationship. This stage involves the computation of the effective stress and the invariants of the stress tensor at each Gauss point. In the event of an increment leading to a stress state lying outside of the yield surface, an iterative procedure is initiated to bring it back on the yield surface, evaluate plastic straining, and update the yield surface (hardening and softening). Convergence is checked at the end of each iteration using the nodal

forces calculated from the current stress state.

After the validation of finite element model FEMASS for the modelling of elastoplastic problems, the proper implementation of the Modified Cam Clay model and the model MASS will be verified.

### 5.6.2 Simulation of a thick cylinder subjected to internal pressure

We validated the finite element program FEMASS using the benchmark provided by Hinton and Owen (1980) of a thick cylinder subjected to an internal pressure  $P$ . A mesh made of eight-node quadrilateral elements was used for the simulation with 4 ( $2 \times 2$ ) Gauss integration points in plane strain conditions (Figure 5.6). In this section we compare the results produced by the code FEMASS with the benchmark solutions (Hinton and Owen, 1980) and the good implementation of the three main stages previously identified (Figure 5.5).

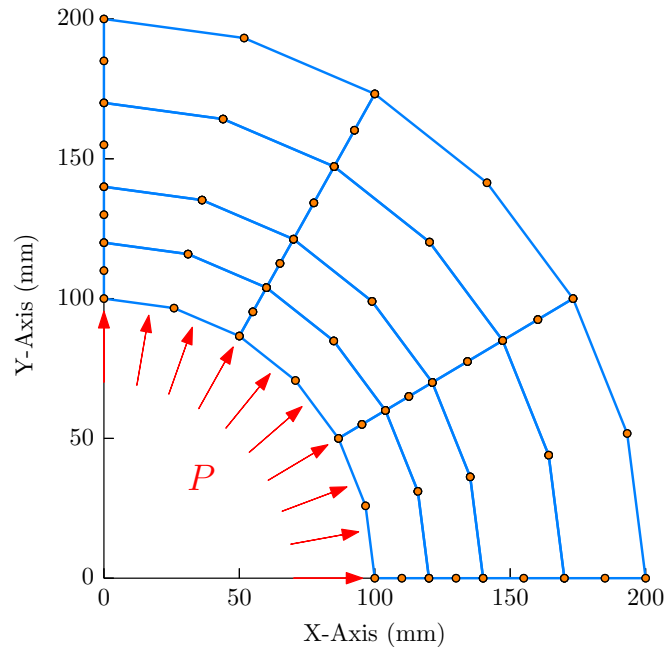


Figure 5.6: Mesh of the thick cylinder used for the validation –  $P$ : Internal pressure

The proper implementation of the FEM was validated using the relative error between the solutions of the FEMASS and the benchmark (Zienkiewicz and Taylor, 1989; Szabó and Babuška, 2011). The relative error, noted  $\Psi$ , of the variable  $y$  is given by

$$\Psi(y) = \left| \frac{\hat{y} - y}{y} \right| \times 100 \quad (5.56)$$

with  $\hat{y}$  the result of the FEMASS and  $y$  the benchmark solution. Parameters used for the simulation are given in Table 5.2.

Table 5.2: Parameters used for the validation.

Parameter	Criteria	Conditions	E (GPa)	$\nu$ (-)	$\sigma_y$ (MPa)	$H'$ (-)
Value	Von Mises	Plane strain	2.10	0.3	2.40	0.0

$H'$ : Strain hardening parameter,  $\sigma_y$ : Yield stress.

The validation was performed using the nodal displacements  $\mathbf{d}$ , the maximum principal strain  $\varepsilon_I$ , and the stress  $\sigma_{xy}$ , which correspond to the results of each of the three main steps of a finite element model (Figure 5.5). Two different internal pressures  $P$  are considered leading in both cases to plastic deformations. The maximum acceptable relative error was set to 1% (Guddati and Yue, 2004; Szabo and Babuska, 2009).

### Computation of the nodal displacements

We consider the displacements in a thick cylinder subjected to an internal pressure of 1.4 MPa. Figure 5.7 gives the relative error  $\Psi(\mathbf{d})$  on the displacements between the model FEMASS and the benchmark. A maximum error of 0.536% is obtained on the inner face of the cylinder, and quickly decreases to 0.431% after the first 15 millimetres.

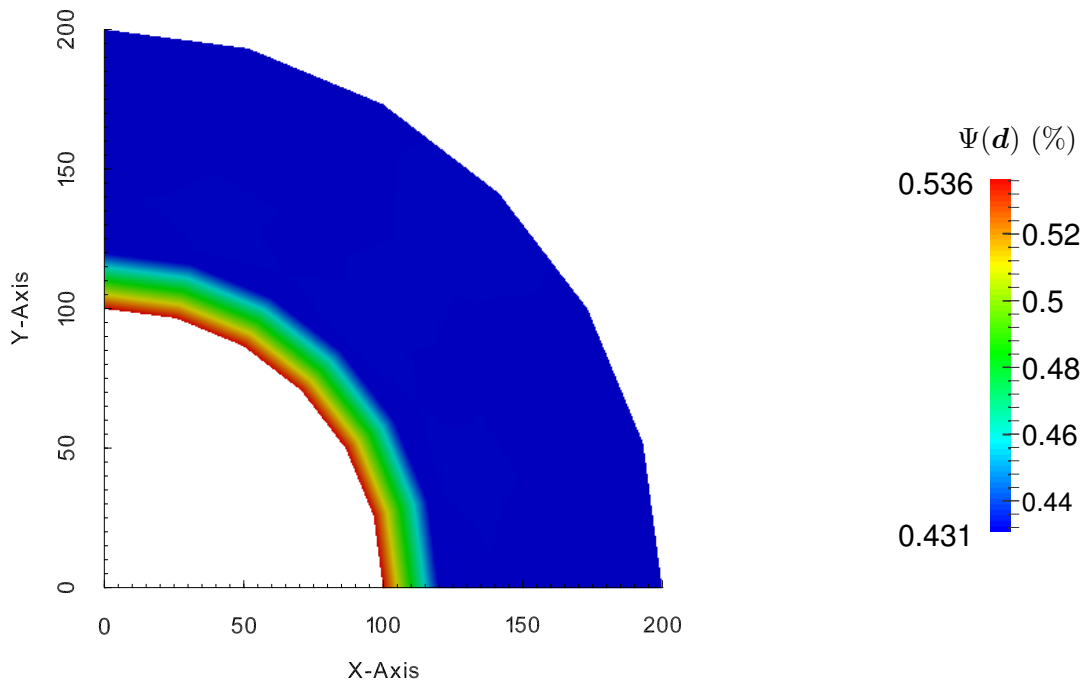


Figure 5.7: Relative error between FEM code and benchmark on displacements ( $P = 1.4$  MPa)

Since the relative error never exceeds 1%, these results validate the proper implementation of the first stage (blue in Figure 5.5) and of all the subroutines involved:

- Generation of the input file using GiD and the ProblemType-FEMASS

## 5. FINITE ELEMENT MODELLING OF STRUCTURED MATERIALS

- Importation of the mesh, connectivity table, boundary conditions, material properties from the input
- Conversion of the boundary conditions (point load, distributed loading, gravity, and prescribed displacements) into nodal forces
- Evaluation of the element stiffness matrix, assembling of the global stiffness matrix, and reduction of the global stiffness matrix using boundary conditions
- Resolution of the linear system  $[\mathbf{K}]\{\mathbf{d}\} = \{\mathbf{f}_{B_i} + \mathbf{f}_{T_i}\}$

### Computation of the strain tensor

The second stage (orange in Figure 5.5) is validated using the first principal strain  $\varepsilon_I$ , which corresponds to the first eigenvalue of the strain tensor  $\underline{\underline{\varepsilon}}$  given by

$$\varepsilon_I = \frac{1}{2} \left( \varepsilon_x + \varepsilon_y + \sqrt{4\varepsilon_{xy}^2 + (\varepsilon_x - \varepsilon_y)^2} \right) \quad (5.57)$$

The relative error  $\Psi(\varepsilon_I)$  is given in Figure 5.8. A maximum error of 0.00268% was measured on the first principal strain. Therefore the difference between the code FEMASS and the benchmark can be considered as negligible.

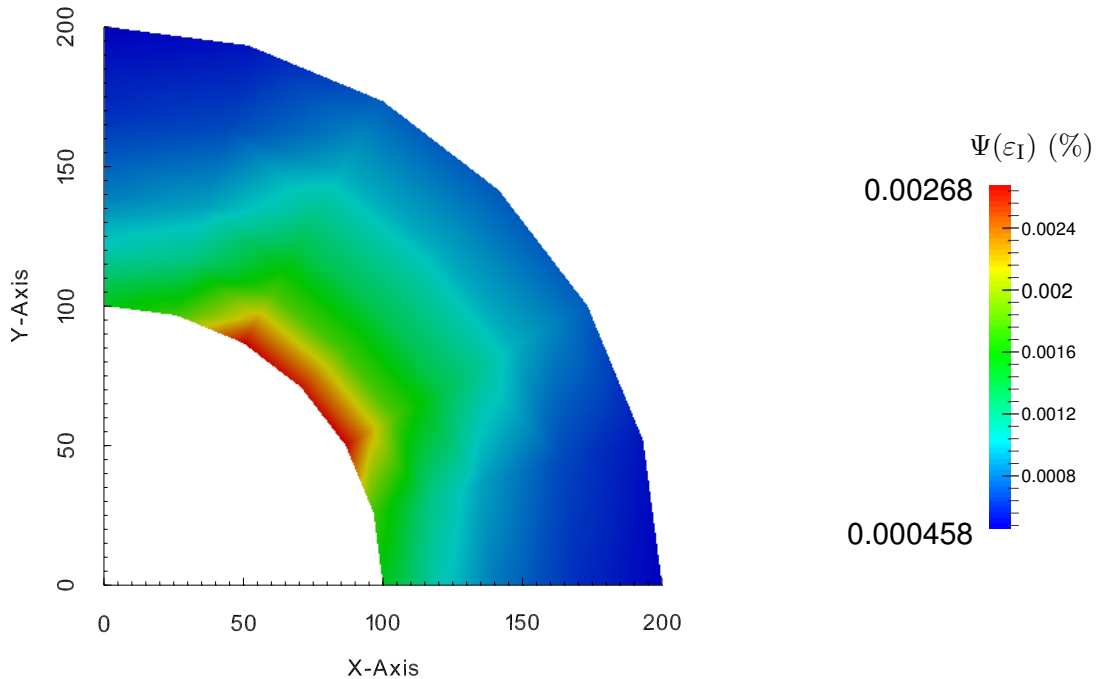


Figure 5.8: Relative error between FEM code and benchmark on principal strains  $\varepsilon_I$  ( $P = 1.4$  MPa)

These results validate the proper implementation of the second stage (orange in Figure 5.5) and of all the subroutines involved:

- Evaluation of the shape functions and their derivatives in local and Cartesian coordinate systems

- Evaluation of the Jacobian matrix and its determinant
- Numerical integration using Gauss-Legend quadrature
- Correct interpolation of the strains at Gauss integration points from the nodal displacements of the element

### Computation of the stress tensor

Yielding of materials is usually described with the yield stress that can be experimentally measured. For this reason, the stress state in the structure is an important result of a simulation that is used to assess the stability of the design. The limit between the elastic and plastic domains is described by the yield surface formulated in the general stress space. Numerically, the stress increment  $d\boldsymbol{\sigma}$  resulting from the strain increment  $d\boldsymbol{\varepsilon}$  can be calculated using the elasticity tensor (Hooke's law) assuming an elastic behaviour. As the stress state gets closer to the yield surface, a strain increment might lead to a stress state lying outside the yield surface, which is something not permitted. Several methods for the projection of the stress state on the yield surface exist, but all of them necessarily introduce a numerical error.

This section is dedicated to the third stage (green in Figure 5.5) during which the stress tensor is evaluated and corrected in the event of plasticity. Since the stress state is used in the design, this step must be thoroughly validated. Figure 5.9 shows the relative error on the shear stress  $\sigma_{xy}$  between the results of the code FEMASS and the benchmark. It can be seen that the maximum relative error observed in the cylinder is equal to 0.445%.

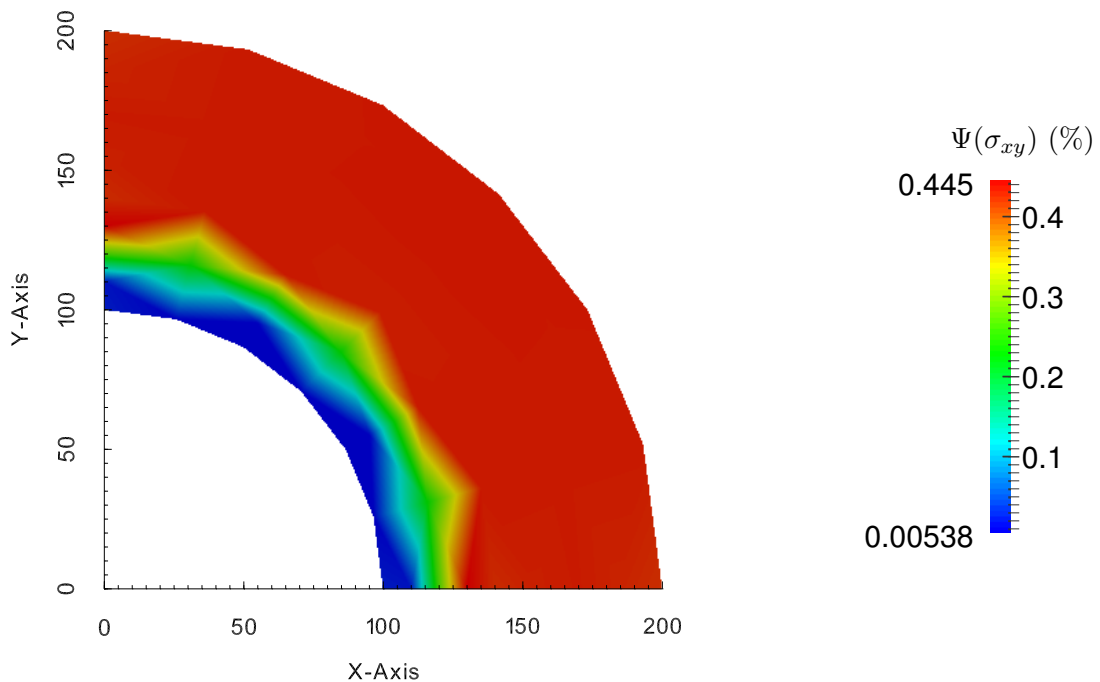


Figure 5.9: Relative error between FEM code and benchmark on  $\sigma_{xy}$  ( $P = 1.4$  MPa)

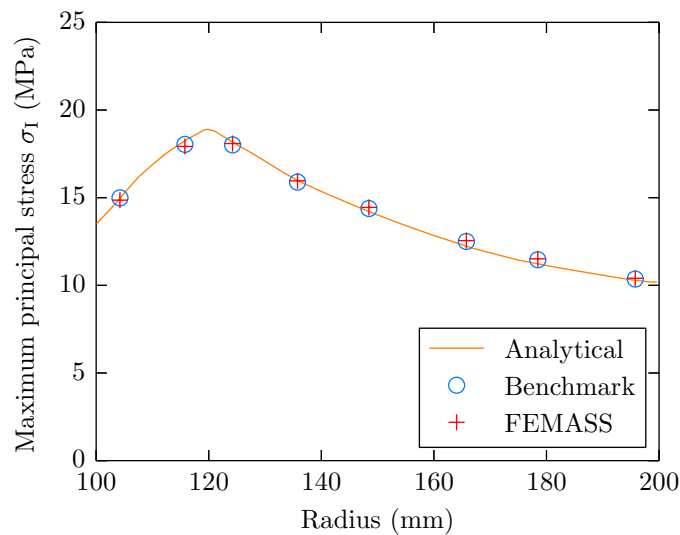
Since the relative error in the cylinder never exceeds 1%, these results confirm the

## 5. FINITE ELEMENT MODELLING OF STRUCTURED MATERIALS

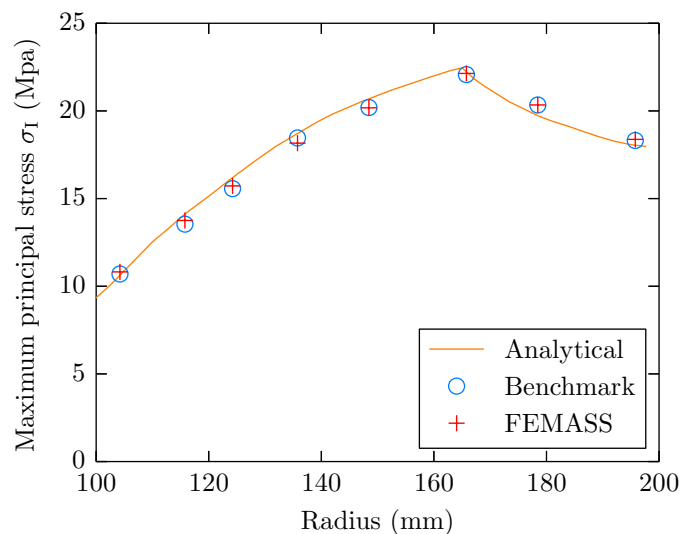
suitability of the code FEMASS for elasto-plastic problems and validate the implementation of all the procedures involved:

- Computation of the stress increment from the strain increment
- Computation of the effective stress, Nayak's coefficient, flow vector, plastic multiplier, and plastic strains
- Algorithm of projection of the yield stress on the yield surface
- Computation of the equivalent nodal forces from the stress tensor
- Verification of the convergence of the results

The problem of a thick cylinder internally pressurised experiencing plasticity has been solved by Hill (1950), who gave an analytical solution for the hoop stress distribution along the radius in the cylinder. The analytical, benchmark, and FEMASS solutions of the first principal stress state for two different internal pressures,  $P = 1.4$  MPa and  $P = 1.8$  MPa, are given in Figures 5.10a and 5.10b respectively.



(a) Hoop stress distribution along radius for  $P = 1.4$  MPa



(b) Hoop stress distribution along radius for  $P = 1.8$  MPa

Figure 5.10: Comparison of the hoop stress distribution along the radius given by the analytical solution, benchmark, and FEMASS.

One can see that there is a very good agreement between the code FEMASS and the analytical solution. Both cases lead to plastic straining in the cylinder and the radius giving the elastic/plastic limit is accurately reproduced by the model FEMASS (120 mm for  $P = 1.4$  MPa, 165 mm for  $P = 1.8$  MPa).

The code FEMASS has been successful to model the elasto-plastic behaviour in a cylinder using the Von Mises yield criterion. For further geotechnical applications, we also need to validate the implementation of the Modified Cam Clay and the MASS yield criteria.

### 5.6.3 Validation of the Modified Cam Clay

The implementation of the Modified Cam Clay is validated on an isotropic compression test and compared with the analytical solution of the specific volume  $v$ . During the simulation, the variation of the the specific  $dv$  resulting from the strain increment  $d\boldsymbol{\varepsilon}$  is given by

$$dv = -v d\boldsymbol{\varepsilon}_p = -v \operatorname{tr}(d\boldsymbol{\varepsilon}) \quad (5.58)$$

The values of the parameters used for the simulation are given in Table 5.3, and the result of the isotropic compression test is given in Figure 5.11. One can see that the finite element program FEMASS gives a good agreement with the analytical solution, the relative error being always lower than 1% on the simulated range of effective pressures.

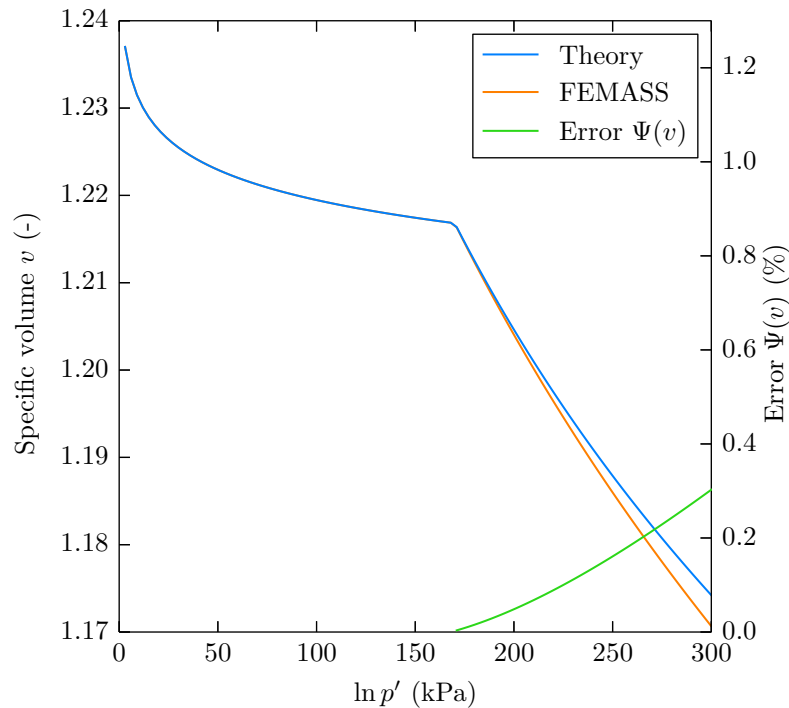


Figure 5.11: Validation of the implementation of the Modified Cam Clay

Table 5.3: Parameters used for the validation of the Modified Cam Clay

Parameter	E (kPa)	$\nu$ (-)	$p'_y$ (kPa)	$N_\lambda$	$\lambda$	$\kappa$	$M$ (-)
Value	50,000	0.2	170	1.602	0.075	0.005	1.13

#### 5.6.4 Validation of the MASS

The same simulation is performed to validate the good implementation of the model for artificially structured soils (MASS) in finite element code FEMASS. Results of the isotropic compression test are given in Figure 5.12 and are compared with the analytical solution of the specific volume given by Equation (4.14). The values of the parameters used for the simulations are given in Table 5.4. One can see that the finite element program gives a good agreement with the theoretical solution; the process of degradation around  $p' = 400$  kPa is properly modelled, and the relative error with the analytical solution is lower than 1%.

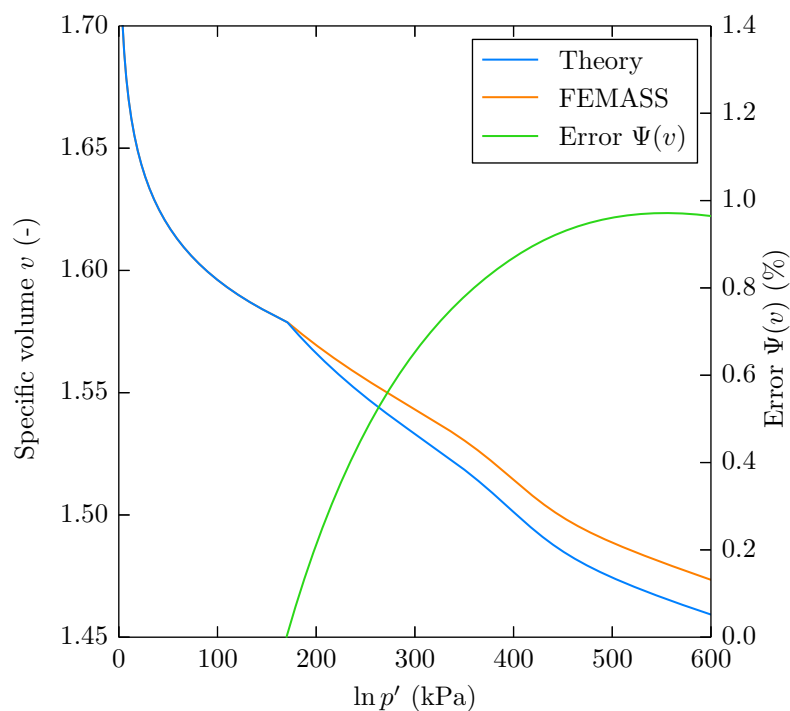


Figure 5.12: Validation of the implementation of the model MASS

Table 5.4: Parameters used for the validation of the model MASS

Parameter	E (kPa)	$\nu$ (-)	$p_y^I$ (kPa)	$N_\lambda$	$\lambda$	$\kappa$	$M$ (-)
Value	50,000	0.2	170	1.602	0.075	0.005	1.13

$p_y^{II}$ (kPa)	$\beta$ (kPa $^{-1}$ )	$\Delta e_i$ (-)	$\Delta e_c$ (-)	$p_b$
400	0.035	0.065	0.046	-41.8



### 5.6.5 Conclusion of the validation

A thorough validation has proven the good implementation of the finite element method in the numerical code FEMASS and its suitability for the modelling of elasto-plastic problems. The relative error between the code FEMASS and the benchmark solutions has shown to be always lower than 1% on the displacements, strains, and stresses.

The code FEMASS is a fully functional finite element program including the pre-processing of the problem using GiD and the post-processing of the results with ParaView. It includes several yield criteria commonly used in soil mechanics that make the code FEMASS particularly suitable for geotechnical problems, in addition to the model MASS for the modelling of the degradation in structured soils at yield.

However, many processes other than the mechanical degradation of the structure are involved in the life cycle of a lime treated soil. The code FEMASS in its current form allows only the modelling of structured soils in geotechnical structures – which is already an interesting feature – but other processes involved in soil treatment (e.g. pozzolanic reactions) should be included to make of the code FEMASS the reliable tool needed by geotechnical companies. Nevertheless, we give in the next section an example of future application of the code FEMASS to illustrate its potential for the design of geotechnical structures involving structured materials.

## 5.7 Potential of the code FEMASS for design optimisation

### 5.7.1 Context

It is common nowadays to include artificially treated materials in geotechnical structures. Although lime treatment is known to improve the mechanical properties, the long term effects are not accounted for in the design for two reasons:

1. Artificially and naturally structured materials experience at yield a degradation of the structure that goes along with a loss of the mechanical improvements
2. No reliable method is available at the moment to model the mechanical behaviour of structured soils

For these reasons, earthworks are designed to avoid plastic straining under any circumstances by staying in the elastic domain. This is done via different methods like safety factors and results in the over design of the structure and the use of unnecessary large amount of resources.

This strategy is legitimate since degradation is due to plastic deformations. However, using the untreated material as reference for the calculations when a lime treatment is actually performed results in the elastic domain being much larger than what the material will experience, even at the ultimate limit state (Figure 5.13a). The method presented in this section aims at accounting for the long term effects in order to reduce the elastic domain (Figure 5.13b) and reduce the amount of resources by optimising the design.

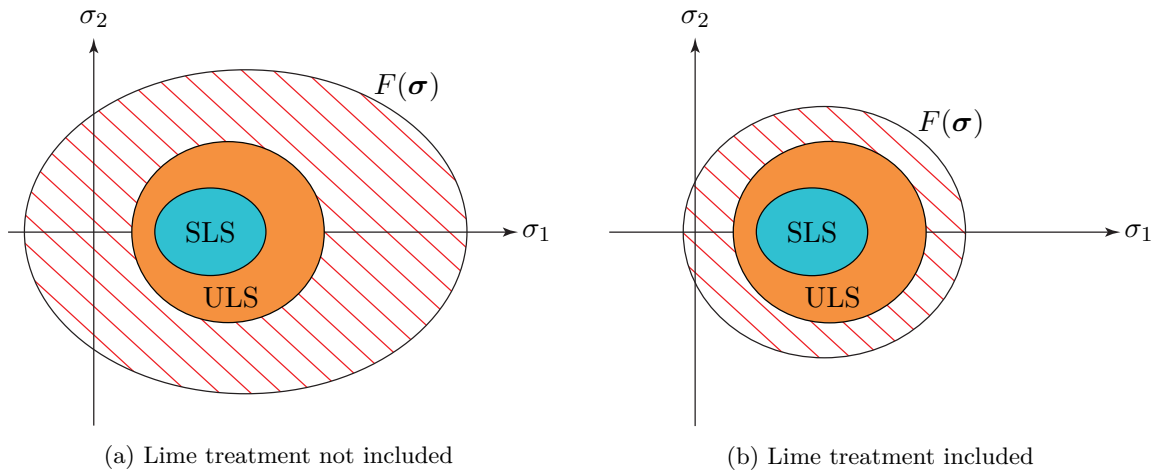


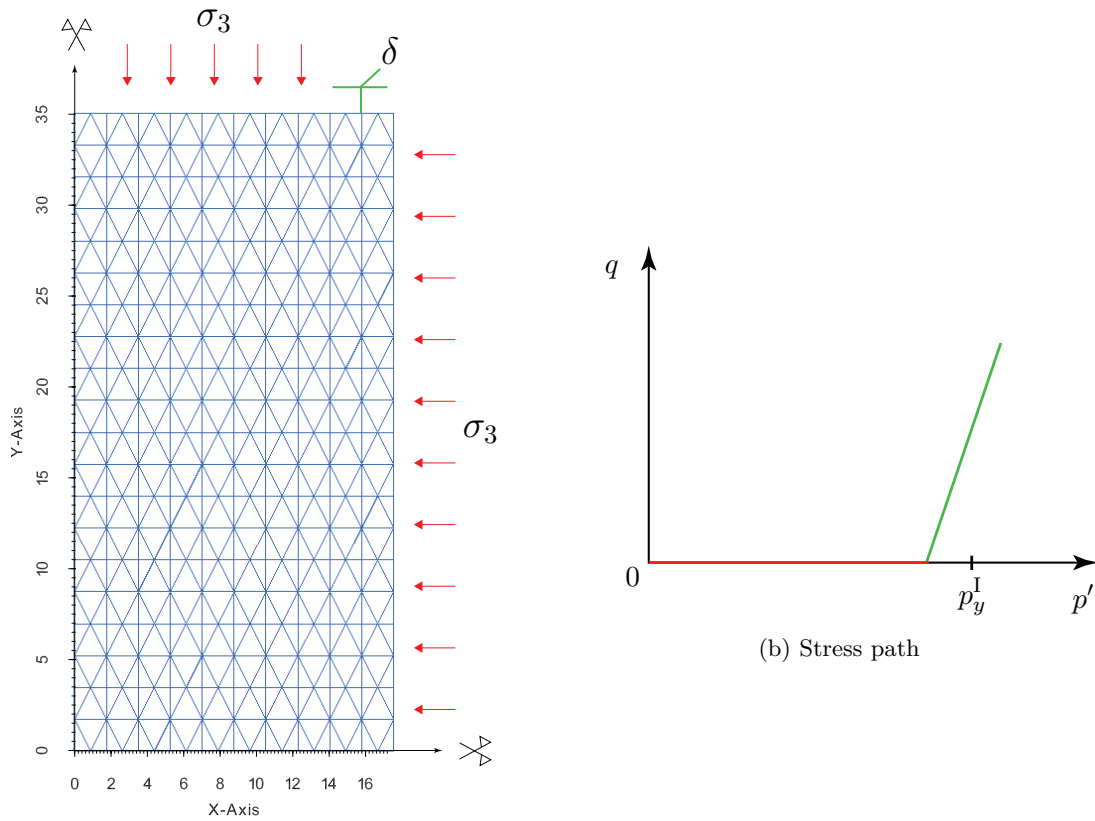
Figure 5.13: Optimisation of the design resulting from the consideration of the lime treatment– SLS: Serviceability Limit State, ULS: Ultimate Limit State, F: Yield function

We now illustrate the potential of a numerical code like the FEMASS for design optimisation purposes.

### 5.7.2 Example of application

The method we expose here is based on the assumption of a better description of the behaviour of structured materials at yield with the model MASS. Finite element method allows to understand where the degradation might take place and how the mechanical properties could be degraded, which can be used to optimise the lime treatment and the design.

To illustrate this approach we consider a lime treated cylindrical specimen (70 cm  $\times$  35 cm) subjected first to an isotropic consolidation, and then to prescribed axial displacements of 4 mm (Figure 5.14a), which can correspond to the kind of mechanical loading inside of a geotechnical structure (Figure 5.14b). The nodes subjected to the prescribed displacements are constrained along the X-axis as well. Due to symmetry, only a quarter of the sample is modelled.



(a) Geometry and boundary conditions of the case study

Figure 5.14: Geometry and stress path of the example for illustration of the potential of the method

Two simulations are performed using two different yield criteria to model the behaviour at yield of a lime treated silt with 1% CaO. The first simulation was performed using the Mohr-Coulomb criterion to describe the plastic behaviour as it is the most commonly used, and a positive strain hardening parameter was introduced to avoid perfect plasticity. The second simulation was performed using the model MASS developed in Chapter 4 which accounts for the degradation of the structure at yield in the mechanical behaviour. The parameters were determined from the experimental results given in Chapter 3 on a 1% lime treated silt and are given in Table 5.5. Since plastic straining is responsible for degradation, we compare the differences of distribution of plastic strains in the samples for each criterion.

Table 5.5: Parameters used for the modelling of a lime treated silt with 1%

Parameter		Simulation 1	Simulation 2
$E$	(kPa)	45,000	45,000
$\nu$	(-)	0.25	0.25
$c$	(kPa)	47.9	-
$\phi$	(°)	28.5	-
$H'$	(kPa <sup>-1</sup> )	0.1	-
$p_y^I$	(kPa)	-	731
$p_y^{II}$	(kPa)	-	1000
$N_\lambda$	(-)	-	1.99
$\lambda$	(-)	-	0.08
$\kappa$	(-)	-	0.032
$M$	(-)	-	1.15
$\Delta e_i$	(-)	-	0.065
$\Delta e_c$	(-)	-	0.046
$p_b$	(kPa)	-	-41.8
$\beta$	(kPa <sup>-1</sup> )	-	0.035

Figure 5.15 shows the results of the simulations at three different increments ( $\delta = 3, 3.5,$  and  $4$  mm). One can see that, although the range of values for  $\varepsilon^P$  are similar, the repartition of plastic straining in the sample is not the same. For an axial displacement of  $3$  mm ( $\varepsilon_a = 8.5\%$ ), both models give a similar distribution of the plastic strains, the model MASS predicting slightly larger values than Mohr-Coulomb. However, as the axial displacement increases, differences in the distribution appear. At  $\delta = 4$  mm ( $\varepsilon_a = 11.4\%$ ), the values are in the same ranges for both models but Mohr-Coulomb – which does not account for the loss of structure – gives a much more scattered distribution of important plastic strains ( $\varepsilon^P > 0.07$ ) in the lower part of the sample (Figure 5.15e) compared to the model MASS (Figure 5.15f). If used to optimise the design of lime treated inclusions where stresses are the most important, Mohr-Coulomb would lead to the lime treatment of part of the earthwork that actually don't need it. The model MASS, on the other hand, would show more accurately where lime treatment is actually necessary and would result in an optimisation of the design.

Although this approach is purely hypothetical and qualitative, it demonstrates the potential of the numerical code FEMASS to account for the long term effects in the design. The model MASS have proven to model accurately the degradation of the structure at yield under isotropic loading and shear strains. Combined with the finite element method, it gives the possibility to identify where in the structure degradation is likely to happen and adjust the design accordingly.

## 5.7. Potential of the code FEMASS for design optimisation

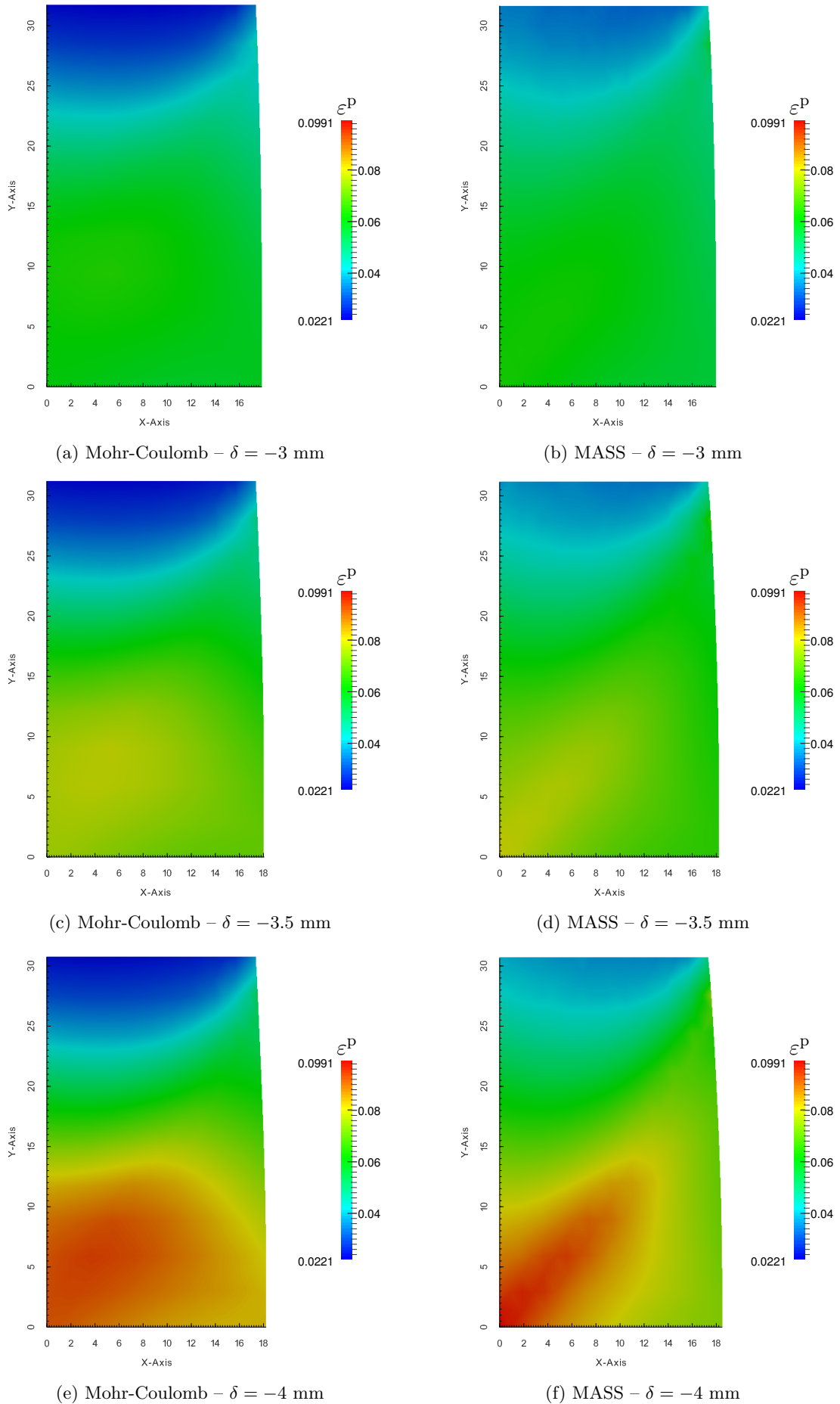


Figure 5.15: Difference in the repartition of the plastic strain in a solid depending on the yield criteria chosen

## 5.8 Conclusion

The study of the theory of the finite element method has allowed to implement efficiently the constitutive law proposed in this study for artificially structured soils. The numerical code FEMASS developed in thesis has passed all the tests ensuring the good implementation of the finite element procedures and the accuracy of the results. The constitutive law for artificially structured soils, generalised for any structured material, has been successfully implemented in the numerical code and allows the modelling of lime treated materials within geotechnical structures.

The potential of the finite element program FEMASS developed in this thesis was demonstrated on a hypothetical case. It was shown that using the model MASS gives a different repartition of the plastic strains within the structure compared to the Mohr-Coulomb criterion commonly used by industry. Based on the quality of prediction given by the model MASS in the previous chapter and its capability to model a large number of key features due to structure, it can be assumed that the results of simulations using the model MASS and the repartition of the plastic strains are more accurate. This would give the possibility to optimise the design of the structure by adjusting accordingly the lime content depending of the position in the structure, and could lead to significant reduction of the resources used in the structure, a cost-effectiveness, and a reduction of the carbon footprint.

There are however some restrictions regarding the use of the code FEMASS at an industrial scale that should be addressed first. As it was said before, lime treatment relies on several important processes that are not accounted for in the finite element program yet. For instance, aspects such as the durability of the treatment subjected to environmental aggressions, or the time dependency of pozzolanic reactions, are key issues that should be considered during the design of structures involving lime treated materials. In the last chapter we discuss the possible methods to account for these aspects in the numerical model FEMASS.

## Chapter 6

# Conclusion of the study

The work undertaken in this thesis fits into the overall context of soil improvement. Because of the current situation promoting the development of environmental and sustainable solutions, geotechnical companies have to deal with the problem of on-site materials with low mechanical properties. Among all the methods available, lime treatment appears to be a good alternative to make use of all the resources available on-site.

Lime treatment is mostly used for its short term effects that make easier the construction works. However, lime treatment also presents long term effects that lead to significant mechanical improvements of the soil. Materials originally unsuitable can be artificially enhanced to meet the mechanical requirements, and since no suitable material would have to be imported and no wastes to be disposed of in landfills, the total amount of resources involved in the works could be significantly reduced. Although lime is not a “green” product, the benefits arising from the lime treatment compensates for the carbon footprint of the lime production. Unfortunately, long term effects are at the moment neglected in the design of the geotechnical structures because of the lack of reliable methods.

This thesis aimed at developing a methodology to account for lime treatment in the design. Three main challenges have been identified:

1. A coupling between the lime content and the magnitude of the mechanical improvements
2. An elasto-plastic model to model the degradation of the structure at yield
3. A numerical model to optimise the lime treatment and the design

The second chapter has given the background common to these three challenges. The study of chemical reactions taking place in the soil has shown that three different compounds can arise from a lime treatment: the portlandite (unreacted lime), the cementitious compounds, and carbonates. Then, we introduced the main mechanical features of lime treated soils and showed that they behave like naturally structured soils. Finally, the study of the current methods used in the design has pointed out

## 6. CONCLUSION OF THE STUDY

their limitations for the modelling of structured materials.

In the third chapter, an extensive experimental program was carried out on a lime treated silt to develop a chemo-mechanical coupling. The modifications of the chemical composition arising from lime treatment in a soil were assessed with thermal analysis (TGA/DTA). In the perspective of developing a constitutive model for lime treated soils, the mechanical modifications were assessed using triaxial apparatus that allows a complete determination of the stress tensor within the sample. The results of triaxial tests have confirmed the potential of lime treatment to improve the mechanical properties, and a coupling was found between the yield stress and the amount in cementitious compounds. It was therefore demonstrated that the methodology proposed for the chemo-mechanical modelling of lime treated soils is suitable, and relies on simple experiments.

The fourth chapter was dedicated to the development of an elasto-plastic model to account for the mechanical improvements and the presence of structure in the design. A new formulation to model the degradation of the structure at yield was developed and introduced in the hardening and softening rule of the Modified Cam Clay. A thorough investigation was carried out to verify the relevance of some fundamental assumptions of the MCC for the modelling of lime treated soils. It was shown that the assumption of associated potential is acceptable for lime treated soils, and the increase of the cohesion was included by expanding the yield surface in the tensile domain. The results showed that the model MASS is successful in reproducing the most important features of both naturally and artificially structured materials. The dilation of the specimen experiencing softening is particularly well predicted by the model. In total, the model MASS requires 4 additional parameters to model the degradation. They all have physical meaning and can be determined from an isotropic compression test on the structured material. It appears that the isotropic behaviour gives enough information to predict the shear behaviour.

In the fifth chapter we described the finite element program developed in this thesis to optimise the design of structures involving lime treated materials. A fully functional finite element model for elasto-plastic applications written in Fortran and Python has been developed, including the pre- and post-processing of the geometry and the results. The code FEMASS (Finite Element Modelling of Artificially Structured Soils) allows the modelling of elasto-plastic problems involving structured materials. The potential of this tool for the improvement of the design was demonstrated on a hypothetical case study. The purpose was to show that the model MASS implemented in the finite element method allows a more accurate description of the distribution of plastic strains in the structure compared to the other criteria used by industry. It was shown that the method allows an optimisation of the design by treating only the area experiencing important mechanical solicitations. The numerical model FEMASS combined with the chemo-mechanical coupling developed for lime treated soils can lead to more sustainable and cost-effective solutions.



In the next chapter we discuss of the limitations for a practical use of the method developed in the fifth chapter. Although its potential was demonstrated, there are several aspects in lime treatment that should be studied in depth. It includes first the durability of the treatment subjected to environmental aggressions such as water circulation. The cementitious compounds being the result of chemical reactions that rely on strict chemical conditions, any changes of the conditions in the porous medium could lead to the dissolution of the structure and the unexpected release of the soil particles. The modelling of leaching is however very complex due to the number of compounds involved. An approach in line with the one used for the chemo-mechanical coupling has been presented. It consists of considering a unique hypothetical compound that accounts for all the hydrates. This reduces considerably the complexity of the problem. Another aspect that has not been studied in this thesis is the time-dependency of the pozzolanic reactions. In this thesis a curing time of 28 days was respected; however, chemical analysis has revealed that for lime contents greater than 1% there is still some unreacted lime (portlandite) in the soil, suggesting that cementitious compounds could still be produced. This would change the mechanical properties of the material and should be included in the calculations.

The fields of application of the three tools developed in this thesis (coupling, elastoplastic model, finite element model) are however very diverse. These may include:

- Reduction and optimisation of the amount of resources required in the construction of geotechnical structures,
- Diminution of the carbon footprint of projects,
- Optimisation of the lime treatment in order to get the mechanical properties required and avoid the oversizing of the design,
- Optimisation of the design using the FEM to account for the mechanical improvements,
- Use of lime treatment where mechanical solicitations are the most important for the stability of the structure.

## 6. CONCLUSION OF THE STUDY

## Chapter 7

# Recommendations for future work

### 7.1 Introduction

The main challenges of this thesis were to develop a reliable methodology to account for the benefits of lime treatment in the design of geotechnical structures. This would result in a diminution of the resources required for the achievement of the works, an optimisation of the lime content, a reduction of the carbon footprint and therefore to the development of a sustainable geotechnical solution.

The first part of the thesis focused on the development of a chemo-mechanical coupling. This was followed by the development of a constitutive law to model the behaviour of artificially structured soils under mechanical loading. Finally, everything was assembled and implemented in a finite element program developed for the modelling of structured materials and their effect on the global behaviour of earthworks.

Although these three tools have proven their usefulness for an optimisation of the design they are still subjected to some assumptions that restrict their use in particular conditions. In this chapter we discuss of these limitations and the possible additional analysis for the development of a complete method for design optimisation using lime treatment. First, we discuss of the influence of water circulation in the treated material on the stability of the cementitious compounds. Then we discuss of the limitation inherent to the Modified Cam Clay in the prediction of the behaviour at yield and the possible enhancements that could be made in the model for artificially structured soils.

### 7.2 Further investigation for the chemo-mechanical modelling of lime treated soils

#### 7.2.1 Durability of lime treatment under water circulation

The second chapter of this thesis has been dedicated to the establishment of a chemo-mechanical coupling for lime treated soils. Since the mechanical improvements following lime treatment rely on chemical reactions, an investigation of the reactions happening between the lime and the soil has been carried out. It turns out that the cementitious compounds are the result of reactions between the soil particles dissolved in solution and the hydrated lime (portlandite). The dissolution of the soil minerals is

## 7. RECOMMENDATIONS FOR FUTURE WORK

made possible at high pH ( $\approx 12.4$ ), and any modification of this parameter could result in the dissolution of the cementitious compounds. In the event of a water circulation in the treated material, the water flow may lead to the leaching of the hydroxide ions  $\text{HO}^-$  and therefore to the decrease of the pH. In these conditions the cementitious compounds, stable in high pH environment, would experience the inverse reaction that would lead to the re-dissolution of the cementitious compounds. This would result in the deterioration of the mechanical improvements and could threaten the stability of the structure (Le Runigo et al., 2009, 2011).

Most of the geotechnical structures are likely to be exposed to environmental aggressions and degradations such as wind or frost. Lime treated materials can be used in many different kinds of earthworks such as embankment (Figure 7.1). These structures are likely to be subjected to seepages, which can lead to a modification of the chemical conditions within the structure and, in the worst scenario, to the leaching of the material. Such processes, known as *leaching*, is a problem frequently met by geotechnical companies in structures that can be subjected to water circulation (e.g. heavy rains or seepages) and could have catastrophic consequences on the stability of the earthwork. The durability of the lime treatment is thus an aspect that must be considered when the mechanical improvements are accounted for in the design.

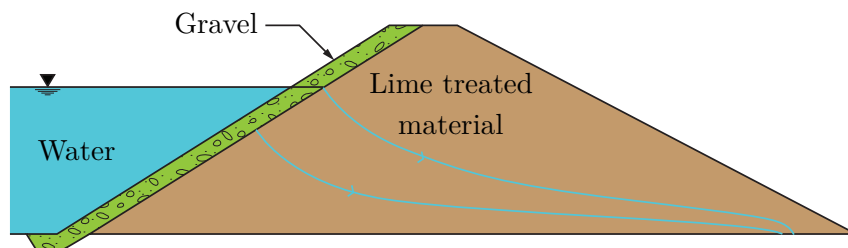


Figure 7.1: Example of leaching: embankment containing lime treated materials subjected to seepages and to the risk of dissolution of the cementitious compounds.

The modelling of the dissolution of the cementitious compounds is a very complex problem because of the large number of compounds belonging to the family of hydrates CSH, CAH, and CASH. Modelling the dissolution of every single cementitious compounds is therefore not possible. Several authors (e.g. Cafaro and Cotecchia, 2001; Pomakhina et al., 2012; De Windt et al., 2014) have studied the effects of leaching on the dissolution of the cementitious compounds in cemented materials. De Windt et al. (2014) used the numerical code HYTEC (van der Lee et al., 2003) coupled with the module CHESS to simulate the dissolution of the hydrated compounds under water circulation. However, this results in a large number of processes being modelled and the determination of the constants controlling the dissolution is difficult. Also, the coupling with the mechanical behaviour is not obvious or straightforward.

A first approach, in line with the one used for the chemo-mechanical modelling, would be to consider a unique hypothetical compound accounting for all the products the pozzolanic reactions. If this does not solve the problem of the determination of the diffusivity coefficient (Legat and Winckelmans, 2007), it leads however to significant simplifications, reducing the problem to three processes to be modelled:

1. The convection-diffusion of the unreacted lime (portlandite) and the hydroxide

## 7.2. Further investigation for the chemo-mechanical modelling of lime treated soils

ions under the water flow

2. The dissolution of the cementitious compounds due to the renewal of the porous medium and the decrease of the pH
3. the convection-diffusion of the products of the dissociation of the cementitious compounds

The convection-diffusion process is governed by

$$\frac{\partial c}{\partial t} + \vec{\nabla} \cdot (\vec{v}c) + \vec{\nabla} \cdot (-D\vec{\nabla}c) = Q \quad (7.1)$$

with  $c$  the concentration in the hypothetical compounds ( $\text{kg.m}^{-3}$ ),  $D$  the diffusion coefficient ( $\text{m}^2.\text{s}^{-1}$ ),  $\vec{v}$  the velocity of the water flow ( $\text{m.s}^{-1}$ ), and  $Q$  a source term that could be compared with the rain fall or the water reservoir sustaining the seepages. The permeability of the soil can be introduced using Darcy's law

$$\vec{v} = \frac{\vec{q}}{n} \quad \vec{q} = -\frac{k}{\mu} (\vec{\nabla}p - \rho\vec{g}) \quad (7.2)$$

with  $q$  the Darcy's velocity ( $\text{m.s}^{-1}$ ),  $n$  the porosity (-),  $k$  the permeability ( $\text{m}^2$ ),  $\mu$  the dynamic viscosity ( $\text{Pa.s}$ ),  $p$  the pressure ( $\text{Pa}$ ),  $\rho$  the density ( $\text{kg.m}^{-3}$ ), and  $g$  the acceleration due to gravity ( $\text{m.s}^{-2}$ ).

The finite difference method was used to model the process of convection-diffusion under water circulation in a soil. This choice was motivated by the fact that the finite element method does not respect the mass conservation law when applied on fluid mechanics problems. We simulated the leaching of a lime treated material embedded in a non treated material (Figure 7.2). The values of the parameters are given in Table 7.1<sup>1</sup>.

---

<sup>1</sup>Note that the magnitude of the values is not relevant for this simulation, the purpose being to highlight the phenomenon of convection-diffusion that might happen in a lime treated soil under water circulation.

## 7. RECOMMENDATIONS FOR FUTURE WORK

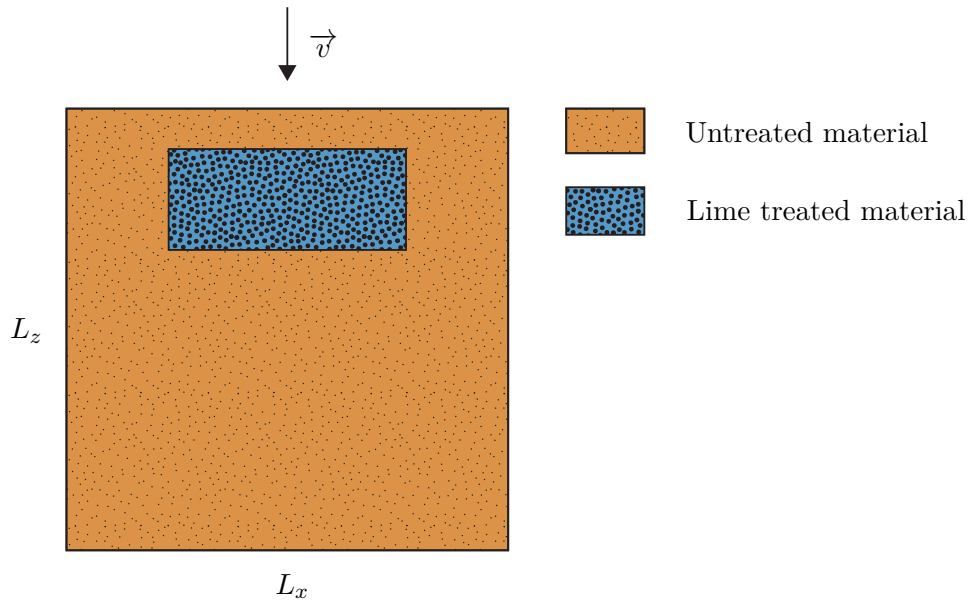


Figure 7.2: Schematic for the modelling of leaching in lime treated soils

The distribution of the lime in the treated area was done randomly to account for the fact that lime cannot be homogeneously distributed in practice. The results are given in Figure 7.3. As expected the convection term prevails on the diffusion term and the compounds is quickly transported elsewhere in the structure. In the framework of lime treatment, this process would first concern the portlandite and the hydroxide ions. The pozzolanic reactions have small equilibrium constant, which means it takes time to dissolve the minerals and have them react with the portlandite. A leaching of the portlandite that has not been used means than no more cementitious compounds can be produced and is a waste of lime. The leaching of the hydroxide ions will results in the decrease of the pH and the re-dissolution of the cementitious compounds which, due to the leaching, are to be transported away from the treated area.

Although very simplistic, this simulation points out the risk of neglecting the effects of the environment on the the durability of the treatment. This aspect, which has been studied in thesis, is an important aspect that should be introduced in the method developed in this study.

Table 7.1: Values of the parameters used for the simulation of the phenomenon of convection-diffusion in a lime treated soil

Parameters	$c_0$ [kg.m <sup>-3</sup> ]	$D$ [m <sup>2</sup> .s <sup>-1</sup> ]	$Q$ [m <sup>3</sup> .s <sup>-1</sup> ]	$\vec{v}$ [m.s <sup>-1</sup> ]	$L_x$ [m]	$L_z$ [m]	$\Delta x$ [m]	$t_{max}$ [s]	$\Delta t$ [s]
Value <sup>†</sup>	1.0	0.001	1.0	1.0	300	300	3	100	0.05

<sup>†</sup>The magnitude of the values is not relevant in this simulation.

7.2. Further investigation for the chemo-mechanical modelling of lime treated soils

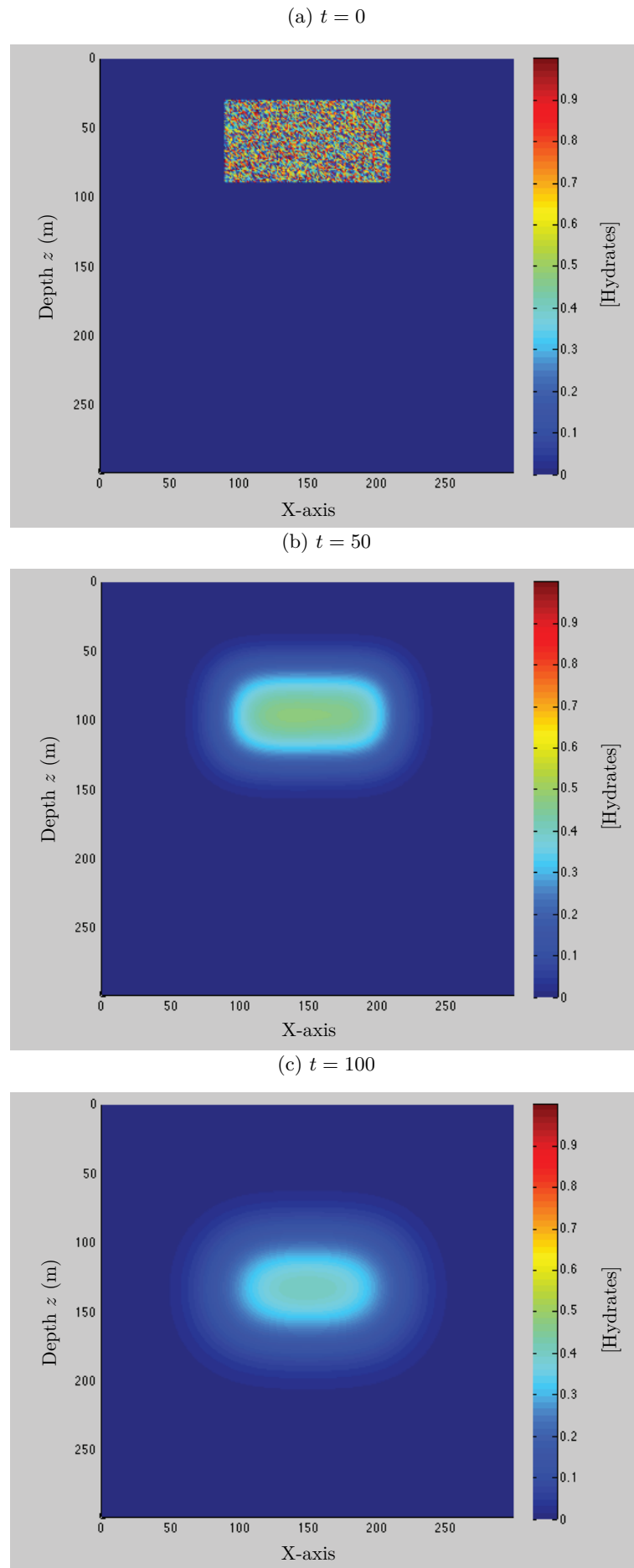


Figure 7.3: Diffusion-convection of the dissolved portlandite under water circulation.

### 7.2.2 Time-dependency of pozzolanic reactions and influence on the long term behaviour

In this study all the experiments were carried out after a curing time of 28 days. This value is commonly accepted to be the duration after which the improvements of the mechanical properties are less significant. However, it does not mean that the pozzolanic reactions stop and one can therefore expect the mechanical behaviour of the material after 6 months to be different from the one at 28 days. This was confirmed by a drained triaxial test performed on 5% lime treated specimen, part of the same batch used for the chemo-mechanical coupling, but tested after 6 months (Figure 7.4). One can see that deviatoric stress peak after 6 months is about 5 times the one at 28 days. This result has to be coupled with the TGA/DTA results. The chemical analysis revealed a large amount of portlandite after 28 days. In the light of these results, it confirms the hypothesis that the unreacted amount of portlandite is used and that pozzolanic reactions keep going.

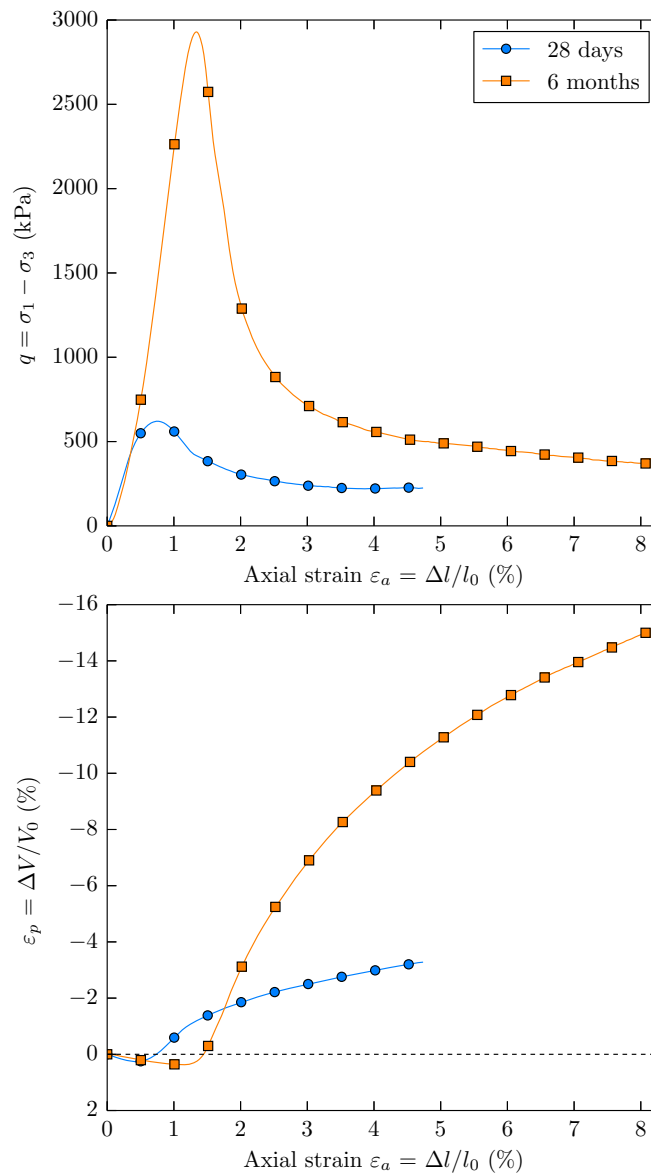


Figure 7.4: Comparison of the same lime treated soil with 5% in lime at 28 days and 6 months for low confining pressure ( $\sigma_3 = 20$  kPa).



### 7.3 Improved yield criterion for structured materials

The model MASS has been developed in the framework of the Modified Cam Clay, which is known to overestimate yield loci at low confining pressures. This inconvenience is enhanced by the formulation chosen in the model which accounts for the increase of cohesion due to structure by expanding the yield surface in the tensile domain.

Several authors (e.g. Matsuoka et al., 1999; Mita et al., 2004) have developed new yield criteria to increase the accuracy of the modelling in such situations. The Mohr-Coulomb criterion is known to be suitable for many types of soil to model the yield loci (Hinton and Owen, 1980), unfortunately it introduces singularities at the transition between the two criteria due to the different sections in the  $\pi$  plane (irregular hexagon and circle).

In numerical analysis, the use of continuous functions is always preferred to avoid numerical instabilities. Instead of using Mohr-Coulomb, one could use Drucker-Prager which is an approximation of the Mohr-Coulomb criterion based on the Von-Mises criterion. Since both criteria have the same section in the deviatoric plane it is possible to develop a formulation for a closed and continuous function. More details can be found in Neto et al. (2009). A representation of such hybrid criterion that might be more suitable for structured materials is given in Figure 7.5.

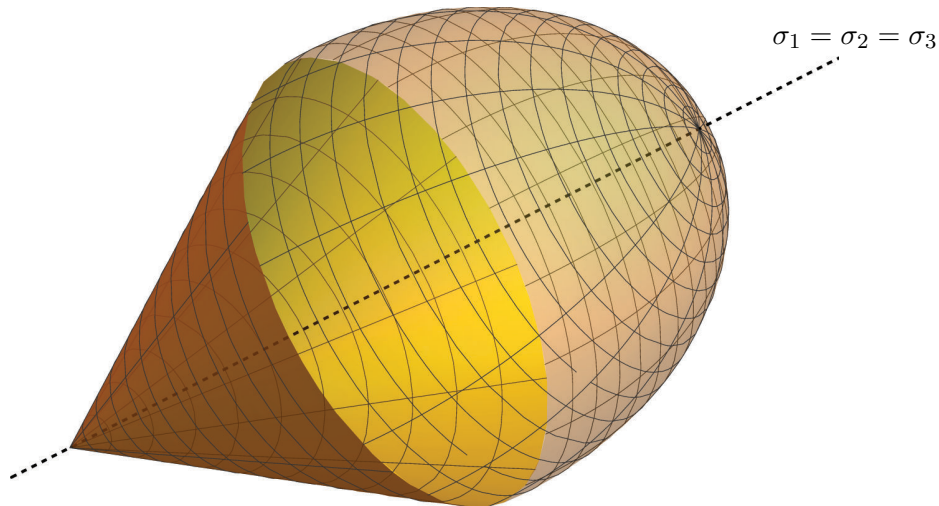


Figure 7.5: Hybrid Modified Cam Clay / Drucker-Prager yield criterion

## 7. RECOMMENDATIONS FOR FUTURE WORK

# Bibliography

- Ahnberg, H., 2007. On yield stresses and the influence of curing stresses on stress paths and strength measured in triaxial testing of stabilized soils. *Canadian geotechnical journal* 44 (1), 54–66.
- Al-Rawi, R. S., 1981. Effect of curing temperature on lime stabilization. In: *The Second Australian Conference on Engineering Materials*, held at Sydney, July 6-8, 1981. pp. 611–662.
- Alarcon-Ruiz, L., Platret, G., Massieu, E., Ehrlacher, A., Mar. 2005. The use of thermal analysis in assessing the effect of temperature on a cement paste. *Cement and Concrete Research* 35 (3), 609–613.
- Anagnostopoulos, a. G., Kalteziotis, N., Tsiambaos, G. K., Kavvas, M., 1991. Geotechnical properties of the Corinth Canal marls. *Geotechnical and Geological Engineering* 9 (1), 1–26.
- Anderson, E., 1992. *LAPACK users' guide*. Society for Industrial and Applied Mathematics, Philadelphia.
- Anderson, E., Bai, Z., Dongarra, J., Greenbaum, A., McKenney, A., Du Croz, J., Hammerling, S., Demmel, J., Bischof, C., Sorensen, D., 1990. LAPACK: A portable linear algebra library for high-performance computers. *Proceedings of the 1990 ACM/IEEE conference on Supercomputing*, 2–11.
- Anderson, S. H., Gantzer, C. J., Boone, J. M., Tully, R. J., 1988. *Rapid Nondestructive Bulk Density and Soil-Water Content Determination by Computed Tomography*.
- Arroyo, M., Ciantia, M., Castellanza, R., Gens, A., Nova, R., 2012. Simulation of cement-improved clay structures with a bonded elasto-plastic model: A practical approach. *Computers and Geotechnics* 45, 140–150.
- ASTM Standard D6276, 2006. Standard Test Method for Using pH to Estimate the Soil-Lime Proportion Requirement for Soil Stabilization. In: *ASTM International*. pp. 1–4.
- ASTM Standard D7181-11, 2011. Method for Consolidated Drained Triaxial Compression Test for Soils. In: *ASTM International*. Vol. i. ASTM International, pp. 1–11.

## BIBLIOGRAPHY

- ASTM Standard D7263-09, 2009. Standard Test Methods for Laboratory Determination of Density (Unit Weight) of Soil Specimens. In: 10.1520/D7263-09 (Ed.), ASTM International, 10th Edition. pp. 1–7.
- Aubry, D., Hujeux, J., Lassoudiere, F., Meimon, Y., 1982. A double memory model with multiple mechanisms for cyclic soil behaviour. In: Proceedings of the International Symposium on Numerical Models in Geomechanics. pp. 3–13.
- Aziz, A. e., 1972. The Mathematical Foundations of the Finite Element Method with Applications to Partial Differential Equations. Academic Press.
- Balasubramaniam, A., Buessucesco, B., Oh, Y.-N. E., Bolton, M. W., Bergado, D., Lorenzo, G., 2005. Strength degradation and critical state seeking behaviour of lime treated soft clay. In: International Conference on Deep Mixing-Best Practice and Recent Advances. Vol. 1. Stockholm, pp. 35–40.
- Baudet, B., Stallebrass, S., 2004. A constitutive model for structured clays. *Géotechnique* 54 (4), 269–278.
- Bell, F., Jul. 1996. Lime stabilization of clay minerals and soils. *Engineering Geology* 42 (4), 223–237.
- Bigoni, D., Piccolroaz, A., Jun. 2004. Yield criteria for quasibrittle and frictional materials. *International Journal of Solids and Structures* 41 (11-12), 2855–2878.
- Bishop, A. W., Henkel, D. J., 1957. The measurement of soil properties in the triaxial test.
- Bonnet, M., Frangi, A., 2006. Analyse des solides déformables par la méthode des éléments finis. Editions Ecole Polytechnique.
- Borja, R. I., Lee, S. R., Jan. 1990. Cam-Clay plasticity, Part I: Implicit integration of elasto-plastic constitutive relations. *Computer Methods in Applied Mechanics and Engineering* 78 (1), 49–72.
- Borja, R. I., Lin, C.-h., Montáns, F. J., 2001. Cam-Clay plasticity, Part IV: Implicit integration of anisotropic bounding surface model with nonlinear hyperelasticity and ellipsoidal loading function. *Computer Methods in Applied Mechanics and Engineering* 190.
- Boussinesq, J., 1885. Application des potentiels à l'étude de l'équilibre et du mouvement des solides élastiques: principalement au calcul des déformations et des pressions que produisent, dans ces solides, des efforts quelconques exercés sur une petite. Gauthier-Villars.
- Brandl, H., 1981. Alteration of soil parameters by stabilization with lime. In: 10th International Conference on Soil Mechanics and Foundation Engineering. Stockholm, pp. 587–594.
- Broms, B. B., Boman, P., 1975. Stabilisation of soil with lime columns. *Ground Engineering* 12 (4), 23–32.

- Broms, B. B., Boman, P., 1979. Lime Columns—A New Foundation Method. *Journal of the Geotechnical Engineering Division* 105 (4), 539–556.
- Burj Khalifa, 2013. The Tallest Building in the World. <http://www.burjkhalifa.ae/en/>.
- Burland, J., Dean, E., Gudehus, G., Muhunthan, B., Collins, I., 2008. Discussion: Interlocking, and peak and design strengths. *Géotechnique* 58 (6), 527–532.
- Burland, J. B., 1990. On the compressibility and shear strength of natural clays. *Géotechnique* 40 (3), 329–378.
- Burland, J. B., Rampello, S., Georgiannou, V. N., Calabresi, G., 1996. A laboratory study of the strength of four stiff clays. *Géotechnique* 46 (3), 491–514.
- Cafaro, F., Cotecchia, F., 2001. Structure degradation and changes in the mechanical behaviour of a stiff clay due to weathering. *Géotechnique* (5).
- Callisto, L., Calabresi, G., 1998. Mechanical behaviour of a natural soft clay. *Géotechnique* 48 (4), 495–513.
- Callisto, L., Rampello, S., 2004. An interpretation of structural degradation for three natural clays. *Canadian Geotechnical Journal* 41 (3), 392–407.
- Chazallon, C., Hicher, P., 1998. A constitutive model coupling elastoplasticity and damage for cohesive-frictional materials. *Mechanics of Cohesive-frictional Materials* 3 (1), 41–63.
- Chazallon, C., Hicher, P. Y., 1995. An elastoplastic model with damage for bonded geomaterials. In: *International Congress of Numerical Methods for Geomechanics*. Vol. V. Balkema, Rotterdam, pp. 22–30.
- Chew, S. H., Kamruzzaman, a. H. M., Lee, F. H., Jul. 2004. Physicochemical and Engineering Behavior of Cement Treated Clays. *Journal of Geotechnical and Geoenvironmental Engineering* 130 (7), 696–706.
- Chiu, C., Zhu, W., Zhang, C., Jan. 2009. Yielding and shear behaviour of cement-treated dredged materials. *Engineering Geology* 103 (1-2), 1–12.
- Choquette, M., Berube, M.-A., Locat, J., Aug. 1987. Mineralogical and microtextural changes associated with lime stabilization of marine clays from eastern Canada. *Applied Clay Science* 2 (3), 215–232.
- Clare, K. E., Cruchley, A. E., 1957. Laboratory Experiments in The Stabilization of Clays With Hydrated Lime. *Geotechnique* 7 (2), 97–111.
- Consoli, N. C., Lopes, L. d. S., Prietto, P. D. M., Festugato, L., Cruz, R. C., 2011. Variables Controlling Stiffness and Strength of Lime-Stabilized Soils. *Journal of Geotechnical and Geoenvironmental Engineering* 137 (6), 628–632.
- Constructing Excellence Limited, 2013. *Sustainability in Construction*.

## BIBLIOGRAPHY

- Corless, R. M., Gonnet, G. H., Hare, D. E. G., Jeffrey, D. J., Knuth, D. E., 1996. On the Lambert W Function. *Advances in Computational Mathematics* 5, 329–359.
- Cotecchia, F., Chandler, R. J., 2000. A general framework for the mechanical behaviour of clays. *Géotechnique* 50 (4), 431–447.
- Coulomb, C. A., 1776. *Essai sur une application des règles de maximis & minimis à quelques problèmes de statique, relatifs à l'architecture*. De l'Imprimerie Royale.
- Craig, R. F., 2004. *Craig's Soil Mechanics*, 7th Edition. Taylor & Francis.
- Croft, J., 1967. The structures of soils stabilized with cementitious agents. *Engineering Geology* 2 (1938), 63–80.
- Croft, J. B., 1964. The processes involved in the lime stabilization of clay soils. In: *Australian Road Research Board (ARRB) Conference, 2nd, 1964, Melbourne*. Vol. 2. pp. 1169–1203.
- Cuisinier, O., Auriol, J.-C., Le Borgne, T., Deneele, D., 2011. Microstructure and hydraulic conductivity of a compacted lime-treated soil. *Engineering Geology* 123 (3), 187–193.
- Cuisinier, O., Masrouri, F., Pelletier, M., Villieras, F., Mosser-Ruck, R., 2008. Microstructure of a compacted soil submitted to an alkaline PLUME. *Applied Clay Science* 40 (1-4), 159–170.
- Cundall, P. A., 1979. A discrete numerical model for granular assemblies (1), 47–65.
- Dafalias, Y. F., 1986. *Bounding Surface Plasticity. I: Mathematical Foundation and Hypoplasticity*.
- Dafalias, Y. F., Popov, E. P., Oct. 1975. A model of nonlinearly hardening materials for complex loading. *Acta Mechanica* 21 (3), 173–192.
- Das, S. K., Mitra, A., Das Poddar, P. K., 1996. Thermal analysis of hydrated calcium aluminates. *Journal of Thermal Analysis and Calorimetry* 47 (3), 765–774.
- Davidson, D. T., Pitre, G. L., Mateos, M., George, K. P., 1962. *Moisture-Density, Moisture-Strength and Compaction Characteristics of Cement-Treated Soil Mixtures*. Highway Research Board Bulletin (353).
- De Windt, L., Deneele, D., Maubec, N., May 2014. Kinetics of lime/bentonite pozzolanic reactions at 20 and 50°C: Batch tests and modeling. *Cement and Concrete Research* 59, 34–42.
- Deneele, D., Lemaire, K., 2012. *Evaluation de la durabilité des effets du traitement des sols: Effet de la circulation d'eau sur la durabilité du limon traité – Approche multi-échelle*. Tech. rep., TerDOUEST.
- Dhatt, G., Touzot, G., 1984. *The finite element method displayed*. Wiley.

- Diamond, S., Kinter, E. B., 1965. Mechanisms of soil-lime stabilization. Highway Research Record (92).
- Diamond, S., Kinter, E. B., 1966. Adsorption of calcium hydroxide by montmorillonite and kaolinite. *Journal of Colloid and Interface Science* 22 (3), 240–249.
- Eades, J. L., Grim, R. E., 1960. Reaction of hydrated lime with pure clay minerals in soil stabilization. Highway Research Board Bulletin (262).
- Eades, J. L., Grim, R. E., 1966. A quick test to determine lime requirements for lime stabilization. Highway Research Record 139, 61–72.
- European Commission, 2013. Horizon 2020 – Energy Efficiency. <http://ec.europa.eu>.
- Gens, A., Nova, R., 1993. Conceptual bases for a constitutive model for bonded soils and weak rocks. *Geotechnical engineering of hard soils-soft rocks* 1 (1), 485–494.
- GiD Customization Manual, 2014. GiD Customization Manual.
- GiD User Manual, 2014. [ftp://www.gidhome.com/pub/GiD\\_Documentation/Tutorials/GiD\\_12\\_User\\_Manual.pdf](ftp://www.gidhome.com/pub/GiD_Documentation/Tutorials/GiD_12_User_Manual.pdf).
- Giraud, A., 2011. *Mécanique des Milieux Continus*, notes de cours.
- Guddati, M. N., Yue, B., Jan. 2004. Modified integration rules for reducing dispersion error in finite element methods. *Computer Methods in Applied Mechanics and Engineering* 193 (3-5), 275–287.
- Haeri, S. M., Hamidi, A., May 2009. Constitutive modelling of cemented gravelly sands. *Numerical models in geomechanics-NUMOG IX* 4 (2), 123–139.
- Henkel, D. J., 1956. The effect of overconsolidation on the behaviour of clays during shear. *Géotechnique* 6 (4), 139–150.
- Hill, R., 1950. *The Mathematical Theory of Plasticity*.
- Hilt, G. H., Davidson, D. T., 1960. Lime fixation in clayey soils. Highway Research Board Bulletin 262, 20–32.
- Hinton, E., Owen, D., 1980. *Finite elements in plasticity: Theory and practice*. Pineridge, Swansea, Wales.
- Horpibulsuk, S., Liu, M. D., Liyanapathirana, D. S., Suebsuk, J., 2010a. Behaviour of cemented clay simulated via the theoretical framework of the Structured Cam Clay model. *Computers and Geotechnics* 37 (1-2), 1–9.
- Horpibulsuk, S., Rachan, R., Chinkulkijniwat, A., Raksachon, Y., Suddeepong, A., Oct. 2010b. Analysis of strength development in cement-stabilized silty clay from microstructural considerations. *Construction and Building Materials* 24 (10), 2011–2021.

## BIBLIOGRAPHY

- Hujeux, J., 1985. Une loi de comportement pour le chargement cyclique des sols. *Génie parasismique*, 278–302.
- Ingles, O. G., 1964. The nature and strength of the interparticle bonds in natural and stabilized soils. In: *Mechanisms of Stabilization, D-9, Pro. Of a Colloquium Held at Syndal Vietora. Syndal Victoria, Australia.*
- Itin, Y., Hehl, F. W., 2013. The constitutive tensor of linear elasticity : its decompositions , Cauchy relations , null Lagrangians , and wave propagation. *Journal of Mathematical Physics* 54 (4).
- Kamon, M., 2001. Environmental issues of geotechnical engineering. <http://www.nce.co.uk/environmental-issues-of-geote>.
- Kavvasdas, M., Amorosi, A., 2000. A constitutive model for structured soils. *Géotechnique* 50 (3), 263–273.
- Kendall, K., Howard, A. J., Birchall, J. D., Pratt, P. L., Proctor, B. A., Jefferis, S. A., 1983. The Relation between Porosity, Microstructure and Strength, and the Approach to Advanced Cement-Based Materials [and Discussion]. *Philosophical Transactions of the Royal Society of London. Series A, Mathematical and Physical Sciences* 310, 139–153.
- Ketcham, R., Carlson, W., 2001. Acquisition, optimization and interpretation of X-ray computed tomographic imagery: applications to the geosciences. *Computers & Geosciences* 27 (4), 381–400.
- Ketcham, R. a., Jul. 2005. Three-dimensional grain fabric measurements using high-resolution X-ray computed tomography. *Journal of Structural Geology* 27 (7), 1217–1228.
- Kissinger, H. E., 1957. Reaction kinetics in differential thermal analysis. *Analytical Chemistry* 29, 1702–1706.
- Lagioia, R., a.M. Puzrin, Potts, D., Jan. 1996. A new versatile expression for yield and plastic potential surfaces. *Computers and Geotechnics* 19 (3), 171–191.
- Lagioia, R., Nova, R., 1995. An experimental and theoretical study of the behaviour of a calcarenite in triaxial compression. *Géotechnique* 45 (4), 633–648.
- Lapierre, C., Leroueil, S., Locat, J., 1990. Mercury intrusion and permeability of Louisville clay. *Canadian Geotechnical Journal* 27 (6), 761–773.
- Le Runigo, B., Cuisinier, O., Cui, Y.-J., Ferber, V., Deneele, D., Nov. 2009. Impact of initial state on the fabric and permeability of a lime-treated silt under long-term leaching. *Canadian Geotechnical Journal* 46 (11), 1243–1257.
- Le Runigo, B., Ferber, V., Cui, Y., Cuisinier, O., Deneele, D., 2011. Performance of lime-treated silty soil under long-term hydraulic conditions. *Engineering Geology* 118 (1-2), 20–28.



- Le Tallec, P., 2011. Modélisation et calcul des milieux continus, les Éditio Edition.
- Legat, V., Winckelmans, G., 2007. Mécanique des fluides et transferts I. Vol. 1321.
- Legay, A., 2012. Calcul des structures par éléments finis.
- Leroueil, S., Vaughan, P. R., 1990. The general and congruent effects of structure in natural soils and weak rocks. *Géotechnique* 40 (3), 467–488.
- Little, D. N., 1995. Stabilization of pavement subgrades and base courses with lime. Kendall Hunt Pub Co.
- Liu, H., Song, E., Ling, H. I., Jul. 2006. Constitutive modeling of soil-structure interface through the concept of critical state soil mechanics. *Mechanics Research Communications* 33 (4), 515–531.
- Liu, M. D., Carter, J. P., 2002. A structured Cam Clay model. *Canadian Geotechnical Journal* 39 (6), 1313–1332.
- Liu, M. D., Carter, J. P., 2003. Volumetric Deformation of Natural Clays. *International Journal of Geomechanics* 3 (2), 236–252.
- Lo, S., Wardani, S., 2002. Strength and dilatancy of a silt stabilized by a cement and fly ash mixture. *Canadian Geotechnical Journal* 39 (1), 77–89.
- Locat, J., Bérubé, M.-A., Choquette, M., 1990. Laboratory investigations on the lime stabilization of sensitive clays: shear strength development. *Canadian Geotechnical Journal* 27 (3), 294–304.
- Locat, J., Tremblay, H., Leroueil, S., 1996. Mechanical and hydraulic behaviour of a soft inorganic clay treated with lime. *Canadian geotechnical journal* 33 (4), 654–669.
- Lorenzo, G., Bergado, D., 2004. Fundamental parameters of cement-admixed clay-new approach. *Journal of geotechnical and geoenvironmental engineering* 130 (10), 1042–1050.
- Lubliner, J., 2008. Plasticity theory. Courier Dover Publications.
- Lubliner, J., Oliver, J., Oller, S., Onate, E., 1989. A plastic-damage model for concrete. *International Journal of solids and structures* 25 (3), 299–326.
- Maccarini, M., 1987. Laboratory studies for a weakly bonded artificial soil. Ph.D. thesis, Imperial College London (University of London).
- MacKenzie, R. C., 1970. Differential Thermal Analysis. Volume 1 : Fundamental Aspects. Academic Press London, London-New York.
- MacKenzie, R. C., 1972. Differential Thermal Analysis. Vol. 2. Applications., academic p Edition. Academic Press London, London-New York.
- Malandraki, V., Toll, D. G., 2001. Triaxial Tests on Weakly Bonded Soil with Changes in Stress Path. *Journal of Geotechnical and Geoenvironmental Engineering* 127 (3), 282–291.

## BIBLIOGRAPHY

- Mathew, P. K., Rao, S. N., 1997. Effect of Lime on Cation Exchange Capacity of Marine Clay. *Journal of Geotechnical and Geoenvironmental Engineering* 123 (2), 183–185.
- Matsuoka, H., Nakai, T., 1982. A new failure criterion for soils in three-dimensional stresses. In: *IUTAM conference on deformation and failure of granular materials*, Delft. Vol. 1. pp. 253–263.
- Matsuoka, H., Yao, Y.-P., Sun, D., 1999. The Cam-clay models revised by the SMP criterion. *Soils and foundations* 39 (1), 81–95.
- Maubec, N., 2010. Approche multi-echelle du traitement des sols a la chaux. Etudes des interactions avec les argiles. Ph.D. thesis, Thèse de Doctorat, Université de Nantes, France.
- Mayniel, K., 1808. *Traité expérimental, analytique et pratique de la poussée des terres et des murs de revêtement*. chez Bachelier, libraire, quai des Augustins.
- Mita, K., Dasari, G., Lo, K., 2004. Performance of a three-dimensional Hvorslev-modified cam clay model for overconsolidated clay. *International Journal of Geomechanics* 4 (4), 296–309.
- Mitchell, J. K., Hooper, D. R., 1961. Influence of time between mixing and compaction on properties of a lime-stabilized expansive clay. *Highway Research Board Bulletin* (304).
- Mitchell, J. K., Soga, K., 2005. Soil Composition and Engineering Properties. In: *Fundamentals of Soil Behavior* (3rd Edition). pp. 83–108.
- Muir Wood, D., 1990. *Soil Behaviour and Critical State Soil Mechanics*. Cambridge University Press.
- Muir Wood, D., 2004. *Geotechnical modelling*. Vol. Applied Ge. CRC Press.
- Müller, C. J., 2005. Pozzolanic Activity of Natural Clay Minerals with Respect to Environmental Geotechnics. Ph.D. thesis, University of Karlsruhe.
- Narasimha Rao, S., Rajasekaran, G., 1996. Reaction products formed in lime-stabilized marine clays. *Journal of Geotechnical Engineering* 122 (5), 329–336.
- Nayak, G., Zienkiewicz, O., 1972. Convenient form of stress invariants for plasticity. *journal of the structural division*. Proceedings of the American Society of Civil Engineers 98 (ST 4), 949–954.
- Neto, E. A. d. S., Peric, D., Owen, D. R. J., 2009. *Computational Methods for Plasticity: Theory and Applications*.
- Nitka, M., Combe, G., Dascalu, C., Desrues, J., Mar. 2011. Two-scale modeling of granular materials: a DEM-FEM approach. *Granular Matter* 13 (3), 277–281.

- Nova, R., 1988. Sinfonietta classica: an exercise on classical soil modelling. In: Constitutive Equations for Granular non-cohesive soils. Balkema: Rotterdam, Cleveland, pp. 501–519.
- Nova, R., Castellanza, R., Tamagnini, C., 2003. A constitutive model for bonded geomaterials subject to mechanical and/or chemical degradation. *International journal for numerical and analytical methods in geomechanics* 27 (9), 705–732.
- Oliveira, P. J. V., Correia, A. A. S., Garcia, M. R., 2013. Effect of Stress Level and Binder Composition on Secondary Compression of an Artificially Stabilized Soil. *Journal of Geotechnical and Geoenvironmental Engineering* 139 (5), 810–820.
- Oliveira, P. V., 2013. Effect of Stress Level and Binder Composition on Secondary Compression of an Artificially Stabilized Soil. *Journal of Geotechnical and Geoenvironmental Engineering* 139 (5), 810–820.
- Pansu, M., Gautheyrou, J., 2006. Handbook of soil analysis: Mineralogical, organic and inorganic methods.
- ParaView User's Guide, 2012. <http://denali.princeton.edu/Paraview/ParaViewUsersGuide.v3.14.pdf>. Kitware, Inc.
- Pekau, O., Gocevski, V., 1989. Elasto-plastic model for cemented and pure sand deposits. *Computers and Geotechnics* 7 (3), 155–187.
- Plante, A. F., Fernández, J. M., Leifeld, J., 2009. Application of thermal analysis techniques in soil science.
- Pomakhina, E., Deneele, D., Gaillot, A.-C., Paris, M., Ouvrard, G., Apr. 2012. <sup>29</sup>Si solid state NMR investigation of pozzolanic reaction occurring in lime-treated Ca-bentonite. *Cement and Concrete Research* 42 (4), 626–632.
- Potts, D., Zdravkovic, L., 1999. Finite element analysis in geotechnical engineering: Theory. Thomas Telford London.
- Potts, D., Zdravkovic, L., 2000. Some Pitfalls when using Modified Cam Clay. Imperial College, London, UK.
- Ramachandran, V., Paroli, R. M., Beaudoin, J. J., Delgado, A. H., 2002. Handbook of Thermal Analysis of Construction Materials.
- Rampello, S., Callisto, L., 1998. A study on the subsoil of the Tower of Pisa based on results from standard and high-quality samples. *Canadian Geotechnical Journal* 35 (6), 1074–1092.
- Rankine, W. J. M., Jan. 1857. On the Stability of Loose Earth. *Philosophical Transactions of the Royal Society of London* 147 (January), 9–27.
- Richards, F., 1959. A flexible growth function for empirical use. *Journal of experimental Botany* 10 (29), 290–300.

## BIBLIOGRAPHY

- Robin, V., Cuisinier, O., Masrouri, F., Javadi, A. A., 2014a. A chemo-mechanical coupling for lime treated soils. In: International Symposium on Geomechanics from Micro to Macro. Cambridge.
- Robin, V., Cuisinier, O., Masrouri, F., Javadi, A. A., 2014b. Chemo-mechanical modelling of lime treated soils. *Applied Clay Science* 95, 211–219.
- Robin, V., Javadi, A. A., Cuisinier, O., Masrouri, F., 2014c. A new formulation to model the degradation in structured soils. In: 8th European Conference on Numerical Methods in Geotechnical Engineering. Delft, pp. 97–102.
- Robin, V., Javadi, A. A., Cuisinier, O., Masrouri, F., 2014d. An Effective Constitutive Model for Lime Treated Soils. *Computers & Geotechnics*, (Accepted with revisions).
- Roscoe, K., Schofield, A., Thurairajah, A., 1963. Yielding of Clays in States Wetter than Critical. *Geotechnique* 13 (3), 211–240.
- Roscoe, K. H., Burland, J. B., 1968. On the generalized stress-strain behaviour of wet clay. *Engineering Plasticity*, 535–609.
- Roscoe, K. H., Schofield, A. N., Wroth, C. P., 1958. On the yielding of soils. *Géotechnique* 8 (1), 22–53.
- Rotta, G. V., Consoli, N. C., Prietto, P. D. M., Coop, M. R., Graham, J., 2003. Isotropic yielding in an artificially cemented soil cured under stress. *Géotechnique* 53 (5), 493–501.
- Rougier, E., Munjiza, a., John, N. W. M., Oct. 2004. Numerical comparison of some explicit time integration schemes used in DEM, FEM/DEM and molecular dynamics. *International Journal for Numerical Methods in Engineering* 61 (6), 856–879.
- Rowe, P. W., 1962. The stress-dilatancy relation for static equilibrium of an assembly of particles in contact. *Proceedings of the Royal Society of London. Series A. Mathematical and Physical Sciences* 269 (1339), 500–527.
- Saikia, N., Sengupta, P., Gogoi, P., Borthakur, P., Feb. 2002. Hydration behaviour of lime-co-calcined kaolin-petroleum effluent treatment plant sludge. *Cement and Concrete Research* 32 (2), 297–302.
- Salençon, J., 2002. *Mécanique des milieux continus - Tome 2: Thermoélasticité*.
- Salençon, J., 2007. *Mécanique des milieux continus - Tome 1: Concepts généraux*.
- Schofield, A., Wroth, P., 1968. Critical state soil mechanics, 310.
- Schofield, R., Samson, H., 1953. The deflocculation of kaolinite suspensions and the accompanying change-over from positive to negative chloride adsorption.
- Scholtès, L., Donzé, F.-V., Feb. 2013. A DEM model for soft and hard rocks: Role of grain interlocking on strength. *Journal of the Mechanics and Physics of Solids* 61 (2), 352–369.

- SETRA, 2007. Traitement des sols à la chaux et/ou aux liants hydrauliques: application à la réalisation des assises de chaussées.
- Sherwood, P. T., 1993. Soil Stabilization with Cement and Lime: State-of-the-Art Review. Transport Research Laboratory, Her Majesty Stationary Office.
- Sokolnikoff, I. S., 1951. Tensor Analysis: Theory and Application. John Wiley & Sons, Inc.
- Sokolnikoff, I. S., 1956. Mathematical Theory of Elasticity. McGraw-Hill.
- Stocker, P. T., 1974. Diffusion and diffuse cementation in lime and cement stabilised clayey soils - studies of plasticity and aggregation. Australian Road Research 5 (6), 51–75.
- Suebsuk, J., Horpibulsuk, S., Liu, M. D., 2010. Modified Structured Cam Clay: A generalised critical state model for destructured, naturally structured and artificially structured clays. Computers and Geotechnics 37 (7-8), 956–968.
- Suebsuk, J., Horpibulsuk, S., Liu, M. D., 2011. A critical state model for overconsolidated structured clays. Computers and Geotechnics 38 (5), 648–658.
- Szabo, B., Babuska, I., 2009. An Introduction to Finite Element Analysis.
- Szabó, B., Babuška, I., 2011. Introduction to Finite Element Analysis: Formulation, Verification and Validation. John Wiley & Sons.
- Tamagnini, C., Castellanza, R., Nova, R., Aug. 2002. A Generalized Backward Euler algorithm for the numerical integration of an isotropic hardening elastoplastic model for mechanical and chemical degradation of bonded geomaterials. International Journal for Numerical and Analytical Methods in Geomechanics 26 (10), 963–1004.
- Tengattini, A., Das, A., Nguyen, G. D., Viggiani, G., Hall, S. a., Einav, I., Oct. 2014. A thermomechanical constitutive model for cemented granular materials with quantifiable internal variables. Part I—Theory. Journal of the Mechanics and Physics of Solids 70, 281–296.
- Tremblay, H., Leroueil, S., Locat, J., 2001. Mechanical improvement and vertical yield stress prediction of clayey soils from eastern Canada treated with lime or cement. Canadian Geotechnical Journal 38 (3), 567–579.
- UK Green Building Council, 2012. Fast facts and stats on key built environment issues.
- van der Lee, J., De Windt, L., Lagneau, V., Goblet, P., Apr. 2003. Module-oriented modeling of reactive transport with HYTEC. Computers & Geosciences 29 (3), 265–275.
- Vatsala, A., Nova, R., Srinivasa Murthy, B. R., 2001. Elastoplastic Model for Cemented Soils. Journal of Geotechnical and Geoenvironmental Engineering 127 (8), 679–687.
- VTK User's Guide, 2010. VTK User's Guide, 11th Edition. Kitware Inc.

## BIBLIOGRAPHY

- Wendlandt, W. W., 1974. Thermal methods of analysis. Wiley-Interscience. New York.
- Wesley, L. D., 1973. Some basic engineering properties of halloysite and allophane clays in Java, Indonesia. *Géotechnique* 23 (4), 471–494.
- Wissa, A. E. Z., 1965. Effective stress-strength behavior of cemented soils. Ph.D. thesis, Thesis (Sc. D.), Massachusetts Institute of Technology.
- Yong, R., Nagaraj, T., 1977. Investigation of fabric and compressibility of a sensitive clay. In: *Proceedings of the International Symposium on Soft Clay*, Asian Institute of Technology. pp. 327–333.
- Zhu, W., Zhang, C. L., Chiu, A. C. F., May 2007. Soil–Water Transfer Mechanism for Solidified Dredged Materials. *Journal of Geotechnical and Geoenvironmental Engineering* 133 (5), 588–598.
- Zienkiewicz, O., Taylor, R., 1991. *The Finite Element Method: Solid and Fluid Mechanics Dynamics and Non-Linearity*, 4th Edition. Vol. 2. McGraw-Hill.
- Zienkiewicz, O. C., Taylor, R. L., 1989. *The Finite Element Method: Basic formulation and linear problems*, 4th Edition. Vol. 1. McGraw-Hill.
- Zienkiewicz, O. C., Taylor, R. L., 2000. *The Finite Element Method Volume 1 : The Basis*, 5th Edition. Vol. 1.
- Zytynski, M., Randolph, M., Nova, R., Wroth, C., 1978. On modelling the unloading-reloading behaviour of soils. *International Journal for Numerical and Analytical Methods in Geomechanics* 2 (1), 87–93.

# Appendices

## BIBLIOGRAPHY



# Appendix A

## Experimental program details

### Determination of the amount lime

The amount of lime is determined from the total mass of wet soil to be treated and is given by

$$m_{\text{CaO}} = [\text{CaO}] \times m_{\text{wet soil}} \quad (\text{A.1})$$

### Amount of material per triaxial specimen

For a triaxial sample of dimension  $D \times L$  the amount of treated material per triaxial sample is given by

$$m_{\text{sample}} = V_{\text{sample}} \times \rho_d \times (1 + w) \quad (\text{A.2})$$

with  $V_{\text{sample}} = \pi \times \left(\frac{D}{2}\right)^2 \times L$ ,  $\rho_d$  the dry density, and  $w$  the water content.

### Lime treatment and moulding of the specimen

1. Sprinkle  $\frac{1}{4}$  of the amount of lime to be added and mix until no trace of lime is visible. Repeat 4 times.
2. The treated material is immediately sealed in a plastic bag for an hour before proceeding to the moulding of the specimens
3. After 1 hour, mould specimens. Use Equation A.2 to determine the amount of material per specimen
4. Each specimen is wrapped into a plastic film and in an aluminium foil to prevent as much as possible carbonation reactions
5. All the specimens are placed in sealed plastic bag for 28 days in a controlled temperature room.

**Details on the saturation of the specimens**

Table A.1: Degrees of saturation for the tested specimens

0%		1%		2%		5%	
Sample	$S_r$ (%)	Sample	$S_r$ (%)	Sample	$S_r$ (%)	Sample	$S_r$ (%)
t0-01	98	t1-01	??	t2-01	100	t5-01	99
t0-02	100	t1-02	100	t2-02	100	t5-02	101
t0-03	102	t1-03	102	t2-03	101	t5-03	100
t0-04	101	t1-04	98	t2-04	101	t5-04	98
t0-05	100	t1-05	100	t2-05	99	t5-05	100
t0-06	101	t1-06	101	t2-06	100	t5-06	100
		t1-07	99	t2-07	101		

tX-Y: X=[CaO], Y=Sample number.

# Appendix B

## Finite element procedures

### B.1 Proof of Equation (5.7)

*Proof.*

$$\begin{aligned}
 \underline{\underline{\sigma}} : \underline{\underline{\nabla \delta \mathbf{u}}} &= (\sigma_{kl} \underline{e}_k \otimes \underline{e}_l) : (\delta u_{i,j} \underline{e}_i \otimes \underline{e}_j) \\
 &= \sigma_{kl} \delta u_{i,j} \delta_{jk} \delta_{il} \\
 &= \sigma_{ki} \delta u_{i,j} \delta_{jk} && \delta_{il} = 1 \text{ if } l = i \\
 &= \sigma_{ji} \delta u_{i,j} && \delta_{jk} = 1 \text{ if } k = j \\
 &= \sigma_{ij} \delta u_{i,j} && \sigma_{ij} = \sigma_{ji} \\
 &= \frac{1}{2} (\sigma_{ij} \delta u_{i,j} + \sigma_{ij} \delta u_{i,j}) = \frac{1}{2} (\sigma_{ij} \delta u_{i,j} + \sigma_{ji} \delta u_{i,j}) \\
 &= \frac{1}{2} (\sigma_{ij} \delta u_{i,j} + \sigma_{ij} \delta u_{j,i}) = \sigma_{ij} \frac{1}{2} (\delta u_{i,j} + \delta u_{i,j}) \\
 &= \sigma_{ij} \delta \varepsilon_{i,j} && \text{after Equation (2.13)} \\
 &= \underline{\underline{\sigma}} : \underline{\underline{\delta \varepsilon}}
 \end{aligned}$$

□

### B.2 Nodal interpolation

#### Context

One of the key aspect of the FEM is that the value of a particular degree of freedom can be evaluated anywhere within the element just from the nodal values. Assume a 3-noded element as given in Figure B.1. The vector of nodal displacements  $\underline{\mathbf{u}} = \{\underline{\mathbf{u}}_1, \underline{\mathbf{u}}_2, \underline{\mathbf{u}}_3\}^T$  is completely defined. How can we determine from  $\{\mathbf{u}\}$  the displacement  $\underline{\mathbf{v}}$ ?

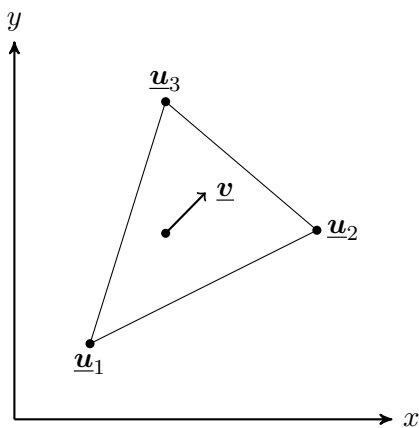


Figure B.1: Interpolation from nodal values

The method is called *nodal interpolation* and is the key aspect in numerical integration.

**Definition B.1** Let  $F$  a metric space,  $G \subset F$  and  $u \in F$ . Given a set of nodal points  $V$ , we define  $\hat{u} \in G$  the best interpolation of  $u$  that verifies  $\max_{x_i \in V} |u(x_i) - \hat{u}(x_i)| = 0$

Different kind of interpolation exist (e.g. Lagrangian or Hermitian) depending on the type of element considered. We present briefly the principles of the Lagrangian interpolation.

### Lagrangian interpolation

Given a set of  $n + 1$  nodal points  $V_{n+1} = \{x_0, x_1, \dots, x_n\}$ , from Definition (B.1) we note

$$\forall x_i \in V_{n+1} \quad \hat{u}(x_i) = u(x_i) = u_i \tag{B.1}$$

with  $u$  the function to be interpolated and  $\hat{u}$  its interpolation. The general form of the polynomial interpolation consists in a linear combination of polynomials such as

$$\hat{u}(x) = \sum_{i=0}^n P_i(x) a_i = \langle P_{n+1} \rangle \{ \mathbf{a} \} \tag{B.2}$$

with  $\langle P_{n+1} \rangle = \langle P_0 \ P_1 \ \dots \ P_n \rangle$  the polynomial basis of the interpolation and  $P_i(x_j) = \delta_{ij}$ . For the Lagrangian interpolation we choose  $\langle P_{n+1} \rangle = \langle 1 \ x \ x^2 \ \dots \ x^n \rangle$ . Equation (B.2) becomes

$$u(x) \approx \hat{u}(x) = \sum_{i=0}^n a_i x^i \tag{B.3}$$

Combined with Equation (B.1) gives a set of  $(n + 1)$  equations

$$\hat{u}(x_i) = u_i \quad \Leftrightarrow \quad \begin{bmatrix} 1 & x_0 & x_0^2 & \cdots & x_0^n \\ 1 & x_1 & x_1^2 & \cdots & x_1^n \\ 1 & x_2 & x_2^2 & \cdots & x_2^n \\ \vdots & \vdots & \vdots & & \vdots \\ 1 & x_n & x_n^2 & \cdots & x_n^n \end{bmatrix} \begin{Bmatrix} a_0 \\ a_1 \\ a_2 \\ \vdots \\ a_n \end{Bmatrix} = \begin{Bmatrix} u_0 \\ u_1 \\ u_2 \\ \vdots \\ u_n \end{Bmatrix} \quad (\text{B.4})$$

and can be written as

$$[\mathbb{V}] \{\mathbf{a}\} = \{\mathbf{u}\} \quad (\text{B.5})$$

with  $\mathbb{V}$  the Vandermonde matrix. If all the  $x_i$  are distinct it can be proven that the determinant of the Vandermonde matrix is non-zero and is given by

$$\det \mathbb{V} = \prod_{0 \leq i < j \leq n} (x_j - x_i) \neq 0 \quad \text{if } x_i \neq x_j \quad (\text{B.6})$$

therefore,

$$[\mathbb{V}] \{\mathbf{a}\} = \{\mathbf{u}\} \quad \Leftrightarrow \quad \{\mathbf{a}\} = [\mathbb{V}]^{-1} \{\mathbf{u}\} \quad (\text{B.7})$$

Combined with Equation (B.2) gives the interpolation  $\hat{u}$  from the nodal points

$$\hat{u}(x) = \langle P_{n+1} \rangle \{\mathbf{a}\} = \langle P_{n+1} \rangle [\mathbb{V}]^{-1} \{\mathbf{u}\} = [\mathbf{N}] \{\mathbf{u}\} \quad (\text{B.8})$$

Therefore,

$$u(x) \approx \hat{u}(x) = \sum_{i=0}^n N_i u_i \quad (\text{B.9})$$

with

$$N_i(x) = \frac{\prod_{\substack{j=0 \\ j \neq i}}^n (x - x_j)}{\prod_{\substack{j=0 \\ j \neq i}}^n (x_i - x_j)} \quad (\text{B.10})$$

called the Lagrange polynomials that verify

$$N_i(x_j) = \delta_{ij} = \begin{cases} 0 & \text{if } i \neq j \\ 1 & \text{if } i = j \end{cases} \quad (\text{B.11})$$

An example of Lagrangian interpolation is given in Figure B.2.

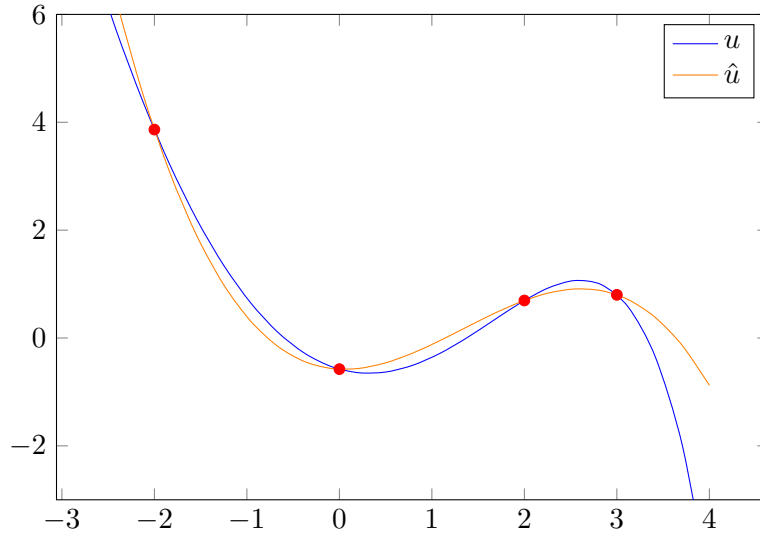


Figure B.2: Lagrangian interpolation of  $u(x) = x^2 - \frac{e^x}{\sqrt{3+x}} - n = 4$ .

### B.3 Explicit formulation of the model MASS

This section gives the explicit formulation of the model MASS for an axisymmetric problem:

$$D = \frac{E(1-\nu)}{(1+\nu)(1-2\nu)} \begin{bmatrix} 1 & \frac{\nu}{1-\nu} & 0 & \frac{\nu}{1-\nu} \\ \frac{\nu}{1-\nu} & 1 & 0 & \frac{\nu}{1-\nu} \\ 1 & 0 & \frac{1-2\nu}{2(1-\nu)} & 0 \\ \frac{\nu}{1-\nu} & \frac{\nu}{1-\nu} & 0 & 1 \end{bmatrix} \quad (\text{B.12})$$

Calculations were performed with the software Mathematica 10.0 Student Edition.

#### Flow vector $\mathbf{a}$

$$\mathbf{a} = \frac{1}{9M^2} \begin{pmatrix} 9(2\sigma_x - \sigma_y - \sigma_z) + M^2(3p_0 + 3p_b + 2(\sigma_x + \sigma_y + \sigma_z)) \\ 9(-\sigma_x + 2\sigma_y - \sigma_z) + M^2(3p_0 + 3p_b + 2(\sigma_x + \sigma_y + \sigma_z)) \\ 54\tau_{xy} \\ 9(-\sigma_x - \sigma_y + 2\sigma_z) + M^2(3p_0 + 3p_b + 2(\sigma_x + \sigma_y + \sigma_z)) \end{pmatrix} \quad (\text{B.13})$$

#### Parameter $A$

$$A = -\frac{A_1}{9(A_2 + A_3)} \quad (\text{B.14})$$

with

$$A_1 = p_0 v \left( e^{\beta(p_0 - p_y^{\text{II}})} + 1 \right)^2 (3p_b + \sigma_x + \sigma_y + \sigma_z) (3p_0 + 3p_b + 2(\sigma_x + \sigma_y + \sigma_z)) \quad (\text{B.15})$$

$$A_2 = \kappa + \beta p_0 (\Delta e_c - \Delta e_i) e^{\beta(p_0 + p_y^{\text{I}} - 2p_y^{\text{II}})} \quad (\text{B.16})$$

$$A_3 = -\lambda + e^{\beta(p_0 - p_y^{\text{II}})} (2(\kappa - \lambda) + \beta p_0 ((\Delta e_c - \Delta e_i))) + (\kappa - \lambda) e^{2\beta(p_0 - p_y^{\text{II}})} \quad (\text{B.17})$$

The formulations of the parameters  $d\lambda$  and  $\mathbf{D}_{ep}$  are too large to be displayed. However, flow vector  $\mathbf{a}$  and parameters  $A$  are sufficient for the evaluation of the elastoplastic matrix  $\mathbf{D}_{ep}$ .

## B.4 Pre-processing procedures

### ProblemType for GiD

Listing B.1: ProblemType developed for GiD

```

=====
                                General Data File
=====

=====
#   DESCRIPTION
=====
Problem_name      *gendata(Problem_name)
Type_of_element  *if(nnode == 4)
QUA4
*elseif(nnode == 8)
QUA8
*elseif(nnode == 9)
QUA9
*endif
Solver_type      *gendata(Solver_type)
Tolerance        *gendata(Tolerance, real)
type             *gendata(Type_of_problem)

=====
#   DIMENSIONS
=====
npoin            *npoin
nelem            *nelem
*Set Cond Prescribed_Displacements *nodes
nvfix            *condnumentities
ntype*if(strcmp(GenData(Type_of_problem), "Plane-Stress")==0)
1
*elseif(strcmp(GenData(Type_of_problem), "Plane-Strain")==0)
2
*elseif(strcmp(GenData(Type_of_problem), "Axisymmetric")==0)

```

## B. FINITE ELEMENT PROCEDURES

```

        3
*endif
nnode  *nnode
nmats  *nmats
ngaus  *GenData(No_Gauss ,int)
nalgo*if(strcmp(GenData(Algorithm),"Initial_Stiffness_Method")==0)
    1
*else
    999
*endif
ncrit*if(strcmp(GenData(Yield_Criterion),"Tresca")==0)
    1
*elseif(strcmp(GenData(Yield_Criterion),"Von_Mises")==0)
    2
*elseif(strcmp(GenData(Yield_Criterion),"Mohr-Coulomb")==0)
    3
*elseif(strcmp(GenData(Yield_Criterion),"Drucker-Prager")==0)
    4
*elseif(strcmp(GenData(Yield_Criterion),"Modified_Cam_Clay")==0)
    5
*elseif(strcmp(GenData(Yield_Criterion),"Lime_Treated_Soils")==0)
    6
*endif
nincs      *GenData(Number_of_increments_S1 ,int)
nstre*if(strcmp(GenData(Type_of_problem),"Axisymmetric")==0)
    4
*else
    3
*endif
ndime  *ndime
epsilon*gendata(Tolerance ,real)
nstage*if(GenData(Stage_2 ,int)==1)
    2
*else
    1
*endif

=====
# CONNECTIVITY TABLE
=====
Element Material          Node1   Node2   Node3   Node4   ...
*loop elems
*elemsnum          *elemsmat          *elemsconec
*end elems

=====
#          MESH
=====
Node      X          Y
*loop nodes
*nodesnum          *nodescoord
*end nodes

=====

```



```

# MATERIAL PROPERTIES
=====
*if(strcmp(GenData(Yield_Criterion),"Modified_Cam_Clay")==0)
Material      Young      Poisson      Thickness      Mass_Density      py
              Hardening_Parameter      Friction_Angle      Nlambda      lambda
              kappa      M
*loop materials
  *matnum *matprop(E,real) *matprop(Poisson,real) *matprop(Thickness
    ,real) *matprop(Mass_Density,real) *matprop(Yield_Stress_pyI,
    real) 0.0 0.0 *matprop(v0_Nlambda,real) *matprop(lambda,
    real) *matprop(kappa,real) *matprop(M,real)
*end
*elseif(strcmp(GenData(Yield_Criterion),"Lime_Treated_Soils")==0)
Material      Young      Poisson      Thickness      Mass_Density      py
              Hardening_Parameter      Friction_Angle      Nlambda      lambda
              kappa      M      pyII      beta      Dei      Dec      pb
*loop materials
  *matnum *matprop(E,real) *matprop(Poisson,real) *matprop(Thickness
    ,real) *matprop(Mass_Density,real) *matprop(Yield_Stress_pyI,
    real) 0.0 0.0 *matprop(v0_Nlambda,real) *matprop(lambda,
    real) *matprop(kappa,real) *matprop(M,real) *matprop(
    Degradation_Stress_pyII,real) *matprop(beta,real) *matprop(Dei,
    real) *matprop(Dec,real) *matprop(pb,real)
*end
*else
Material      Young      Poisson      Thickness      Mass_Density
              Simga_y/Cohesion      Hardening_Parameter      Friction_Angle
*loop materials
  *matnum *matprop(E,real) *matprop(Poisson,real) *matprop(Thickness
    ,real) *matprop(Mass_Density,real) *matprop(Simga_y/Cohesion,
    real) *matprop(Hardening_Parameter,real) *matprop(
    Friction_Angle,real)
*end
*endif

=====
#      BOUNDARY CONDITIONS
#      STAGE 1
=====

# Prescribed displacements:
*Set Cond Prescribed_Displacements *nodes
*Add Cond Prescribed_Displacements *nodes
Number of nodes blocked: *condnumentities
*condnumentities
*if(GenData(Prescribed_Disp,int)==1)
Node      Type      X-Value Y-Value
*loop nodes *OnlyInCond
*NodesNum      *cond(Type,int) *cond(X-Value,real) *cond(Y-Value,real)
*end
*endif

# Internal pressure:
*Set Cond Point_Load *nodes

```

## B. FINITE ELEMENT PROCEDURES

```

Point_Load      *condnumentities
*Set Cond Distributed_Loading *elems *CanRepeat
Distributed_Loading      *condnumentities
Gravity      *GenData(Gravity_Loading)
*if(GenData(Point_Load ,int)==1)

# Point Load:
*Set Cond Point_Load *nodes
*Add Cond Point_Load *nodes
Number of nodes loaded: *condnumentities
Node      FX-Value      FY-Value
*loop nodes *OnlyInCond
*NodesNum      *cond(FX-Value ,real)      *cond(FY-Value ,real)
*end
*endif
*if(GenData(Distributed_Loading ,int)==1)

# Distributed Loading:
*Set Cond Distributed_Loading *elems *CanRepeat
Number of elements loaded: *condnumentities
*condnumentities
*if(CondNumEntities(int)>0)
*loop elems *OnlyInCond
*elemsnum() *globalnodes
*cond(Normal-Pressure ,Real) *cond(Tangent-Pressure ,Real) *cond(
    Normal-Pressure ,Real) *cond(Tangent-Pressure ,Real) *cond(Normal-
    Pressure ,Real) *cond(Tangent-Pressure ,Real)
*end
*endif
*endif
*if(GenData(Gravity_Loading ,int)==1)

# Gravity Loading:
theta      gravity
*GenData(theta)      *GenData(g_force)
*endif

*if(GenData(Stage_2 ,int)==1)
=====
#      BOUNDARY CONDITIONS
#      STAGE 2
=====
nincs      *GenData(Number_of_increments_S2 ,int)

# Prescribed displacements:
*Set Cond Prescribed_Displacements_S2 *nodes
*Add Cond Prescribed_Displacements_S2 *nodes
Number of nodes blocked: *condnumentities
*condnumentities
*if(GenData(Prescribed_Disp_S2 ,int)==1)
Node      Type      X-Value Y-Value
*loop nodes *OnlyInCond
*NodesNum      *cond(Type_S2 ,int) *cond(X-Value_S2 ,real) *cond(Y-
    Value_S2 ,real)

```

```

*end
*endif

# Internal pressure:
*Set Cond Point_Load_S2 *nodes
Point_Load      *condnumentities
*Set Cond Distributed>Loading_S2 *elems *CanRepeat
Distributed>Loading      *condnumentities
Gravity      *GenData(Gravity>Loading_S2)
*if(GenData(Point_Load_S2 ,int)==1)

# Point Load:
*Set Cond Point_Load_S2 *nodes
*Add Cond Point_Load_S2 *nodes
Number of nodes loaded: *condnumentities
Node      FX-Value      FY-Value
*loop nodes *OnlyInCond
*NodesNum      *cond(FX-Value_S2 ,real)      *cond(FY-Value_S2 ,real)
*end
*endif
*if(GenData(Distributed>Loading_S2 ,int)==1)

# Distributed Loading:
*Set Cond Distributed>Loading_S2 *elems *CanRepeat
Number of elements loaded: *condnumentities
*condnumentities
*if(CondNumEntities(int)>0)
*loop elems *OnlyInCond
*elemsnum() *globalnodes
*cond(Normal-Pressure_S2 ,Real) *cond(Tangent-Pressure_S2 ,Real) *cond(
      (Normal-Pressure_S2 ,Real) *cond(Tangent-Pressure_S2 ,Real) *cond(
      Normal-Pressure_S2 ,Real) *cond(Tangent-Pressure_S2 ,Real)
*end
*endif
*endif
*if(GenData(Gravity>Loading_S2 ,int)==1)

# Gravity Loading:
theta      gravity
*GenData(theta_S2)      *GenData(g_force_S2)
*endif

*endif

```

### Example of input file generated by GiD

Listing B.2: Example of input generated by GiD

```

=====
                          General Data File
=====

=====
#      DESCRIPTION

```

## B. FINITE ELEMENT PROCEDURES

```

=====
Problem_name      Example-Input-file
Type_of_element  QUA8
Solver_type      Automatic
Tolerance        1e-06
type             Axisymmetric

=====
#      DIMENSIONS
=====
npoin           21
nelem           4
nvfix           9
ntype           3
nnode           8
nmats           1
ngaus           3
nalgo           1
ncrit           6
nincs           20
nstre           4
ndime           2
epsilon         1e-06
nstage          2

=====
# CONNECTIVITY TABLE
=====
Element          Material          Node1          Node2          Node3
                Node4          ...
1                1              17 8 4 14 12 7 10 15
2                1              21 18 8 17 19 11 12 20
3                1              8 5 1 4 6 3 2 7
4                1              18 13 5 8 16 9 6 11

=====
#      MESH
=====
Node            X            Y
1                0            1
2                0            0.75
3                0.25        1
4                0            0.5
5                0.5          1
6                0.5          0.75
7                0.25        0.5
8                0.5          0.5
9                0.75        1
10               0            0.25
11               0.75        0.5
12               0.5          0.25
13               1            1
14               0            0
15               0.25        0

```

```

16          1          0.75
17          0.5          0
18          1          0.5
19          1          0.25
20          0.75          0
21          1          0

```

```

=====
# MATERIAL PROPERTIES
=====

```

Material	Young Nlambda	Poisson lambda	Thickness kappa	Mass_Density M	py
1	45000.0	0.2	0.0	0.0	
	170.0	1.99	0.032	1.15	

```

=====
# BOUNDARY CONDITIONS
# STAGE 1
=====

```

# Prescribed displacements:

Number of nodes blocked: 9

9

Node	Type	X-Value	Y-Value
1	10	0	0
2	10	0	0
4	10	0	0
10	10	0	0
14	11	0	0
15	1	0	0
17	1	0	0
20	1	0	0
21	1	0	0

# Internal pressure:

Point\_Load 0

Distributed>Loading 4

Gravity 0

# Distributed Loading:

Number of elements loaded: 4

4

2 21 18 19	170	0	170	0	170
		0			
3 5 1 3	170	0	170	0	170
		0			
4 13 5 9	170	0	170	0	170
		0			
4 18 13 16	170	0	170	0	170
		0			

## B. FINITE ELEMENT PROCEDURES

```
=====
#      BOUNDARY CONDITIONS
#      STAGE 2
=====

nincs          1000

# Prescribed displacements:
Number of nodes blocked: 10
10
Node      Type      X-Value Y-Value
1         11         0       -0.25
3         1         0       -0.25
5         1         0       -0.25
9         1         0       -0.25
13        1         0       -0.25
14        11         0         0
15        1         0         0
17        1         0         0
20        1         0         0
21        1         0         0

# Internal pressure:
Point_Load      0
Distributed_Loading  0
Gravity         0
```

## B.5 Finite element algorithm for elasto-plastic problems

The algorithm for the finite element procedure in elasto-plasticity using initial stiffness matrix is given as follows:

---

**Algorithm 1** Finite element resolution for elasto-plasticity – Initial stiffness method

---

```

1: for each increment  $\Delta \mathbf{f}$  do
2:   Compute  $\mathbf{B}$ ,  $\mathbf{N}$ 
3:   Assemble  $\mathbf{K}$ ,  $\mathbf{d}$ ,  $\mathbf{f}$ 
4:    $\mathbf{R}^0 \leftarrow \mathbf{f}$ 
5:   while  $\|\mathbf{R}^r\| > \varepsilon_{\max}$  do
6:     Solve  $[\mathbf{K}] \{\mathbf{d}^r\} = \mathbf{R}^r$ 
7:      $d\boldsymbol{\varepsilon}^r \leftarrow \mathbf{B} \cdot \mathbf{d}^r$ 
8:      $\boldsymbol{\varepsilon}^r \leftarrow \boldsymbol{\varepsilon}^{r-1} + d\boldsymbol{\varepsilon}^r$ 
9:     Compute  $d\boldsymbol{\sigma}_e^r = \mathbf{D}d\boldsymbol{\varepsilon}^r$ 
10:    Compute  $I_1, I_2, I_3, J_2, J_3$ 
11:    Compute  $C_1, C_2, C_3$ 
12:    Compute  $\bar{\sigma}^r$ 
13:    if  $\bar{\sigma}^r > \sigma_y^r$  then
14:      Compute reduction factor  $R_\sigma = \frac{\bar{\sigma}_e^r - \sigma_y^r}{\bar{\sigma}_e^r - \bar{\sigma}^{r-1}}$ 
15:      Compute  $\boldsymbol{\sigma} \leftarrow \boldsymbol{\sigma} + (1 - R_\sigma)d\boldsymbol{\sigma}$ 
16:      Compute  $d\lambda$ ,  $\mathbf{a}$ ,  $d_D$ 
17:       $\boldsymbol{\sigma}^r \leftarrow \boldsymbol{\sigma} + d\boldsymbol{\sigma}_e^r - d\lambda d_D$ 
18:    else
19:       $\boldsymbol{\sigma}^r \leftarrow \boldsymbol{\sigma}^{r-1} + d\boldsymbol{\sigma}_e^r$ 
20:    end if
21:    Compute  $\mathbf{f}^r = \int_{\Omega} \mathbf{B}^t \boldsymbol{\sigma}^r d\Omega$ 
22:     $\mathbf{R}^r \leftarrow \mathbf{R}^r - \mathbf{f}^r$ 
23:  end while
24: end for

```

---

## B.6 Python script for vtk file generation

Listing B.3: Python script for vtk file generation

```

from __future__ import print_function
import os
import platform
import numpy as np

# Get platform
syst = platform.system()

# Get current directory
base=os.path.dirname(os.path.abspath(__file__))

# Import parameters
File=base+'/Output/parameters.txt'
data=np.loadtxt(File,skiprows=0)

# Save main parameters
nelem=int(data[0])
nnode=int(data[1])
npoint=int(data[2])
nincs=int(data[3])+1
ntype=int(data[4])

# Loop over each increment
for iincs in range(0,nincs):

    # Display progress
    sys.stdout.write("\r{0} %".format((float(iincs)/float(nincs+1.0))
        *100))
    sys.stdout.flush()

    # Open output file for increment
    f = open('vtkmovie/vtk_'+str(iincs)+'.vtk','w')

    # Print header in vtk file
    print("# vtk DataFile Version 1.0", file=f)
    print("2D Unstructured Grid of Linear Triangles", file=f)
    print("ASCII", file=f)
    print("", file=f)
    print("DATASET UNSTRUCTURED_GRID", file=f)
    print("POINTS "+str(npoint)+" float", file=f)

    # Import displacements of the nodes
    File=base+'/Output/output_increm/displacements/'+str(iincs)+'.dat
    ,
    data=np.loadtxt(File,skiprows=0)

    # Save displacements of each nodes for this increment
    coord=[]
    for i in range(0,len(data)):
        coord.append([])

```



```

coord[i].append( float(data[i,0])+float(data[i,2]) )
coord[i].append( float(data[i,1])+float(data[i,3]) )

# Print displacements in vtk file
for i in range(0,len(coord)):
    print(str(coord[i][0])+" "+str(coord[i][1])+" "+str(coord[i][2])+" "+str(coord[i][3]), file
          =f)

print("", file=f)

# Import connectivity table
File=base+'/Output/conntable.txt'
data=np.loadtxt(File,skiprows=0)

# Save connectivity table
lnods=[]
if (nelem>1):
    for i in range(0,len(data)):
        lnods.append([])
        for j in range(0,nnode):
            lnods[i].append((int(data[i,j+1])-1))

if (nelem==1):
    for i in range(0,nelem+1):
        lnods.append([])
        for j in range(0,nnode):
            lnods[i].append((int(data[j+1])-1))

# Print header of connectivity table in vtk file
print("CELLS "+str(nelem)+" "+str(nelem*(nnode+1)), file=f)

#Re-order nodes according to vtk format
for i in range(0,len(lnods)):
    myorder=[0,2,4,6,1,3,5,7]
    lnods_temp = [ lnods[i][j] for j in myorder]
    lnods[i]=lnods_temp

# Print connectivity table in vtk file
for i in lnods:
    var=str(i)
    var=var[0:-1]
    var = var.replace("[",str(nnode)+" ")
    newstr = var.replace(","," ")
    print(newstr, file=f)

print("", file=f)

# Print type of element
print("CELL_TYPES "+str(nelem), file=f)
if (nnode==8):
    type=23
elif (nnode==4):
    type=9
elif (nnode==4):

```

## B. FINITE ELEMENT PROCEDURES

```
    type=28

for i in range(0,nelem):
    print(type, file=f)

#START PLOTTING THE RESULTS: POINTS TYPE
print("", file=f)
print("POINT_DATA "+str(npoint), file=f)

#-----
# STRAINS
#-----
# Import strains
File=base+'/Output/output_increm/strains/'+str(iincs)
data=np.loadtxt(File,skiprows=1)

x=y=eps_xx=eps_yy=eps_xy=eps_zz=ps_max=[]

for i in range(0,len(data)):
    if data[i,0]==0:
        x.append((float(data[i,3])))
        y.append(float(data[i,4]))
        eps_xx.append(float(data[i,5]))
        eps_yy.append(float(data[i,6]))
        eps_xy.append(float(data[i,7]))
        eps_zz.append(float(data[i,8]))
        ps_max.append(float(data[i,9]))

strains=[eps_xx,eps_yy,eps_xy,eps_zz,ps_max]

# Choose name of parameters depending of the type of problem
if ntype==3:
    names=['eps_rr','eps_zz','eps_rz','eps_tt','eps_max_principal
    ']
else:
    names=['eps_xx','eps_yy','eps_xy','eps_zz','eps_max_principal
    ']
compt=-1

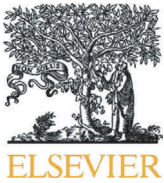
# Output all the strains in the vtk file
for res in strains:
    compt += 1
    print("SCALARS "+names[compt]+" float", file=f)
    print("LOOKUP_TABLE default", file=f)
    for i in res:
        print(i, file=f)
    print("", file=f)

# Close file
f.close()

#-----
#          END
#-----
```

## Appendix C

Paper published in *Applied Clay Science*



Contents lists available at ScienceDirect

Applied Clay Science

journal homepage: [www.elsevier.com/locate/clay](http://www.elsevier.com/locate/clay)

Research paper

## Chemo-mechanical modelling of lime treated soils

V. Robin <sup>a,b</sup>, O. Cuisinier <sup>a,\*</sup>, F. Masrouri <sup>a</sup>, A. A. Javadi <sup>b</sup><sup>a</sup> LEMTA, UMR 7563 CNRS, Laboratoire d'Energétique et de Mécanique Théorique et Appliquée, Université de Lorraine, France<sup>b</sup> Computational Geomechanics Group, Department of Engineering, University of Exeter, United Kingdom

## ARTICLE INFO

## Article history:

Received 21 January 2014

Received in revised form 9 April 2014

Accepted 10 April 2014

Available online xxxxx

## Keywords:

Quicklime

Mechanical behaviour

Chemo-mechanical coupling

Constitutive modelling

## ABSTRACT

Lime treatment has been widely used to improve mechanical properties of soils. However, less has been done to account for the effect of the treatment on constitutive relationships. In this study, a comprehensive programme of isotropic consolidation tests and drained triaxial experiments were designed and carried out on saturated specimens of a silt treated with quicklime. The chemical composition in hydrates, portlandite, and carbonates was determined using thermogravimetric analysis and differential thermal analysis. The modifications to the mechanical parameters of the soil were evaluated in the framework of the Cam Clay elastoplastic model. The experimental results revealed that the addition of lime leads to the modification of the critical state. For concentrations in lime higher than 1%, the treated specimens displayed a different normal compression line compared to the untreated state. Chemical analysis revealed the production of cementitious compounds for every concentration tested. A constitutive model was proposed to describe the observed behaviour of lime treated soils in the framework of the Structured Cam Clay. The model accounts for the modifications on the mechanical parameters of the soil. A chemo-mechanical coupling was established between the yield stress and the mass concentration in cementitious compounds.

© 2014 Elsevier B.V. All rights reserved.

### 1. Introduction

For economic and environmental considerations, engineering companies are highly encouraged to use on site materials to construct earth structures like embankment, river levees, and earth dams. For soils with low mechanical characteristics, lime treatment (CaO) is an efficient method to improve their properties and allow their use in geotechnical structures (e.g. Little, 1995). It is of the greatest interest to account for artificial treatments in geotechnical design.

When added to the soil, quicklime reacts with the free water to produce hydrated lime, known as portlandite ( $\text{Ca}(\text{OH})_2$ ). Then, calcium cations  $\text{Ca}^{2+}$  and hydroxides anions  $\text{HO}^-$  are released in the soil, which increase the pH of the porous medium. Cation exchange process combined with the presence of large amounts of calcium ions adsorbed on the clay particles surface leads to a reduction of the size of the double diffuse layer of the clay particles. This results in the lowering of the repelling forces between clay particles and thereby giving rise to the flocculation of the clay particles. It is generally accepted that cation exchange and flocculation processes occur immediately after the addition of lime and result in a decrease of the soil plasticity (e.g. Eades and Grim, 1966; Rogers and Glendinning, 1996). Moreover, the addition of lime leads to a high pH environment (near 12.4), which enables the

dissolution of both silica and alumina present in the soil (e.g. North et al., 2008). These later react with the calcium. As a result of these chemical reactions, known as pozzolanic reactions, cementitious compounds such as calcium silicate hydrates (CSH), calcium aluminate hydrates (CAH), and calcium aluminosilicate hydrates (CASH) can be formed (e.g. Metelková et al., 2012; Pomakhina et al., 2012). The formation of these compounds leads to a modification in the soil mechanical properties (e.g. Little, 1995).

Many authors have studied the mechanical behaviour of materials treated with lime or cement (e.g. Consoli et al., 2011; Cuisinier et al., 2008; Cuisinier et al., 2011; Malandraki and Toll, 2001; Oliveira et al., 2013; Stoltz et al., 2012). In most of the cases, the addition of quicklime leads to a modification of the mechanical parameters such as the cohesion, the friction angle, and the yield stress. Improvements obtained with lime treatment regarding tensile strength and Young's modulus have been integrated in the design of pavement (Thompson, 1965). Nevertheless, less has been done to consider these improvements in the design of structures for global stability or settlement analysis. This last issue could be associated with the fact that there is no specific constitutive relationship accounting for the specific aspects of the mechanical behaviour of lime-treated soils and for the coupling between physicochemical processes and mechanical behaviour. Such relationship is required to account for the treatment in the design of geotechnical structures, in the short term and also to foretell the long term behaviour of earthen structures built with lime-treated soils.

\* Corresponding author at: LEMTA UMR 7563, Université de Lorraine / CNRS 2 Rue du Doyen Marcel Roubault TSA 7060554518 Vandœuvre-les-Nancy Cedex France.  
E-mail address: [Olivier.Cuisinier@ensg.univ-lorraine.fr](mailto:Olivier.Cuisinier@ensg.univ-lorraine.fr) (O. Cuisinier).

Lime treatment induces the formation of cementitious compounds that bind soil particles. Some studies (Leroueil and Vaughan, 1990; Liu and Carter, 2003) have shown that naturally structured soils and artificially treated materials have common mechanical features, treatment appearing to create a “structure” in the soil. In this paper, “structure” refers to the combination of the fabric and the bonding of the soil skeleton (Burland, 1990). Fabric accounts for the arrangement of particles, which depends on the state of compaction and their geometry.

Several constitutive models have been proposed for structured materials (Baudet and Stallebrass, 2004; Cotecchia and Chandler, 2000; Gens and Nova, 1993; Lee et al., 2004; Nova et al., 2003; Vatsala et al., 2001). Liu and Carter (2002) proposed a Cam Clay based constitutive model for structured materials, adding only three extra parameters to the original Modified Cam Clay (Roscoe and Burland, 1968). Since then several enhancements (Horpibulsuk et al., 2010a; Suebsuk et al., 2011, 2010) have been proposed. Most of these constitutive models use the destructured state as reference to describe the mechanical behaviour of the structured soils. The destructured state accounts for the intrinsic parameters of the soil, and especially the geometry of the particles. Artificial cementation arising from the treatment involves chemical reactions that could alter the soil particles. This aspect should be considered to adapt the existing framework to the case of lime stabilised compacted soils.

A key aspect of lime stabilisation is the fact that the structure, and thus the mechanical behaviour, relies on physicochemical processes that need to be quantified. Based on the soil water transfer method (Zhu et al., 2007), Chiu et al. (2009) used centrifuge method to determine the variation of soil water composition in dredged materials with high water content. A different approach was used in this study to assess the chemical composition of lime treated compacted soils with lower water content. Chemical composition in hydrates and portlandite in cement and concrete was successfully determined using thermogravimetric analysis (TGA) and differential thermal analysis (DTA). Some studies (Horpibulsuk et al., 2010b; Maubec, 2010) have shown the suitability of this method to determine the chemical modifications following a lime treatment. The objective of the paper is to investigate the couplings between mechanical behaviour and physicochemical processes, and then to introduce these aspects in a constitutive relationship.

To account for the treatment in the structure design, a chemo-mechanical coupling is required to predict the mechanical improvements resulting from the addition of a given amount of lime. This implies a good understanding of the mechanical behaviour of lime treated soils and of the chemical modifications arising from the treatment. To this end, the paper aims at shedding light on three aspects:

- How can the effects of a lime treatment on a material and its consequences on the mechanical properties be described?
- How can a chemo-mechanical coupling be established between the mechanical improvements and the chemical modifications?
- How can a lime treated soil be modelled?

## 2. Material and methods

### 2.1. Tested soil and specimens preparation

The material selected in this study is a silt from the east part of France. The mineral composition is as follows: quartz (55%), kaolinite (12%), feldspar (11%), illite (10%), montmorillonite (4%), chlorite (1%), goethite (6.4%), and carbonates (0.6%). The lime fixation point is near 1% and was determined according to the ASTM Standard D6276 (2006). Before proceeding to the moulding of the specimen, the material was first heated at 60 °C and then sieved to get particles smaller than 2 mm. The main characteristics of the soil are listed in Table 1.

Five concentrations in quicklime were considered in this study: 0, 0.5, 1, 2, and 5% expressed on a soil dry weight basis. The non-treated

**Table 1**  
Characteristics of the silt.

	Value
<i>Geotechnical properties</i>	
Liquid limit LL (%)	31.2
Plastic limit PL (%)	7.8
Plasticity index PI	23.4
Particle density $\rho_s$ ( $\text{Mg}\cdot\text{m}^{-3}$ )	2.66
Methylene blue value (g/100 g of dry soil)	2.1
USCS <sup>a</sup>	ML
<i>Physical chemistry properties</i>	
pH (–)	5.7
Cation-exchange capacity (cmol+/100 g)	7.41
Carbonate mass concentration (%)	0.6
<i>Initial conditions</i>	
Dry density ( $\text{Mg}\cdot\text{m}^{-3}$ )	1.68
Water content $w$ (%)	20
Initial void ratio $e_i$ (–)	0.6

<sup>a</sup> Unified Soil Classification System.

specimen (0%) was used as reference to assess the mechanical and the chemical modifications arising from the treatment.

All the specimens used for the mechanical characterisation of the soil, with or without treatment, were prepared at the same moisture content and dry density. Indeed, the optimal moisture content and maximum dry density of the silt used in this study were not significantly modified by the lime-treatment (Table 2). Therefore, all the specimens have been prepared at the same mean initial water content of 20% and a dry density of  $1.68 \text{ Mg}\cdot\text{m}^{-3}$ . Thus, any modification of the mechanical behaviour of the soil after treatment can be attributed mostly to structure modification, i.e. fabric and bonding, but not to density.

The soil was first prepared at the target water content. After an equilibration period of several days, quicklime was added to the soil, both being mixed thoroughly until a homogenous mixture was obtained. Before the specimens were compacted, the quicklime–soil mixture was sealed in hermetic plastic bags for 1 h before compaction. Then, 35 mm × 70 mm triaxial specimens were statically compacted up to the target dry density. After these steps, the actual water content of the specimens was determined. It varied between 19.6% and 20.2%. The specimens were then wrapped in plastic bags to prevent any exchange with the atmosphere, and a curing time of 28 days was respected.

### 2.2. Drained triaxial experiments

To determine the shape of the yield function, three kinds of stress path were performed in this study: isotropic consolidation, drained paths ( $\sigma'_3$  constant), and same stress ratio paths ( $\eta = p'/q = 0.39$ ).

Saturation was achieved by first creating an upward water flow through the specimen. This was achieved by applying a pressure gradient between the bottom and the top of the specimen. Deaerated water was used to maximise the dissolution of air. Pore pressure was then increased in three stages (Table 3) while maintaining a constant effective mean stress.

**Table 2**  
Results of proctor compression test for different concentrations in lime.

Lime content (%)	Optimal moisture content (%)	Optimal dry density ( $\text{Mg}\cdot\text{m}^{-3}$ )
0	17.9	1.76
1	18.8	1.72
2	20.3	1.68
3	20.9	1.64

**Table 3**  
Saturation stages performed.

	Stage 1	Stage 2	Stage 3
Duration (days)	≈7	≈7	≈7
$\sigma_3$ (kPa)	50	100	200
$P_{bottom}$ (kPa)	30	80	180
$P_{top}$ (kPa)	20	70	170
$\bar{\sigma}_3$ (kPa)	25	25	25

$P_{bottom}$ : pressure at the bottom of the specimen;  $P_{top}$ : pressure at the top of the specimen.

After every triaxial experiment, saturation of the specimen was checked by determining the degree of saturation with paraffin according to the ASTM Standard D7263-09 (2009).

To ensure full drainage of the specimens during the experiments, filter paper strips were applied to the surface of the specimens. Low rates of consolidation and axial deformation were chosen in order to generate small excess of pore pressure. An external probe was used to measure accurately the pore pressure at the bottom of the specimen during shearing.

For isotropic consolidation, a rate of  $3.47 \text{ Pa} \cdot \text{s}^{-1}$  was chosen and specimens were consolidated up to a total effective stress of 3320 kPa. Validation tests were performed to verify that there was no excess pore pressure in the specimen under this rate.

Triaxial compression tests were carried out with an axial displacement rate of  $2.46 \mu\text{m} \cdot \text{min}^{-1}$ , leading to an axial deformation of about 5% per day. Validation tests have confirmed the suitability of this rate. All the experiments were performed following the procedure described in the ASTM Standard D7181-11 (2011). The initial conditions of the specimens are given Table 4.

2.3. Monitoring of the physicochemical reactions

Lime can react with soil particles to produce only three different chemical compounds: portlandite, hydrates (cementitious compounds CAH, CSH, and CASH), and carbonates. Portlandite is produced by the hydration of quicklime introduced in the material, according to the following reaction:



Dissociation of portlandite induces release of hydroxide anions, thus increasing the pH. Once a suitable pH is reached in the porous medium, portlandite is consumed by pozzolanic reactions to produce hydrates.

Due to the high sensibility of lime with carbon dioxide, we also considered the evolution in carbonates in the specimens. Carbonates are produced by reaction of quicklime and carbon dioxide according to the following reaction:



Therefore, to monitor the progress of the physicochemical processes in the specimens, it is necessary to determine the amount of portlandite, hydrates, and carbonates.

Thermogravimetric analysis (TGA) consists of measuring the mass loss of a specimen as a function of the increasing temperature. This

**Table 4**  
Characteristics of the specimens.

Lime content (%)	Water content (%)	$\rho_d$ ( $\text{Mg} \cdot \text{m}^{-3}$ )	$e_o$ (-)	Hydraulic permeability k (m/s)
0	20.0	$1.67 \pm 0.01$	$0.60 \pm 0.02$	$10^{-9}$ – $10^{-8}$
0.5	19.6	$1.67 \pm 0.01$	$0.60 \pm 0.01$	$10^{-9}$ – $10^{-8}$
1	20.2	$1.67 \pm 0.01$	$0.60 \pm 0.01$	$10^{-9}$ – $10^{-8}$
2	19.6	$1.67 \pm 0.01$	$0.60 \pm 0.01$	$10^{-8}$ – $10^{-7}$
5	20.2	$1.66 \pm 0.01$	$0.60 \pm 0.02$	$10^{-8}$ – $10^{-7}$

test is completed with a differential thermal analysis (DTA), which compares any temperature difference between the specimen and an inert reference (MacKenzie, 1970). Each peak on the curves is correlated to a chemical compound. Using the associated mass loss, the mass concentration of the species can be estimated (Mackenzie, 1972).

TGA/DTA analysis was first used successfully to determine the chemical composition of cements and concretes in hydrated products, portlandite, and carbonates. Some studies have shown that the decarboxylation processes of these three compounds were associated with three temperature domains (Alarcon-Ruiz et al., 2005; Das et al., 1996; Saikia et al., 2002). Recent studies have applied TGA/DTA analysis on artificially treated soils to assess the mass concentration in portlandite (unreacted lime), cementitious compounds, and calcium carbonates in artificially treated specimens (Horpibulsuk et al., 2010b; Maubec, 2010).

The procedure for the determination of the chemical composition is illustrated in Fig. 1. TGA/DTA analysis provides three different curves: the variation of the energy (TDA), the mass loss (TG), and the first derivative of the weight loss (DTG). First, TDA and DTG results were used to determine accurately the three temperature domains (Table 5).

Each peak on the DTG curve (Fig. 1) is associated to a variation of the weight loss and corresponds to the decarboxylation of a chemical compound. The two temperatures delimitating the peak correspond to the temperature domains, and the chemical compound is assumed to have completely disappeared when the upper temperature limit was reached. Therefore, the variation of weight (TG curve) between these two temperatures gives the mass of the chemical compound. Analyses were performed using a NETZSCH STA 409 PC/PG device. The accuracy of the TGA weighing scale was 0.01 mg.

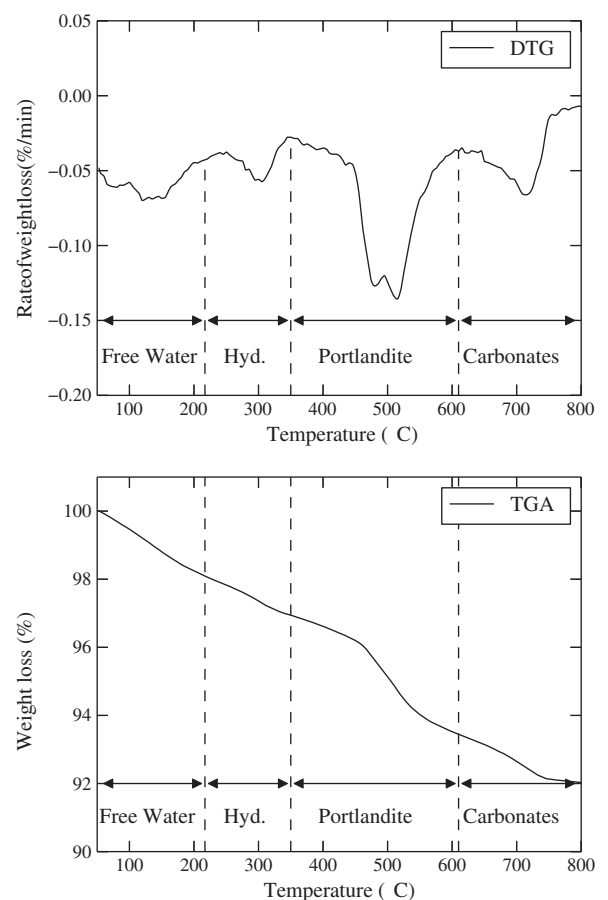


**Fig. 1.** TGA/DTA results for a lime treated specimen with the three temperatures domains – Hyd.: hydrates, DTG: differential thermo gravimetric, TGA: thermogravimetric analysis.



**Table 5**  
Ranges of temperatures used for the determination of the TGA/DTA.

Range of temperature	Chemical compound
20 °C–217 °C	Free and adsorbed water
217 °C–350 °C	Cementitious compounds
350 °C–610 °C	Portlandite (Ca(OH) <sub>2</sub> )
610 °C–800 °C	Carbonates (CaCO <sub>3</sub> )

**3. Results**

The experiments performed in this paper aimed: 1) to determine the effects of the quicklime on the intrinsic parameters of soils, 2) to assess the shape of the yield function in order to choose the most suitable model for lime-treated soils, and 3) to measure the concentrations in portlandite, hydrates, and carbonates of lime-treated specimens.

**3.1. Mechanical behaviour**

**3.1.1. Isotropic consolidation**

To assess the effects of the treatment on the yield stress, isotropic consolidation tests were performed on 0, 0.5, 1, 2, and 5% lime-treated specimens. For concentrations greater than 1%, three isotropic tests were carried out to ensure the highest representativeness. Only one result is reported in Fig. 2. The yield stress was determined using Casagrande's method.

Yield occurred for an effective mean stress of 177 kPa for the untreated specimen (Fig. 2). When lime was added to the soil, the yield stress was increased even for low lime content of 0.5%. The evolution of the yield stress as a function of the lime content is given in Fig. 3. For concentrations between 0.5% and 2%, the gradient of the curve was significantly increased. Above 2% the slope decreased, and as concentration increased, yield stress value seemed to approach 2000 kPa. One can note that there exists a one-to-one correspondence between the lime content and the resulting yield stress after 28 days of curing.

At yield the treated soil displayed higher specific volume compared to the reference state (Fig. 2). This could be due to the structure. When the effective mean stress reached the yield stress, the additional specific volume began to decrease as the effective mean stress was increased until a new normal compression line was reached, parallel to the one

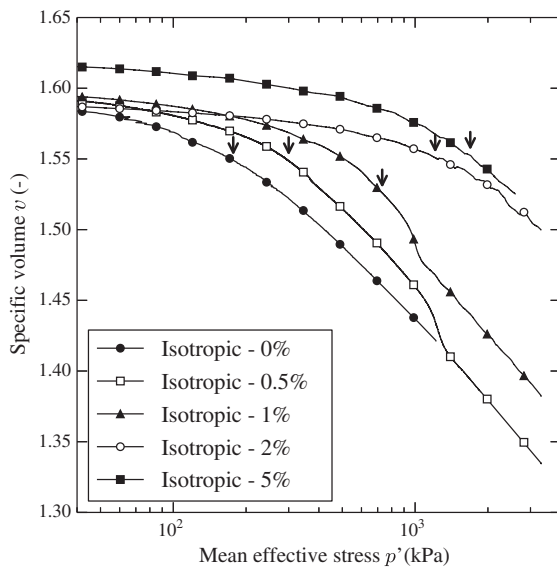


Fig. 2. Isotropic consolidation curves for five concentrations in lime.

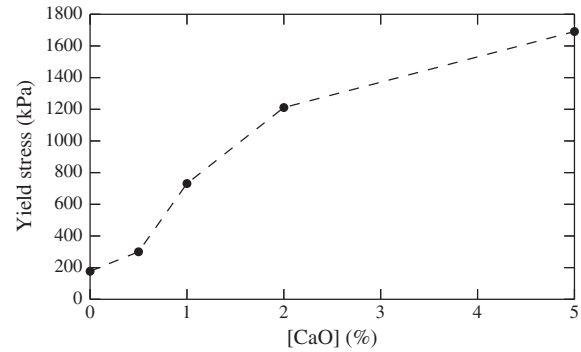


Fig. 3. Evolution of the yield stress after 28 days of curing with the lime.

of the non-treated state. This decrease of the additional specific volume corresponds to the loss of the structure. Only 0.5% lime treated specimen has shown to completely lose the additional specific volume at high mean stresses. In this case, the normal compression line matched the one of the non-treated state. For lime contents greater than 1%, specimens did not appear to converge to the non-treated state for mean effective stresses lower than 3320 kPa. At some point, a secondary normal compression line, different from the non-treated state but still parallel, seems to be reached. This feature is particularly noteworthy for the 1% treated specimen. The 2% and 5% lime-treated specimens have shown such significant improvements in mechanical properties that this feature could not be seen because of the limits of the applied pressure in the triaxial cell (3500 kPa).

**3.1.2. Shear behaviour**

Drained triaxial experiments were performed to assess the shape of the yield function and the gradient of the critical state line. Different stress paths and pre-consolidation pressures were performed on 0, 1, 2, and 5% lime-treated specimens.

The shear behaviour of the non-treated specimens (Fig. 4a) was significantly improved with 5% lime treatment (Fig. 4b). For an isotropic pre-consolidation pressure of 245 kPa, the yield locus of the reference state was reached for a deviatoric stress of 400 kPa. With 5% of lime, this value was increased up to 1250 kPa.

As the confining pressure was increased, one can see that contraction behaviour was gradually observed. This feature was particularly marked for the 5% lime-treated specimens (Fig. 4b). For a confining pressure of 20 kPa, the specimens had significant dilation behaviour. As the confining pressure increased, the specimens started to exhibit a contraction behaviour.

**3.2. Yield loci for lime-treated soils**

Yield loci and critical states were determined from the previous results and plotted in the (p', q) plane (Fig. 5). Results from the same stress ratio paths (η = 0.39) were also included.

To use these results in a constitutive model, yield loci and critical states were determined based on the critical state theory (Muir Wood, 1991). Yield was assumed to occur when plastic deformation appeared (ε<sub>q</sub><sup>p</sup> > 0), and critical state was reached when:

$$\frac{\partial p'}{\partial \epsilon_q} = \frac{\partial q}{\partial \epsilon_q} = \frac{\partial v}{\partial \epsilon_q} = 0 \tag{3}$$

The elastic domain showed to be significantly increased with the increase of lime content, without any significant anisotropic behaviour, and the critical state lines appeared to be modified with the treatment. The gradient and the y-intercept of the critical state lines both increased with the increase of the amount in lime. The results appear to be well described by the Modified Cam Clay model.

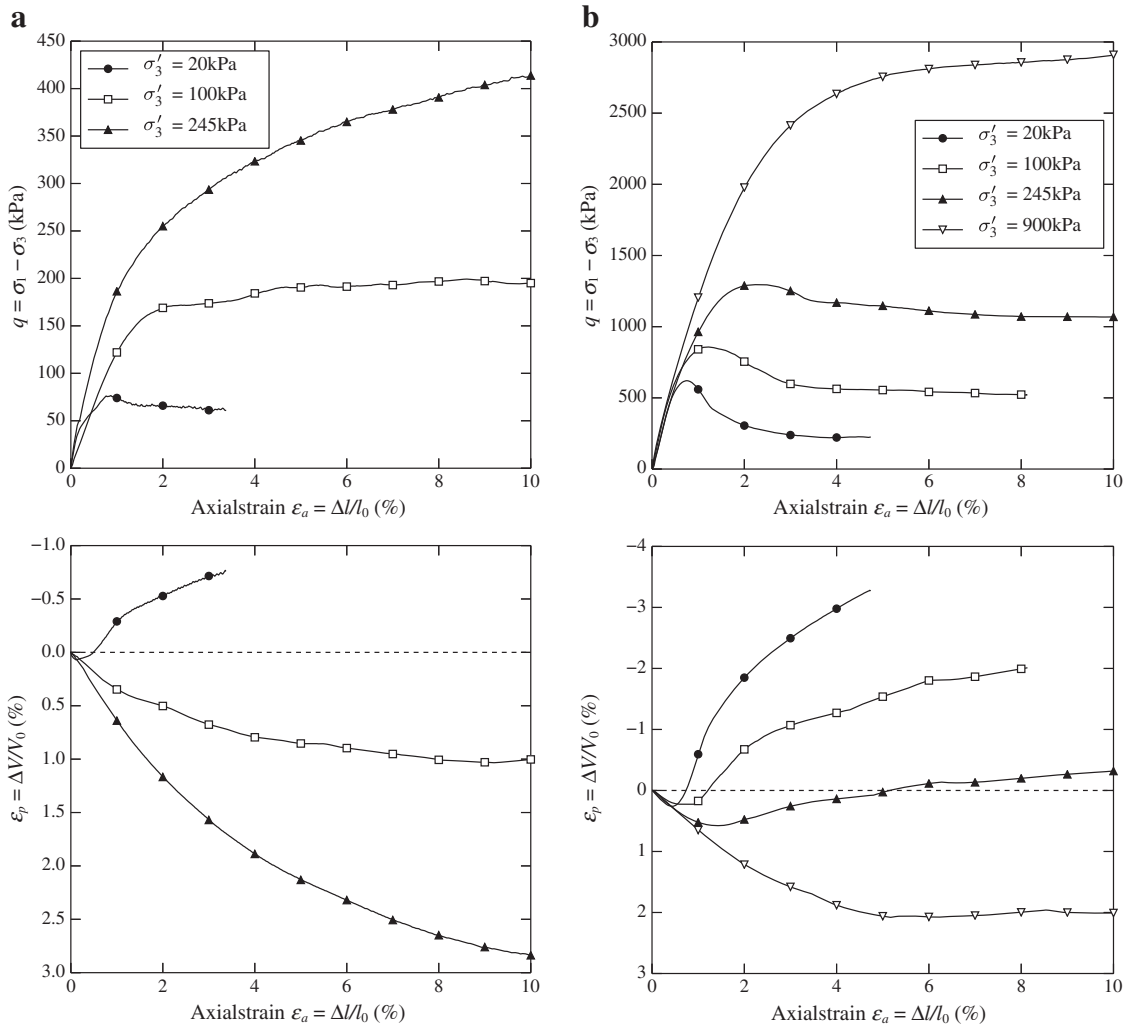


Fig. 4. Drained triaxial results on 0% and 5% lime treated specimens –  $\epsilon_v$ : volumetric deformations,  $\epsilon_a$ : axial strain,  $q$ : deviatoric stress. a: shear behaviour for untreated specimens; b: shear behaviour for 5% lime treated specimens.

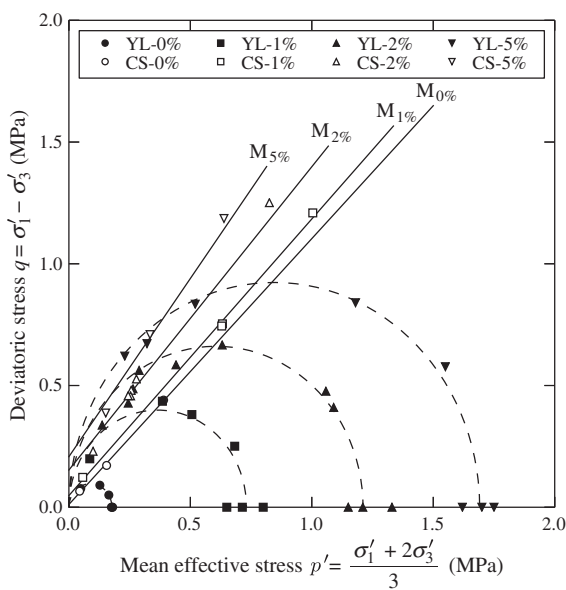


Fig. 5. Yield loci and critical states of 0%, 1%, 2%, and 5% lime treated specimens – YL: yield loci, CS: critical state, M: gradient of critical state line.

### 3.3. Chemical analysis

The results of TGA/DTA tests to measure the chemical composition in portlandite, hydrates, and carbonates on 0, 0.5, 1, 2, and 5% lime treated specimens are plotted in Fig. 6. The y-axis values correspond to the variation of mass compared to the untreated specimen.

The chemical composition of the soil appears to be modified after addition of lime and a curing time of 28 days. Concentration in portlandite is increased only for lime contents greater than 0.5%. The latter is used by pozzolanic reactions to produce cementitious compounds. For a concentration of 0.5%, all the portlandite produced by the hydration of the quicklime was used by pozzolanic reactions.

Concentration in hydrates was increased for all the lime contents. It is worth to note that there is a one-to-one correspondence between the lime content and the mass concentration in hydrates. The fact that neo-portlandite is measured for high lime contents means that pozzolanic reactions are unfinished and concentration in hydrates is likely to evolve if the curing time is extended.

Concentration in carbonates revealed to be increased only for high lime contents. Probability of carbonation is higher at high lime contents and this could explain the sudden formation of carbonates. It is more likely that these new carbonates are the result of the reaction of the unhydrated lime with the atmospheric carbon dioxide.



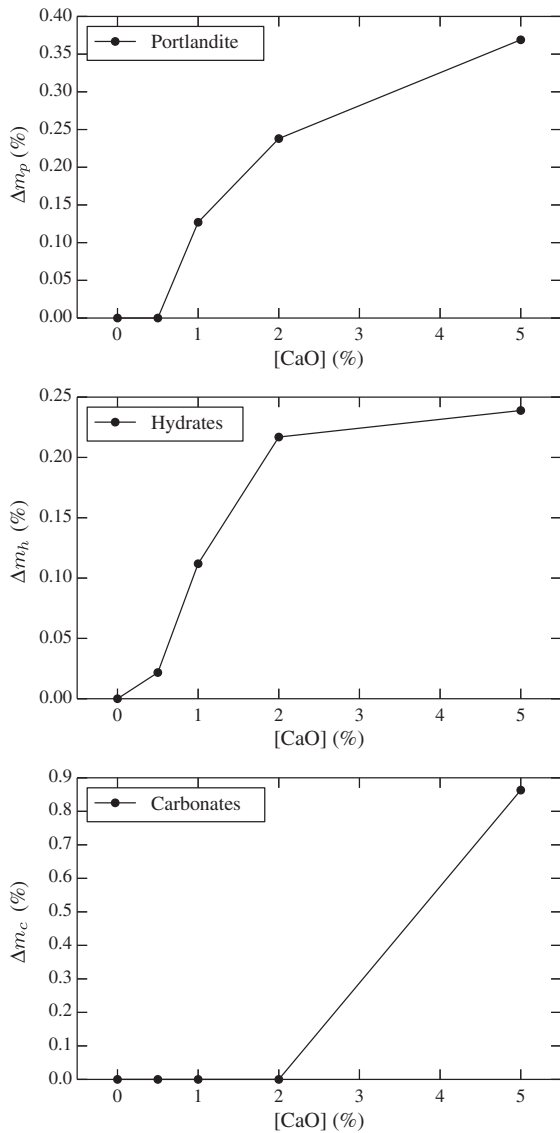


Fig. 6. Influence of a lime treatment on the variation of the mass concentration in hydrates (cementitious compounds), portlandite, and carbonates for a curing time of 28 days. —  $\Delta m_p$ : mass concentration in portlandite,  $\Delta m_h$ : mass concentration in hydrates,  $\Delta m_c$ : mass concentration in carbonates.

4. Discussion

In the first part of the Discussion section, the influence of lime on the mechanical properties of soil is discussed. Moreover, a quantification of the physicochemical processes induced by lime-treatment after 28 days of curing is provided. The main objective of the second part of the Discussion section is to highlight the coupling between the mechanical behaviour and the amount of the different compounds formed during the curing period and to propose an equation for the coupling. In the last part, a framework to account for the effects of the treatment on the intrinsic parameters is proposed.

4.1. Influence of lime on mechanical parameters

Lime has appeared to modify the mechanical behaviour of the soil and parameters like the position of the virgin consolidation line and the slope of the critical state line, M. Following the definition proposed by Burland (1990), “structure” consists of the combination of the

cementation and the fabric. In the case of structured soils, Leroueil and Vaughan (1990) showed that isotropic consolidation induced a progressive loss of structure at yield. After total loss of structure, the normal compression line of the structured soil converges to that of the same soil prepared in a remoulded state before compression.

In the case of a treated soil with quicklime, this assumption was only valid for a soil treated with 0.5% of quicklime. Isotropic consolidation results revealed a full loss of the structure for 0.5% lime treated specimens, which displayed the same virgin consolidation line as the non-treated specimens at a mean stress value of 1340 kPa. However, for concentrations equal or greater than 1% it could be assumed that the position of the virgin consolidation line following the destructuration is shifted. This feature is usually controlled by the fabric, and especially by the geometry of the particles. Therefore, one may assume that the geometry of the particles is modified by the treatment and is lime content-dependent. This observation is corroborated by the drained triaxial test results, which revealed a modification of the critical state line. The increase of the y-intercept is a result of the cementation (Fig. 5). The slope of the critical state line, M, is a direct function of the angle of friction (Schofield and Wroth, 1968) and describes the relationship between the particles and their geometry. A modification of M (Table 6) implies a modification of the angle of friction, and therefore of the geometry of the particles (Stocker, 1974; Wissa, 1965). Therefore, in the framework of the lime-treated soils, our results show that these mechanical parameters are modified.

Parameters like M and the normal compression line are considered as intrinsic and invariable in the framework of naturally structured soils (Liu and Carter, 2002). For these materials, reconstituted state is used as reference to assess the mechanical improvements due to the structure. In this case, the soil particles have already experienced cementation processes. The soil particles of the untreated state have not been in contact with lime and hence no modification of their geometry has occurred. From this point of view, the use of the mechanical parameters of the non-treated state as reference appears to be inappropriate to assess the effects of the treatment. This is important to describe the improvements, but not enough to fully describe the mechanical behaviour of treated soils. To do this, an intermediate state appears to be required, the destructured state of the lime treated soil. This state would account for the effects of the treatment on the mechanical parameters.

These results have showed that mechanical parameters of a soil are modified with the addition of quicklime. Therefore, it appears of the greatest interest to compare those with the chemical modifications arising from the treatment.

4.2. Correlation between physicochemical processes and yield stress

It has appeared that lime treatment modified the nature of the soil by altering parameters classically considered as intrinsic. In light of these results and using the approach proposed by Chiu et al. (2009), the yield stress was chosen as the mechanical coupling parameter. Apart from controlling the size of the initial yield function in most of

Table 6 Influence of lime on the mechanical properties.

Parameters	Values				
	0%	0.5%	1%	2%	5%
$\rho'_y$ (kPa)	177	300	731	1211	1691
$v_0$	1.602	1.609	1.612	1.606	1.626
$\lambda$	0.075	0.088	0.085	N/A	N/A
$\kappa$	0.005	0.005	0.005	0.005	0.005
M	1.092	N/A	1.136	1.246	1.464
$\varphi$ (°)	27.5	N/A	28.5	31.1	36.0
c (kPa)	11.4	N/A	47.9	152.9	207.6

c: cohesion,  $\varphi$ : angle of friction.

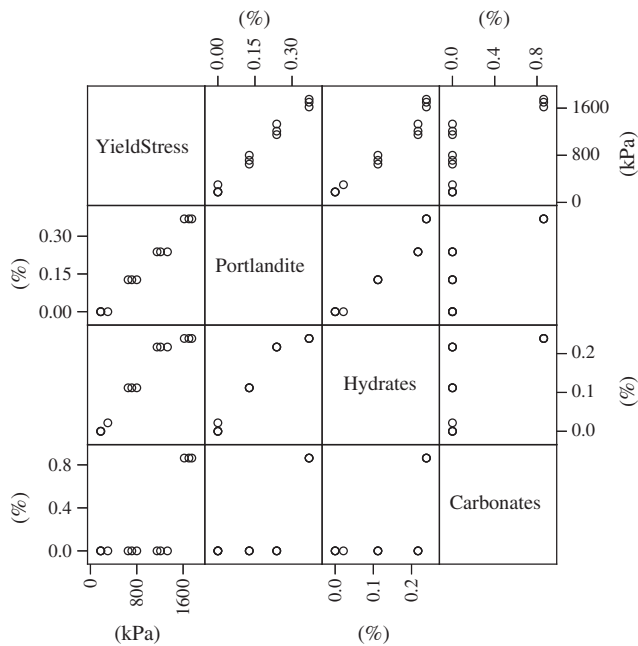


Fig. 7. Scatterplot matrix between the yield stress and the mass concentrations in cementitious compounds, portlandite, and carbonates.

the constitutive models, there is a one-to-one correspondence between the lime content and the resulting yield stress. The mechanical results and the chemical compositions are plotted in a scatterplot matrix (Fig. 7) to assess the trends between the yield stress and the mass concentration in cementitious compounds, portlandite, and carbonates.

The trends between the yield stress and the portlandite, and carbonates and hydrates are given in Fig. 7. The results show a linear correlation between the yield stress and the portlandite. Hydrates also appear to be linearly correlated to the yield stress. The production of hydrates was noted for every lime content and a one-to-one correspondence with the lime content. A second trend can be noticed between the yield stress and the portlandite. Chemical analysis revealed that all the portlandite has been consumed by pozzolanic reactions for low lime-contents (<0.5%). However, mechanical results showed that this lime-content is enough to increase the yield stress. Therefore, portlandite cannot be considered as a relevant parameter for a chemo-mechanical coupling.

Production of carbonates was only observed for concentrations greater than 2%, but mechanical improvements can be measured for small lime contents. Maubec (2010) has shown that the contribution of the carbonates in the mechanical behaviour can be neglected. For the same reasons as the portlandite, carbonates are not suitable for a chemo-mechanical coupling. Lime can be easily carbonated in contact with  $\text{CO}_2$  (Eq. (2)).

In light of these observations, mass concentration in hydrates is the only parameter systematically modified by the addition of lime and presenting a one-to-one correspondence with the lime content. Since yield stress has also a one-to-one correspondence with the lime content, a coupling between these two parameters appears to be the most relevant choice.

In order to establish a coupling, a relationship was established between yield stress and the mass concentration in hydrates. To model accurately a lime-treated soil, the regression function must fulfil the following criteria:

- (a) The point of lime fixation describes the minimum lime-content required to measure mechanical improvements. Thus, for low concentrations in hydrates (<0.05%), regression function must show a low gradient.

- (b) Above a critical lime content, yield stress does not increase anymore (Rotta et al., 2003). To account for this feature in the coupling, the interpolation function must converge to a finite value for high concentrations in hydrates.

To account for these two conditions, we chose a generalised logistic function (also known as Richards's curve) of the form:

$$\forall \Delta m_h \in \mathbb{R}^+ f(\Delta m_h) = p_{y,\min} + (p_{y,\max} - p_{y,\min}) \cdot \frac{1}{1 + e^{-\beta(\Delta m_h - \Delta x)}} \quad (4)$$

with:

- $p_{y,\min}$  The lower asymptote
- $p_{y,\max}$  The upper asymptote
- $\beta$  The growth rate
- $\Delta x$   $\Delta m_h$  value for which the first derivative is maximum and  $\frac{df^2}{d^2 \Delta m_h} = 0$ .

Using a non-linear least square method, the 4 variables  $p_{y,\min}$ ,  $p_{y,\max}$ ,  $\beta$ , and  $\Delta x$  were calculated to determine the optimal set of parameters (Table 7) based on the results of the isotropic tests. For lime concentrations greater than 1%, three isotropic tests were performed to reduce the error. The interpolation appears to satisfactorily describe the results (Fig. 8) and fulfil the conditions (a) and (b).

The same procedure can be applied to link the mass concentration in hydrates with the lime content. If introduced in the Eq. (7), this will result in a direct coupling between the amount in lime introduced in the soil and the resulting yield stress. This correlation is allowed since there is a systematic one-to-one correspondence between all the variables, which proves that a robust coupling between the mechanical behaviour and chemical composition exists.

#### 4.3. Modification of the Structured Cam Clay model for application on lime treated soils

Several studies (Leroueil and Vaughan, 1990; Liu and Carter, 2003) have shown that naturally structured soils exhibit similar behaviour to artificially treated materials. Under isotropic consolidation, structured and treated soils display at yield a higher void ratio compared to the remoulded/untreated state (Callisto and Rampello, 2004; Coop and Atkinson, 1993). This additional void ratio tends to disappear as the mean effective stress is increased to finally match the behaviour of the remoulded/untreated state (Burland et al., 1996). For drained experiments, Leroueil and Vaughan (1990) noted that a structured material exhibits a rate of maximum dilatation after the peak while this occurs before the peak for a non-structured material. Based on these considerations and the results of this study, one can assume that naturally structured soils and lime treated materials have a similar mechanical behaviour for both isotropic and shear stresses.

We propose in this paper a simple modification to the Structured Cam Clay model (SCCM) (Liu and Carter, 2002) to account for the effects of lime treatment on the intrinsic parameters. The SCCM was originally designed for naturally structured soils, but the results prove that it can be applied to lime treated specimen, provided that a modification is

Table 7  
Optimal set of parameters for a logistic interpolation.

Parameter	$p_{y,\min}$	$p_{y,\max}$	$\beta$	$\Delta x$	$R^2$
Value	100	2000	17.4	0.16	0.95

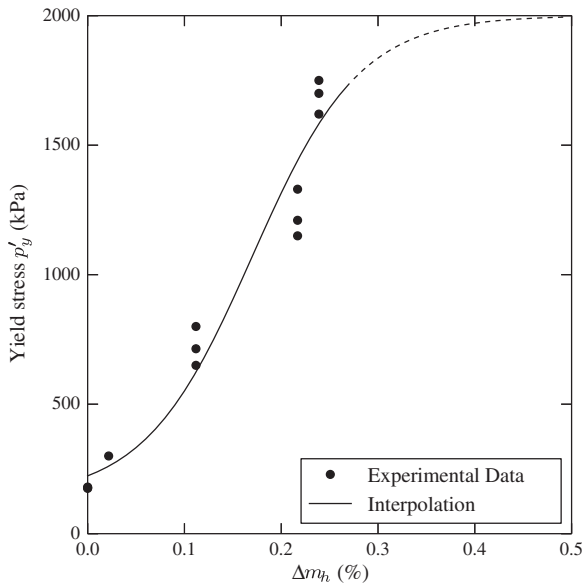


Fig. 8. Logistic interpolation for a chemo-mechanical coupling –  $\Delta m_h$ : mass concentration in hydrates.

implemented to introduce the secondary normal compression line for lime treated materials.

The SCCM models structured soils by introducing an additional void ratio  $\Delta e$  to the Cam Clay equation of the void ratio as:

$$e = e^* + \Delta e = e^* + \Delta e_i \left( \frac{p'_{y,i}}{p'} \right)^b \xrightarrow{p' \rightarrow +\infty} e^* \quad (5)$$

where:

- $e^*$  is the void ratio for the reconstituted soil,
- $\Delta e_i$  is the additional void ratio at yield compared to the reconstituted soil at the same stress state,
- $p_{y,i}$  is the yield stress of the structured soil, and
- $b$  is the destructuring index.

The formulation of the additional void ratio is chosen to converge to zero for high levels of mean stress. In the case of a lime treatment, normal compression line appears to be vertically translated by a constant void ratio, called  $\Delta e_c$ . The modified equation of the additional void ratio can be written as follows:

$$\Delta e = \left[ (\Delta e_i - \Delta e_c) \left( \frac{p'_{y,i}}{p'} \right)^b \right] + \Delta e_c \xrightarrow{p' \rightarrow +\infty} \Delta e_c. \quad (6)$$

This formulation ensures the convergence toward the destructured state (intermediate state), rather than the untreated state. This additional parameter  $\Delta e_c$  can be measured from the same isotropic test used for the determination of  $\Delta e_i$  and  $p_{y,i}$ . In the case where  $\Delta e_c = 0$ , Eq. (5) reverts back to the formulation of the MSCC. For use in constitutive modelling Eq. (5) can be written in an incremental form:

$$dv = -\lambda \frac{dp'}{p'} - (\Delta e_i - \Delta e_c) \cdot \left( \frac{p'_{y,i}}{p'} \right)^b \cdot b \cdot dp' \cdot (p')^{-b-1}. \quad (7)$$

The first part is the classic incremental form of the normal compression line from the Cam Clay model and describes the untreated state. The second part adds the effects of the structure as an additional void ratio.

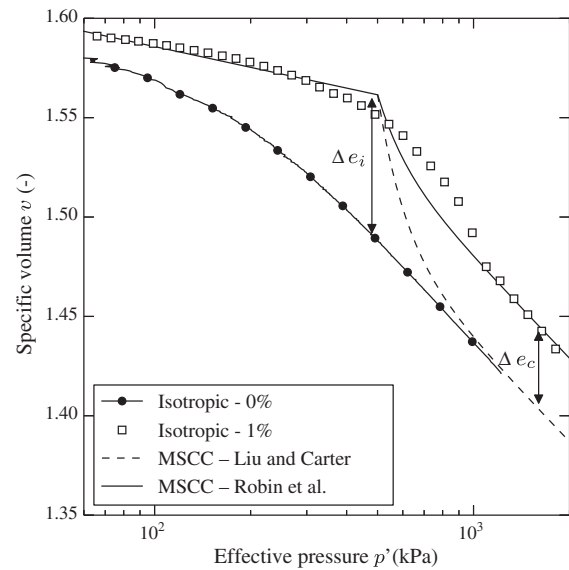


Fig. 9. Isotropic compression for 0% and 1% lime treated specimens – MSCC: Modified Structured Cam Clay;  $\Delta e_i$ : additional void ratio at yield;  $\Delta e_c$ : vertical translation of the virgin compression line.

The suitability of this formulation for the 1% lime treated specimen of this study is given in Fig. 9. Parameters used for the simulation are given in Table 8.

### 5. Conclusion

This study has shown the potential of lime treatment to improve the mechanical properties of the materials initially unsuitable for geotechnical structures. Thus, a chemo-mechanical coupling to account for the treatment in the design is of the greatest interest.

This paper aimed first to describe in details the effects of lime on the mechanical behaviour of a soil and also on parameters usually considered as constant. The results have shown that there was an improvement of the mechanical parameters due to the chemical reactions occurring after the addition of the lime. For lime contents greater than 1%, the specimens converged toward a normal compression line different from the untreated state but parallel to it. Therefore, in the framework of the lime treated soils, the mechanical parameters of treated soils could be different from those of the untreated state.

The chemical composition of lime treated specimens has been successfully assessed using thermogravimetric and thermodifferential analyses. The results have shown that concentrations in cementitious compounds and portlandite increased with the lime content. They permitted to explain the mechanical results and especially the modification of some parameters such as the angle of friction. The production of the cementitious compounds involves several preliminary reactions where soil particles experience dissolution due to the high pH. From this point of view, the nature of soil is seriously altered, leading to an evolution of the mechanical parameters. Chemical results revealed that cementitious compounds were produced for every concentration tested. A chemo-mechanical coupling was established using a logistic

Table 8  
Parameters for the Structured Cam Clay model adapted for lime treated soils.

MSCC parameters	Lime content				
	0%	0.5%	1%	2%	5%
$b$	0.0	1.8	7.2	–	–
$\Delta e_i$	0.0	0.027	0.066	0.129	0.159
$\Delta e_c$	0.0	0.0	0.046	–	–

MSCC: Modified Structured Cam Clay.

function between the amount of cementitious compounds and the yield stress. The proposed equation appears to describe accurately the observations and ensures a one-to-one correspondence between the mass concentration in cementitious compounds and the yield stress.

A modification of the formulation of the Structured Cam Clay model was proposed by introducing a new parameter  $\Delta e_c$  describing the position of the second normal compression line. Simulations proved the suitability of the new formulation for use in constitutive modelling.

The proposed coupling may be used to account for the treatment in the design of geotechnical structures. However, one must be aware of the durability of the treatment. The bonding structure resulting from chemical reactions occurring at high pH environment and treated materials are often subjected to environmental conditions. For example, in the event of a continuous rainfall, water flow may occur changing the pH environment and altering the chemical equilibriums. This would result in the dissolution of the cementitious compounds and, therefore, in the extinction of the bonding structure. It is thus important to assess the durability for the treatment in the design of geotechnical structures.

## References

- Alarcon-Ruiz, L., Platret, G., Massieu, E., Ehrlicher, A., 2005. The use of thermal analysis in assessing the effect of temperature on a cement paste. *Cem. Concr. Res.* 35, 609–613. <http://dx.doi.org/10.1016/j.cemconres.2004.06.015>.
- ASTM Standard D6276, 2006. Standard Test Method for Using pH to Estimate the Soil–Lime Proportion Requirement for Soil Stabilization. pp. 1–4.
- ASTM Standard D7181-11, 2011. Method for consolidated drained triaxial compression test for soils. *ASTM Int.* 1–11. <http://dx.doi.org/10.1520/D7181>.
- ASTM Standard D7263-09, 2009. Standard test methods for laboratory determination of density (unit weight) of soil specimens. *ASTM Int.* 1–7. <http://dx.doi.org/10.1520/D7263-09>.
- Baudet, B., Stallebrass, S., 2004. A constitutive model for structured clays. *Geotechnique* 54, 269–278.
- Burland, J.B., 1990. On the compressibility and shear strength of natural clays. *Geotechnique* 40, 329–378.
- Burland, J.B., Rampello, S., Georgiannou, V.N., Calabresi, G., 1996. A laboratory study of the strength of four stiff clays. *Geotechnique* 46, 491–514. <http://dx.doi.org/10.1680/geot.1996.46.3.491>.
- Callisto, L., Rampello, S., 2004. An interpretation of structural degradation for three natural clays. *Can. Geotech. J.* 41, 392–407. <http://dx.doi.org/10.1139/T03-099>.
- Chiu, C.F., Zhu, W., Zhang, C.L., 2009. Yielding and shear behaviour of cement-treated dredged materials. *Eng. Geol.* 103, 1–12. <http://dx.doi.org/10.1016/j.enggeo.2008.07.007>.
- Consoli, N.C., da Lopes, L.S., Prietto, P.D.M., Festugato, L., Cruz, R.C., 2011. Variables controlling stiffness and strength of lime-stabilized soils. *J. Geotech. Geoenviron. Eng.* 137, 628–632. [http://dx.doi.org/10.1061/\(ASCE\)GT.1943-5606.0000470](http://dx.doi.org/10.1061/(ASCE)GT.1943-5606.0000470).
- Coop, M.R., Atkinson, J.H., 1993. The mechanics of cemented carbonate sands. *Geotechnique* 43, 53–67.
- Cotecchia, F., Chandler, R.J., 2000. A general framework for the mechanical behaviour of clays. *Geotechnique* 50, 431–447.
- Cuisinier, O., Masroui, F., Pelletier, M., Villieras, F., Mosser-Ruck, R., 2008. Microstructure of a compacted soil submitted to an alkaline PLUME. *Appl. Clay Sci.* 40, 159–170. <http://dx.doi.org/10.1016/j.clay.2007.07.005>.
- Cuisinier, O., Auriol, J.-C., Le Borgne, T., Deneele, D., 2011. Microstructure and hydraulic conductivity of a compacted lime-treated soil. *Eng. Geol.* 123, 187–193. <http://dx.doi.org/10.1016/j.enggeo.2011.07.010>.
- Das, S.K., Mitra, A., Das Poddar, P.K., 1996. Thermal analysis of hydrated calcium aluminates. *J. Therm. Anal. Calorim.* 47, 765–774.
- Eades, J.L., Grim, R.E., 1966. A quick test to determine lime requirements for lime stabilization. *Highw. Res. Rec.* 139, 61–72.
- Gens, A., Nova, R., 1993. Conceptual bases for a constitutive model for bonded soils and weak rocks. *Geotech. Eng. Hard Soils-Soft Rocks* 1, 485–494.
- Horpibulsuk, S., Liu, M.D., Liyanapathirana, D.S., Suebsuk, J., 2010a. Behaviour of cemented clay simulated via the theoretical framework of the Structured Cam Clay model. *Comput. Geotech.* 37, 1–9. <http://dx.doi.org/10.1016/j.compgeo.2009.06.007>.
- Horpibulsuk, S., Rachan, R., Chinkulkijniwat, A., Raksachon, Y., Suddepong, A., 2010b. Analysis of strength development in cement-stabilized silty clay from microstructural considerations. *Constr. Build. Mater.* 24, 2011–2021. <http://dx.doi.org/10.1016/j.conbuildmat.2010.03.011>.
- Lee, K., Chan, D., Lam, K., 2004. Constitutive model for cement treated clay in a critical state frame work. *Soils Found.* 44, 69–77.
- Leroueil, S., Vaughan, P.R., 1990. The general and congruent effects of structure in natural soils and weak rocks. *Geotechnique* 40, 467–488.
- Little, D.N., 1995. Stabilization of Pavement Subgrades and Base Courses with Lime. National Lime Association, Arlington.
- Liu, M.D., Carter, J.P., 2002. A structured Cam Clay model. *Can. Geotech. J.* 39, 1313–1332. <http://dx.doi.org/10.1139/T02-069>.
- Liu, M.D., Carter, J.P., 2003. Volumetric deformation of natural clays. *Int. J. Geomech.* 3, 236–252. [http://dx.doi.org/10.1061/\(ASCE\)1532-3641\(2003\)3:2\(236\)](http://dx.doi.org/10.1061/(ASCE)1532-3641(2003)3:2(236)).
- MacKenzie, R.C., 1970. Differential thermal analysis. *Fundamental Aspects*, vol. 1. Academic Press London, London–New York.
- Mackenzie, R.C., 1972. Differential thermal analysis. In: Academic, P. (Ed.), *Applications*, vol. 2. Academic Press London, London–New York.
- Malandraki, V., Toll, D.G., 2001. Triaxial tests on weakly bonded soil with changes in stress path. *J. Geotech. Geoenviron. Eng.* 127, 282–291.
- Maubec, N., 2010. Approche multi-échelle du traitement des sols à la chaux. Etudes des interactions avec les argiles. Université de Nantes, France, Thèse de Doctorat.
- Metelková, Z., Boháč, J., Příkryl, R., Sedlářová, I., 2012. Maturation of loess treated with variable lime admixture: pore space textural evolution and related phase changes. *Appl. Clay Sci.* 61, 37–43. <http://dx.doi.org/10.1016/j.clay.2012.03.008>.
- Muir Wood, D., 1991. *Soil Behaviour and Critical State Soil Mechanics*.
- North, J.M., Becker, J.G., Seagren, E.A., Ramirez, M., Peot, C., 2008. Methods for quantifying lime incorporation into dewatered sludge. I: Bench-scale evaluation. *J. Environ. Eng.* 134, 750–761.
- Nova, R., Castellanza, R., Tamagnini, C., 2003. A constitutive model for bonded geomaterials subject to mechanical and/or chemical degradation. *Int. J. Numer. Anal. Methods Geomech.* 27, 705–732.
- Oliveira, P.J.V., Correia, A.A.S., Garcia, M.R., 2013. Effect of stress level and binder composition on secondary compression of an artificially stabilized soil. *J. Geotech. Geoenviron. Eng.* 139, 810–820. [http://dx.doi.org/10.1061/\(ASCE\)GT.1943-5606.0000762](http://dx.doi.org/10.1061/(ASCE)GT.1943-5606.0000762).
- Pomakhina, E., Deneele, D., Gaillot, A.-C., Paris, M., Ouvrard, G., 2012. <sup>29</sup>Si solid state NMR investigation of pozzolanic reaction occurring in lime-treated Ca-bentonite. *Cem. Concr. Res.* 42, 626–632. <http://dx.doi.org/10.1016/j.cemconres.2012.01.008>.
- Rogers, C.D.F., Glendinning, S., 1996. The role of lime migration in lime pile stabilization of slopes. *Q. J. Eng. Geol. Hydrogeol.* 29, 273–284. <http://dx.doi.org/10.1144/GSL.QJEGH.1996.029.P4.02>.
- Roscoe, K.H., Burland, J.B., 1968. On the generalized stress-strain behaviour of wet clay. *Eng. Plast.* 535–609.
- Rotta, G.V., Consoli, N.C., Prietto, P.D.M., Coop, M.R., Graham, J., 2003. Isotropic yielding in an artificially cemented soil cured under stress. *Geotechnique* 53, 493–501. <http://dx.doi.org/10.1680/geot.2003.53.5.493>.
- Saikia, N.J., Sengupta, P., Gogoi, P.K., Borhthakur, P.C., 2002. Hydration behaviour of lime-calcined kaolin-petroleum effluent treatment plant sludge. *Cem. Concr. Res.* 32, 297–302. [http://dx.doi.org/10.1016/S0008-8846\(01\)00676-7](http://dx.doi.org/10.1016/S0008-8846(01)00676-7).
- Schofield, A.N., Wroth, C.P., 1968. *Critical State Soil Mechanics*. McGraw-Hill.
- Stocker, P.T., 1974. Diffusion and diffuse cementation in lime and cement stabilised clayey soils – studies of plasticity and aggregation. *Aust. Road Res.* 5, 51–75.
- Stoltz, G., Cuisinier, O., Masroui, F., 2012. Multi-scale analysis of the swelling and shrinkage of a lime-treated expansive clayey soil. *Appl. Clay Sci.* 61, 44–51. <http://dx.doi.org/10.1016/j.clay.2012.04.001>.
- Suebsuk, J., Horpibulsuk, S., Liu, M.D., 2010. Modified structured cam clay: a generalised critical state model for destructured, naturally structured and artificially structured clays. *Comput. Geotech.* 37, 956–968. <http://dx.doi.org/10.1016/j.compgeo.2010.08.002>.
- Suebsuk, J., Horpibulsuk, S., Liu, M.D., 2011. A critical state model for overconsolidated structured clays. *Comput. Geotech.* 38, 648–658. <http://dx.doi.org/10.1016/j.compgeo.2011.03.010>.
- Thompson, M.R., 1965. *Shear Strength and Elastic Properties of Lime-Soil Mixtures*. Bureau of Public Roads/US, Washington.
- Vatsala, A., Nova, R., Srinivasa Murthy, B.R., 2001. Elastoplastic model for cemented soils. *J. Geotech. Geoenviron. Eng.* 127, 679–687.
- Wissa, A.E.Z., 1965. *Effective Stress–Strength Behavior of Cemented Soils*. (Thesis (Sc. D.)) Massachusetts Institute of Technology.
- Zhu, W., Zhang, C.L., Chiu, A.C.F., 2007. Soil–water transfer mechanism for solidified dredged materials. *J. Geotech. Geoenviron. Eng.* 133, 588–598. [http://dx.doi.org/10.1061/\(ASCE\)1090-0241\(2007\)133:5\(588\)](http://dx.doi.org/10.1061/(ASCE)1090-0241(2007)133:5(588)).

## Appendix D

Paper published in *Computers & Geotechnics*



# An Effective Constitutive Model for Lime Treated Soils

V. Robin<sup>1,2</sup>, A. A. Javadi<sup>1</sup>, O. Cuisinier<sup>2</sup>, F. Masrouri<sup>2</sup>

<sup>1</sup>*Computational Geomechanics Group, Department of Engineering, University of Exeter, United-Kingdom*

<sup>2</sup>*LEMETA – UMR 7563 CNRS, Laboratoire d’Énergétique et de Mécanique Théorique et Appliquée, Université de Lorraine, France*

---

## Abstract

The effect of lime on the yield stress, and more generally the presence of structure in the soil, is usually not accounted for in the design of geotechnical structures. As a result the potential of lime treatment or of a structured soil has not been fully exploited. This paper presents a new formulation to account for the effect of structure on the mechanical behaviour for structured soils. A constitutive model is proposed in the framework of the Modified Cam Clay model to describe the behaviour of lime treated soils. The new formulation introduces a limited number of additional parameters, all of which have a physical meaning and can be obtained from an isotropic compression test. Due to similarity in behaviour of lime treated soils and naturally structured soils, the formulation can be applied to both types of soil. It is shown that the proposed model can successfully reproduce the main features of both structured soils such as maximum rate of dilation at softening and degradation at yield. The model can be applied for any structured material regardless of the origin of cementation.

*Keywords:*

lime treated soils, structured soils, degradation, constitutive modelling.

---

## 1. Introduction

The use of on-site materials has become a central issue for civil engineering companies, but it is sometimes difficult to deal with all the resources available on site. For soils with low mechanical characteristics, lime treatment appears to be an efficient method to improve their mechanical properties and allow their use in geotechnical earth structures (e.g. [Little, 1995](#)). The effects of the addition of lime on the soil parameters such as cohesion and friction angle have been extensively studied. Nevertheless, lime is still mostly used to dry soils with high water contents and increase the bearing capacity. However, it is also generally known that adding lime leads to a significant increase of the yield stress and modifies other mechanical parameters in compacted soils. In lime-treated soils, the modification of the mechanical behaviour results from several physico-chemical processes associated with the increase in calcium concentration and pH (i.e. cation exchange, pozzolanic reactions, etc...).

20 From an economical point of view, it is becoming increasingly important to account for the properties  
21 of treated materials in the design of the geotechnical structures. However, despite its proven efficacy, the  
22 use of treated materials suffers from several major drawbacks: there is no reliable method to account for  
23 the structure in the calculations. At yield, and for an increasing mechanical loading, treated materials  
24 experience what is called the "loss of structure", resulting in the degradation of the structure in different  
25 ways. To model the behaviour of these materials, a constitutive law describing the behaviour at yield is a  
26 requirement.

27 Some studies ([Leroueil and Vaughan, 1990](#); [Liu and Carter, 2003](#)) have shown that naturally structured  
28 soils and artificially treated materials have common mechanical features; artificial treatment appears to  
29 create a "structure" in the soil. In this paper, "structure" refers to Burland's definition ([Burland, 1990](#)),  
30 and is seen as the combination of the fabric and the bonding of the soil skeleton. Fabric accounts for the  
31 arrangement of particles, which depends on the state of compaction and their geometry.

32 Several constitutive models have been proposed for structured materials. Most of these models use the  
33 destructured state as reference to describe the mechanical behaviour of structured soils. [Liu and Carter](#)  
34 ([2002](#)) proposed a constitutive model, based on the Modified Cam Clay model (MCC), by adding three  
35 additional parameters to the original MCC ([Roscoe and Burland, 1968](#)). Since then, several enhancements  
36 (e.g. [Horpibulsuk et al., 2010](#); [Suebsuk et al., 2011](#)) have been proposed. However, various modes of de-  
37 structuration have been identified, and the original formulation fails to model some of them. A number of  
38 other formulations have been developed ([Gens and Nova, 1993](#); [Cotecchia and Chandler, 2000](#); [Kavvas](#)  
39 [and Amorosi, 2000](#); [Vatsala et al., 2001](#); [Nova et al., 2003](#); [Baudet and Stallebrass, 2004](#); [Nguyen et al.,](#)  
40 [2014](#)) and some of which give good agreement with experimental results. However, it often comes at the  
41 cost of a larger number of parameters, or high computational resources (e.g. mapping rule). Parameters do  
42 not always have a physical meaning, and some of them can be difficult to determine. All these limitations  
43 make these models difficult to be used in engineering practice.

44 The main objective of this paper is to propose a general and simple formulation capable of fulfilling some  
45 fundamentals criteria regarding the degradation of the structure. This model must be capable of modelling  
46 any kind of degradations, and require a limited number of parameters to account for the maximum number  
47 of features of structured materials. These parameters should be rapidly obtained from classic experimental  
48 tests, and they all must have a physical meaning. To this end, the paper will focus on two aspects:

- 49 • How can the key features of structured or lime treated materials be described?
- 50 • How can these features be efficiently accounted for in a constitutive model?

51 This paper is divided into four parts. The first part gives a review of the main characteristics of naturally  
52 and artificially structured materials that must be reproduced by the model. The second part introduces the  
53 theoretical framework chosen for the model for lime treated soils (MLTS) and the new formulation developed

54 to model the degradation of the structure. In the third part, the developed formulation is used to calculate  
55 the compliance matrix and obtain the stress-strain relationship. Finally, in the last part, we assess the  
56 suitability of the model in predicting experimental results obtained from triaxial tests on artificially (i.e.  
57 lime treated) and naturally structured materials.

## 58 **2. Features of structured soils**

59 The mechanical behaviour of naturally and artificially structured material has been extensively studied  
60 (Leroueil and Vaughan, 1990; Burland et al., 1996; Malandraki and Toll, 2001; Cuisinier et al., 2008, 2011;  
61 Consoli et al., 2011; Oliveira, 2013; Robin et al., 2014) and some specific features have been identified.  
62 Several studies have pointed out that naturally and artificially structured soils have a similar mechanical  
63 behaviour. In this section, we identify the key features common to naturally and artificially structured soils  
64 that should be properly reproduced by a model.

### 65 *2.1. Naturally structured soils*

66 It has been shown that naturally structured soils have a higher yield stress compared to the destructured  
67 state (Burland et al., 1996), the latter being usually considered as the reference state. For the same stress  
68 state, a higher yield stress leads to a higher void ratio at yield compared to the destructured state, called  
69 the additional void ratio  $\Delta e$ . Once plastic deformations take place, one can observe that the additional  
70 void ratio decreases. Depending on the material, the additional void ratio can quickly or slowly decrease  
71 until the material reaches a normal compression line (ncl), which can correspond to the ncl of the reference  
72 state ( $ncl_d$ ), or a different one, parallel to the reference ncl but vertically translated along the  $v$  axis ( $ncl_r$ )  
73 (Baudet and Stallebrass, 2004; Callisto and Rampello, 2004; Suebsuk et al., 2011). More generally, 4 modes  
74 of degradation can be identified (Figure 1):

75 **Mode 1:** Destructuration takes place immediately at yield. The additional void ratio progressively de-  
76 creases until it converges toward the destructured state (Yong and Nagaraj, 1977; Lagioia and Nova,  
77 1995).

78 **Mode 2:** Destructuration takes place immediately at yield, but it does not converge toward its destructured  
79 state. A different ncl appears parallel to the destructured state, but a residual additional void ratio  
80 still remains (Burland et al., 1996; Rampello and Callisto, 1998).

81 **Mode 3:** No significant destructuration is observed immediately after yield. The process of degradation is  
82 initiated later on for a higher effective mean stress and the additional void ratio completely disappears  
83 (Callisto and Rampello, 2004).



84 **Mode 4:** No destructuration is observed immediately after yield. The process of degradation is initiated  
 85 later on for a higher effective mean stress. However, a residual additional void ratio remains (Rotta  
 86 et al., 2003).

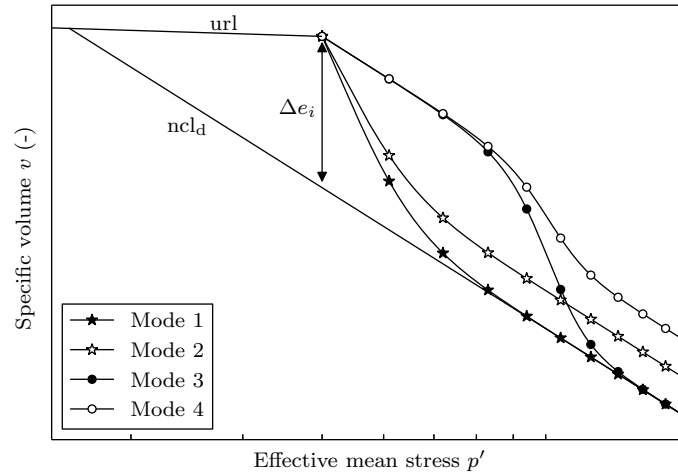


Figure 1: The four different modes of destructuration in structured soils – ncl<sub>d</sub>: Normal compression line of the destructured state, url: Unloading-reloading line.

87 Additionally, the volumetric behaviour of naturally structured soils was compared with the destructured  
 88 state by Leroueil and Vaughan (1990) on heavily overconsolidated specimens from drained triaxial test  
 89 results. They identified two different mechanisms taking place. While the maximum rate of dilation was  
 90 measured before the peak of the deviatoric stress for the destructured soil, it was observed after the peak  
 91 of the deviatoric stress for structured soils. This is due to the structure, which binds soil particles together.  
 92 To allow the particles to move freely, the structure has to be degraded first to release particles (Leroueil and  
 93 Vaughan, 1990).

## 94 2.2. Lime treated soils

95 Several studies have shown that addition of lime leads to an increase of the yield stress compared to the  
 96 untreated state (Tremblay et al., 2001; Ahnberg, 2007). As for naturally structured soils, the additional void  
 97 ratio appears to decrease at yield, i.e. the degradation of the artificial structure takes place. Robin et al.  
 98 (2014) have assessed the mechanical behaviour of a lime treated silt under isotropic loading (Figure 2). It  
 99 can be seen that the mode of degradation depends on the amount of lime. For 0.5% in lime, the additional  
 100 void ratio completely disappears at high stress states (Mode 3), when it is not the case for 1% lime treated  
 101 specimens (Mode 4). This latter reaches a different ncl compared to the untreated specimen. Details about  
 102 the samples and experimental conditions can be found in Robin et al. (2014).

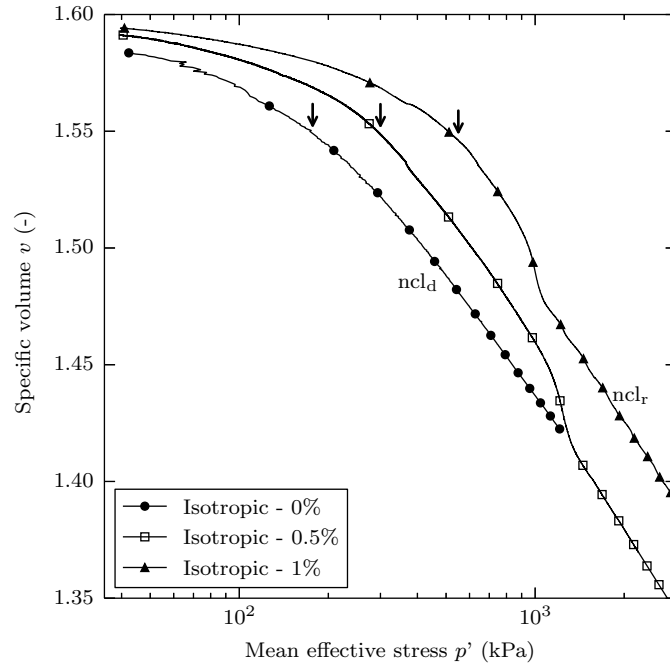


Figure 2: Isotropic consolidation curves obtained from specimens of silt treat at 0.5% and 1% in lime – Arrows mark the yield stress  $p'_y$ ,  $ncl_d$ : Normal compression line of the destructured state,  $ncl_r$ : Normal compression line of the residual state (Robin et al., 2014).

103 The maximum rate of dilation at shear for specimens experiencing softening also appears after the  
 104 peak for artificially structured soils, which indicates that the same kind of mechanism is taking place. This  
 105 common feature was pointed out by Leroueil and Vaughan (1990), and was also observed for the lime treated  
 106 specimens from the current study (Figure 3).

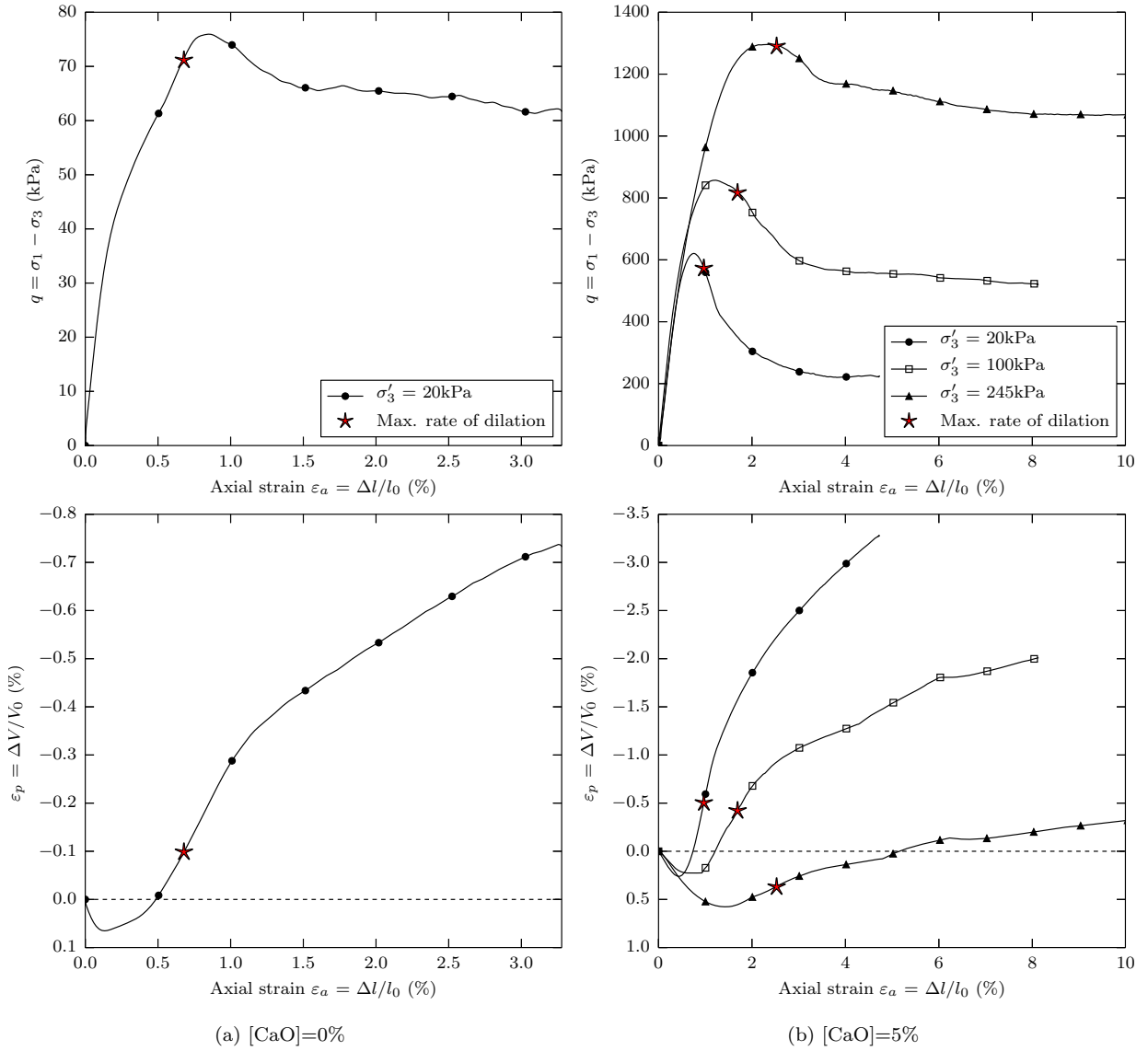


Figure 3: Drained triaxial results on (a) untreated and (b) lime treated soils – Stars mark the location where the rate of dilation is maximum (Robin et al., 2014).

107 The influence of a lime treatment on the cohesion and the friction angle has been studied by several  
 108 authors (Wissa et al., 1965; Balasubramaniam et al., 2005). Both cohesion and friction angle appear to  
 109 increase with the amount of lime. The slope of the critical state line is directly related to the friction angle,  
 110 and the increase of cohesion, which increases the tensile strength, has an influence on the shape of the yield  
 111 function. Therefore, in the framework the critical state theory, these features should be accounted for in the  
 112 model.

### 113 2.3. Summary

114 Based on the previous observations, a model for lime treated soils might be suitable for naturally struc-  
115 tured soils, and therefore should be able to reproduce the four modes of destructuration and account for the  
116 following features:

- 117 • The cohesion increases following pozzolanic reactions,
- 118 • The yield stress increases for lime treated soils compared to the reference state,
- 119 • At yield, there exists an additional void ratio compared to the reference state,
- 120 • At yield, degradation of the structure takes place, which follows one of the four modes identified  
121 previously,
- 122 • Overconsolidated specimens at shear show a maximum rate of dilation after the peak, describing the  
123 degradation of the structure,
- 124 • The friction angle is modified due to the effects of the chemical reactions on the texture of the soil,  
125 and therefore the critical state as well.

## 126 3. Theoretical framework of the model

127 The model proposed in this paper was developed in the framework of the Modified Cam Clay model  
128 (MCC) to model the key features of lime treated soils previously identified. We introduced only parameters  
129 with a physical meaning that can be determined from isotropic compression tests. We present in this section  
130 a new formulation to model the four modes of degradation in structured soils under isotropic loading. This  
131 will then be used as a hardening rule for the determination of the compliance matrix.

### 132 3.1. Modelling the structure and its degradation under isotropic loading

133 To model the degradation of the structure under isotropic loading, we propose the framework given  
134 in Figure 4. We introduce the *primary yield stress*  $p_y^I$ , which corresponds to the apparition of plastic  
135 deformations. To describe the stress states for which the degradation of the structure takes place (hatched  
136 area in Figure 4), we also introduce the *degradation stress*  $p_y^{II}$ . In the case of an immediate degradation  
137 of the structure at yield (modes 1 & 2 in Figure 1), which can happen for some structured soils, we have  
138  $p_y^{II} = p_y^I$ . The additional void ratio  $\Delta e_i$  at  $p_y^I$  quantifies the initial additional void ratio at yield.  $\Delta e_c$  is  
139 measured at an effective mean stress above which the additional void ratio remains constant ( $p' \gg p_y^{II}$ ).  
140 By setting the parameters as given in Table 1, this framework is capable of describing the four modes of  
141 degradation.

142 In this study, the structure is quantified through the additional void ratio in comparison to the  $ncl_d$  and  
 143 is assumed to be made of two components. The first one, referred to as the *available structure*, corresponds  
 144 to the part of structure that will be available during the process of destructuration ( $\Delta e_i - \Delta e_c$ ). The  
 145 second one, referred to as the *residual structure*, corresponds to the persisting additional void ratio at high  
 146 effective mean stress ( $\Delta e_c$  at  $p' \gg p_y^I$ ). The latter can be the consequences of chemical reactions, e.g. a lime  
 147 treatment, which leads to a permanent modification of the fabric of the soil (Robin et al., 2014).

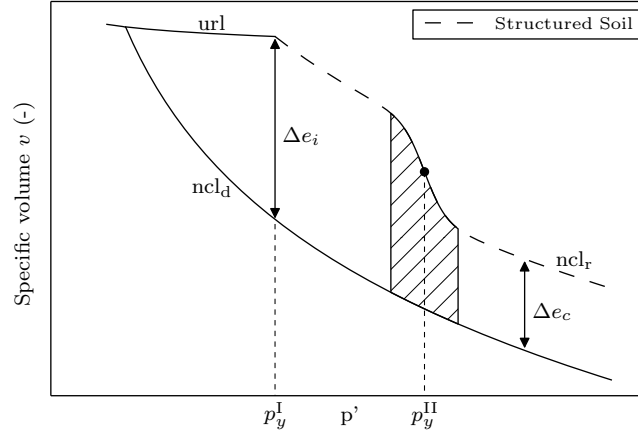


Figure 4: General framework of the degradation of structured soils –  $\Delta e_i$ : Initial additional void ratio,  $\Delta e_c$ : Residual additional void ratio,  $p_y^I$ : Primary yield stress,  $p_y^II$ : degradation stress, hatched area: degradation of the structure,  $ncl_d$ : Normal compression line of the destructured state,  $ncl_r$ : Normal compression line of the residual state, url: Unloading-reloading line.

Table 1: Conditions on the parameters  $p_y^II$  and  $\Delta e_c$  for the 4 modes of degradation

Parameters	Values			
	Mode 1	Mode 2	Mode 3	Mode 4
$p_y^II$	$p_y^I$	$p_y^I$	$> p_y^I$	$> p_y^I$
$\Delta e_c$	0	$> 0$	0	$> 0$

### 148 3.1.1. Mathematical Formulation

To model these four mechanisms, a flexible formulation using all the parameters previously introduced is required. Richards's equation (Richards, 1959) for the sigmoid provides many degrees of freedom to control the shape of the function. This function is frequently used for the modelling natural phenomena where there exists a threshold above which a process is activated, in this case the degradation. This equation can be written as follows:

$$\forall p' \in [p_y^I, +\infty[ \quad \pi(p') = 1 - \frac{1}{1 + e^{-\beta(p' - p_y^II)}} \quad (1)$$

149 where  $p_y^{\text{II}}$  [Pa] corresponds to the position of the inflection point ( $\pi''(p_y^{\text{II}}) = 0$ ) and describes the stress  
 150 state for which the degradation occurs (hatched area in Figure 4), and  $\beta$  [ $\text{Pa}^{-1}$ ] describes the rate of  
 151 degradation.

Therefore, we have

$$\forall p' \in \mathbb{R} \quad 0 \leq \pi(p') \leq 1 \quad (2)$$

### 152 3.1.2. Scaling of $\pi$

The function  $\pi$  is scaled to ensure that  $\forall \beta, \forall p_y^{\text{II}} \quad \pi(p_y^{\text{I}}) = 1$ , which leads to the following final formulation:

$$\forall p' \in [p_y^{\text{I}}, +\infty[ \quad \pi(p') = \frac{e^{\beta p_y^{\text{I}}} + e^{\beta p_y^{\text{II}}}}{e^{\beta p'} + e^{\beta p_y^{\text{II}}}} \quad (3)$$

153 which verifies  $\pi(p_y^{\text{I}}) = 1$  and  $\lim_{p' \rightarrow +\infty} \pi(p') = 0$ .

154 The ability to control the rate of degradation at yield of this formulation is demonstrated in Figure 5. It  
 155 can be seen that the function  $\pi$  can either slowly decrease with a low  $\beta$  or quickly with a high  $\beta$  as  $p'$  gets  
 156 close to  $p_y^{\text{II}}$ .

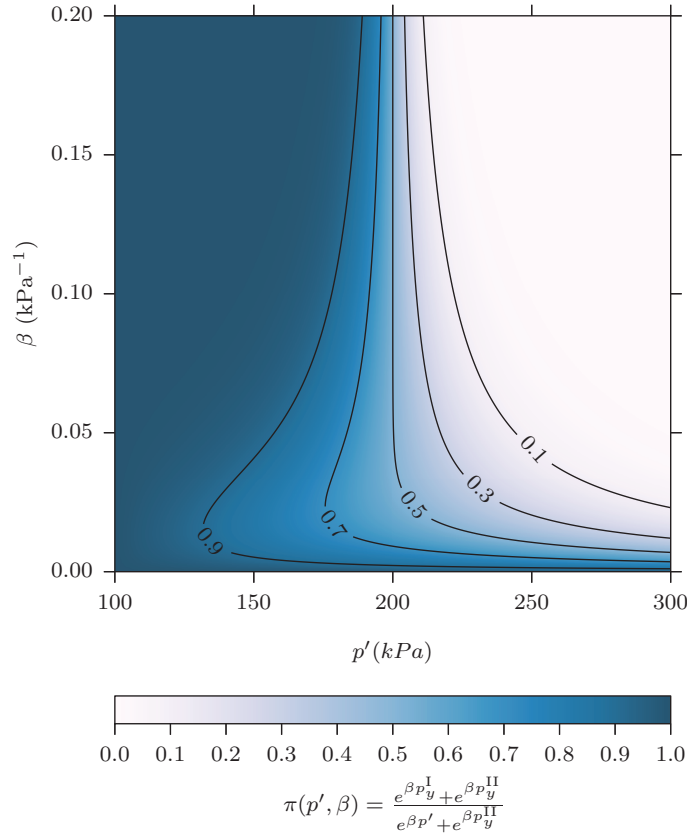


Figure 5:  $\pi$  values as a function of  $p_y^{\text{II}}$  and  $\beta - p_y^{\text{I}}=100$  kPa,  $p_y^{\text{II}}=200$  kPa.

157 3.1.3. Relationship between the specific volume and the effective mean stress for structured soils

The presence of structure can be accounted for in the relationship between the specific volume and the effective mean stress ( $v : p'$  relationship) using the following general formulation:

$$\forall p' \in \mathbb{R}_+^* \quad v(p') = N_\lambda - \lambda \ln(p') + \Delta e(p') \quad (4)$$

158 with  $N_\lambda$  the intercept on the reference normal compression line  $ncl_d$  and  $\lambda$  the slope of the reference  $ncl$   
159 in  $v : \ln(p')$  plane.

160 Using the function  $\pi$  (Equation 3), the equation for the additional void ratio is given by:

$$\forall p' \in [p_y^I, +\infty[ \quad \Delta e(p') = (\Delta e_i - \Delta e_c) \cdot \left[ \frac{e^{\beta p_y^I} + e^{\beta p_y^{II}}}{e^{\beta p'} + e^{\beta p_y^{II}}} \right] + \Delta e_c \quad (5)$$

which fulfils the boundary value problems:

$$\Delta e(p') = \begin{cases} \Delta e_i & \text{if } p' = p_y^I \\ \Delta e_c & \text{if } p' \rightarrow +\infty \end{cases} \quad (6)$$

Introducing Equation 5 in Equation 4 gives the final equation of the specific volume for structured soils at yield:

$$\forall p' \in [p_y^I, +\infty[ \quad v_s(p') = N_\lambda - \lambda \ln(p') + (\Delta e_i - \Delta e_c) \cdot \left[ \frac{e^{\beta p_y^I} + e^{\beta p_y^{II}}}{e^{\beta p'} + e^{\beta p_y^{II}}} \right] + \Delta e_c \quad (7)$$

161 3.1.4. Determination of  $\beta$

162  $\beta$  can be directly determined from the results of an isotropic compression test. Practically,  $\beta$  is related  
163 to the gradient  $\xi$  on the  $v : p'$  curve at  $p' = p_y^{II}$  (Figure 6). For consistency and stability, the function  $v_s$   
164 the specific volume in the  $v : p'$  plane must be strictly monotonic decreasing on  $[p_y^I, +\infty[$ , which imposes  
165  $\beta \geq 0$ .

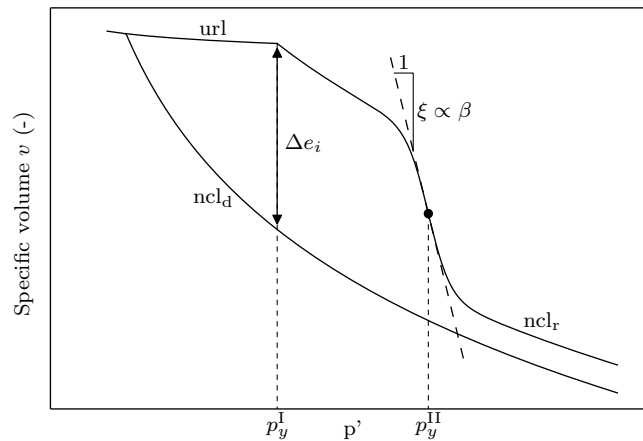


Figure 6: Physical meaning of  $\beta$  –  $ncl_d$ : Normal compression line of the destructured state,  $ncl_r$ : Normal compression line of the residual state,  $url$ : Unloading-reloading line.

Calling  $\xi$  the gradient of the specific volume curve at  $p' = p_y^{\text{II}}$ , the appropriate value for  $\beta$  is obtained by solving the following equation:

$$\left(\frac{dv}{dp'}\right)_{p'=p_y^{\text{II}}} = \xi \Leftrightarrow -\frac{1}{4} \left(1 + e^{\beta(p_y^{\text{I}} - p_y^{\text{II}})}\right) \times \beta(\Delta e_i - \Delta e_c) - \frac{\lambda}{p_y^{\text{II}}} = \xi \quad (8)$$

166 There is no analytical solution to this equation, known as the Lambert W function, due to the non-  
 167 linearity in  $\beta$ . However, this equation can be solved graphically or numerically using methods such as the  
 168 Newton-Raphson algorithm (Corless et al., 1996).

### 169 3.1.5. Suitability of the formulation

170 The  $v : p'$  relationship (Equation 7) is used to demonstrate the ability of the formulation to describe  
 171 the four modes (Figure 7). Parameters used for the simulations are given in Table 2. The influence of  
 172 the parameters  $\beta$  (Figure 8) and the degradation stress  $p_y^{\text{II}}$  (Figure 9) is assessed and the case  $p_y^{\text{I}} = p_y^{\text{II}}$  is  
 173 considered in Figure 10.

174 Figure 8 shows that it is possible to describe the mode 3. Changing the value of  $\beta$  permits to achieve  
 175 different rates of degradation. In this figure, a non-zero  $\Delta e_c$  was chosen ( $\Delta e_c > 0$ ), but mode 4 can be  
 176 achieved by setting  $\Delta e_c = 0$ . The influence of  $p_y^{\text{II}}$  is shown in Figure 9. One can see that this parameter  
 177 controls the initiation of the process of degradation, and is successful in describing modes 2 and 4. As  
 178 previously, modes 1 and 3 can be achieved by setting  $\Delta e_c = 0$ . Finally, the case  $p_y^{\text{I}} = p_y^{\text{II}}$  is considered in  
 179 Figure 10. This case corresponds to an immediate loss of structure at yield. This case does not lead to any  
 180 instabilities of the formulation.



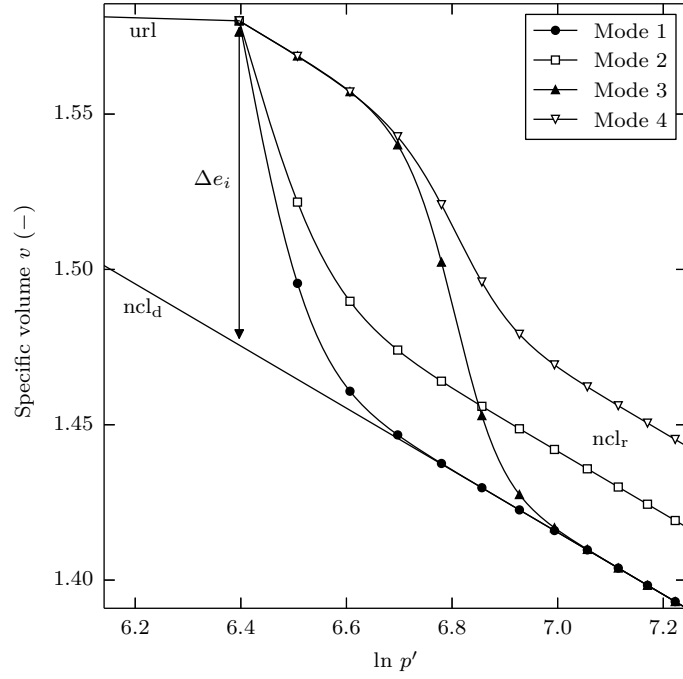


Figure 7: Possibility of the formulation to model the four modes –  $ncl_d$ : Normal compression line of the untreated state,  $url$ : Unloading-reloading line.

Table 2: Model parameters used for simulations of the four modes in Figure 7

Mode	$p_y^I$ (kPa)	$p_y^{II}$ (kPa)	$\Delta e_i$	$\Delta e_c$	$\beta$ (kPa $^{-1}$ )
Mode 1	600	600	0.104	0.0	0.025
Mode 2	600	600	0.104	0.026	0.02
Mode 3	600	900	0.104	0.0	0.025
Mode 4	600	900	0.104	0.052	0.02

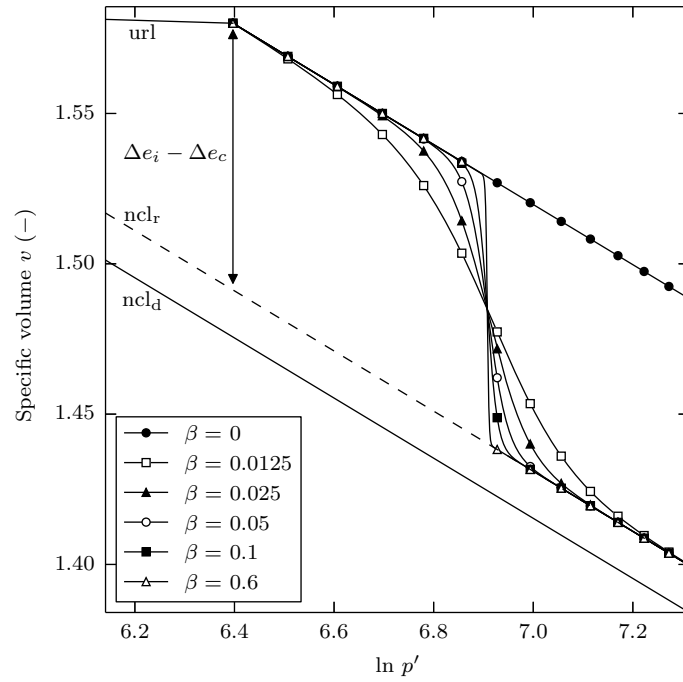


Figure 8: Influence of  $\beta$ :  $p_y^I = 600$  kPa,  $p_y^{II} = 1000$  kPa,  $\Delta e_c > 0$  – Mode 4.

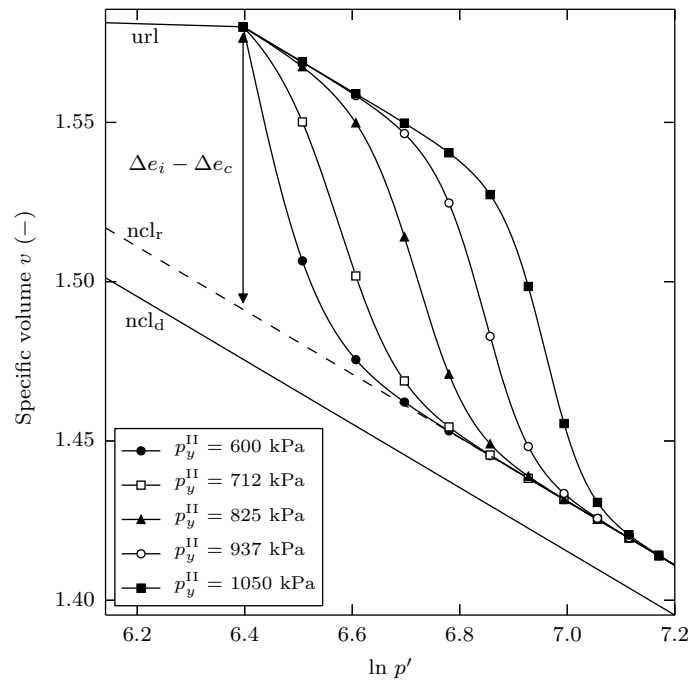


Figure 9: Influence of  $p_y^{II}$ :  $p_y^I = 600$  kPa,  $\beta = 0.025$ ,  $\Delta e_c > 0$  – Modes 2 and 4.

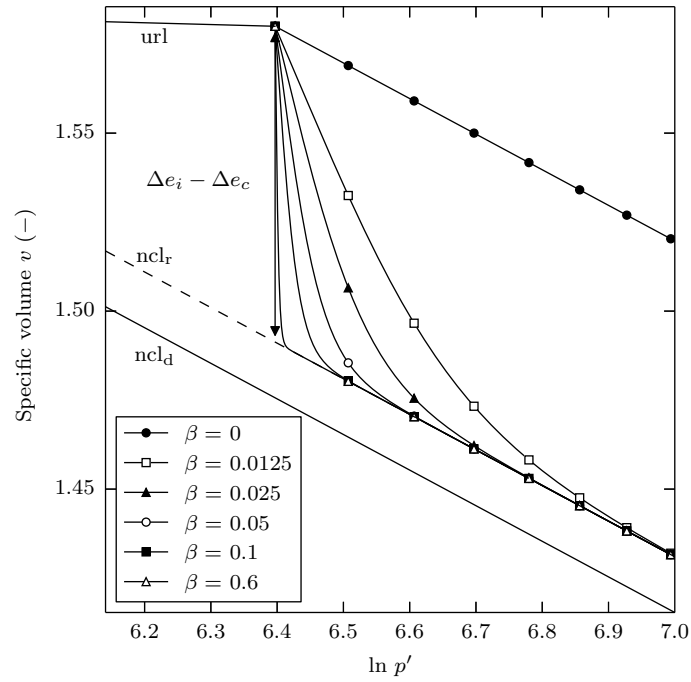


Figure 10: Influence of  $\beta$ :  $p_y^{\text{II}} = p_y^{\text{I}} = 600$  kPa,  $\Delta e_c > 0$  – Mode 2.

181 3.2. Yield function  $f$

182 The addition of lime leads to an increase of the cohesion and the friction angle compared to the untreated  
 183 soil. Therefore, the equation of the MCC for the yield function  $f$  is not sufficient in its original form. One  
 184 way to account for the increase of cohesion is to consider it as an increase of the tensile strength. This can  
 185 be modelled by expanding the yield function in the negative stress domain (Figure 11). The parameter  $p_b$  is  
 186 introduced to control the expansion of the yield function due to the increase of the cohesion and is directly  
 187 obtained from the equation of the CSL. The critical state line does not necessarily pass through the origin  
 188 anymore.

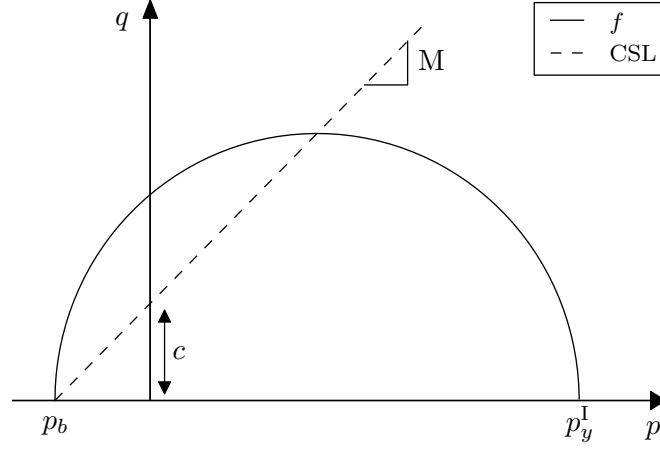


Figure 11: Theoretical yield function for lime treated soils.

The equation chosen for the yield function can therefore be expressed as:

$$f \equiv q^2 + M^2(p' - p_y^I)(p' - p_b) \equiv 0 \quad (9)$$

### 189 3.3. Plastic potential $g$

The choice of the formulation for the plastic potential  $g$  is a major issue in the constitutive modelling of soils. The use of non-associated potentials comes at the cost of several additional parameters with, in most of the cases, no straightforward physical meaning and whose values can rarely be determined from experimental results. This study aims to develop a model based on meaningful parameters determined from classic experimental tests. To this end, this model assumes that lime treated materials follow an associated flow rule and therefore

$$g \equiv f \quad \Rightarrow \quad g \equiv q^2 + M^2(p' - p_y^I)(p' - p_b) \quad (10)$$

which leads to the following flow rule for lime treated materials:

$$\frac{\delta \varepsilon_p^p}{\delta \varepsilon_q^p} = \frac{\partial g / \partial p'}{\partial g / \partial q} = \frac{M^2(p' - p_b)}{2p'\eta} - \frac{p'\eta}{2(p' - p_b)} \quad (11)$$

190 with  $\eta = q/p'$ . The suitability of this hypothesis will be verified in the [Model evaluation](#) section.

### 191 3.4. Summary of the model parameters

192 Using the sigmoid equation, a new formulation has been developed to model the degradation of structure  
 193 at yield for lime treated soils (Equation 7). This formulation has the significant advantage to add only 5  
 194 additional parameters to the original MCC, which all have a physical meaning and can all be determined  
 195 from an isotropic consolidation test performed on the lime treated material. To model the influence of the  
 196 cohesion on the deviatoric behaviour the parameter  $p_b$ , directly related to the equation of the CSL, was

197 introduced. Finally, 6 parameters appear sufficient to account for the effects of a lime treatment on the  
 198 mechanical behaviour of a material:

199

- $p_y^I$  : Primary yield stress
- $p_y^{II}$  : Degradation stress
- $\Delta e_i$  : Additional void ratio at  $p_y^I$
- 200  $\Delta e_c$  : Additional void ratio for  $p' \rightarrow +\infty$
- $\beta$  : Rate of degradation
- $p_b$  : Tensile strength due to the increase of the cohesion

## 201 4. Stress-strain relationship

### 202 4.1. Elastic behaviour

It is assumed that only elastic deformation occurs for stress states lying within the yield surface. According to the Modified Cam Clay model, the elastic volumetric increments are given by

$$\delta \varepsilon_p^e = \kappa \frac{\delta p'}{v p'} \quad (12)$$

$$\delta \varepsilon_q^e = \frac{\delta q}{3G'} \quad (13)$$

203 with  $G'$  the shear modulus.

### 204 4.2. Plastic behaviour

#### 205 4.2.1. Compliance matrix for hardening case

The general plastic stress:strain relationship is given by

$$\begin{bmatrix} \delta \varepsilon_p^p \\ \delta \varepsilon_q^p \end{bmatrix} = \frac{-1}{\left[ \frac{\partial f}{\partial p'_0} \left[ \frac{\partial p'_0}{\partial \varepsilon_p^p} \frac{\partial g}{\partial p'} + \frac{\partial p'_0}{\partial \varepsilon_q^p} \frac{\partial g}{\partial q} \right] \right]} \begin{bmatrix} \frac{\partial f}{\partial p'} \frac{\partial g}{\partial p'} & \frac{\partial f}{\partial q} \frac{\partial g}{\partial p'} \\ \frac{\partial f}{\partial p'} \frac{\partial g}{\partial q} & \frac{\partial f}{\partial q} \frac{\partial g}{\partial q} \end{bmatrix} \cdot \begin{bmatrix} \delta p' \\ \delta q \end{bmatrix} \quad (14)$$

206 The new formulation of the  $v : p'$  relationship given by Equation (7) is now used as the new hardening  
 207 rule. For the sake of simplicity, it was assumed that hardening is only controlled by the plastic volumetric  
 208 strains ( $f(\boldsymbol{\sigma}, \varepsilon_p^p)$ ). The volumetric plastic strains for lime treated soils is therefore expressed as

$$\delta \varepsilon_p^p = \left[ \left( \frac{M^2(2p' - p'_0 - p_b) + 6q}{M^2(p' - p_b)} \right) \left( \frac{\partial p'_0}{\partial \varepsilon_p^p} \right)^{-1} \right] \cdot \delta p' \quad (15)$$

and the deviatoric plastic strains can be calculated using the flow rule:

$$\delta \varepsilon_q^p = \left[ \frac{M^2(p' - p_b)}{2p'\eta} - \frac{p'\eta}{2(p' - p_b)} \right]^{-1} \cdot \delta \varepsilon_p^p \quad (16)$$

#### 209 4.2.2. Compliance matrix for softening case

210 Lime treated specimens experiencing softening at shear show a maximum rate of dilatation after the peak  
 211 due to the degradation of the structure. If Equation (5) is used to model the softening behaviour on  $]0, p_y^I]$ ,  
 212 the formulation leads to  $\Delta e \geq \Delta e_i$  and no degradation of the structure is modelled. To model the softening  
 213 behaviour, we propose a new softening rule in the same framework as the one chosen for the hardening  
 214 case, where the degradation of the structure is described by the sigmoid equation. To avoid the addition of  
 215 meaningless parameters, an automatic procedure is proposed based on experimental considerations.

Since  $\Delta e_c$  arises from the lime treatment and modifies the texture of the soil, it is assumed that the material converges toward the same  $ncl_r$  as under isotropic loading. Based on experimental observations (Robin et al., 2014) the inflexion point, called  $p_{y,s}^{II}$ , was chosen as the intersection of the  $url$  and the  $ncl_r$  (Figure 12) and is given by

$$p_{y,s}^{II} = \exp \left( \frac{N_\lambda - N_\kappa + \Delta e_c}{\lambda - \kappa} \right) \quad (17)$$

which does not require any additional parameter. This leads to the following expression of the softening rule:

$$\forall p' \in ]0, p_y^I] \quad v_s(p') = N_\lambda - \lambda \ln(p') + (\Delta e_i - \Delta e_c) \cdot \left[ \frac{e^{-\beta_s p_y^I} + e^{-\beta_s p_{y,s}^{II}}}{e^{-\beta_s p'} + e^{-\beta_s p_{y,s}^{II}}} \right] + \Delta e_c \quad (18)$$

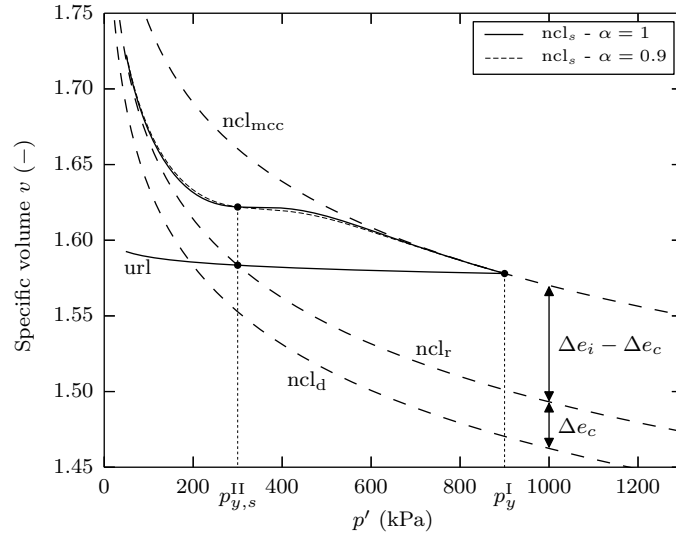


Figure 12: Modelling of the behaviour at yield for softening case.

The parameter  $\beta_s$  describes the rate of destructuration which is calculated automatically. During the post-yield behaviour, the maximum rate of dilatation is observed right after the deviatoric stress reaches its

maximum. This is due to the structure experiencing an extensive degradation. Such feature can be modelled by using as  $\beta_s$ , the maximum rate of degradation  $\beta_0$ , leading to  $v_s$  monotonically decreasing (not strictly). In this case, the first derivative being zero only for a single effective mean stress (which is not necessarily  $p_{y,s}^{\text{II}}$ ). This method presents the advantage that  $\beta_0$  can easily be determined graphically or numerically. However, for consistency and numerical stability,  $v_s$  is preferred to be strictly monotonic decreasing on  $]0, p_y^{\text{I}}]$ . For this purpose, we introduced a constant  $\alpha$  such that

$$\beta_s = \alpha \times \beta_0 \quad (19)$$

216 the bijection (one-to-one correspondence) being ensured by  $\alpha \in ]0, 1[$ . Practically,  $\alpha$  can control the  
 217 smoothness of the process of destructuration. In this model,  $\alpha$  is arbitrarily set to 0.9, which ensures a  
 218 bijective function and an appropriate rate of degradation at yield (Figure 12).

219 This two-step method is the simplest and most reliable way to calculate  $\beta_s$ , simply because the deter-  
 220 mination of  $\beta_0$  is independent of the stress state and does not require information about the gradient at  
 221  $p_{y,s}^{\text{II}}$ , which can not be determined from experimental results, and may lead to numerical instabilities. The  
 222 suitability of this method will be demonstrated during the [Model evaluation](#) section.

223 The strain-strain relationship for the softening case is obtained by introducing Equation 18 into Equa-  
 224 tion 14. Such softening rule respects the associated potentials hypothesis.

## 225 5. Model evaluation

226 The robustness of the model for lime treated soils (MLTS) is assessed in predicting the behaviour of  
 227 artificially and naturally structured materials under isotropic loading and drained paths for different con-  
 228 fining pressures. As a first step, we assess the suitability of an associated flow rule for the modelling of lime  
 229 treated soils using the experimental results from [Robin et al. \(2014\)](#). Then, the model is used to predict the  
 230 behaviour of silt specimens treated with different lime contents (0.5%, 1%, 2%, and 5% CaO) ([Robin et al.](#),  
 231 [2014](#)). The model is finally tried out on naturally structured specimens of calcarenite ([Lagioia and Nova](#),  
 232 [1995](#)). For both cases, the additional parameters to the Modified Cam Clay were determined from a single  
 233 isotropic compression test performed on the structured specimens (Table 3).

Table 3: Values of the model parameters

Parameters		[CaO]				Calcarenite
		Robin et al. (2014)				Lagioia and Nova (1995)
		0.5%	1%	2%	5%	
MCC	$p_y^I$ (kPa)	255	600	1260	1900	2300
	$N_\lambda$ (-)	1.95	1.99	1.97	2.00	3.76
	$\lambda$ (-)	0.08	0.08	0.08	0.08	0.23
	$\kappa$ (-)	0.019	0.032	0.014	0.015	0.020
	M (-)	-	1.15	1.22	1.42	1.42
	E (kPa)	-	45000	55000	70000	77000
MLTS	$p_y^{II}$ (kPa)	1200	1000	2200	3500	2300
	$\Delta e_i$ (-)	0.027	0.065	0.129	0.159	0.134
	$\Delta e_c$ (-)	0.0	0.046	0.109	0.136	0.0
	$p_b$ (kPa)	-	-41.8	-120.3	-144.7	-25.6
	$\beta$ (kPa <sup>-1</sup> )	0.020	0.035	0.020	0.020	0.047

MCC: Modified Cam Clay model, MLTS: Model for Lime Treated Soils.

### 234 5.1. Associated flow rule hypothesis

235 In this section, we assess the validity of an associated flow rule for lime treated soils. Plastic strain  
236 increment vectors from drained triaxial tests performed on specimens treated with 1%, 2%, and 5% in  
237 lime were determined. The yield loci values were normalized with respect to the primary yield stress  $p_y^I$ .  
238 Figure 13 shows that it seems reasonable to assume that plastic strain increment vectors are normal to  
239 the yield surface. The hypothesis of an associated flow rule for the modelling of lime treated soils appears  
240 therefore suitable.



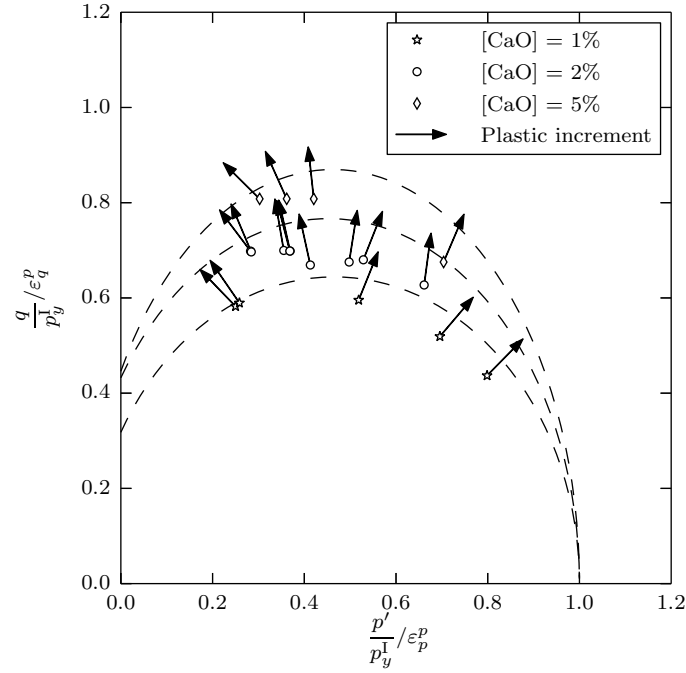


Figure 13: Vectors of plastic strain increment plotted at yield points obtained from drained triaxial tests on lime treated specimens.

241 *5.2. Lime treated specimens*

242 *5.2.1. Isotropic consolidation*

243 The new formulation to model the degradation of the structure at yield (Equation 7) was applied on  
 244 lime treated specimens. Two sets of experimental results of isotropic compressions tests were used to verify  
 245 the general nature of the formulation. The first set was treated with 0.5% CaO and follows the mode 3  
 246 ( $\Delta e_c = 0$ ), and the second with 1% CaO and follows the mode 4 ( $\Delta e_c > 0$ ) (Figure 14). For the two sets the  
 247 parameter  $\beta$  was determined from the gradient of the curve at  $p' = p_y^{\text{II}}$  using the Newton-Raphson algorithm.

248 The use of the sigmoid equation appears very appropriate to model the degradation experienced at yield  
 249 by lime treated materials. For both concentrations in lime, there is a very good agreement between the  
 250 experimental results and the model. The degradation is initiated at the right effective mean stress and with  
 251 the correct rate, and both sets converge toward the correct normal compression line.

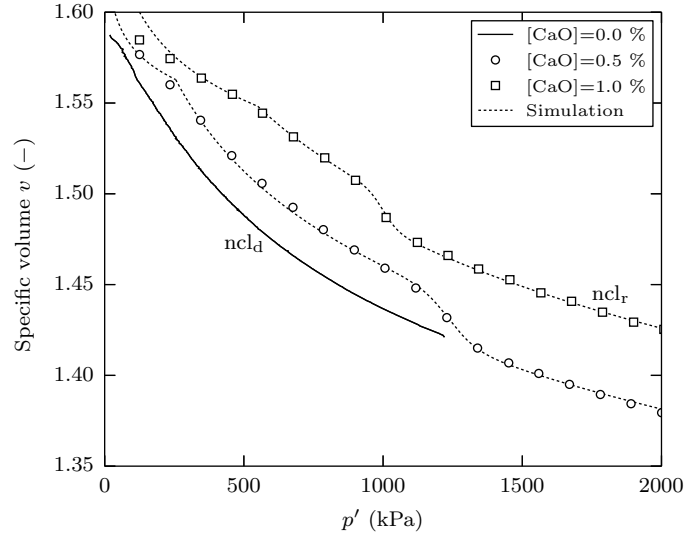


Figure 14: Validation of the formulation on 0.5% and 1% lime treated specimens –  $ncl_d$ : normal compression line of the untreated state,  $ncl_r$ : normal compression line of the residual state.

### 5.2.2. Shear behaviour

No additional parameters to the MCC are required by this model to describe the degradation of the structure at shear apart from  $p_b$  that is derived from the equation of the CSL. The model was applied on lime treated specimens along different drained stress paths and confining pressures (Figures 15-17). Three concentrations in lime were tested to consider various degrees of structure: 1%, 2% and 5% CaO.

The yield loci and critical states appear satisfactory modelled for all the lime contents tested. They confirm the appropriateness of the equation of the yield function  $f$  and the suitability of the parameter  $p_b$  to account for the influence of the lime treatment on the cohesion and the critical state.

For both hardening and softening cases, the volumetric deformations are very accurately predicted by the model. This supports the assumption of the volumetric deformations being mostly controlled by the structure. The evolution of the specific volume for the softening case is particularly accurate (Figure 18). The model is successful to reproduce the dilation post-yield of the specimens and the maximum rate of dilation after the deviatoric stress peak, which is one of the key features of structured soils.

The framework chosen for the softening case appears suitable and very powerful. The assumptions made to calculate automatically in the background the parameters  $p_{y,s}^{\Pi}$  and  $\beta_s$  (Figure 12) are therefore relevant and successful to reproduce the majority of the main features of behaviour of lime treated soils, and that using only information from isotropic test results. It also ensures that the material experiences dilation at yield for samples in the dry side.

The MLTS appears very satisfactory to model the key features of lime treated soils considering the limited number of parameters and the straightforwardness of their determination. Nevertheless, the model

272 tends to deviate from the experimental results during the post-yield stage before converging back toward  
273 the critical state at high axial strains for some samples subjected to a high preconsolidation pressure (600  
274 kPa in Figure 15, 900 kPa in Figure 16). In this model, potentials  $f$  and  $g$  are associated and hardening  
275 is controlled by the plastic volumetric deformations  $\varepsilon_p^p$  only ( $f(\boldsymbol{\sigma}, \varepsilon_p^p)$ ). This has for consequences to reflect  
276 the degradation of the structure on the deviatoric stress. However, lime treated specimens experiencing  
277 hardening do not show any sign of this phenomenon for any of the concentrations tested. This might come  
278 from the fact that the contribution of  $\varepsilon_q^p$  was neglected in this model, and/or that the ‘amount’ of structure  
279 is too low to significantly affect the stresses.

280 For samples in the dry side, the model predicts larger values for the yield loci than what is experimentally  
281 observed. One of the known limitations of the MCC is that it overestimates the values in such situation;  
282 the fact that we extended the yield function in the tensile domain with  $p_b$  amplifies this feature.

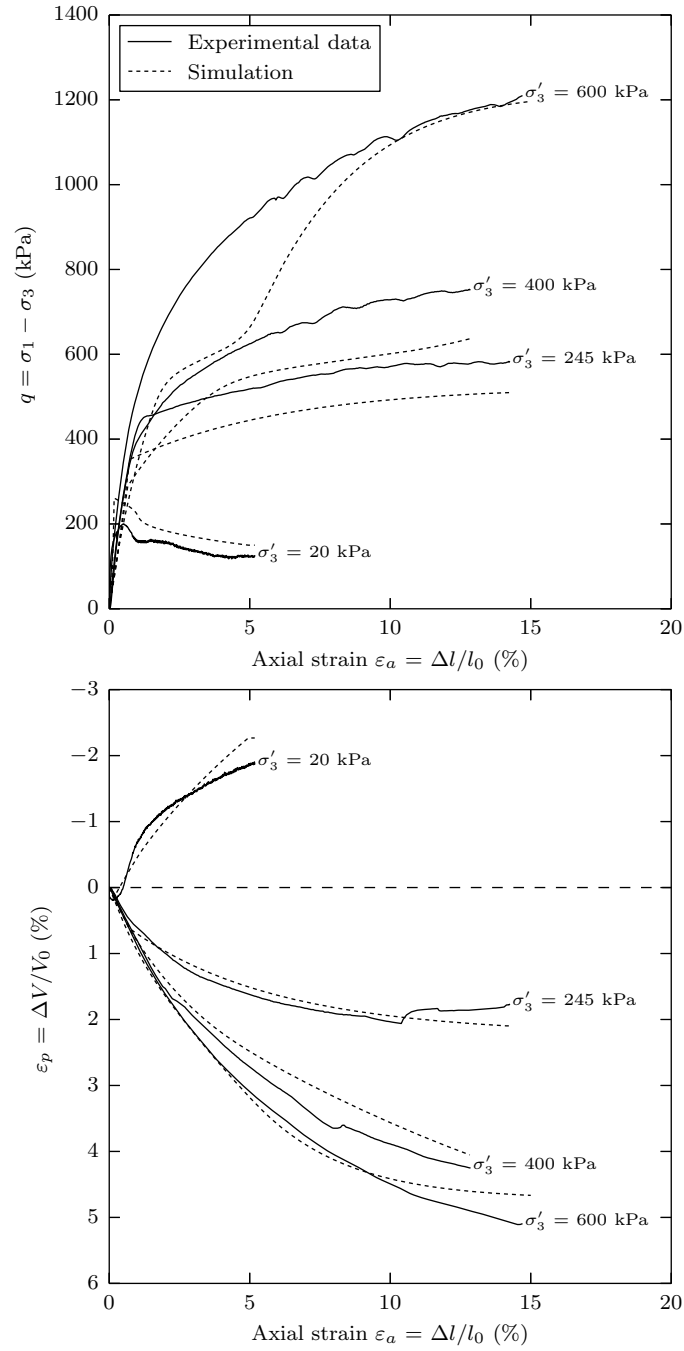


Figure 15: Comparison between experimental results and the model of drained triaxial tests performed on lime treated specimens with 1% CaO (Robin et al., 2014).

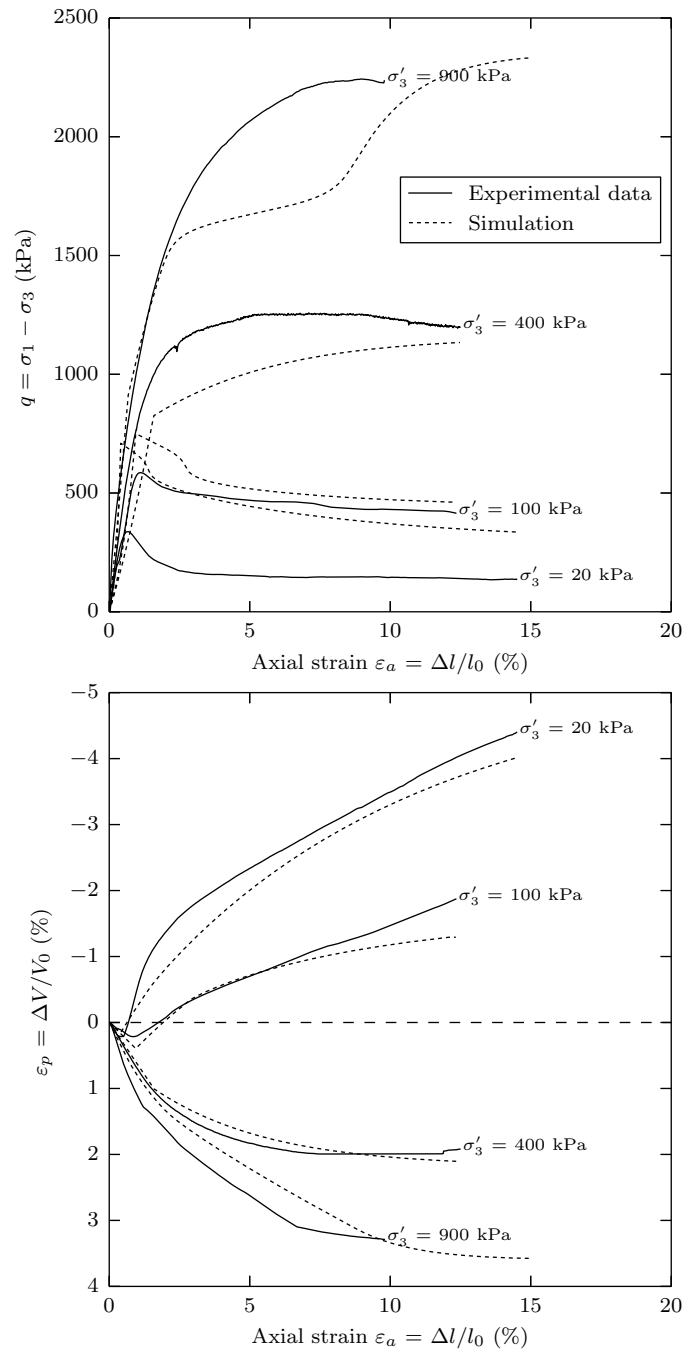


Figure 16: Comparison between experimental results and the model of drained triaxial tests performed on lime treated specimens with 2% CaO (Robin et al., 2014).

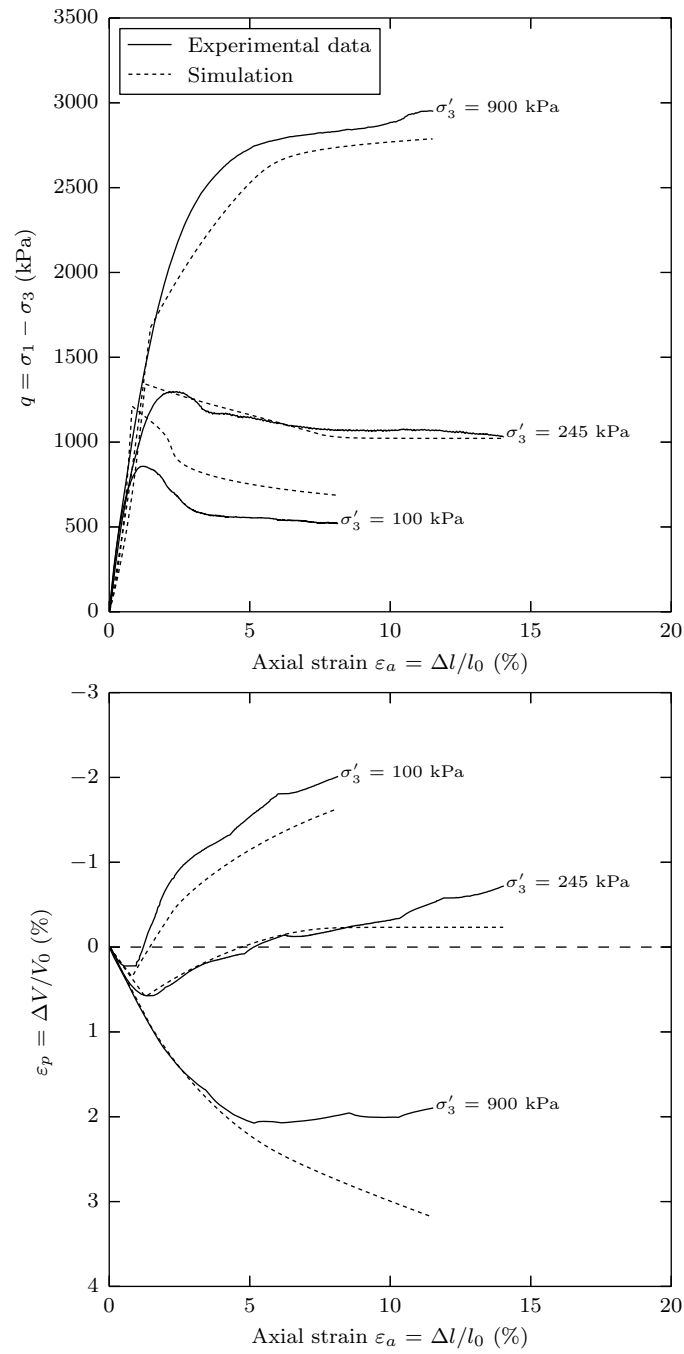


Figure 17: Comparison between experimental results and the model of drained triaxial tests performed on lime treated specimens with 5% CaO (Robin et al., 2014).

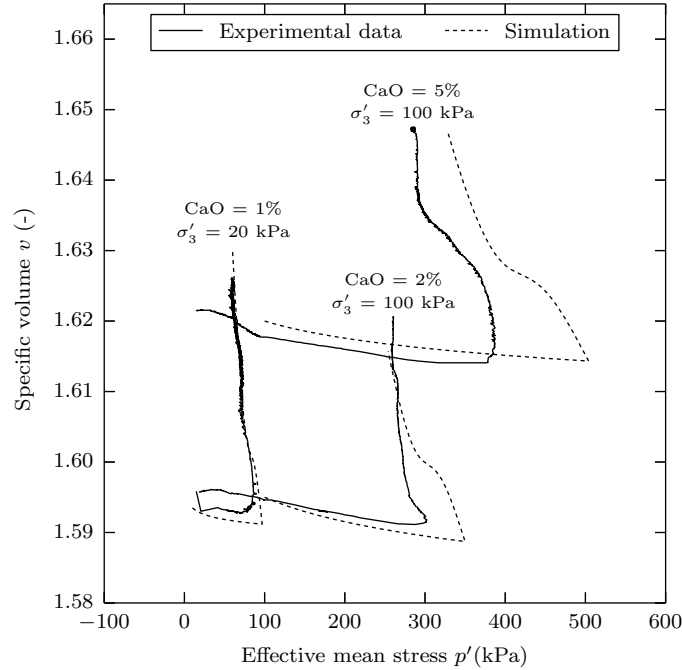


Figure 18: Comparison between drained triaxial results and the model of the specific volume for different lime contents (Robin et al., 2014).

### 283 5.3. Naturally structured soils

284 Although the formulation was originally designed for lime treated soils, there are several common features  
285 of behaviour between artificially and naturally materials that could also make it suitable for the latter.

#### 286 5.3.1. Isotropic consolidation

287 The suitability of the formulation to model the degradation of naturally structured soils under isotropic  
288 loading is verified using the results from Lagioia and Nova (1995) on natural calcarenite (Figure 19). Likewise  
289 the lime treated specimens, calcarenite experiences a degradation of the structure at yield but that occurs  
290 immediately at yield ( $p_y^I = p_y^{II}$ ) and at a very high rate. Again,  $\beta$  was solved numerically using the Newton-  
291 Raphson procedure. There is no information about the behaviour of the destructured calcarenite under  
292 isotropic loading, and therefore no information is given about the value of the residual void ratio  $\Delta e_c$ .  
293 However, Lagioia and Nova (1995) considered that calcarenite converges toward the ncl of the destructured  
294 state. Thus, it is assumed that calcarenite has no residual void ratio ( $\Delta e_c = 0$ ) and follows the mode 1.  
295 The parameters used for the simulations are given in Table 3.

296 Though the origin of the cementation is different, the MLTS appears suitable to model naturally struc-  
297 tured materials under isotropic loading. As for the lime treated specimens, the degradation is initiated at  
298 the right effective mean stress and at the correct rate till it reaches the normal compression line of the  
299 destructured state.

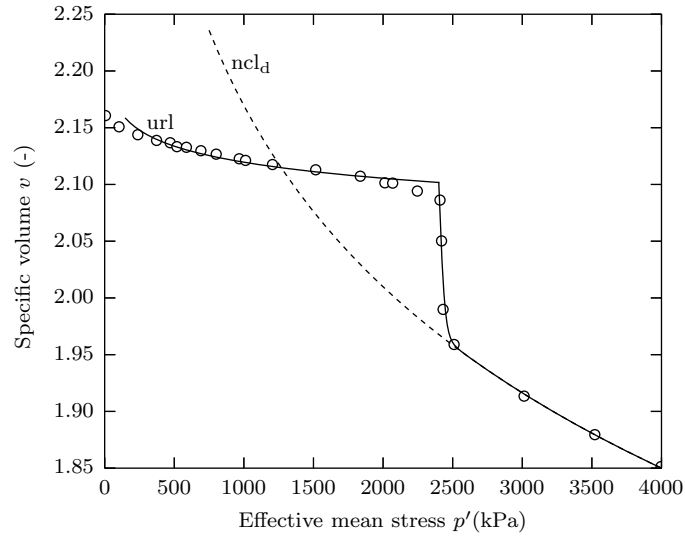


Figure 19: Validation of the formulation on natural calcarenite (after [Lagioia and Nova \(1995\)](#)) – ncl: normal compression line.

300 *5.3.2. Shear behaviour*

301 The model is now tried to reproduce the behaviour of samples naturally structured calcarenite at shear  
 302 submitted to drained triaxial tests. The parameter  $p_b$  was determined from the equation of CSL given in  
 303 [Lagioia and Nova \(1995\)](#).

304 For samples of calcarenite experiencing hardening ([Figure 20](#)) the MLTS gives a very good agreement  
 305 with the experimental results of the yield loci and the critical state. At yield, the degradation of the structure  
 306 seems to affect the deviatoric stress, which is successfully described by model. The specific volume at yield  
 307 ([Figure 21](#)) is accurately modelled and the trends of the volumetric deformations ([Figure 20](#)) are satisfactory,  
 308 although the values appear underestimated at large deformations.

309 For samples experiencing softening ([Figure 22](#)) the MLTS gives an accurate prediction of the yield loci  
 310 and the critical state. However, samples revealed an unusual behaviour in the framework of the MCC and  
 311 the critical state theory regarding the volumetric deformations. It is generally accepted that for the softening  
 312 case samples experience dilation at yield. However, the calcarenite seems to behave differently and keeps  
 313 contracting at yield, although the deviatoric stress decreases.



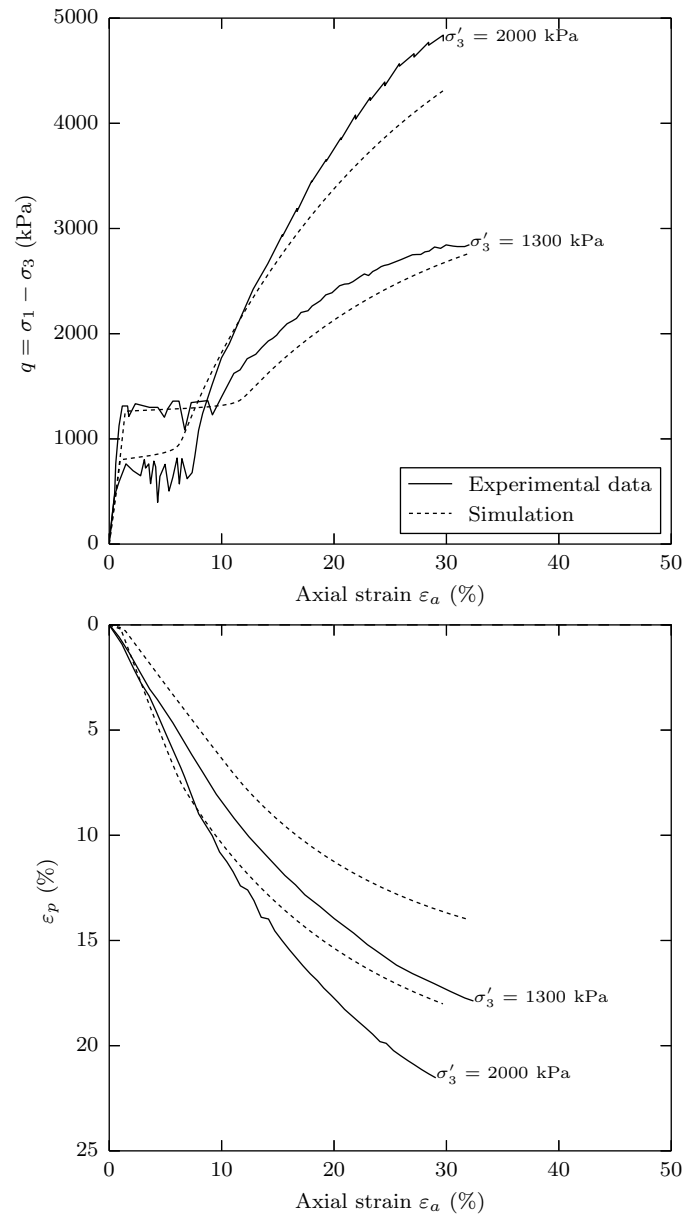


Figure 20: Comparison between experimental results and the model of drained triaxial tests performed on calcarenite and experiencing hardening (Lagioia and Nova, 1995).

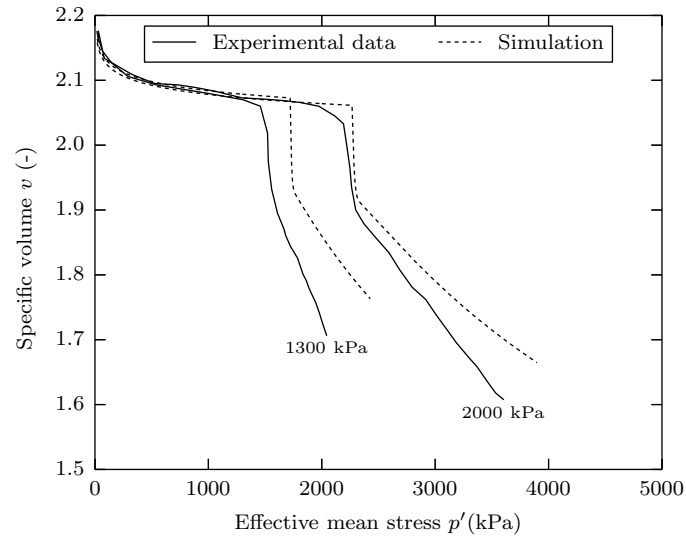


Figure 21: Comparison between the experimental results and the model for the specific volume (Lagioia and Nova, 1995)

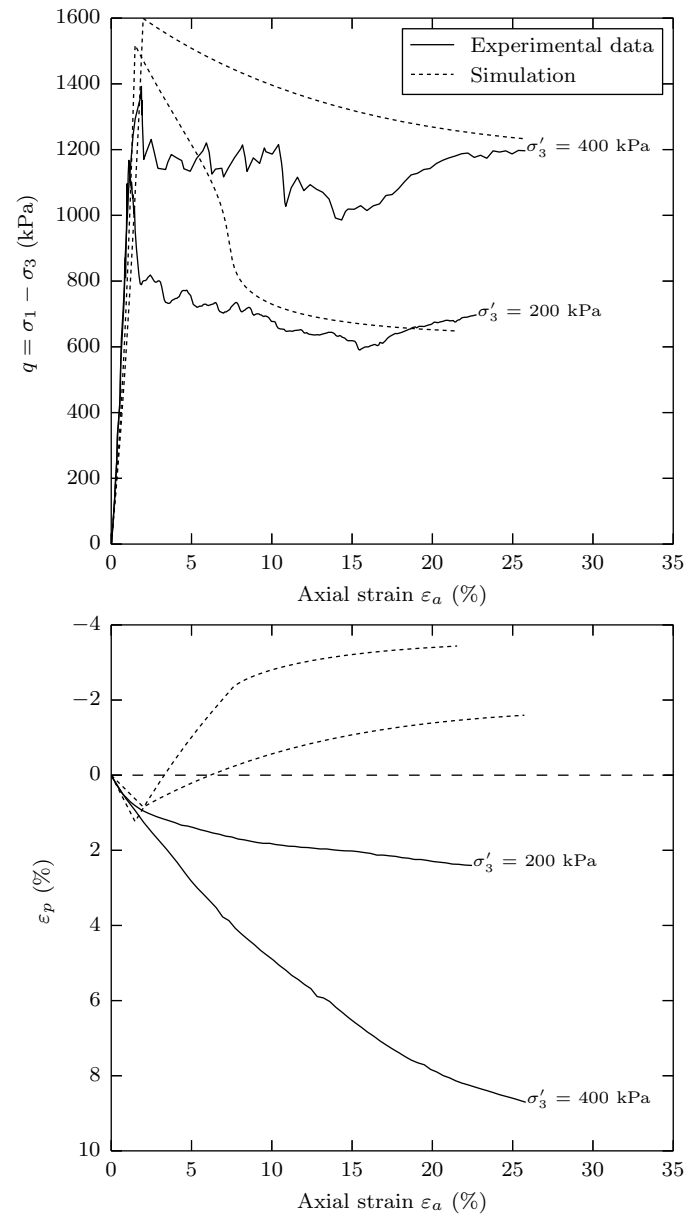


Figure 22: Comparison between experimental results and the model of drained triaxial tests performed on calcarenite and experiencing softening (Lagioia and Nova, 1995).

314 *5.4. Discussion: influence of the initial void ratio on the degradation mode*

315 The MLTS can successfully reproduce a large number of features of both lime treated soils and naturally  
316 structured soils. However, the model deviates from the experimental results for 1) lime treated specimens  
317 subjected to high preconsolidation pressures experiencing hardening, and 2) samples of calcarenite experi-  
318 encing softening. In this section, we propose a hypothesis to explain these limitations using the initial void  
319 ratio of the material.

320 During the early post-yield stage, the degradation of the structure seems to affect the stress:strain  
321 response for samples of calcarenite experiencing hardening, but not for the lime treated specimens. Fur-  
322 thermore, for the softening case, lime treated specimens experience dilation, as predicted by the critical  
323 state theory, but this is not the case for the samples of calcarenite, which experience contraction despite the  
324 decrease of deviatoric stress at yield.

325 For the calcarenite, the initial additional void ratio at yield  $\Delta e_i$  and the range of stresses are similar to  
326 those measured on lime treated soils with 5% CaO. The only difference between the two materials lies in  
327 the initial specific volume (around 1.6 for the lime treated specimens and 2.2 for the calcarenite). When  
328 the calcarenite starts yielding, the structure is rapidly degraded due to the brittleness of the material.  
329 [Lagioia and Nova \(1995\)](#) stated that some softening could take place under isotropic loading, and explained  
330 that the plateau of the deviatoric stress is associated with debonding. However, what was interpreted as  
331 *softening* under isotropic loading is more likely to be collapse since the specific volume decreases during the  
332 destructuration. Once the particles are released from the cementation, they immediately collapse and start  
333 filling the voids as the axial deformation increases. During this stage, there is no effective friction inside the  
334 material and therefore no additional deviatoric stress is necessary to increase the axial deformation. The  
335 effective friction is restored once the particles are close enough and the porosity is significantly reduced,  
336 which leads to an increase of the deviatoric stress followed by convergence toward the critical state. This  
337 mechanism also explains why samples experiencing softening do not have a dilatant behaviour at yield as  
338 predicted by the critical state theory. The dilation process is the direct result of the interlocking of the  
339 particles; in the case of the calcarenite, the fast degradation of the structure leads to the collapsing of the  
340 particles and therefore to the contraction of the sample. Although the deviatoric stress decreases at yield,  
341 since there is no interlocking of the particles, there is no dilation of the sample.

342 For the lime treated specimens of this study, the initial conditions were chosen to match those used  
343 on-site and obtained from the Proctor compaction test ([Robin et al., 2014](#)). In these conditions, the void  
344 ratio is too low to generate a noticeable collapse in the material, and the destructuration is a slower process.  
345 The degradation of the structure takes place but particles are already in contact, which maintains a friction  
346 between them and leads to increase in the deviatoric stress with the axial deformation. Therefore, the  
347 degradation of the structure is not observed directly on the stress:strain response. If the conditions imply  
348 strain softening, interlocking happens and therefore dilation, which is observed on the experimental results

349 and properly reproduced by the MLTS.

350 In light of these observations, it appears that the initial void ratio has a key impact on the behaviour of  
 351 the material than the degree and the origin of cementation. As matter of fact, the mode of degradation of a  
 352 large number of structured materials seems to be closely related to the initial void ratio (Table 4). Further  
 353 work must be carried out to identify the parameters responsible for the different behaviours. Nevertheless,  
 354 the MLTS appears to reproduce the main features of behaviour of lime treated soils, and is also successful  
 355 in modelling the main trends that are observed in naturally structured soils.

Table 4: Correlation between the initial void ratio and the mode of degradation

	Origin of structure	Material	$v_i$ (-)	Study
Mode 1	Natural	Pisa clay	2.8	<a href="#">Callisto and Calabresi (1998)</a>
	Artificial	St-Alban clay	6.0	<a href="#">Tremblay et al. (2001)</a>
Mode 2	Natural	Louiseville clay	3.0	<a href="#">Lapierre et al. (1990)</a>
	Artificial	Louiseville clay	$\gg 3$	<a href="#">Tremblay et al. (2001)</a>
Mode 3	Natural	Corinth marl	1.6	<a href="#">Anagnostopoulos et al. (1991)</a>
	Artificial	Silt	1.6	<a href="#">Robin et al. (2014)</a>
Mode 4	Natural	Vallericca clay	1.8	<a href="#">Callisto and Rampello (2004)</a>
	Artificial	Sandstone	$<1.6$	<a href="#">Rotta et al. (2003)</a>

$v_i$ : initial specific volume.

## 356 6. Conclusion

357 A new model in the framework of the Modified Cam Clay model was developed for lime treated soils.  
 358 In order to introduce only relevant parameters, the most important features of lime treated materials and  
 359 naturally structured soils that should be reproduced by a model were identified. Experimental results reveal  
 360 that both naturally and artificially soils have a very similar mechanical behaviour at yield.

361 To account for the effects of structure on the behaviour of soils, a new formulation was developed based on  
 362 Richards's equation. In the framework of the simplicity and easiness, only 4 new additional parameters to the  
 363 MCC were introduced: the degradation stress  $p_y^{\text{II}}$ , the rate of degradation  $\beta$ , the additional void ratio at  $p_y^{\text{I}}$ ,  
 364 and the additional void ratio  $\Delta e_c$  at  $p' \rightarrow +\infty$ . The power of this model is that all the additional parameters  
 365 have a physical meaning and can be determined from a single isotropic consolidation test performed on the

366 structured material. A transparent and powerful procedure was developed for the softening rule. The two  
367 parameters required by the sigmoid function to model the degradation are automatically determined from  
368 the 4 parameters obtained from the isotropic tests.

369 The model was applied for lime treated soils and naturally structured samples of calcarenite. The  
370 formulation is in good agreement with the experimental results and the main trends are properly reproduced.  
371 The formulation proposed as softening rule is successful to model the dilation observed on lime treated  
372 samples at yield and the maximum rate of dilation after the peak, one of the most representative features  
373 of structured soils. However, the results on the calcarenite have risen interesting considerations for the  
374 modelling of the structured materials in general, naturally or artificially.

375 The initial porosity appeared to be the key parameter controlling the influence of the degradation of the  
376 structure on the mechanical behaviour of lime treated specimens and the calcarenite. Once the material  
377 starts yielding the degradation of the bonding structure takes place, and therefore the release of the particles.  
378 Depending on the initial void ratio, the material can either experience dilation (particles are in contact and  
379 expand due to the interlocking) or collapse until particles start interacting again. This can lead to compaction  
380 even for heavily over consolidated samples.

381 Further work must be carried out to develop a model capable of accounting for the influence of the initial  
382 void ratio on the post-yield behaviour.

## 383 **Appendix A. Notation**

<b>Symbol</b>	<b>Definition</b>
CSL	Critical State Line
$E$	Young's modulus
$f$	yield function
$g$	plastic potential
$G'$	shear modulus
$M$	slope of critical state line
MCC	Modified Cam Clay Model
MLTS	Model for Lime Treated Soils
ncl	normal compression line
ncl <sub>d</sub>	normal compression line of the destructured state
ncl <sub>r</sub>	normal compression line of the residual state

<b>Symbol</b>	<b>Definition</b>
$ncl_{mcc}$	normal compression line of modified Cam Clay model
$N_\lambda$	specific volume at $p' = 1$ kPa
$p'$	effective mean stress
$p_b$	tensile stress
$p_y^I$	primary yield stress
$p_y^{II}$	degradation stress
$p_{y,s}^{II}$	degradation stress for softening case
$q$	deviatoric stress
url	unloading-reloading line
$v$	specific volume
$v_s$	specific volume for the structured soil
$\alpha$	parameter of bijection for softening case
$\beta$	rate of degradation
$\beta_s$	rate of degradation for softening case
$\beta_0$	rate of degradation for monotonic decreasing function $v_s$
$\Delta e_c$	residual additional void ratio at $p' \rightarrow +\infty$
$\Delta e_i$	initial additional void ratio at $p' = p_y^I$
$\varepsilon_p, \varepsilon_p^e, \varepsilon_p^p$	total, elastic, and plastic volumetric strains
$\varepsilon_q, \varepsilon_q^e, \varepsilon_q^p$	total, elastic, and plastic deviatoric strains
$\kappa$	elastic stiffness parameter for changes in effective mean stress
$\lambda$	plastic stiffness parameter for changes in effective mean stress
$\xi$	gradient of the curve ( $v : p'$ ) at $p' = p_y^{II}$
$\sigma_1, \sigma_3$	axial, radial stress

## 384 7. References

- 385 Ahnberg, H., 2007. On yield stresses and the influence of curing stresses on stress paths and strength measured in triaxial  
386 testing of stabilized soils. *Canadian geotechnical journal* 44 (1), 54–66.
- 387 Anagnostopoulos, a. G., Kalteziotis, N., Tsiambaos, G. K., Kavvas, M., 1991. Geotechnical properties of the Corinth Canal  
388 marls. *Geotechnical and Geological Engineering* 9 (1), 1–26.
- 389 Balasubramaniam, A., Buessuceso, B., Oh, Y.-N. E., Bolton, M. W., Bergado, D., Lorenzo, G., 2005. Strength degradation  
390 and critical state seeking behaviour of lime treated soft clay. In: *International Conference on Deep Mixing-Best Practice*  
391 *and Recent Advances*. Vol. 1. Stockholm, pp. 35–40.
- 392 Baudet, B., Stallebrass, S., 2004. A constitutive model for structured clays. *Géotechnique* 54 (4), 269–278.
- 393 Burland, J. B., 1990. On the compressibility and shear strength of natural clays. *Géotechnique* 40 (3), 329–378.
- 394 Burland, J. B., Rampello, S., Georgiannou, V. N., Calabresi, G., 1996. A laboratory study of the strength of four stiff clays.  
395 *Géotechnique* 46 (3), 491–514.
- 396 Callisto, L., Calabresi, G., 1998. Mechanical behaviour of a natural soft clay. *Géotechnique* 48 (4), 495–513.
- 397 Callisto, L., Rampello, S., 2004. An interpretation of structural degradation for three natural clays. *Canadian Geotechnical*  
398 *Journal* 41 (3), 392–407.
- 399 Consoli, N. C., Lopes, L. d. S., Prietto, P. D. M., Festugato, L., Cruz, R. C., 2011. Variables Controlling Stiffness and Strength  
400 of Lime-Stabilized Soils. *Journal of Geotechnical and Geoenvironmental Engineering* 137 (6), 628–632.
- 401 Corless, R. M., Gonnet, G. H., Hare, D. E. G., Jeffrey, D. J., Knuth, D. E., 1996. On the Lambert W Function. *Advances in*  
402 *Computational Mathematics* 5, 329–359.
- 403 Cotecchia, F., Chandler, R. J., 2000. A general framework for the mechanical behaviour of clays. *Géotechnique* 50 (4), 431–447.
- 404 Cuisinier, O., Auriol, J.-C., Le Borgne, T., Deneele, D., 2011. Microstructure and hydraulic conductivity of a compacted  
405 lime-treated soil. *Engineering Geology* 123 (3), 187–193.
- 406 Cuisinier, O., Masrouri, F., Pelletier, M., Villieras, F., Mosser-Ruck, R., 2008. Microstructure of a compacted soil submitted  
407 to an alkaline PLUME. *Applied Clay Science* 40 (1-4), 159–170.
- 408 Gens, A., Nova, R., 1993. Conceptual bases for a constitutive model for bonded soils and weak rocks. *Geotechnical engineering*  
409 *of hard soils-soft rocks* 1 (1), 485–494.
- 410 Horpibulsuk, S., Liu, M. D., Liyanapathirana, D. S., Suebsuk, J., 2010. Behaviour of cemented clay simulated via the theoretical  
411 framework of the Structured Cam Clay model. *Computers and Geotechnics* 37 (1-2), 1–9.
- 412 Kavvas, M., Amorosi, A., 2000. A constitutive model for structured soils. *Géotechnique* 50 (3), 263–273.
- 413 Lagioia, R., Nova, R., 1995. An experimental and theoretical study of the behaviour of a calcarenite in triaxial compression.  
414 *Géotechnique* 45 (4), 633–648.
- 415 Lapierre, C., Leroueil, S., Locat, J., 1990. Mercury intrusion and permeability of Louiseville clay. *Canadian Geotechnical*  
416 *Journal* 27 (6), 761–773.
- 417 Leroueil, S., Vaughan, P. R., 1990. The general and congruent effects of structure in natural soils and weak rocks. *Géotechnique*  
418 40 (3), 467–488.
- 419 Little, D. N., 1995. *Stabilization of pavement subgrades and base courses with lime*. Kendall Hunt Pub Co.
- 420 Liu, M. D., Carter, J. P., 2002. A structured Cam Clay model. *Canadian Geotechnical Journal* 39 (6), 1313–1332.
- 421 Liu, M. D., Carter, J. P., 2003. Volumetric Deformation of Natural Clays. *International Journal of Geomechanics* 3 (2), 236–252.
- 422 Malandraki, V., Toll, D. G., 2001. Triaxial Tests on Weakly Bonded Soil with Changes in Stress Path. *Journal of Geotechnical*  
423 *and Geoenvironmental Engineering* 127 (3), 282–291.
- 424 Nguyen, L. D., Fatahi, B., Khabbaz, H., 2014. A constitutive model for cemented clays capturing cementation degradation.  
425 *International Journal of Plasticity* 56, 1–18.



- 426 Nova, R., Castellanza, R., Tamagnini, C., 2003. A constitutive model for bonded geomaterials subject to mechanical and/or  
427 chemical degradation. *International journal for numerical and analytical methods in geomechanics* 27 (9), 705–732.
- 428 Oliveira, P. V., 2013. Effect of Stress Level and Binder Composition on Secondary Compression of an Artificially Stabilized  
429 Soil. *Journal of Geotechnical and Geoenvironmental Engineering* 139 (5), 810–820.
- 430 Rampello, S., Callisto, L., 1998. A study on the subsoil of the Tower of Pisa based on results from standard and high-quality  
431 samples. *Canadian Geotechnical Journal* 35 (6), 1074–1092.
- 432 Richards, F., 1959. A flexible growth function for empirical use. *Journal of experimental Botany* 10 (29), 290–300.
- 433 Robin, V., Cuisinier, O., Masrouri, F., Javadi, A. A., 2014. Chemo-mechanical modelling of lime treated soils. *Applied Clay  
434 Science* 95, 211–219.
- 435 Roscoe, K. H., Burland, J. B., 1968. On the generalized stress-strain behaviour of wet clay. *Engineering Plasticity*, 535–609.
- 436 Rotta, G. V., Consoli, N. C., Prietto, P. D. M., Coop, M. R., Graham, J., 2003. Isotropic yielding in an artificially cemented  
437 soil cured under stress. *Géotechnique* 53 (5), 493–501.
- 438 Suebsuk, J., Horpibulsuk, S., Liu, M. D., 2011. A critical state model for overconsolidated structured clays. *Computers and  
439 Geotechnics* 38 (5), 648–658.
- 440 Tremblay, H., Leroueil, S., Locat, J., 2001. Mechanical improvement and vertical yield stress prediction of clayey soils from  
441 eastern Canada treated with lime or cement. *Canadian Geotechnical Journal* 38 (3), 567–579.
- 442 Vatsala, A., Nova, R., Srinivasa Murthy, B. R., 2001. Elastoplastic Model for Cemented Soils. *Journal of Geotechnical and  
443 Geoenvironmental Engineering* 127 (8), 679–687.
- 444 Wissa, A. E., Ladd, C. C., Lambe, T. W., 1965. Effective stress strength parameters of stabilized soils. In: *International  
445 conference on soil mechanics and foundation engineering*. Montréal, pp. 412–416.
- 446 Yong, R., Nagaraj, T., 1977. Investigation of fabric and compressibility of a sensitive clay. In: *Proceedings of the International  
447 Symposium on Soft Clay*, Asian Institute of Technology. pp. 327–333.